Feasibility of Solar Energy and its Ability to Support Libyan Grid in Facing its Energy Crisis

HUSSIN ABOULGASIM ZAHLOUL

Feasibility of Solar Energy and its Ability to Support Libyan Grid in Facing its Energy Crisis

Mr Hussin Aboulgasim Zahloul

Supervisors: Dr Hamed Bahmani

Dr Sergii Veremieiev

Department of Engineering, University of Durham

Thesis submitted in fulfilment of the requirement for the degree of Doctor of Philosophy

April, 2024

ABSTRACT

The escalating global energy demand, driven by population growth and industrial expansion, necessitates a shift towards clean, renewable energy sources. Presently, fossil fuels dominate global energy production, despite their adverse environmental impacts. Consequently, numerous countries are exploring renewable energy, with solar power leading the charge. Libya, grappling with energy challenges exacerbated by past conflicts, is focusing on enhancing its renewable energy sector, particularly solar and wind power. To this end, 2MW GCPV system was modelled using the MATLAB/SIMULINK software tool. The system was configured as a double-stage grid-connected system, comprising five PV arrays of 400kW each. The system underwent comprehensive evaluation from various perspectives. Initially, tests were conducted under diverse levels of irradiance and temperature, accompanied by FFT analysis. The findings reveal that solar irradiance exerts a more pronounced impact on the system's performance compared to temperature. The control strategy of the system demonstrated its efficacy on maintaining constant DC voltage, irrespective of changes in weather conditions. The FFT analysis further indicates that the LC filter effectively upheld the THD level for both voltage and current well below 5%, adhering to the acceptable threshold established by the IEEE 519 standard. Then the system underwent evaluation under Line to Ground (L-G) short circuit, and three phase Line to Ground (3L-G) short circuit faults. These faults were applied at varying distances from the Common Coupling Point (CCP). The study found that during L-G faults, the DC side of the system remained stable, maintaining constant output power and voltage. However, on the AC side, there were voltage dips and current surges during the fault period. Notably, the system swiftly returned to its normal operational state with a settling time of less than 0.2 ms after fault clearance. In the case of 3L-G faults, when the fault occurred near the CCP, significant fluctuations were observed on both sides of the system. Following fault clearance, the system remained in a transient state for approximately 3.5 seconds before returning to normal. Conversely, when faults were applied far from the CCP, the system maintained its stability with minor transients. Despite voltage sags and current surges, the system quickly recovered to its normal state in less than 0.2 ms after fault clearance. The system's performance was evaluated across nine locations in Libya, utilizing satellite data from NASA's database and measurements from the Libyan Centre for Solar Energy Research and Studies (CSESR). Assessment across nine Libyan locations highlighted significant solar energy potential, with Murzuqh City emerging as a key producer, Collectively, the nine sites produced approximately 33,180.84 MWh/year, meeting the energy demand of 4544 houses.

DECLARATION

I hereby declare that, except where specific reference is made, the work described in this project is the result of the investigation carried out by the researcher and that neither this project nor any part of it has been presented, or is currently being submitted in candidature for any award other than in part of the fulfilment for the degree of Doctor of Philosophy in Department of Engineering, University of Durham.

Signature: HUSSIN ABOULGASIM ZAHLOUL

Date: April/2024

STATEMENT OF COPYRIGHT

ACKNOWLEDGMENT

All deepest thanks are due to Almighty ALLAH for helping me achieve this work.

In the first place, I would like to express my sincere gratitude to my research and academic supervisors, **Dr. Hamed Bahmani** and **Dr. Sergii Veremieiev**, for their continuous supervision, advice, and guidance from the very beginning of this research. I would also like to thank my Ph.D. committee members: **Professor Simon Hogg** and **Dr. Oliver Vogt** for their assistance throughout my annual review meetings, which greatly contributed to assessing my work and my progress.

I would like to show my deepest gratitude and respect to my family, especially my parents, to whom I owe all the success in my life. No words can express my gratitude to them, but I pray to Allah to bless and reward them. My father, who passed away while I was here working on this project, this is my gift to you. You have always been with me during this journey, and I am sorry I couldn't see you before you left. May Allah grant you paradise. To my mother, I ask Allah to give you health and a long life. I am sorry for leaving you alone during these difficult years, and thank you for your prayers, which were my light in the darkness.

To my wife, without you, I could have never been able to achieve this work. Your patience and encouragement were always a source of strength for me. You are the shining moon that lights my way. Thanks for your support during my difficult periods.

In my final words, I would like to express my deepest gratitude and respect to my sponsor, the Libyan embassy as a representer on behalf of the Libyan government, and my home institute for giving me this opportunity to complete my postgraduate studies.

TABLE OF CONTENTS

LIST OF FIGURES

Chapter 1:

Chapter 2:

Chapter 3:

Chapter 4:

Chapter 5:

Chapter 6:

Chapter 7:

LIST OF TABLES

Chapter 2:

Chapter 3:

Chapter 4:

Chapter 6:

LIST OF ABBERVIATION

PV	Photovoltaic
c-Si	crystalline silicon
CdTe	Cadmium Telluride
MERE	The Ministry of Electricity and Renewable Energy
REAoL	The Renewable Energy Authority of Libya
GECOL	The General Electric Company of Libya
IEA	The International Energy Agency
GHI	Global Horizontal Irradiation
DNI	Direct Normal Irradiation
NASA	Aeronautics and Space Administration
PV-SWH	Photovoltaic-solar water heating
PV-PV/T	Photovoltaic-photovoltaic/thermal
PTC CSP	Parabolic Trough Concentrated Solar Power
TES	Thermal Energy Storage
POWER	Prediction of Worldwide Energy Resource
BESS	Battery Energy Storage Systems
DG	Distributed Generators
RE	Renewable Energy
STC	Standard Test Conditions
BiPV	Building Integrated Photovoltaics
DGPV	Distributed Generation Photovoltaics
MPPT	Maximum Power Point Tracking
THD	Total Harmonic Distortion
GCPVs	Grid connected Photovoltaic Systems
P&O	Perturb and Observe
HC	Hill Climbing
IncCon	Incremental Conductance
AI	artificial intelligence
FLCs	fuzzy logic controllers
ANNs	artificial neural networks
PSO	particle swarm optimization
NB	negative big

NS	negative small
ZE	zero
PB	positive big
PS	positive small)
VSCs	Voltage Source Converters
LVRT	Low Voltage Ride-Through
RESs	Renewable Energy Systems
PWM	Pulse Width Modulation
CCP	Common Coupling Point
NEC	National Electric Code
PLL	Phase locked loop
STC	Standard test condition
SOC	Standard Operating Condition
CSESR	Libyan Centre for Solar Energy Research and Studies
FFT	Fast Fourier Transform

NOMENCLATURE

Symbol	Description
ΔI_L	The current ripple
ΔV_C	The voltage ripple
C_b	The output capacitor
C_{in}	The input capacitor
E_g	Energy gap
G_N	The irradiance value at standard temperature
I	Current
I_{0_1}, I_{0_2}	The saturation currents
I_D	The diode current
$I_{L,max}$	The maximum current
I_{Ph}	The photon current
I_{Phn}	The photon current value at reference conditions
I_{SH}	The shunt current flow through
I_{array}	The current of the array
$I_{d,ref}$	The reference current value $dq0$ reference frame
I_{on}	The reverse saturation current at standard temperature
I_{sc}	Short-circuit current
L_b	The inductor of DC-DC boost converter
L_f	The filter inductor
N_{PV}	The number of the PV modules used in the system
N_s	The number series connected cells in a single module
P_{array}	The power of the array
P_r^{PV}	The rated power of the PV panel
R_P	Shunt resistances
R_s	Series resistance
T_{NOCT}	The nominal operating cell temperature
T_{amb}	The ambient temperature
T_c	The cell temperature
T_{cof}	The PV module temperature coefficient
T_{ref}	The reference temperature

V_{DC}	DC link voltage
V_{array}	The voltage of the array
$V_{in} = V_{PV}$	The input voltage
V_{oc}	Open circuit voltage
V_{out}	The output voltage
V_{th}	The thermal voltage
e_{Vdc}	The error signal of the DC voltage
v_{ph}	The RMS phase voltage
ω_t	The reference Phase angle
$\Delta I_{L,max}$	The maximum current ripple
CO2	Carbon dioxide
E	The error signal
f	The switching frequency
I_{mp}	Current maximum point
N_p	The number of PV modules connected in parallel
N_s	The number of modules connected in series
V_{cell}	The Voltage of the PV cell
V_{mp}	Voltage maximum point
V_{ref}	Reference voltage
ΔE	The rate of change of the error
D	The duty cycle
G	The irradiance value
K	Boltzmann constant
KI	The current temperature coefficient
MPP	Maximum power point
T	The cell temperature
V	Voltage
a	The diode ideality factor
dI	The Change in current
dP	The change in power
dV	The change in voltage
q	The charge of an electron

Chapter 1:

Introduction

1.1 Introduction

The world is experiencing significant growth in terms of population, commerce, and industry, resulting in an escalating demand for energy. Projections indicate that energy demands are expected to increase by about 50% over the next two decades. Furthermore, approximately 80% of the world's energy is currently sourced from non-renewable resources such as oil, gas, and coal. These resources not only have a detrimental impact on the environment but are also contributing factors to global warming [1][2]. It is argued that the global community bears a collective responsibility to confront numerous challenges in the 21st century, particularly concerning climate change. There is an imperative need to make substantial efforts to mitigate the prevailing dependence on fossil fuels, as they constitute 40% of the identified factors contributing to global warming [3]. The global power system predominantly relies on burning fossil fuels, which are non-renewable and finite energy resources. Additionally, these fuels generate a substantial amount of greenhouse gases with detrimental impacts on the global environment and human health. Furthermore, considering the fluctuating prices of fossil fuels over time and global political conflicts, there is significant pressure on global energy security. This has prompted a comprehensive re-evaluation of available energy resources to identify sustainable and clean alternatives. It is, therefore, important to explore alternative energy resources that can meet the rapid growth in the world's energy demands. Renewable energies are considered the most suitable energy resource for the future and could play a major role in reducing CO2 emissions, a significant contributor to global warming. It is anticipated that renewable energy will play a substantial role in minimizing CO2 emissions in the world's power system by 3.6 gigatons in 2035 [1].

Considering all the aforementioned factors, over the past few decades, the demand for sustainable energy installations based on renewable energy resources has experienced rapid growth. Power generation from clean energy resources has been acknowledged as an effective means to mitigate the impacts of climate change by providing a sustainable energy source [4] [5]. There are various types of renewable and clean energy technologies capable of providing a clean and sustainable energy supply. Among these technologies, hydro, solar, and wind technologies are the most common. Many countries are striving to achieve their targets of

meeting their energy needs through safe, clean, and renewable energy resources, including wind turbines, solar PV systems, fuel cells, geothermal, and hydro turbines [6].

Renewable energy resources are garnering significant global attention due to their clean, sustainable, and environmentally friendly nature, making them capable of securing the energy supply for current and future human generations. It is anticipated that the utilization of renewable energy resources will experience rapid growth, and by 2030, it could surpass the use of coal in the global energy sector, reaching approximately 35% of total energy production by 2040. This growth is evident across various types of renewable energy technologies, with the highest growth rate observed in solar photovoltaic (PV) systems [7]. Among all renewable resources, PV systems dominate other alternatives due to their advantages of easy installation, simple operation, and low maintenance costs [8][9]. It is expected that by 2035, the use of solar PV technology will have increased approximately 26-fold compared to 2010, growing from 67 GW in 2011 to 600 GW. This projection is contingent on government support and decreasing technology expenses [1]. The installation capacity of solar PV systems has doubled over the last decade, and it is anticipated to contribute to 25% of the total energy production by the year 2050. Since 2014, China and India have been at the forefront of the growth in PV technology, achieving approximately 100 GW of energy production in 2017, with China alone accounting for an annual installation of 53 GW [10].

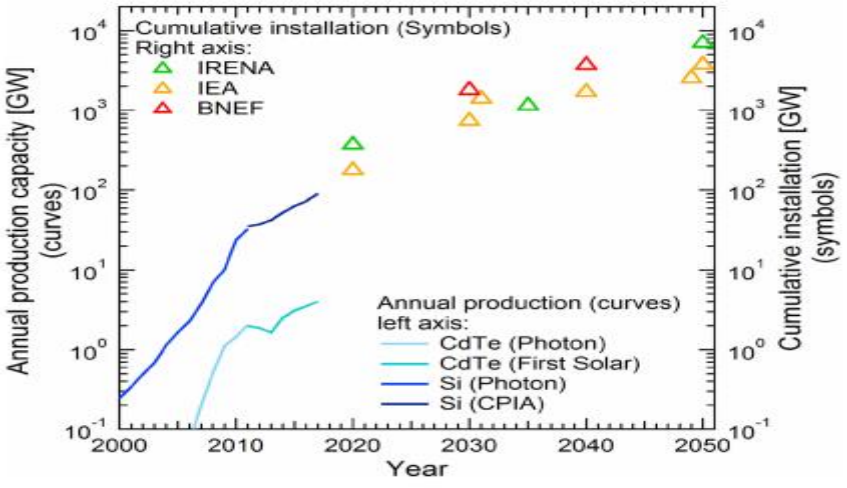

Fig. 1.1. The annual production capacity (curves) and cumulative installation (symbols) over time [10].

Globally, the new installation of PV systems in 2017 reached 90 GWp, enabling a cumulative total of 415 GWp with an annual growth rate of 29.3% over the previous year. This substantial growth surpasses the global installed PV capacity up to 2012. All the

aforementioned facts indicate the competitiveness of solar PV systems, with large PV power plants leading the way [7]. Figure 1.1 depicts the annual production capacity (curves) and cumulative installation (symbols) over time. The annual energy production from crystalline silicon (c-Si) reaches 98 GW, whereas the annual energy production from cadmium telluride (CdTe) was 4 GW [10].

1.2 Motivation

Solar energy is increasingly recognized as a crucial renewable resource worldwide, sought after by many countries striving to meet emissions reduction targets and enhance energy system diversity. Despite its vast potential compared to global energy needs, solar energy availability varies in quantity and quality across different locations, rendering it unpredictable [11]. The sun, a vast energy source, converts a significant portion of its mass into energy continuously, emitting solar radiation in all directions, although only a minute fraction of this energy reaches the Earth after an approximately 8-minute journey. With a staggering energy of about 3.8×10^{23} kW with 1.8×1014kW reaching the Earth's surface[12]-[13]. solar energy manifests in various forms such as light and heat. However, substantial losses occur due to factors like reflection, scattering, and cloud absorption. Despite these losses, recent studies suggest that solar energy has the potential to satisfy global energy demand cost-effectively and mitigate energy crises [14]. Nevertheless, solar energy presents limitations, including its intermittent nature, fluctuating irradiance levels throughout the day, and dependence on favourable climatic conditions. Overall, while solar energy holds promise as a primary energy source for the future, its effectiveness is contingent upon addressing these inherent limitations [15].

Solar energy, derived from sunlight, serves as the foundation for various alternative energy sources, including hydro, biomass, wind, and fossil fuels. [16]. Its utilization spans multiple applications such as solar desalination, electricity generation, and heating [17]. PV solar technology, a subset of solar energy, exhibits negligible carbon dioxide emissions throughout its operational phase, with emissions primarily occurring during the manufacturing process [18]. Solar energy technologies encompass solar PV, solar heaters, and concentrating solar panels, collectively demonstrating substantial annual growth over the past two decades, particularly with solar PV technology leading the advancement.[19].

1.3 Problem statement

Libya currently relies entirely on fossil fuels for its energy supply. The nation's energy infrastructure predominantly comprises conventional power generation facilities, including gas

turbines, steam turbines, and combined cycle power plants. In light of this, the Libyan government has expressed intentions to diversify its energy mix by harnessing the solar and wind potential inherent in the country. Initially, Libya aimed to source 7% of its electricity from renewable sources by 2020, a target that remains unmet due to ongoing instability. Subsequently, there is a planned increase in this objective to 10% by the year 2025 [20]. This necessitates a comprehensive reassessment of energy infrastructure and consumption patterns in Libya, alongside further research into the feasibility of integrating renewable energy resources across diverse regions of the country. Given that a substantial portion of Libya is situated within the sunbelt region, it emerges as a promising locale for advancing the adoption of solar energy technology.

1.4 The aim of the project

The primary aim of this project is to conduct advanced research into the feasibility of solar energy resource in Libya. This involves a specific focus on regional climate, geographical and technical considerations. Furthermore, the project aims to create a potential map for installing grid connected PV systems across the country to support the national grid to overcome the shortage in the energy needed.

1.5 The project's objectives

The main objectives of this project are highlighted as follows:

1. Identify a realistic horizon for renewable energy technology in Libya.
2. Develop a computer-based dynamic model for typical solar cell based on the criteria and requirements of the Libyan power system.
3. A feasibility study on solar energy resources for different regions of Libya, based on geographical, regional climate and technical issues.

The developed models will be implemented under normal operations and/or transient fault conditions. The aims of this project align with the relevant national and international standards on energy harvesting from solar and wind energy resources.

1.6 Thesis structure

Chapter One provide a background of the system, the motivation, the problem statement, aim and objective of this work.

Chapter Two discusses the current energy situation of the energy system in Libya highlighting the current energy crisis and the potential of renewable energy resources mainly solar energy.

Chapter Three provide a dilated background and previous related work related to this topic including solar energy, Photovoltaic phenomenon, Photovoltaic cell, grid connected PV system, different part of PV system, different MPPT technique and some standard and requirement for safe integration finally some short circuit faults.

Chapter Four discusses the dynamic modelling of grid connected PV system and its control strategies focusing on the modelling of different component of the system.

Chapter Five study the dynamic behaviour of grid connected PV system under different weather conditions and evaluating the impact of solar irradiance and temperature on the behaviour of the system.

Chapter Six discusses the dynamic behaviour of grid connected PV system under different short circuit scenarios taking into account the most frequent short circuit fault scenario which is line to ground as well as the most sever short circuit fault scenario which is three line to ground.

Chapter Seven study the dynamic performance of the grid connected PV system under the Libyan weather condition. The system was evaluated at nine different locations across Libya, using data resources one based on satellite data, the other one based on actual measurement.

Chapter Eight this chapter summarising the findings of the thesis and provide some future work.

Chapter 2:

Energy Crisis and Renewable Energy Horizon in Libya

2.1 Introduction

As each day unfolds, the quest for renewable, dependable, and eco-friendly solutions becomes an increasingly paramount objective. Consequently, numerous countries around the globe have set forth ambitious plans to bolster their dependence on renewable energy resources, with solar and wind power leading the charge. Libya is one of the developing nations grappling with a swift surge in its energy demand. Despite being rich in oil resources and having its energy sector entirely dependent on fossil fuels, Libya still encounters challenges in meeting its energy requirements and aligning with global targets to reduce reliance on non-renewable energy sources [21]. This chapter provides an overview of the current energy situation in the country and explores the potential of solar energy as a future energy source.

2.2 An overview of Libya

Libya is an African country located in the northern part of the continent, bordered by six countries, including Egypt, Tunisia, Algeria, Chad, Niger and Sudan. Moreover, Libya has maritime borders with some European countries such as Italy Greece and Malta. It spans longitudes between 10°E to 25°E and latitudes between 20°N to 32°N [22]. Libya is considered as one of the largest countries in Africa, covering an area of about 1,750,000 km² with a coastal line of 2000 km, making it one of the main gateways to Europe. Its strategic location links the Eastern region with the Western region of Africa, as well as connecting the southern part of Europe with Africa [23]. However, its population is relatively low compared to other countries in Africa, with around 6 million inhabitants spread across three main regions: South, West, and East [24]. Furthermore, Libya is blessed with high reserves of hydrocarbon products, making it the largest in Africa and fifth in the world. This positions Libya as one of the top leaders in providing electricity and petroleum products to the neighbouring countries as well as international market [25]. Libya has the largest oil reserves in Africa and ranks ninth in the world. The country's approved crude oil reserves are approximately 48 billion barrels, along with 158 billion cubic feet of approved natural gas reserves [22].

In recent decades significant changes have occurred in the global energy market. For instance, the oil spill that happened in the Gulf of Mexico in 2010 had destructive impacts on the welfare

of people, local areas, and the economy. Additionally, the earthquake and tsunami that occurred in Japan led to the Fukushima nuclear disaster, prompting several top leaders in the energy sectors in the Middle East, including Libya, to reconsider diversifying their economy and reducing reliance on fossil fuels as energy providers and sources of income. This is an essential criteria to ensure a sustainable economic future [25]. Therefore, creating alternative renewable energy resources has become a critical matter to secure a source of income and reduce the carbon emissions generated by burning fossil fuels [26]. Back in 2007, the Libyan government, represented by the Ministry of Electricity and Renewable Energy (MERE), established the Renewable Energy Authority of Libya (REAoL) to evaluate different renewable energy resources and enhance their presence and utilization across the country. The authority conducted feasibility studies on renewable energy resources and aimed to maximize their integration with the national grid. Furthermore, they launched policies and legislations to support the use of these technologies [27]. As a result of the ongoing instability situation in the country, most of the largest oil and gas fields have been significantly affected [25]. In the same context, all available indicators point to Libya's wealth in renewable energy resources, with solar and wind energy leading the way. The growing fascination with harnessing renewable energy is palpable worldwide, and this fervour is particularly evident in Europe, the Middle East, and North Africa. These regions are renowned for their copious renewable energy sources, making them an attractive hub for energy markets and investors alike. This is primarily due to the exciting prospect of interconnecting these regions with Europe. Numerous studies have been conducted to explore the viability of supplying Europe's energy needs by tapping into the abundant renewable resources present in Africa, particularly in the northern region, which includes Libya [25]. Taking into consideration the imminent depletion of hydrocarbon resources, it becomes increasingly crucial to prepare for a future where these valuable assets are likely to be exhausted within the next century, if not decades. Additionally, it is anticipated that oil prices will soar, potentially reaching a staggering of $200 per barrel by the year 2050. This price surge further emphasizes the need for proactive measures and alternative solutions to cope with the escalating energy challenges. This predicament will leave the country with two choices: either selling its oil production or utilizing it for its own energy generation. Hence, it becomes of utmost importance for the decision makers and people of Libya to forge a path towards alternative and sustainable energy resources for the generations to come. Undoubtedly, this pursuit holds the key to satisfying the energy demands of the nation while safeguarding its future. [27]. According to a study conducted by Nottingham Trent University, renewable

energy resources are poised to take centre stage in oil-rich countries. They are set to not only fulfil their own peak energy requirements but also to generate a substantial surplus to cater to the global energy demand [26].

2.3 The current energy situation in Libya

As Libya experiences an upward trajectory, the nation finds itself in a phase of growth, with both its economy and population on the rise. Consequently, this surge has given birth to a heightened demand for energy resources [28]. Furthermore, the nation's energy consumption stands at a notably elevated level [29]. This arises from a multitude of factors, encompassing energy culture, societal norms, and the government's subsidized electricity scheme, which serves as a pivotal influencer. However, this subsidization widens the gap significantly between the production costs and the consumption tariffs extended to consumers [30].

The Libyan electricity demand over the past two decades is illustrated in Figure 2.1 [29][31]. As per the General Electric Company of Libya (GECOL), the appetite for energy is burgeoning at an impressive pace, expanding by 8-10% annually. [23]. During the past few years, its pinnacle requirement of energy has exceeded a remarkable amount of 7000 MW [28]. Unfortunately, the entire energy landscape in Libya remains shackled to conventional power plants that rely on burning fossil fuels to meet the nation's energy needs [4][32]. Hence, an increase in fossil fuel consumption would inevitably lead to a direct decline in the country's revenues, adversely affecting its income a scenario that's far from desirable [33].

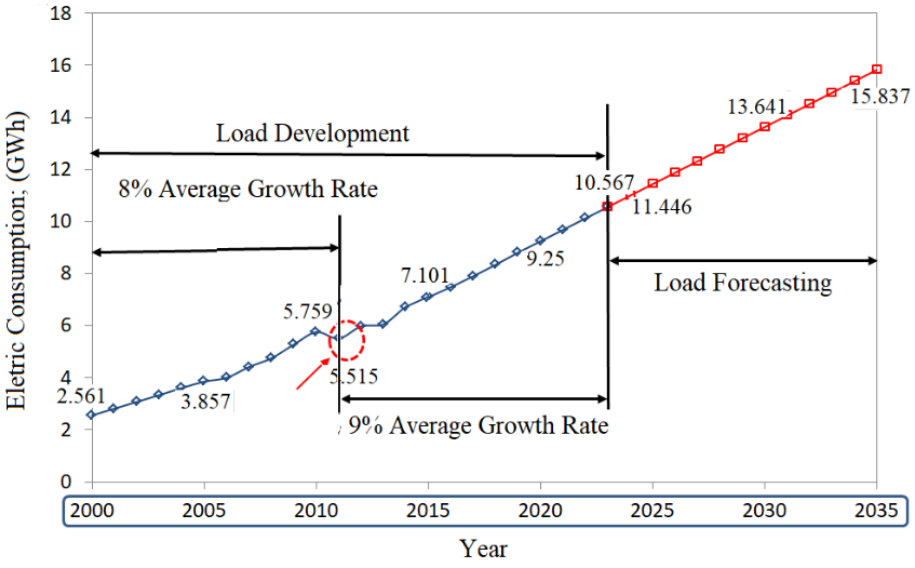

Fig. 2. 1. Electric Power Consumption [31].

Moreover, the surge in energy demand would usher in a corresponding rise in CO2 and greenhouse gas emissions, further exacerbating environmental concerns [34]. Information sourced from the International Energy Agency (IEA) reveals that Libyan electricity consumption in 2017 amounted to 2580 kilo tonnes of oil, surpassing the levels observed back in the year 2000 [27]. Furthermore, back in 1984, the General Electric Company of Libya was founded, and ever since, it has taken the helm of the nation's energy sector, overseeing the realm of power plants and distribution systems. Impressively, the energy distribution network spans extensively, reaching 99% of the country and providing all residents with access to the utility grid [33]. The intricate web of Libya's utility grid comprises 15 conventional power stations, encompassing a total of approximately 68 units that vary in size and technological specifications, as illustrated in Figure 2.2. Nonetheless, not all these power stations are currently operational, as some have incurred damages due to the prevailing conditions in the country. Additionally, 7 of these units are approaching the end of their operational lifespans [35]. These power stations operate using a variety of fuels, ranging from light fuel and heavy fuel to natural gas, each with its unique usage percentage, as shown in Figure 2.3 [36]. Furthermore, spanning across the landscape, the power stations at pivotal points west of Tripoli, east of Tripoli, Misrata, and Tobruk stand as the backbone of the nation's energy infrastructure, boasting rated capacities of 600MW, 1400MW, 600MW, and 740MW respectively. For a comprehensive overview, previous and current power stations in Libya are shown in Tables 2.1 and 2.2.

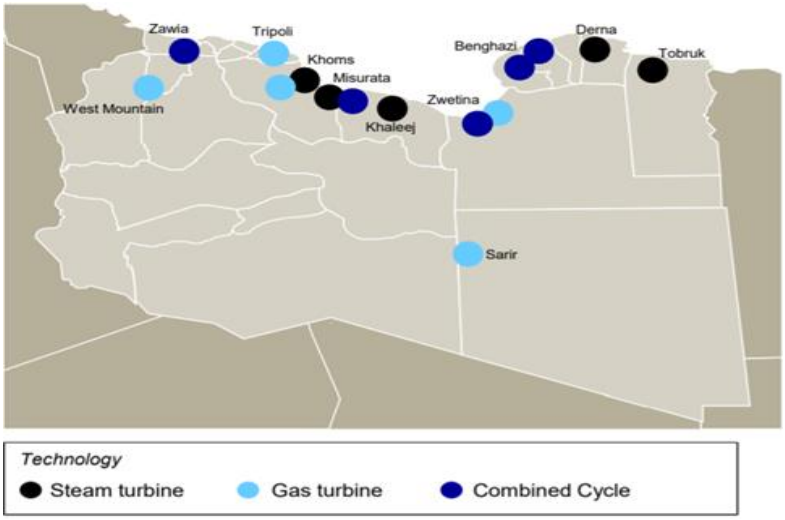

Fig. 2. 2. The map of installed power plants in Libya [35]**.**

Most of these power plants are underpinned by three distinct technologies: gas turbines, steam turbines, and combined cycle turbines. Recent studies carried out in 2019 revealed that the utilization of natural gas for energy generation accounted for a substantial 26.7% of the country's total natural gas production, equating to a staggering of 581 million cubic feet. Moreover, the symphony of Libyan electricity production is orchestrated as follows: a dominant 63% emanates from the incandescent burn of natural gas, a harmonious 29% is conducted through oil-fired stations, while the remaining cadence emerges from the melodic ensemble of non-fuel combined steam power stations. Gas turbines compose a vibrant of 39.3% of Libya's electricity, while the combined cycle turbines contribute a resounding 48.2%, and steam turbines generate 10.6% [27]. Some other small diesel based power plants are in operation to supply energy for remote areas [23]. Yet, in a bid to paint a greener future, GECOL has elevated its reliance on natural gas, a move aimed at diminishing the exhalations of CO2 into the atmosphere [37].

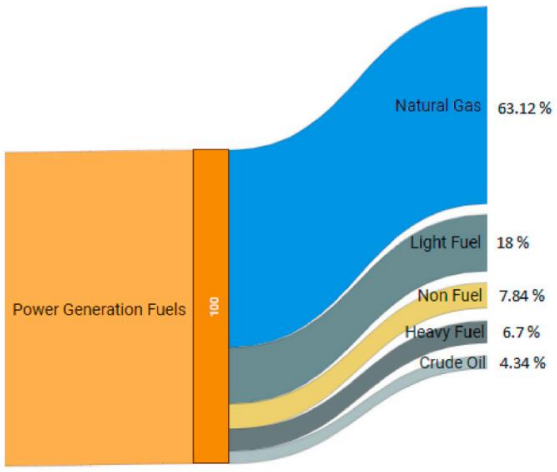

Fig. 2. 3. Breakdown of fuel types for power generation in Libya.

The total installed capacity is approximately 14,500 MW. Yet, the reality unveils a more modest picture, with an available production barely exceeding half that, measuring at 6,320 MW. According to GECOL's vigilant watch, the crescendo of peak load reached a harmonious 7000 MW in the year 2016 [34]. On the other hand, according to on-site investigations in 2019, the zenith of load demand reached an impressive amount of 7,500 MW during the summer season, and a still commanding 7,200 MW during the winter. These notes reveal a poignant gap of approximately 1200 MW, painting a realistic picture of the energy deficit [22]. This shortfall arises due to the absence of essential maintenance mandated for each turbine after a specific duration of operation, compounded by the dearth of progress in expanding the national

grid. While GECOL, in its pursuit of upkeep, has forged agreements with foreign enterprises to undertake essential maintenance, the dissonant notes of instability have deterred these companies from dispatching their skilled professionals and engineers to the country [29]. With a keen awareness of the escalating energy consumption, the visionary minds at GECOL have orchestrated a strategic shift in energy production. They have chosen to bolster their reliance on combined cycle and steam turbines, orchestrating this move to harmonize with the crescendo of energy demand. In tandem, the Libyan Government and GECOL have unveiled their plan of progress, meticulously crafting a plan to elevate the national grid, ensuring it resonates with the future's demands [22]. Table 2.3 shows planned power stations in vision of GECOL.

Table 2. 1. The previous and current power stations in Libya.

Power plant	Phases	Generation Units		Rated Capacity per Unit (MW)	Date of Operation and Status	Current Output (MW)
Al Khums	Phase 1	4	Steam	127	1982	400
	Phase 2	4	Gas	150	1995	560
	Phase 3	2	Gas	275	2017-out of service	0
North Benghazi	Phase 1	4	Steam	40	1979-out of service	0
	Phase 2	3	Gas	150	1995	240
	Phase 3	1	Gas	165	2002	75
		2	CC	150	2007	0
	Phase 4	2	Gas	285	2009	500
		1	CC	250	2012	0
Al Zawiya	Phase 1	4	Gas	165	2000	575
	Phase 2	2	Gas	165	2005	270
	Phase 3	3	CC	150	2007	185
	Phase 4	2	Gas	25	2014	45
Misrata CC	Phase 1	2	Gas	285	2010	530
	Phase 2	1	CC	250	2013	225

As the pathways to diminish the country's reliance on fossil fuels remain scarce, the spotlight turns to renewable energy technologies as the most viable remedy. These innovative solutions offer a feasible avenue for the nation to harmonize its ecological impact, countering the emissions generated by the combustion of various fossil fuels. Especially with their intrinsic attributes, these solutions come crowned with the virtue of being readily available within the

nation's borders. Among them, solar energy emerges as the best option, revered for its environmental harmony and friendliness.

Table 2. 2. The previous and current power stations in Libya

Power plant	Phases	Generation Units		Rated Capacity per Unit (MW)	Date of Operation and Status	Current Output (MW)
South Tripoli	Phase 1	5	Gas	100	1994	330
	Phase 2	2	Gas	47	2016	0
Sarir	Phase 1	2	Gas	285	2010	400
	Phase 2	1	Gas	285	2013	
Zwitina CC	Phase 1	4	Gas	50	1994	90
	Phase 2	2	Gas	285	2010	500
		1	CC	250	Suspended	0
Al Jabal Algharbi-Ruwais	Phase 1	2	Gas	156	2005	785
	Phase 2	2	Gas	156	2006	
	Phase 3	1	Gas	156	2010	
	Phase 4	1	Gas	156	2012	
West Tripoli	Phase 1	5	Steam	65	1976-out of service	0
	Phase 2	2	Steam	120	1980-out of service	0
	Phase 3	4	Steam	350	Contracted	0
	Phase 4	3	gas	25	2014	60
Darna	Phase 1	5	Steam	65	1985	0
Tubruk	Phase 1	5	Steam	65	1985	0
Alkhalij-Sert	Phase 1	4	Steam	350	2014(1 unit on operation)	280
Alzahra	Phase 1	2	gas	15	1971	0
	Phase 2	4	gas	47	Under construction	0
Ubari	Phase 1	4	gas	165	2019	240
Abu Kammash	Phase 1	6	gas	15	1982	0
Zliten	Phase 1	3	gas	15	1975	0
Alfurnaj	Phase 1	2	gas	15	1971	10
Lamluda	Phase 1	1	gas	33	1975	0
Alkufrah	Phase 1	3	gas	25	1975	0
Misrata Kerzaz	Phase 1	3	gas	15	1984	20

Table 2. 3. The planned power stations in vision of GECOL.

Stuts	Plant name	Capacity (MW)
Projects Under Construction	Misurata Combined Cycle Power Plant I	690 MW
	Benghazi North Combined Cycle Power Plant I	690 MW
	West Sarir Gas Power Plant	690 MW
	Extension of West Mountain Gas Power Plant	260 MW
	Zwetina Power Plant	690 MW
	Gulf steam Power Plant	1400 MW
Contracted Projects	Ubari Gas Power Plant	600 MW
	Tripoli West Steam Power Plant	1400 MW
Proposed Projects	Bumba Gulf Power Plant	1400 MW
	Misurata Combined Cycle Power Plant II	690 MW
	Militah Power Plant	1200 MW
	Tripoli East Power Plant	1400 MW
	Zwetina Power Plant II	690 MW
	Abutraba Power Plant	700 MW

In the rhythm of pursuing global currents toward a more sustainable energy landscape, the Libyan government has composed its own plan. This strategic orchestration seeks to amplify the harmonious contribution of renewable energy sources to response to the country's energy demand. The central aim is to generate 10% of the overall electricity demand pirouettes from renewable energy sources by 2025, which is equivalent to 2,219 MW. Table 2.4 shows the national renewable energy plan for Libya. Nevertheless, this visionary strategy was abruptly paused by the political upheaval back in 2011 [23].

As a consequence of the political instability gripping the country since 2011, many sectors have been significantly affected [38]. The energy sector emerges as a pivotal concern demanding concerted efforts for resolution. Over the past decade, the country has recurrently grappled with widespread blackouts, underscoring the imperative need for intervention. Since 2011, the country's infrastructure, in general, and the energy sector have borne the brunt of extensive damage. Numerous power stations and transmission networks across Libya have been severely impacted, with the eastern and western regions particularly affected [34].

This imbalance has led to energy production falling short of peak demand, resulting in energy shortages that have left GECOL grappling with the inability to meet the escalating energy demands [39]. Subsequently, the situation further deteriorated, prompting numerous companies

to halt maintenance and developmental activities due to prevailing security concerns and financial constraints. In order to avert a nationwide blackout, GECOL resorted to the implementation of rolling blackouts on a regional basis. This measure, unfortunately, left homeowners, healthcare facilities, and businesses with limited alternatives, often compelled to rely on mobile diesel generators. Nevertheless, this approach faces its own challenges, including fuel and spare component shortages, coupled with maintenance issues, rendering it an imperfect solution to address the prevailing issue [29]. While a significant portion of the Libyan population remains without reliable access to grid, receiving only a few hours of supply each day [22][40].

Table 2. 4. The national renewable energy plan for Libya.

Renewable Energy Targets						
	Wind	Solar PV	Solar CSP	Total MW	Share %	date
National Plan for Renewable Energy	260	124	0	384	3	2015
	600	344	125	1069	7	2020
	1000	844	375	2219	10	2025

In addition to the severe damages inflicted upon the national grid, the impending expiration of certain power stations, coupled with acts of vandalism and shutdowns affecting oil fields and refineries, constitute the primary factors contributing to the prevalent electricity shortage. The majority of damages occurred in the eastern region, impacting numerous power substations and disrupting connections between the North Benghazi power station and other facilities such as Zwitina, Sarir, and the western region. As a consequence, these events have given rise to concerns of stability and reliability within the national grid. Moreover, the western region has borne the brunt of extensive damages due to military operations occurring in and around the capital, Tripoli. Consequently, this has led to the propagation of power shortages throughout the entire country. In the western region, the populace endures energy scarcity for 5 to 8 hours daily, whereas in the eastern region, blackouts persist for 1 to 4 hours per day. [34][38].

The annual power generation has witnessed substantial growth, surging from 21.31 TWh in 2005 to 30.61 TWh in 2010, showcasing a remarkable 44% increase over a period of five-year. Similarly, from 2011 to 2013, it elevated from 24.44 to 35.64 TWh [27]. To counteract the electricity shortage, Libya has turned to neighbouring countries for assistance, importing over 300 GWh of power to address its deficit. In addition, the country has resorted to renting MW-

scale diesel generators. Nonetheless, while diesel generators provide a transient solution, their economic inefficiency and environmental detriments render them a short-term solution to a persistent problem [22].

2.3.1 Grid connections and supporting infrastructure.

In Libya, the utility grid boasts a well-structured design, extending its reach to encompass 99% of the Libyan population. Nevertheless, a handful of remote villages continue to rely on small distributed diesel generators to cater to their individual energy requirements [28]. Furthermore, considering the concentrated habitation of the Libyan population along the coastal stretch of the country, it follows that a significant portion of the national grid is situated on the coast. The Libyan transmission power system is systematically divided into six primary regions: the western, Tripoli, central, Benghazi, eastern, and southern regions [41]. Similar to other power systems, Libya's national power grid encompasses various voltage levels. These include ultra-high voltage lines operating at 400 kV with a circuit length spanning 442 km, high voltage lines of 220 kV employed for transmission over a circuit length of 13,677 km, 66 kV lines utilized for sub-transmission spanning 13,973 km, and 30 kV lines covering a distance of 6,583 km. The distribution network of the country operates at 11 kV. The power system of Libya is interconnected with neighbouring countries through 220 kV and 225 kV lines. Unfortunately, these lines are currently non-operational [23]. Furthermore, around 2,422 km of the Libyan grid underwent upgrades to accommodate 400 kV, a step taken to enhance the grid's capacity to accommodate the surging energy demand. Nevertheless, as mentioned earlier, this network has incurred substantial damages over the past decade [22]. Additionally, in pursuit of bolstering and enhancing the national grid's capabilities, GECOL initiated a techno-economic feasibility study in 2010. This study was aimed at exploring the potential for interconnecting the Libyan grid with that of Europe. The objective of this study was to facilitate the export of 500 to 1000 MW through a high-voltage direct current (HVDC) submarine power cable. The study's focus was on interconnecting the Mellitah Oil & Gas complex, situated in the northwestern part of the country, with Sicily Island in southern Italy. Unfortunately, due to the turbulence following 2011, the project remains incomplete. Libyan electric transmission network is illustrated in Figure 2.4 [23].

This network has encountered extensive damages over the past decade, incurring a cost of approximately $1 billion. These damages have impacted around 300 substations, 2000 km of power lines, and 6000 km of distribution lines. Since then, substantial funds have been invested

in this sector to maintain and re-stablish the power network. However, due to the persisting instability and corruption, a number of power stations remain non-operational or are only partially functional [22].

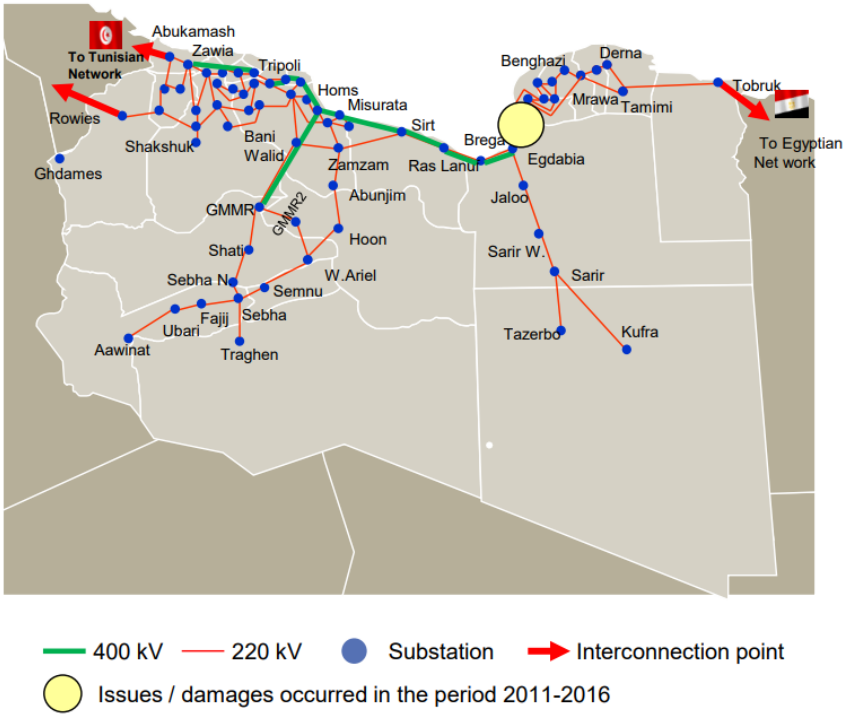

Fig. 2. 4. Map of national transmission grid of Libya (220 kV & 400 kV)[35]**.**

2.3.2 Libyan load profile

As previously stated, the energy demand of the country is experiencing a rapid increase [26]; with an average growth rate of 5% annually [42]. In 2010, the annual per capita consumption soared to 4200 kWh, compared to 1900 kWh in 2000, marking a notable 12% annual increase [32].

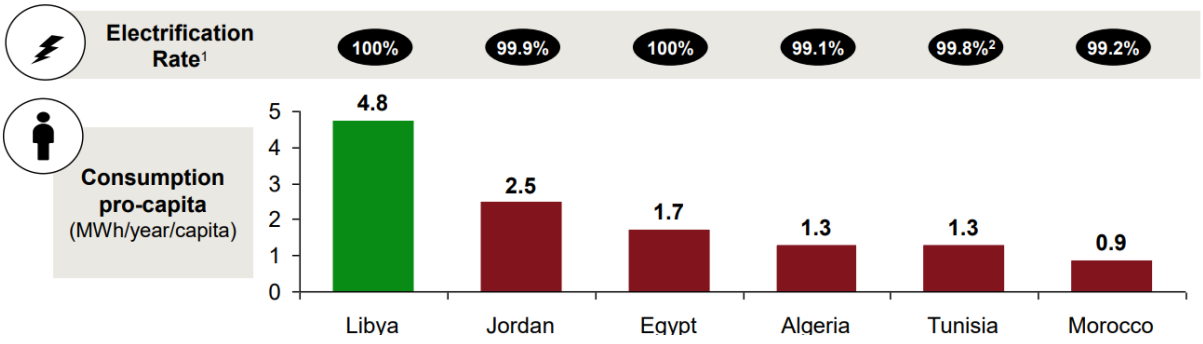

Fig. 2. 5. Annual energy consumption per capita of Libya[27]**.**

Nevertheless, when compared with neighbouring North African countries, this rate stands notably higher. For instance, Algeria, Tunisia, Morocco and Egypt exhibit annual per capita

consumption ranging between 900 kWh and 1804 kWh, as shown in Figure 2.5. This variance is attributed to the elevated daily energy consumption per Libyan household, which has surged to 22.88 kWh/day [27].

Due to the prevailing weather conditions and energy customs in Libya, peak load occurs during the summer season. This surge can be attributed to the widespread usage of air conditioners across both commercial and residential sectors. Analysis of Libya's historical load profile reveals that the residential sector commands the highest energy consumption, trailed by the commercial and industrial sectors, as depicted in Figure 2.6 [22]. Furthermore, street lighting assumes its own portion in the country's load profile, accounting for 19% of the electricity demand [43]-[29].

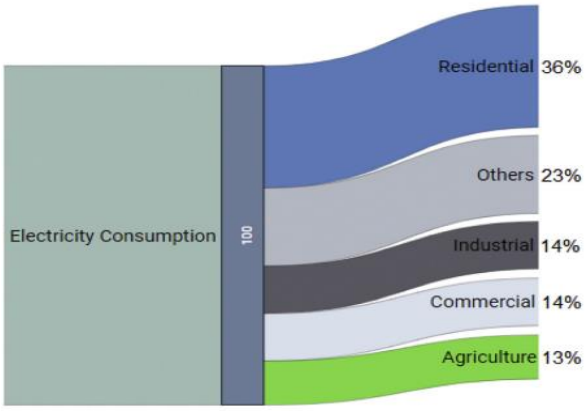

Fig. 2. 6. Breakdown of electric energy consumption per sector[22]**.**

According to [28] from the start of 2013 to the end of 2016, the Libyan energy demand experienced fluctuations, culminating in a peak of 7000 MW, as depicted in Figure 2.7. However, due to the prevailing instability within the country, the generation capacity struggled to reach a mere of 5050 MW, resulting in a significant disparity of up to 1950 MW between generation and consumption. Due to these circumstances, GECOL found itself compelled to implement a strategy of partial blackouts to prevent a nationwide breakdown. Despite these concerted efforts, certain regions encountered widespread blackouts. For instance, the western region suffered a complete blackout in June 2017, while similar incidents unfolded in January 2017 for the eastern and southern regions. Conversely, in tandem with the country's expansion, GECOL anticipates a surge in the maximum load, projecting it to reach 14,834 MW by 2030 and escalate further to 21,669 MW by 2050 [34].

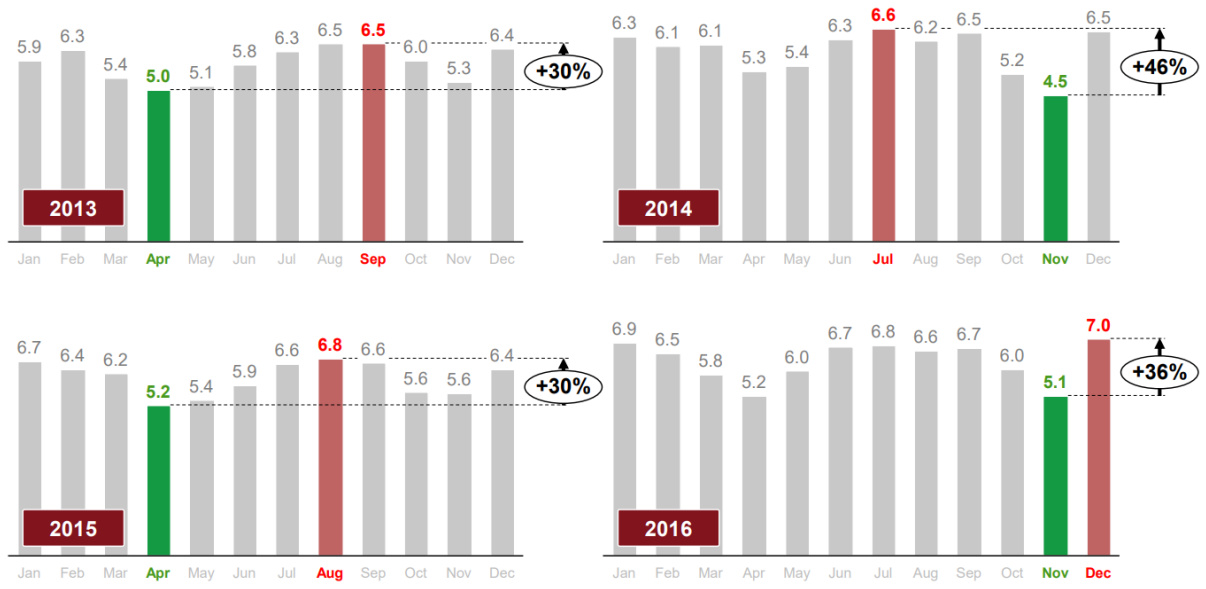

Fig. 2. 7. Monthly electric energy consumption [28].

As evident, the energy demand reaches its highest level during the summer and winter seasons, with a concentration in the Tripoli region. Figure 2.8 illustrates the regional energy consumption distribution across the country.

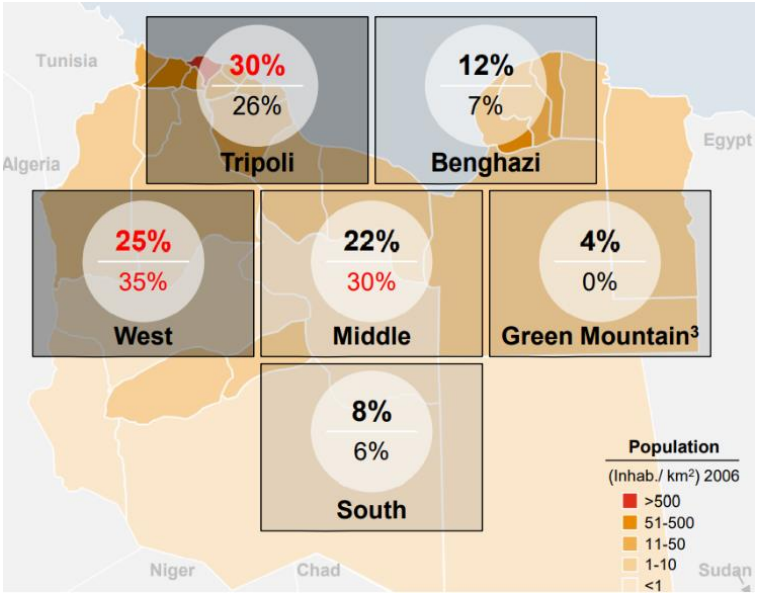

Fig. 2. 8. The regional electric energy consumption distribution across Libya.

2.4 Renewable energy potential in Libya

In the contemporary landscape, renewable energy technologies and resources have garnered substantial interest, notably in Europe. Numerous investors and energy markets have turned their focus toward the Middle East and North Africa, considering these regions' abundance of renewable energy resources, particularly solar energy. Furthermore, these areas present a viable

link to Europe. Consequently, over the past two decades, various initiatives have been devised to address Europe's energy demand by harnessing the renewable energy resources abundant in North African countries, including Libya [25]. Even though Libya boasts substantial fossil fuel reserves, including oil and gas, also blessed with renewable energy resources such as wind and solar. the feasibility of solar energy is higher due to the localized availability of wind resources. Regrettably, none of these resources have been fully utilized within the country, primarily due to the prevailing political situation [29]. Most of the regions across the country benefit from elevated levels of solar radiation, as it located on sunny belt; with daily average solar radiation ranges from 7 kWh/m^2 in the northern region to 8 kWh/m^2 in the southern parts, accompanied by an abundance of annual sunshine lasting for approximately 3500 hours. Notably, 88% of the nation's landmass consists of desert areas, and the solar radiation received per square kilometre equates to approximately 1.5 million oil barrels [40]. While the wind resource is primarily concentrated along the coastal areas, typical wind speeds range from 6 to 7.5 m/s at a height of 40 meters [44]. The substantial potential of solar and wind resources holds the promise of satisfying the entirety of the country's energy demand. However, the ample presence of fossil fuels may pose a hurdle to fully harnessing the available renewable energy resources within the country. In the current scenario, Libya is urgently required to formulate and implement a comprehensive strategy aimed at augmenting the proportion of renewable energy resources to fulfil its energy requirements. This need is particularly pronounced following the extensive infrastructure damage incurred since 2011. Continued reliance on fossil fuels stands to exhaust the nation's primary source of revenue while also inflicting detrimental consequences on the global environment. Libya should capitalize on the accessible renewable energy resources within the country, particularly solar, wind, and biomass. Photovoltaic technology is anticipated to wield substantial influence in Libya's energy sector due to its advantages over other technologies, encompassing cost-effectiveness, environmental friendliness, and technical efficiency. The annual solar energy potential in Libya is vast, amounting to approximately 140,000 TWh. However, this should not dissuade the exploration of other technologies like wind and biomass. It is advantageous for the country to diversify its energy portfolio, reducing reliance on a solitary source and ensuring a consistent supply even in cases of inadequate solar radiation [45].

2.4.1 Solar energy availability

The adoption of solar power technologies is garnering significant attention due to its notable features, particularly its environmental friendliness and absence of greenhouse gases that contribute to global environmental damage and the issue of global warming. Moreover, its versatility in application, spanning residential, industrial, and agricultural sectors, further underscores its potential. These factors collectively underscore the considerable potential of this technology in fulfilling the energy demand across diverse domains [46].

The geographical position of Libya positions it as a nation abundant in renewable energy resources, particularly solar energy. Furthermore, it stands out as one of the sunniest regions on a global scale, characterized by a relatively low average annual rainfall of no more than 150 mm across all areas of the country [47]. Solar energy is anticipated to emerge as a prominent energy contributor in the future of the country, primarily due to the elevated levels of radiation received across the majority of regions within its borders [43].. Additionally, the country boasts a high average solar radiation of approximately 7.5 kWh/m²/day [48]. The southern region of the country experiences notably higher levels of solar radiation compared to other areas. Consequently, it is imperative to promptly and efficiently harness this energy resource, which holds the potential to satisfy the nation's energy requirements and alleviate the persistent issue of extended power shortages. [33]. The solar radiation in different cities in Libya is shown in Figure 2.9 [22].

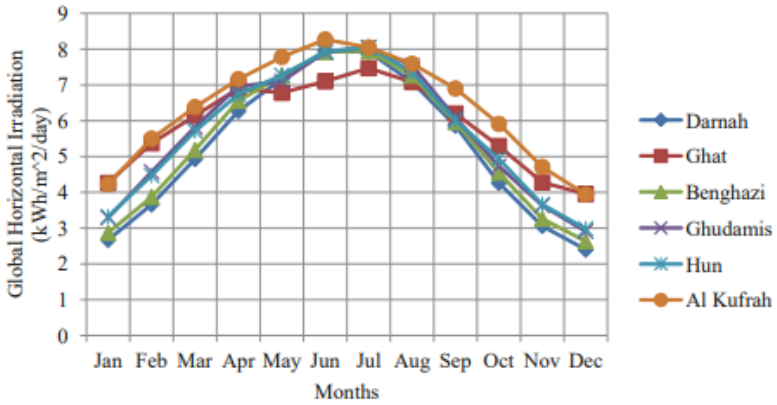

Fig. 2. 9. The solar radiation in different cities in Libya [22]**.**

The intensity of solar radiation reaches its peak during the summer season, spanning from June to October, which coincides with the hottest period of the year. Correspondingly, the load demand surges to its peak during this time due to heightened usage of air conditioning units. In the winter season, the load also increases owing to the utilization of heating systems, albeit

at a significantly lower level compared to the summer season. One of the favourable aspects of deploying solar energy in Libya is the alignment between the solar radiation pattern and the country's load profile. This congruence can facilitate the fulfilment of peak demand, particularly during the summer season [26]. Figure 2.10 shows the relationship between the load demand and the temperature during the year [48]:

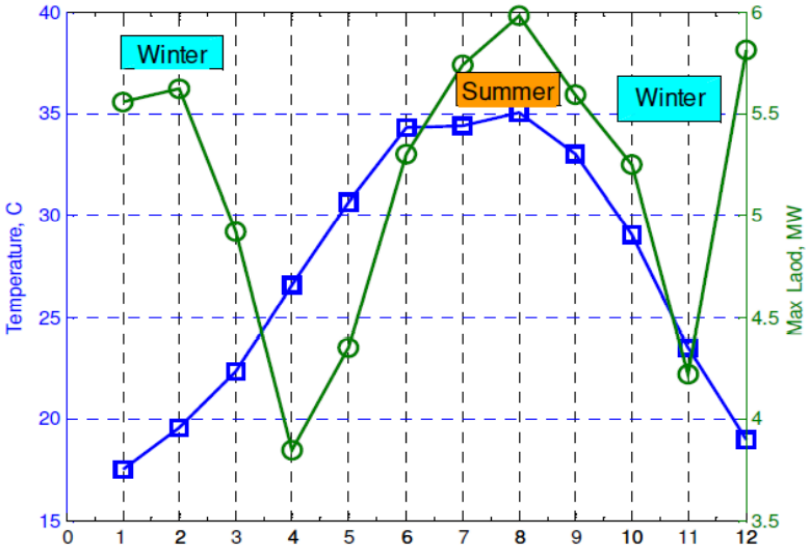

Fig. 2. 10. Monthly load demand and temperature in Libya [48]**.**

Data recorded by Solar GIS between 1994 and 2018 reveals Libya's substantial solar energy potential. Figures 2.11 depict the distribution map of the average annual Global Horizontal Irradiation (GHI) and the Direct Normal Irradiation (DNI) across the country [49]. The average solar radiation in Libya is approximately double that of the UK (2.95 kWh/m^2/day), as depicted in Figure 2.12. However, despite its substantial potential for renewable resources, Libya is in dire need of comprehensive energy strategies to optimize their utilization.

According to Figure 2.11 a and b, it becomes evident that the average annual GHI ranges from approximately 2000 kWh/m²/year in the Northern regions to over 2600 kWh/m²/year in the Southern regions, while the average annual DNI fluctuates roughly between 1900 kWh/m²/year in the coastal region and 2500 kWh/m²/year in the South. With an annual average solar radiation of 6.2 kWh/m²/day and a conversion efficiency of 15%, harnessing merely 0.1% of Libya's land area could yield a staggering energy output of 598 TWh/yr. Notably, this figure is twentyfold greater than the current energy demand of Libya [27].

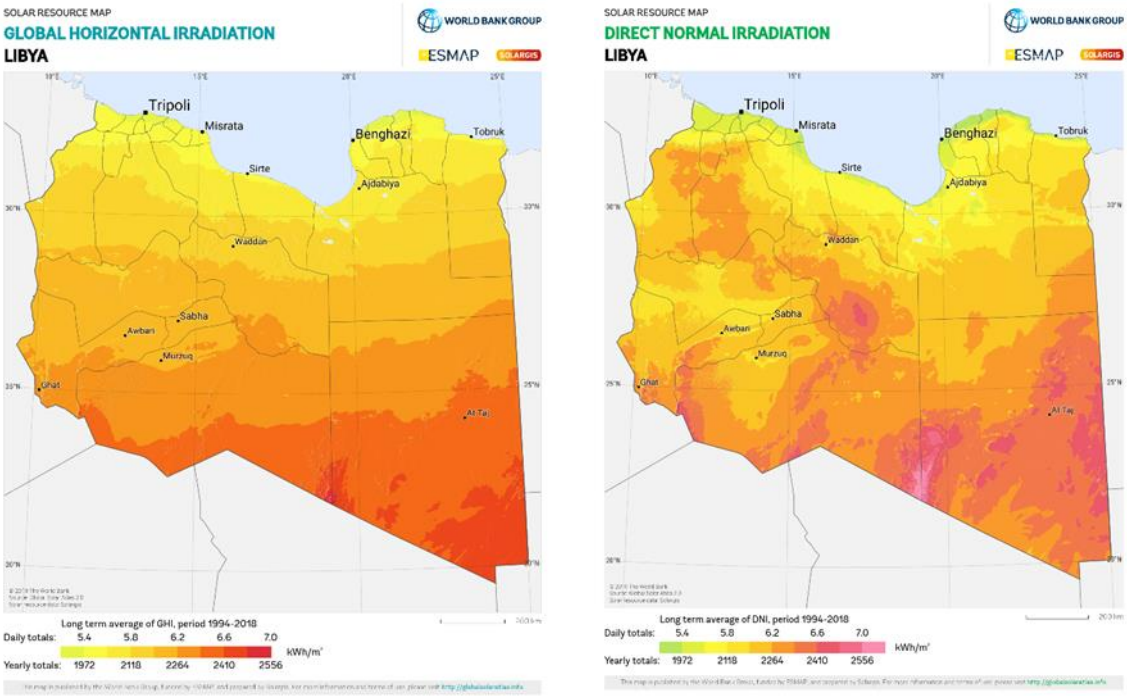

(a) (b)

Fig. 2. 11. a: The average annual Global Horizontal Irradiation, b: The average annual Direct Normal Irradiation [49]**.**

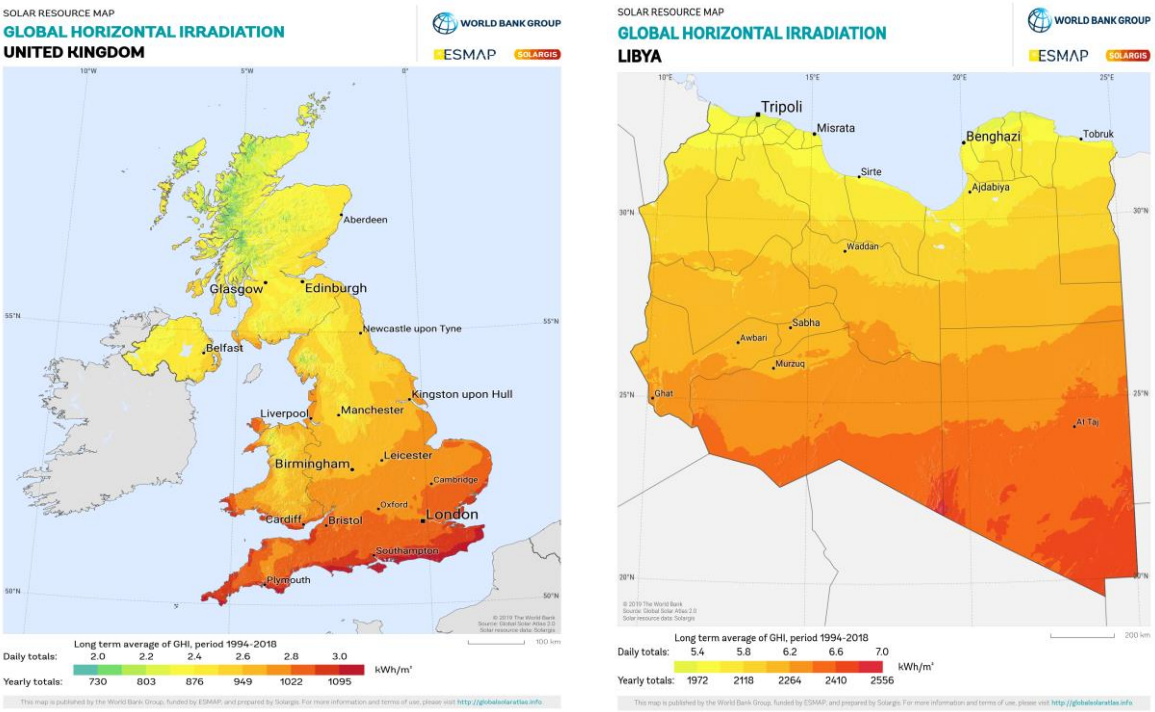

(a) UK Global horizontal irradiation (b) Libya Global horizontal irradiation

Fig. 2. 12. The average annual GHI: comparison for the UK and Libya

A substantial effort needs to be directed towards enhancing the existing infrastructure, encompassing power stations, transmission and distribution lines. Moreover, there's a pressing need to augment the proportion of renewable energy resources within Libya's energy sector,

all in order to effectively accommodate the escalating energy demand. [29]. Given the insights presented above, the potential of harnessing solar energy emerges as substantial. Therefore, capitalizing on this resource holds the potential to align with Libya's objective of augmenting the portion of renewables within its energy sector. Furthermore, this effort could aid in addressing the disparity between energy production and consumption that presently underpins the nation's energy crisis. However, a comprehensive feasibility study is imperative to model the implementation of this energy source and identify optimal installation sites.

2.4.2 Application of solar PV in Libya

Solar photovoltaic technology was initially introduced in Libya around four decades ago. The inaugural installation took place in 1976 within an oil field, aimed at supplying energy to a cathodic protection system, thereby mitigating corrosion along oil pipelines. Despite this early adoption of solar technology, its widespread utilization remains restricted and relatively underdeveloped within the country[50]. In 1979, the initial solar system was established within the communication sector to cater to the energy demands of the southern microwave repeater station, located near the village of Zella. This system encompassed over 500 individual stations. Subsequently, in 1980, solar systems were deployed to fulfil the entire energy requisites of nine stations, four of which continue to operate to this day. Additionally, solar technology was introduced to the agricultural domain in 1983, primarily aimed at energizing water pumps. Another instance of adoption occurred in 1984, when solar systems were employed for irrigation purposes in the village of El-Agailat [26]. Since that time, over 40 PV systems have been installed in the Osis of Ojlah region, situated 400 km to the south of Benghazi. The peak capacity of these systems reached 120 kWp. Additionally, 40 decentralized PV systems, each with a capacity of 48 kWp, were established in the village of Mrrair-Gabis to provide power to 39 families. Data were collected from January 2004 to July 2006 for 30 of these systems. This dataset indicated that no failures or instances of vandalism occurred, and no operational costs were incurred. Moreover, the average power generated by a 1.2 kWp system was 6 kWh/day [27]. The use of solar technology became more widespread, and in 2003, solar systems were first implemented in street lighting for remote areas [29][51]. The successful implementation of these systems attracted many other remote areas that began requesting the installation of similar systems in their regions [27]. Some other remote areas relied on using hybrid systems consisting of solar panels with a backup diesel generator for nighttime when the PV system is not operational. The mechanism of these systems is as follows: the PV systems supply power from 8:00 am to 6:00 pm, while generators supply power from 6:00 pm to 8:00 am. The use of

such systems was primarily to provide power to fuel stations, mosques, and hospitals. Table 2.5 illustrates the PV systems installed in some hospitals [51].

Table 2. 5. The PV systems installed in some hospitals.

Name of Hospital	City
Ali Omar Askar Neuro	Tripoli
Abu-sleem Hospital	Tripoli
Tripoli Heart Centre	Tripoli
Cordoba Centre for Services in Tripoli	Tripoli
Al Gwarsha clinic in Benghazi	Benghazi
Benghazi Al-Kwefia Hospital	Benghazi
Benghazi Dermatology Hospital	Benghazi
Sabha Hospital	Sabha
Kikla Municipality	Kikla
Rujban Hospital	Rujban
Zintan General Hospital	Zintan
Zintan Emergency and Surgery	Zintan
Zintan Obstetrics and Gynecology Hospital	Zintan
Ubari General Hospital	Ubari
Ubari General Hospital – Dialysis	Ubari

Several renewable energy projects were initially planned by the Ministry of Electricity and Renewable Energy authority of Libya to be conducted in 2013. However, all these projects were postponed due to the unstable situation within the country, these projects are as follow [29]-[52].

- 40 MW Solar PV project in Sebha city.
- 14 MW solar PV plant in Hun (Al-Jufra district).
- 100 MW solar PV power plant in Al-Kufra city.

Before the instability situation began in 2011, the Libyan government had ambitious goals to promote the use of renewable energy technologies. The plan established by REAoL in 2010 aimed to integrate renewable energy technologies into the national utility grid. The goal of this plan was to achieve 10% of Libya's energy demand to be met by renewables by 2025, which is equivalent to 2219 MW [15]. Globally, grid-connected PV systems are a well-established technology. However, in Libya, the integration of such systems has only recently begun. A grid-connected PV system with a total power capacity of 24 kWp was installed at Tripoli

University. The performance assessment of the system showed that it operates more effectively than anticipated in terms of output ratio, efficiency, and annual yield [53].

Numerous studies have been conducted to assess the potential of renewable energy resources. Reference [38] examined the feasibility of employing onshore wind farms and solar PV systems to assess their potential in alleviating the energy crisis affecting the country. Data for this study were sourced from National Aeronautics and Space Administration (NASA). The study identified specific locations suitable for the installation of these technologies. However, it did not account for the potential of other renewable technologies. A study was conducted in [26] to assess the current status and future potential of renewable energy technologies in Libya. The study involved interviews with decision-makers, managers, and consultants, from various government organizations. The findings indicate that renewable energy technologies are poised to play a significant role in meeting the country's energy demands. Moria and Elmnifi reviewed the potential of different renewable energy resources including wind, solar and solid waste by depending on recent reports [54]. Similarly, the government's plan was primarily focused on solar and onshore wind technologies. Authors in [51] investigated the potential of renewable energy resources and their role in enhancing the current and future Libyan energy sector. The results of this study demonstrated that the utilization of renewable energy technologies will help the country achieve its target of diversifying its energy sector, as well as reducing the CO2 emissions caused by burning fossil fuels in the energy sector. Likewise, authors in [42] studied the future of renewable energy resources by focusing on the solar and wind potential. The results showed that there is massive potential for both solar and wind energy, which are capable of serving various purposes, including electricity generation. In a captivating research journey detailed in [55], the authors delved into the potential of harnessing photovoltaic-solar water heating (PV-SWH) and photovoltaic-photovoltaic/thermal (PV-PV/T) systems in a typical Libyan household. Their mission to replace the conventional electrical heating system and alleviate the peak load burden. The results indicates that the adept use of PV-SWH could render a remarkable 69.79% energy conservation. Even more astounding, the strategic employment of PV-PV/T demonstrated a grand total energy savings of 75.02% of the overarching energy demand. Similarly, Authors in [40] evaluated the utilization of a solar-powered LED street lighting system as a substitute for the conventional grid-connected HPS-lamp street lighting system. The results highlighted that the implementation of a solar-powered street lighting system is capable of reducing CO2 emissions, saving fuels, and proving to be cost-effective. Authors in [56] proposed a 50MW PV solar plant in Al-Kufra, located in the

southeast of Libya. The outcome of this study indicated a payback period of 2.7 years. The performance of a 1.2 kWp PV system for a water pumping system in Marada city was evaluated in [57]. The results showed that using such a system for water pumping, particularly in remote areas, is economically and technically feasible. Performance evaluation of a 14 MW grid-connected Photovoltaic power plant in Hun city was conducted by [58] as well as techno-economic study for the same power plant was carried out in [59]. The results indicates that the performance ratio of this power plant is 79.9% and installing such power plant economically feasible. Author in [23] conducted a thermo-economic study of a 50 MW Parabolic Trough Concentrated Solar Power (PTC CSP) power plant equipped with a 7.5-hour Thermal Energy Storage (TES) system. The chosen location for this power plant was in Tripoli. The performance of the simulated plant was compared with the Andasol-1 power plant installed in Spain. The results demonstrated that the annual energy production by the Tajoura plant was 175 GWh/yr with a thermal efficiency of 47%. In contrast, the average energy generated by the Andasol-1 power plant was 172 GWh/yr with a thermal efficiency of 40%. The overall efficiency of both power plants was 17% and 13% respectively. The levelized cost of energy calculated for the CSP power plant in Tajoura was equal to $24/kWh. Ref [27] The Direct Normal Irradiation (DNI) of six locations across the country was evaluated over a 28-year period from 1990 to 2018. The data was collected using the solar database provided by Prediction of Worldwide Energy Resource (POWER). It was determined that the highest average DNI occurred in Al Kufra city, with an average daily radiation of 8.07 kWh/m2/day and an annual average of 2957 kWh/m2/yr. This was followed by Sirt city, which had the second highest DNI. Table 2.6 demonstrate the average monthly DNI of six locations. Reference [60] investigated the application of distributed solar generation to enhance the reliability of the energy supply in the southeastern region of Libya. The study utilized Digsilent software to model the network. The proposed system consisted of Photovoltaic (PV) panels along with Battery Energy Storage Systems (BESS) and Distributed Generators (DG). The findings of this study indicated a strong recommendation for adopting the combination of DG with PV and BESS. This approach is particularly advantageous given the substantial solar radiation potential in Al Kufra city. Authors in [45] asserted that Libya possesses substantial potential in terms of Renewable Energy (RE) resources, which have the capacity to generate a daily energy output equivalent to approximately 7 million barrels of oil. Notably, the solar potential alone is estimated to reach around $140*10^6$ GWh/yr.

Table 2. 6. The average monthly DNI, kWh/m2, for six locations in Libya.

Month	Tripoli	Al Kufra	Hun	Sirt	Sabha	Sarir
Jan	3.77	6.28	4.92	5.45	5.13	5.05
Feb	4.74	7.84	6.22	6.34	6.34	6.48
Mar	5.47	7.95	7.13	6.97	7.17	6.76
Apr	6.7	8.19	7.69	7.65	7.34	7.28
May	7.39	8.8	7.86	7.88	6.82	7.82
Jun	8.47	9.67	8.95	8.93	8.27	9.32
Jul	8.94	9.31	9.4	9.54	8.76	9.21
Aug	8.23	8.86	8.67	8.76	8.01	8.68
Sep	6.45	8.57	7.16	7.55	7.16	7.53
Oct	4.84	8.21	6.72	6.74	6.98	6.83
Nov	3.59	7.14	5.41	5.55	5.37	6.11
Dec	3.35	6.03	4.49	5.14	4.57	4.97
Average	5.99	8.07	7.05	7.21	6.83	7.17

2.5 Conclusions

Considering all the aforementioned information concerning the current energy situation and crisis in Libya, coupled with the availability of solar energy, it is imperative for the country's decision-makers to take further steps toward enhancing the utilization of this energy source. The potential for solar energy is substantial in many locations throughout the country, rendering it the foremost choice for meeting the country's energy demands from clean and renewable sources at a cost-effective rate. Moreover, this transition aids the country in reducing its dependence on fossil fuels and aligning with global sustainability goals. Furthermore, beyond catering to the country's energy needs, it could potentially supply energy to Europe by establishing connections with Italy or Malta. This also could open up a new source of income, which in turn would bolster the country's economy.

Chapter 3:

Literature Review

3.1 Introduction

In this chapter, the researcher has placed a strong emphasis on providing an overview of photovoltaic systems and their components. This overview also includes a spotlight on the most recent research activities in the field of integrating renewable energy resources, with a particular focus on solar systems. Additionally, the chapter delves into various issues and challenges associated with the PV systems integration into the utility grid.

3.2 Solar energy

The energy harnessed from the sun is immensely significant when considered in relation to global energy demand. This energy source can be utilized for various purposes, including electricity generation and heating. Nevertheless, its availability is not constant; it varies in terms of both quality and quantity based on location and time. Additionally, this energy source encompasses two primary components: direct and diffuse irradiance. Every single second, the sun undergoes a process in which approximately 4 million tonnes of its mass are transformed into energy, primarily in the form of solar radiation and neutrinos. However, only a minute fraction of this energy embarks on a 150-million-kilometre journey, taking approximately 8 minutes to traverse and reach the Earth [12]. This energy arrives at the Earth's surface in various forms, including heat and light. Throughout its journey, a significant portion of this energy is lost due to several factors, including reflection, absorption, and scattering by clouds. Solar energy is anticipated to emerge as one of the most dependable options to meet the global energy demand for several compelling reasons. One such reason is its consistent availability, with the sun emitting an average of 3.8×10^{23} kW of energy. However, only a fraction of this colossal amount, around 1.8×10^{14} kW, actually reaches the Earth [13]. Several studies have demonstrated that this energy resource can fulfil the global energy demand. A proper application of this technology could be the optimal solution to address the global energy crisis [14]. Despite its advantages, this energy source has some drawbacks. These include its unavailability at night, its inconsistency with fluctuations during the daytime, and the requirement of solar radiation to generate electrical energy, which can incur additional costs. Moreover, it is important to note that solar radiation may be obstructed and fail to reach the

surface of PV panels under adverse weather conditions [15]. Virtually all other energy resources, including renewable energy resources such as hydro, wind, biomass, and nun renewable energy resources such as fossil fuels, ultimately trace their origins back to sunlight [16]. Solar power, as an energy resource, finds applications in various domains, including solar desalination, electricity generation, and heating. Some of its key advantages include safety, cleanliness, and sustainability. Notably, it produces no emissions throughout its operational lifespan; any emissions associated with solar power occur solely during the manufacturing stage. It is anticipated that the installation of diverse solar systems across more than 2% of the Earth's landmass could prove adequate to meet the global energy demand [61]. Over the past two decades, there has been a substantial surge in the utilization of various solar technologies compared to other renewable energy alternatives. Solar photovoltaic (PV) technology has exhibited the most substantial annual growth, followed by concentrating solar panels and solar heaters, as illustrated in Figure 3.1 [62][63].

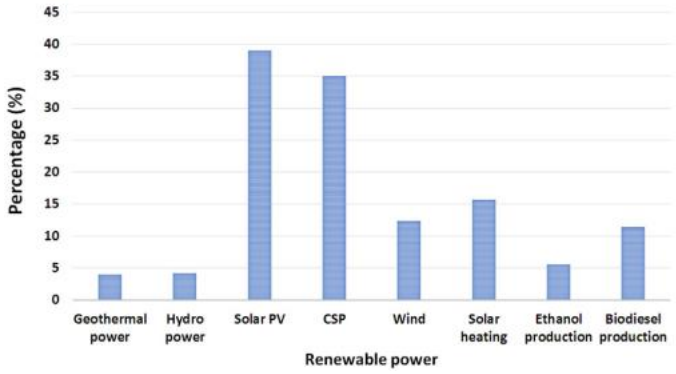

Fig. 3. 1. The percentage of growth for different renewable energy resources [62][63]**.**

The noteworthy features and advantages of solar power production can be summarized as follows [64].

- Abundance: Solar energy is the most readily available resource on Earth.
- Longevity: Photovoltaic (PV) solar panels exhibit minimal degradation, ensuring a lengthy operational lifespan of approximately 25 years.
- Durability: PV modules contain no moving parts, minimizing wear and tear unless equipped with a two-axis tracking system for solar tracking.
- Low maintenance: Solar power systems require minimal maintenance, primarily periodic cleaning.
- Cost reduction: Technological advancements have substantially reduced the cost of solar power production over recent decades.

- Construction cost reduction: The construction costs of solar power systems have decreased by approximately 10%–15%.
- Cost-effectiveness: Solar energy production could be cheaper than conventional power systems if considering cost reduction and improvements as well as government support schemes such as feed in tariff.
- Environmental friendliness: Solar power production generates no environmental or atmospheric pollution during operation period, contrasting with other energy production methods.
- High efficiency: With strategic planning and installation, solar power systems achieve high efficiency when situated near consumption points, minimizing transmission, transformation, and generation losses.

3.3 Photovoltaic phenomenon

Going back to 1839, Alexander-Edmond Becquerel discovered the PV phenomenon. In the later part of the 19th century, physicists observed that when light falls on a surface, whether metallic or liquid, the electrons of the material are emitted. However, during that era, there was no comprehensive explanation for this phenomenon until Albert Einstein introduced his theory. This breakthrough earned him the Nobel Prize in physics and laid the groundwork for the understanding of the photoelectric effect. The mechanism of the effect involves incident light striking the surface of a metal, causing the liberation of electrons. These electrons are subsequently drawn towards a positively charged plate, resulting in the generation of photoelectric current. This phenomenon was elucidated by Einstein through the application of the theory of quantized energy levels, as initially proposed by Max Planck. The theory's observation depicted light as composed of minute packets of energy termed photons. When these photons impinge upon metals or semiconductors, they dislodge electrons from their atomic orbits. In the 1930s, as a consequence of the observation of these theories, a new field in physics was established known as quantum mechanics. This development subsequently led to the innovation of transistors and semiconductor electronics [64]. Afterwards, the first solar cell was developed in 1946 by Russell Ohl, using silicon as the primary material. In the initial stage of this technology, PV solar cells were constructed from thin silicon wafers, which convert solar radiation into electrical power. However, due to the advancements in this technology, modern solar PV cells are manufactured using two distinct layers based on the theory of electron-hole creation. Each cell comprises two separate semiconductor materials, namely p-type and n-type materials as shown in Figure 3.2 [15].

When solar rays, charged with photons, strike the surface of the solar cell, the atoms lose their electrons in a phenomenon known as the photoelectric effect leaving behind a number of holes.

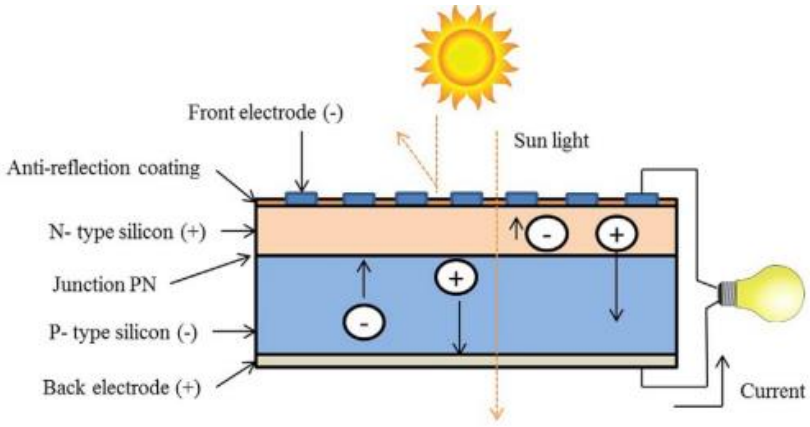

Fig. 3. 2. Construction of a silicon photovoltaic cell [19].

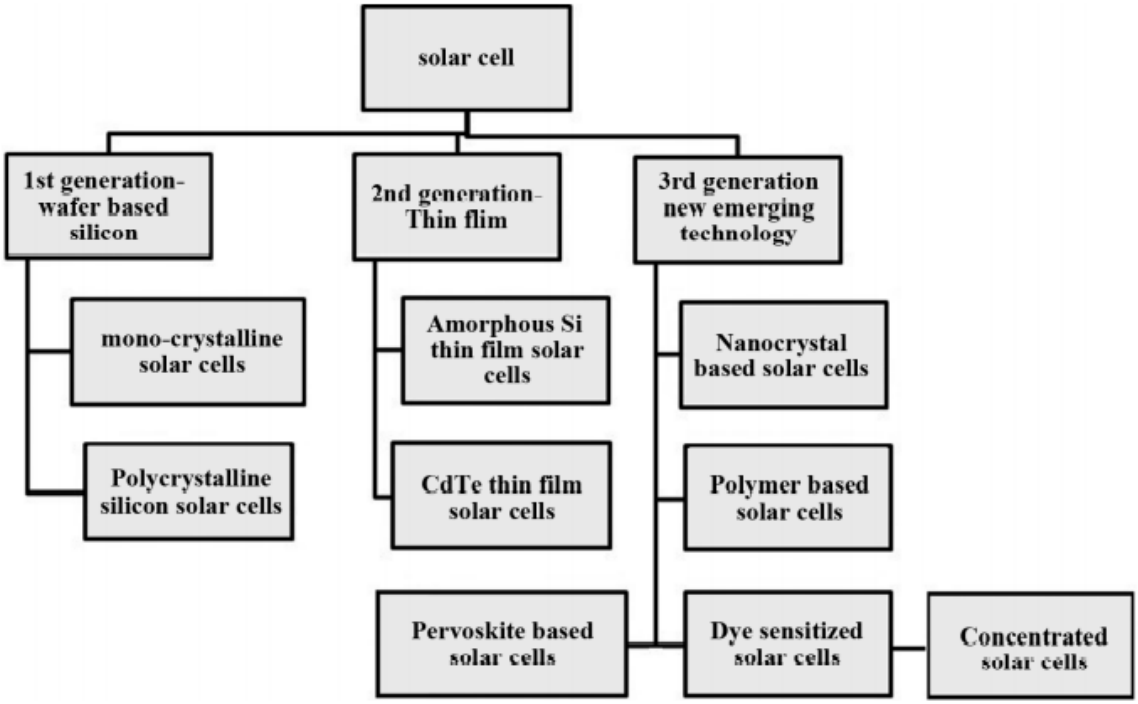

Fig. 3. 3. Various types of solar cell technologies [15].

The energy carried by the photons is transferred to the electrons in the valence region, prompting their movement to the conduction area within the negative layer. Concurrently, the positively charged gaps migrate to the conduction area of the positive layer. This disparity in charge creates a voltage difference between the two layers of the cell. These surfaces can be linked using an electrical conductor to establish a current within an electrical circuit. Electrons flow from the N-type side to the P-type side within the electrical circuit [65]. Various materials

are employed in the fabrication of photovoltaic solar cells, with silicon being the primary material utilized. Consequently, photovoltaic solar cells can be classified into several categories based on these materials, as depicted in the Figure 3.3 [15].

3.4 The Photovoltaic Solar Cell

A photovoltaic solar cell is a device that converts the solar radiation that falls to the earth's surface into electrical energy [66]. The operation mechanism of these cells is similar to semiconductor devices, such as transistors and diodes. Moreover, the majority of solar cells are constructed from semiconductor materials, with silicon being the most commonly utilized material. These cells consist of two main layers, including positive and negative layers. [67]. The positive layer is situated on the surface of the cell and is composed of a slice extracted from monocrystalline silicon injected with impurities from a trivalent element, such as boron. The subsequent electrical contact layer (negative) is made up of pure silicon and includes impurities of a pentavalent element, such as phosphorous. Both layers collaboratively facilitate the transfer of electrical current to and from the solar cell.

When solar radiation, charged with photons, strike the surface of the solar cell, the atoms undergo the photoelectric phenomenon, resulting in the loss of electrons and leaving behind several charge carriers known as holes. The photons' energy is converted to electrons in the valence region, after which they migrate to the conduction area in the N-type layer. Simultaneously, the positive gaps are displaced to the conduction area of the P-type layer, creating a voltage difference between the two layers of the dual link. The resulting current can be extracted from the two surfaces via an electrical conductor in an electrical circuit. Electrons flow from the negative terminal to the positive terminal in the electrical circuit, thereby transforming light energy into electrical energy [65][68].

These kinds of devices have advantages over other kinds of energy production, as no pollution come out except the pollution that results from the manufacturing stage, there are no fuel costs, maintenance is confined to cleaning and replacing damaged mirrors, and they emit no noise. Furthermore, this technology possesses the capability to generate energy by harnessing the most abundant energy resource available in this era. This attribute positions it as one of the most dependable energy resources for the future [64]. A typical photovoltaic system consists of numerous photovoltaic solar cells. Each solar cell is able to generate up to 2W, depending on the kind of material the cell made of [1]. Figure 3.4 shows the internal solar cell interconnections within a photovoltaic module [64].

Photovoltaic solar systems do not incorporate any moving parts, except for systems that facilitate sun tracking mechanisms. Furthermore, a typical PV module has a long operation lifetime of about 25 years.

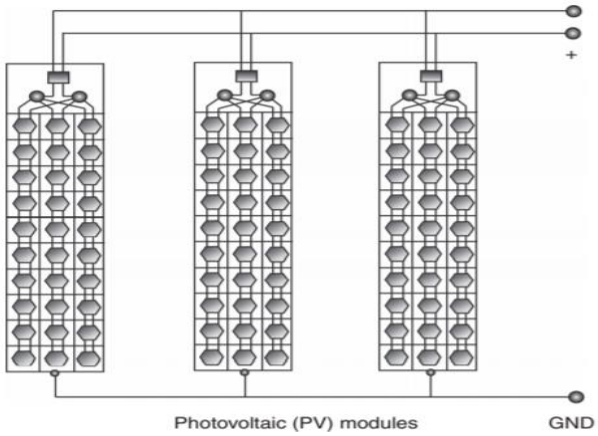

Fig. 3. 4. Interconnection of solar cells within a photovoltaic module.

Likewise, from an economic perspective, the construction costs of solar systems have reduced during last two decades by about 10 to 15%. Figure 3.5 illustrates a PV module assembly cross-section [1].

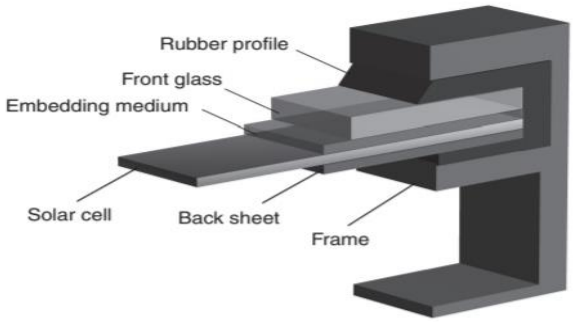

Fig. 3. 5. PV module assembly cross-section [1].

From technical point of view, the energy production from a photovoltaic solar system is influenced by several environment parameters, which include temperature, solar radiation, changes of solar angle through different seasons, atmospheric pressure, air mass, dusting, wind speed, humidity, panel tilt angle, clouds and environmental shading [64].

A combination of several photovoltaic solar cells, connected in parallel and in series, forms a single solar panel (module) capable of converting solar radiation into electrical energy. A typical solar panel consists of 60 or 72 small solar cells (12.5 cm^2 or 15.6 cm^2), developed using materials that facilitate the conversion of sunlight into electrical energy. These panels can vary in their power output, ranging from 40W to 400W. It is anticipated that in the next decade, the

average output power of a 60-cell PV panel will increase from 275Wp (watt peak) in 2017 to 350Wp, while for the 72-cell PV panel, it is expected to increase from 325Wp to 395Wp [7]. The typical power output of a single PV system ranges from hundreds of watts to megawatts. Therefore, PV systems can be installed for both domestic and utility-scale applications [15].

Solar radiation and ambient temperature are the two main factors that directly impact the behaviour of PV modules. PV modules have several parameters, including open-circuit voltage, short-circuit current, and the maximum power point for both voltage and current (V_{mp} & I_{mp}). Furthermore, the point at which the PV module operates at its maximum capacity is defined by the maximum power point, which is the product of V_{mp} and I_{mp} [69]. The operation mechanism of solar cells is depending on different parameters as listed below.

1. Absorption of light, resulting in the generation of charge carriers, namely holes (p-type) and electrons (n-type).
2. charge carriers' separation.
3. The accumulation of charge carriers at the respective electrodes establishes the potential difference across the p-n junction.

The voltage difference generated at the p-n junction due to incident radiation is harnessed to perform the work. In the past, several semiconductor materials and technologies were employed to produce cost-effective solar cells with high conversion efficiency [15].

PV arrays have nonlinear characteristics, with the output fluctuating in response to variations in temperature and radiation. Consequently, it is essential to examine the primary components of the PV cell and its characteristics to assess generated energy, evaluate power quality, gauge conversion performance, and the control algorithms. PV cells fall into two categories: single diode PV cells and double diode PV cells [70][71]. The equivalent circuits of both types are shown in Figure 3.6. The single diode PV cell is the simplest model, consisting of a current source connected in parallel with a single diode. The output of this cell is directly influenced by solar radiation. For the I-V characterization curve, only three parameters are needed: Short-circuit current (I_{sc}), open-circuit voltage (V_{oc}) and the diode ideality factor (a) [72]. However, to achieve a more accurate representation of the behaviour of the PV cell, an improvement of this model is conducted by including $series\ resistance\ R_s$ [73]. It is known as the R_s-model, with some features like simplicity and efficiency. However, it has some limitations, especially during temperature variations, resulting in a decrease in its accuracy. To

overcome this issue, additional resistance is included, known as shunt resistance, and this model is widely known as the R_p-model. [74]. Making it more practical in presenting the behaviour of the PV cell. On the other hand, the two-diode cell (double diode) stands out above the single diode cell for its accuracy in representing the behaviour of the PV cell. However, it is more complex, requiring seven unknown parameters. Its performance is similar to that of the Rp-model under Standard Test Conditions (STC). Nevertheless, at low levels of solar radiation, the double diode model is more accurate. The seven unknown parameters for this model are I_{ph} which is the photon current, I_{0_1}, I_{0_2} which are the saturation currents for both diodes, R_s and R_P which are the series and shunt resistances respectively. Finally, a_1 and a_2 which are the diode ideal factors for both diodes respectively [75][73].

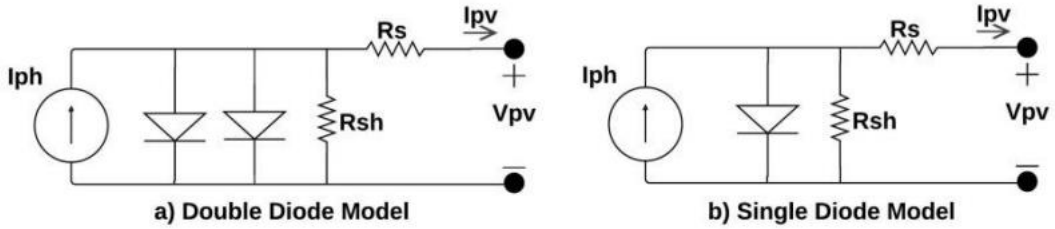

Fig. 3. 6. Equivalent non-linear circuit of solar cell (a) double diode (b) single diode model.

The current for the single diode can be obtained using the following equation (3.1)[76][77]. However, for a double diode PV cell, an additional current component should be taken into consideration, which represents the current flow through the second diode.

$$\boldsymbol{I = I_{Ph} - I_O\left[exp\left(\frac{V+I\,R_S}{N_s a\,V_{th}}\right) - 1\right] - \frac{V+I\,R_S}{R_P}} \qquad (3.1)$$

where I and V are the current and voltage of the PV module, I_{ph} is the photon current which can be expressed using equation (3.2), I_0 is the saturation current, R_s and R_P are the series and shunt resistances respectively, N_s and a are the number of series connected cells in a single PV module and the diode ideal factor while V_{th} is the thermal voltage which can be obtained using the equation (3.3)

$$I_{Ph} = \left[I_{Phn} + KI\left(T - T_{ref}\right)\right] * \frac{G}{G_N} \qquad (3.2)$$

where, I_{Phn} is the photon current value at reference conditions, KI is the current temperature coefficient, T_{ref} is the reference temperature = 273.19K, T is the cell temperature, G is the irradiance value and G_N is the irradiance value at standard temperature.

$$V_{th} = \frac{KT}{q} \tag{3.3}$$

where, $K = 1.38 * 10^{-23}$ J/K is Boltzmann constant, T is the cell temperature an $q = 1.6 * 10^{-19}$ C is the charge of an electron. The I-V and P-V characteristics of the PV array for different temperature and radiation are illustrated in Figure 3.7-a and 7.7-b, respectively.

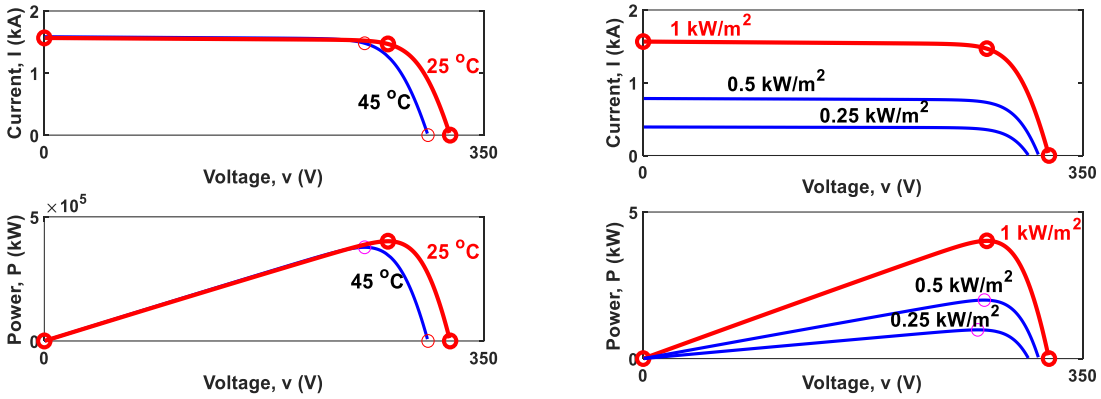

(a) **(b)**

Fig. 3. 7. I-V and P-V characteristics of the PV array (a): at different temperature (b): at different radiation

The PV arrays composed of strings connected in parallel. Each single string has a number of modules connected in series. Therefore, the generated voltage and current of the PV array can be obtained by using the following equations [78]:

$$V_{array} = N_s\,(V_{cell} - IR_s) \tag{3.4}$$

$$I_{array} = N_p I \tag{3.5}$$

$$P_{array} = V_{array} I_{array} \tag{3.6}$$

where N_p is the number of PV modules connected in parallel, N_s the number of modules connected in series and V_{cell} is the Voltage of the PV cell. However, connecting PV modules in series and parallel configurations can lead to a reduction in overall efficiency if obstructions, like clouds or shadows, prevent solar radiation from reaching the surface of the PV modules. To address this issue, bypass diodes can be integrated, but this does not provide a complete solution [79]. To clarify, electrical mismatch conditions can occur in the PV module due to non-uniform solar radiation, partial shading, or the use of solar cells from different manufacturers. Partial shading conditions are frequently encountered in Building Integrated Photovoltaics (BIPVs) and can result from various factors, including trees, dirt, nearby buildings, poles, and antennas [80]. Keeping in mind the theory that in a series connection, the current is the same in all components, it applies similarly to the series-connected solar

cells that make up the PV module. Therefore, in the event of a partially shaded condition, the current decreases, which, in turn, reduces the overall output power. Additionally, the temperature of the shaded cells increases significantly, potentially leading to the hotspot phenomenon in the PV cell [81]. Therefore, addressing this issue involves the employment of bypass diodes integrated in parallel with the PV cells, as depicted in Figure 3.8. These diodes offer an alternative pathway for the current to pass through, so the shaded cells is bypassed [82] [83].

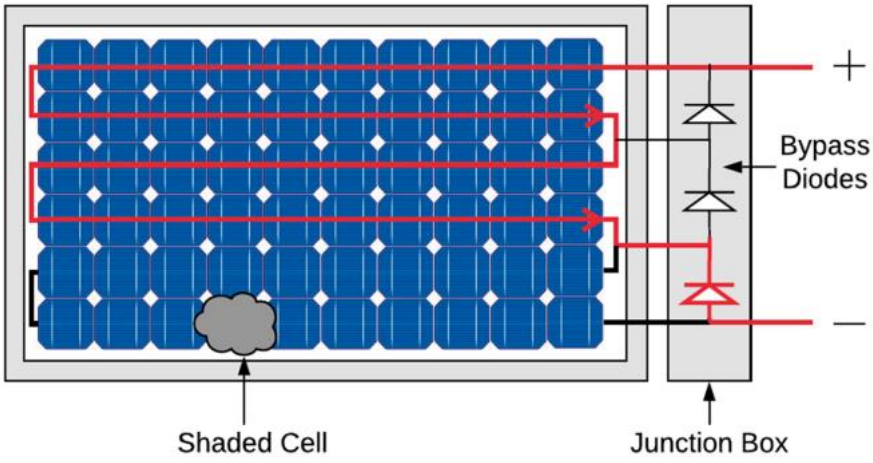

Fig. 3. 8. PV module with one shaded cell [80].

Furthermore, photovoltaic solar systems are typically classified based on their connection and function. The most well-known configurations include grid-connected solar systems and stand-alone (off-grid) solar systems [84][1]. Stand-alone solar systems are primarily employed in remote areas that lack access to the national grid. Such systems typically comprise a solar PV array connected with a DC-DC converter that works to elevate the DC voltage to appropriate align with the DC-AC inverter requirements as well as sometime backup batteries are used to supply energy at night [46]. Conversely, grid-connected solar systems shine brighter than their stand-alone counterparts due to their captivating features. In these systems, energy can flow in both directions, signifying their ability to seamlessly exchange power with the utility grid according to the ever-changing load demands. Consequently, these systems can play a significant role in reducing electricity bills by generating energy at a lower cost, thereby reducing the reliance on the grid for power. Furthermore, there is no need for energy storage as a backup system, leading to higher overall efficiency as there are no storage-related losses involved [69]. Due to the aforementioned features, it's anticipated that the reliance on these systems will surge over the next two decades. However, this surge requires a reliable integration into the national grid [85].

3.5 Grid-connected solar PV system

To ensure a continuous power supply, most grid-connected PV systems (GCPVs) are interconnected in parallel with the utility grid. These systems fall into two primary categories: Building Integrated Photovoltaics (BiPV) and Distributed Generation Photovoltaics (DGPV). In the first category, the generated power is utilized to supply specific loads, with any surplus power being redirected to the grid. In the second category, the entirety of the generated power is directly supplied to the grid. Typically, GCPV systems can consist of a PV array as the primary energy source, or they can operate as hybrid systems in conjunction with other energy resources like wind turbines, diesel systems, or energy storage units [86]. Utilizing such systems can reduce the amount of energy drawn from the grid and even enable energy supply to the grid, potentially leading to reduced energy bills and additional income. Furthermore, installing these systems near consumption points can help mitigate transmission and distribution losses [87]. A typical GCPV system consists of a PV array, a DC-DC boost converter used to elevate the voltage to a specified level and implement the Maximum Power Point Tracking (MPPT) technique to gain maximum power consistently. This is followed by the DC-AC inverter, a critical component responsible for converting the DC signal from the DC converter into a sinusoidal waveform that aligns with the grid's specifications. The inverter's output is directed into a filter to eliminate high-frequency components and reduce Total Harmonic Distortion (THD) to an acceptable level. Ultimately, these generated signals are channelled into a step-up transformer to align with the grid voltage. In situations of energy deficit, the control strategy will halt energy feed to the grid to meet the load demand. Conversely, when there's a surplus of energy, the system will continue supplying the utility grid [88] A typical configuration of the GCPV system is shown in Figure 3.9, with all parts indicated in separate blocks.

In BiPV systems, the size is determined by the necessary load demand and the power required for the grid, whereas in DGPV systems, the size is contingent on the grid's power demand [86]. Some systems are installed and equipped with backup energy storage (batteries) to provide the required power throughout the night or cloudy weather conditions. However, these systems cost more than those without a backup unit and entail higher losses, maintenance, and equipment. Conversely, systems without a backup unit will need to shut down during periods of insufficient solar radiation. Nevertheless, to address this issue, energy can be exchanged with the grid to satisfy the load demand [89].

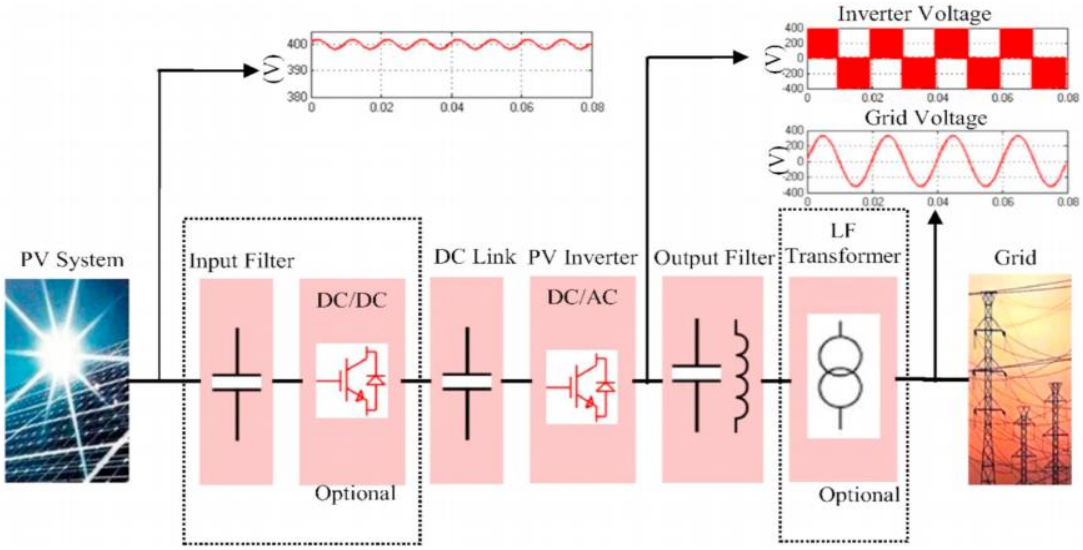

Fig. 3. 9. A typical configuration of the double stage grid-connected PV system [89].

GCPV systems can be structured as double-stage, comprising both a DC-DC converter with a DC-AC inverter as shown in Figure 3.9 or as single-stage, consisting of a DC-AC inverter only as depicted in Figure 3.10 [90]. Single-stage systems encounter challenges in maintaining voltage stability in the DC bus during rapid changes in atmospheric conditions. Therefore, double-stage systems offer the opportunity to apply MPPT to track the MPP and stabilize the DC bus voltage to meet the inverter's requirements. Making it as the most appropriate power interface for any cases [46].

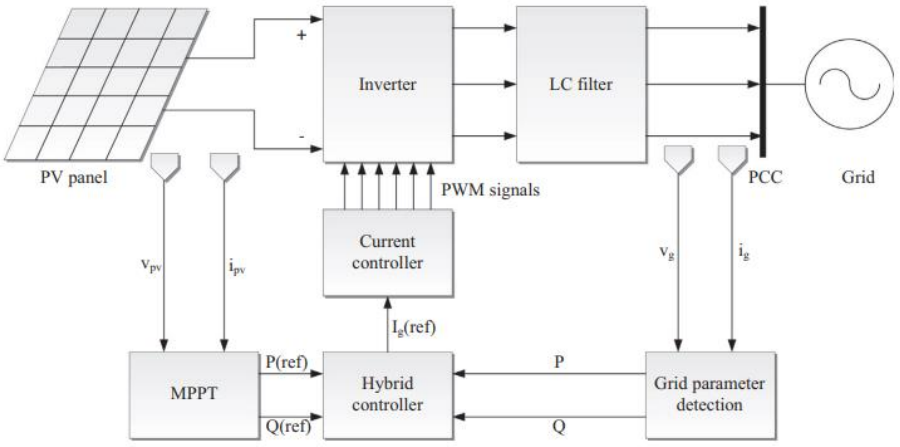

Fig. 3. 10. A typical configuration of the double stage GCPV system [90].

3.5.1 Configuration and topology of PV inverter

Integrating the PV system in parallel with the grid requires several interfacing components, including a DC-DC converter used to maintain a specific voltage level at the DC link bus and implement the MPPT technique.

Additionally, a DC-AC inverter is employed to convert the generated voltage into an AC signal. The output power of the PV system is influenced by factors such as solar radiation levels and temperature, as well as shading caused by obstacles. A well-designed system configuration can help mitigate the impact of shading on the system. Therefore, there are four system topologies to consider including Centralised configuration, String configuration, Multistring configuration and Modular configuration [91]. These systems are briefly explained in the following subsections, and schematically shown in Figures 3.11-a to 3.11-d.

- Centralised configuration

In this topology, thousands of PV modules are connected to a single inverter. Hundreds of these modules are connected in both parallel and series configurations, forming the PV array. Each PV array comprises hundreds of PV strings.

- String configuration

In this topology, each PV string is interfaced with a DC-AC inverter. However, if the voltage level is not within the acceptable range, a DC-DC boost converter can be integrated on the DC side to elevate the voltage to the desired level.

- Multistring configuration

In this topology, each PV string is connected to a DC-DC converter, and every four or five PV strings are then collectively connected to a DC-AC inverter.

- Module configuration

In this configuration each PV module is connected to a single DC-AC inverter.

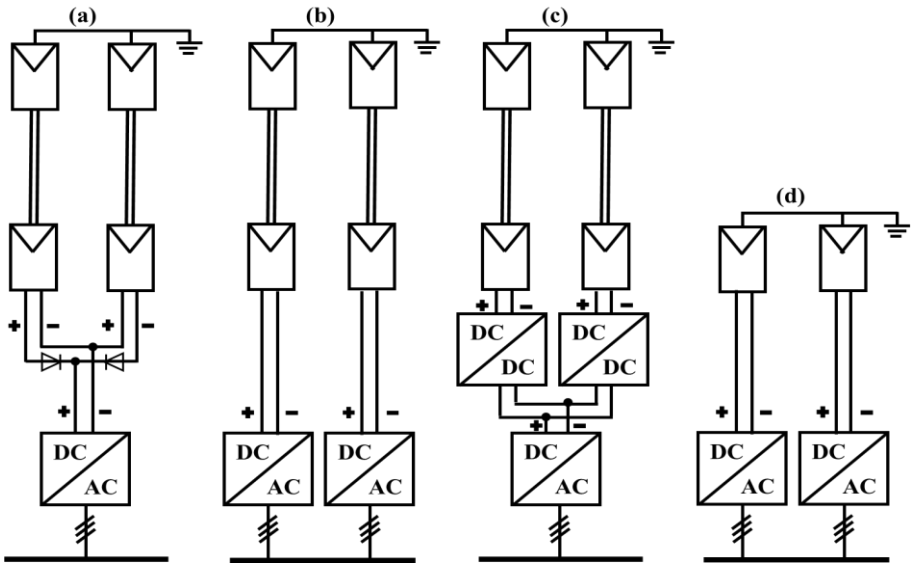

Fig. 3. 11. PV inverter topologies. (a) Central, (b) string, (c) multistring, and (d) module integrated.

These four topologies are categorised and assessed under four criteria which includes performance, power losses, power quality and cost as summarised in Table 3.1.

Table 3. 1. Main characteristics of PV inverter topologies.

Characteristics		Central	String	Multistring	Module integrated
Performance	Reliability	L	H	M	H-H
	Robustness	H	L	M	L-L
	Flexibility	L	H	M	H-H
	MPPT efficiency	L	H	M	H-H
Power losses	Mismatching	H	L	L	L-L
	Switching	H	L	M	L-L
	AC power losses	L	M	M	H
	DC power losses	H	L	M	L-L
	AC voltage variation	L	H	M	H-H
Power quality	DC voltage variation	H-H	M	H	L-L
	Voltage balance	H	M	L	L
cost	Installation cost	M	H	M	H-H
	DC cables	H	L	M	L-L
	AC cables	H	M	M	H
	maintenance	L	M	H	H-H

The following nomenclature is used: H–H: very high, H: High, M: Medium, L: Low, L–L: very low.

3.5.2 DC-DC Boost converter

The DC-DC boost converter stands as one of the pivotal components within GCPVs. Its primary role revolves around managing the DC voltage originating from the PV arrays by manipulating its duty cycle. This converter is also responsible for elevating the voltage level, ensuring it surpasses the input voltage. The typical DC-DC boost converter comprises an inductor, a capacitor, and a power electronic switch as shown in Figure 3.12. Voltage amplification occurs when the switch is open, and the summation of voltage across these components yields the boosted voltage. The duty cycle of the converter can be derived from the following equation.

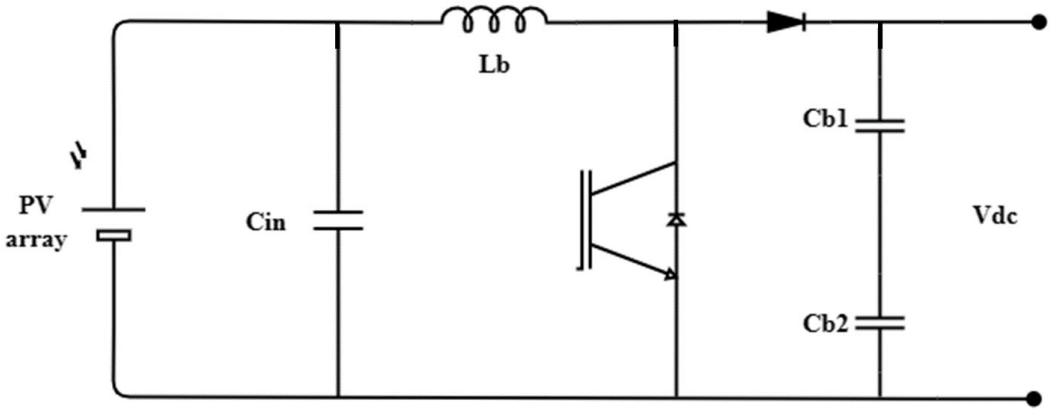

Fig. 3. 12. Equivalent circuit of a DC-DC boost converter

$$D = 1 - \frac{V_{in}}{V_{out}} \qquad (3.7)$$

Typically, the DC-DC boost converter has the capacity to elevate the voltage level up to 450V in single-phase systems and up to 700V in three-phase systems. This assurance is predicated on the requirement that the DC voltage must exceed the peak value of the phase voltage in single-phase systems or the peak value of phase-to-phase voltage in three-phase systems [7]. A DC-DC boost converter plays a crucial role in elevating the DC voltage level generated by the PV array. Furthermore, it provides a pathway for implementing the MPPT technique, thereby enhancing the system's voltage quality and controllability [7]-[92]. The signal produced by the boost converter is under the control of the MPPT unit, which manages the converter's duty cycle [93] [46]. The output of the DC-DC converter is then supplied to the inverter, which converts the DC voltage into a Pulse Width Modulation (PWM) voltage signal.

3.6 Maximum power point tracking

The primary function of the Maximum Power Point Tracking (MPPT) is to extract the maximum power from the PV array, irrespective of any fluctuations in solar radiation or temperature levels [94]. The MPPT controls the DC voltage at the DC bus, adjusting it either up or down in response to weather condition variations to ensure it aligns with the inverter's input limits. This process is carried out by adjusting the duty cycle of the DC-DC converter to control the voltage level. This adjustment is achieved by altering the operational period of the semiconductor switch within the DC-DC converter. As a result of this process, the maximum power of the PV array is extracted through a balanced adjustment of the I-V characteristics of the PV module [95]. MPPT techniques are typically implemented at the DC-DC stage in double-stage topologies or at the DC-AC stage in single-stage topologies. Among these, the DC-DC boost converter is widely employed in solar power systems [46].

Tracking the Maximum Power Point (MPP) of a PV array to extract the maximum power is a crucial requirement in the modelling of PV systems. Consequently, several MPPT techniques have been developed for this purpose [87] [96]. These techniques differ in terms of the number of sensors required, complexity, hardware implementation, convergence speed, effectiveness, and cost [97]. Numerous techniques have been developed and implemented for both double-stage and single-stage topologies. These techniques can be classified into two categories: indirect and direct techniques, with each category comprising several specific techniques. Among the most common techniques in the indirect category are the open-circuit, constant voltage, short-circuit, and pulse methods. Some of these techniques necessitate mathematical calculations, while others demand a deep understanding of the characteristics of the PV array. Conversely, direct techniques are considered the most commonly used, including Perturb and Observe (P&O), Hill Climbing (HC), and Incremental Conductance (IncCon) [46]. These techniques offer several advantages over indirect methods, including improved efficiency, simplicity, ease of implementation, and not demanding extensive prior knowledge of the PV array's characteristics [46].

The operational principle of P&O and IncCon techniques is rooted in the hill-climbing concept. These techniques rely on shifting the operational point of the PV array in a manner that facilitates an increase in power output. These techniques are among the most commonly used due to their simplicity, ease of implementation, and high performance. However, they do have some drawbacks, including the occurrence of oscillations around the MPP, and during rapid changes in weather conditions, they may lose track of the MPP in an effective manner

[97]. The fractional open-circuit voltage or short-circuit current methods provide an approximate MPP rather than an exact output. Under normal operating conditions, the power curve of the PV array exhibits a single MPP. However, in cases of partial shading, the power curve might have multiple MPPs [1]. In recent years, many improvements have been developed in the implementation of MPPT algorithms, and new methods have been newly established based on artificial intelligence (AI). For instance, fuzzy logic controllers (FLCs), artificial neural networks (ANNs), particle swarm optimization (PSO) algorithms offering higher efficiency and faster response compared to indirect and direct methods [46]. Some of the most common MPPT techniques are:

1. Perturb and Observe (hill climbing method).
2. Incremental Conductance method.
3. Fractional short circuit current.
4. Fractional open circuit voltage.
5. Fuzzy logic.
6. Neural networks.
7. Ripple Correlation Control.
8. Current Sweep.
9. DC-link capacitor droop control.
10. Load current or load voltage maximization.
11. dP/dV or dP/dI feedback control.

3.6.1 Perturb and Observe & Hill climbing

The P&O algorithm, sometimes referred to as the Hill Climbing (HC) algorithm, is one of the most popular and widely implemented algorithms due to its simplicity and ease of implementation [88]. This technique requires single voltage sensor to measure the PV array voltage, leading to a lower cost of implementation. In this technique, perturbations in the duty cycle or the voltage level of the converter are introduced [98] [1]. The operational concept of this technique depends on perturbing the voltage level, sensing the output power, and comparing it with the previous measurement. The algorithm tracks the MPP in both directions

by comparing the voltage change and the response of the power output. If the perturbation led to increase in the power output the algorithm continues the tracking process of the MPP in the same direction. If not, the algorithm changes the direction of tracking the MPP of the PV array. If not, the algorithm changes the direction of MPP tracking [46]. In this technique, the direction of the next perturbation is determined based on the power measurement. If the previous perturbation was to the left of the MPP, the next perturbation should increase the voltage, leading to an increase in power. Conversely, if the last perturbation was to the right of the MPP, the following perturbation must decrease the voltage level to increase the power output, as shown in the Figure 3.13.

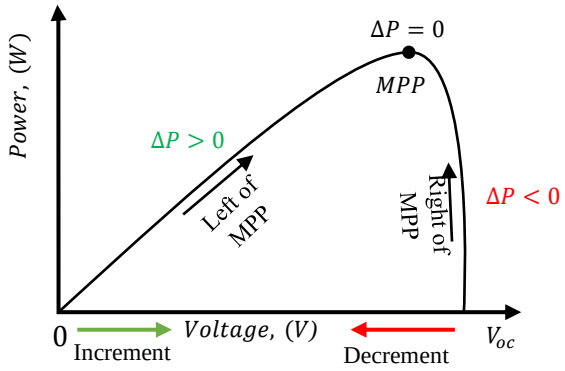

Fig. 3. 13. PV characteristics of P&O MPPT technique

This process can be summarized as follows: whenever the power increases, the perturbation process continues at same direction, and when the power decreases, the afterwards perturbation must follows the opposite direction, as illustrated in the Table 3.2 [97]. The flowchart of this technique is shown in Figure 3.14 [99] [1].

Table 3. 2. Principle of the P&O algorithm

Perturbation	Change in Power	Next perturbation
Positive	Positive	Positive
Positive	Negative	Negative
Negative	Positive	Negative
Negative	Negative	Positive

The technique repeats its steps until the MPP is achieved [1]. Afterward, the system will continue to fluctuate around the MPP, but the level of this oscillation can be reduced by using a smaller perturbation step size. However, this will lead to a slower MPPT technique. An

effective solution for this is to implement a variable perturbation step size that becomes smaller as it approaches the MPP [97]. Moreover, this technique is not suitable for rapidly changing weather conditions where the voltage will continue to fluctuate around the MPP and may never precisely reach the MPP value [98].

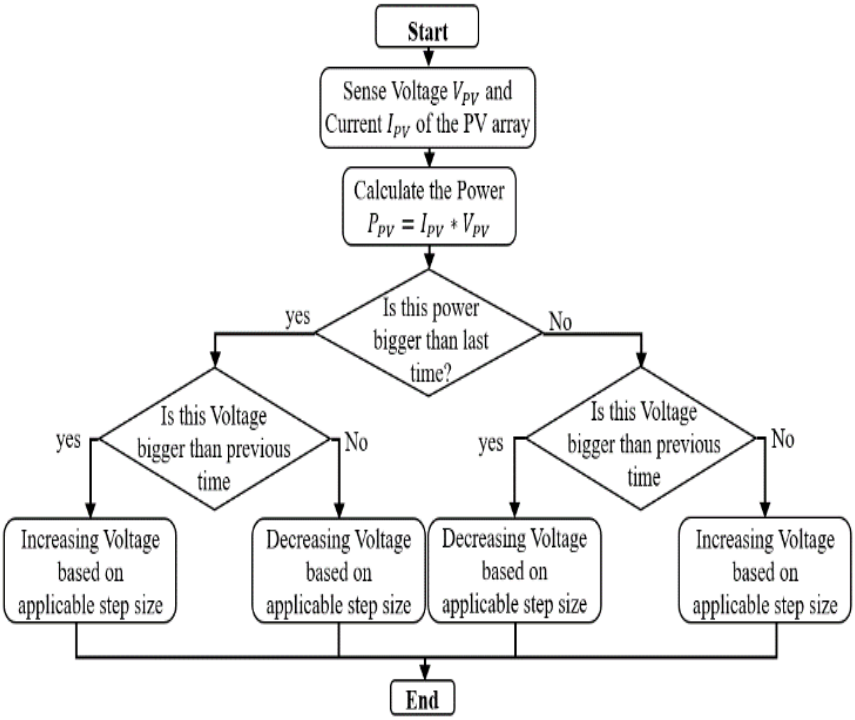

Fig. 3. 14. Flowchart of P&O MPPT technique

3.6.2 Incremental Conductance

In this MPPT technique, double sensors are involved to measure the output voltage and current of the PV array. The output voltage of the PV array is adjusted based on the MPP of the voltage [1].

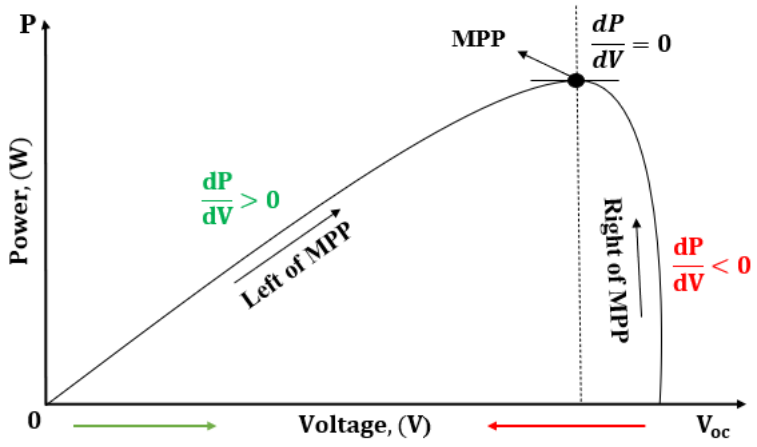

Fig. 3. 15. The principle of the Incremental Conductance algorithm

The principle of the IncCon algorithm depends on the slope of the PV curve. The MPP is achieved when the slope is zero, as shown in the Figure 3.15 [46][100]. There are some similarities with the P&O technique as can be seen in Figure 3.15. The basic equations of this technique are as follows [101]:

$$\frac{dI}{dV} = -\frac{I}{V};\ \left(\frac{dP}{dV} = 0\right);\ at\ MPP \tag{3.8}$$

$$\frac{dI}{dV} > -\frac{I}{V};\ \left(\frac{dP}{dV} > 0\right);\ at\ left\ of\ MPP \tag{3.9}$$

$$\frac{dI}{dV} < -\frac{I}{V};\ \left(\frac{dP}{dV} < 0\right);\ at\ right\ of\ MPP \tag{3.10}$$

In this technique, the reference voltage calculation is conducted based on the incremental value used, and this procedure is repeated until the MPP is achieved. Once the V_{ref} is determined for the MPP, the technique continues tracking this value to ensure the maximum power is consistently extracted from the PV array. If any changes occur in the PV array generated current, denoted as dI, the algorithm recommences its steps to determine the new V_{ref} value by adjusting the previous one. The Equation (3.8-3.10) and the flowchart presented in Figure 16 are rooted in the instantaneous conductance (I/V) and the incremental conductance (dI/dV) of the PV array [46]. Typically, in the conventional Incremental Conductance technique, the step size remains fixed and directly affects the tracking speed and accuracy of the MPPT. A larger fixed step size results in a quicker tracking process, but it also leads to higher power losses due to significant oscillations around the MPP, akin to the behaviour in the P&O technique. Thus, adopting a smaller step size can help alleviate these oscillations [102]. However, during rapidly changing weather conditions, this technique falters and struggles to accurately track the MPP [87]. Considering these factors, numerous advancements have been made by incorporating a variable step size. This adaptive step size is automatically adjusted in response to changes in the PV array's characteristics. The Flowchart of conventional incremental conductance MPPT technique and variable step size IncCon MPPT technique are shown in Figures 3.16 and 3.17, respectively.

As solar radiation directly influences the outputs of the PV array, an increase in solar radiation leads to higher voltage output, shifting the MPP to the right side of the PV curve. Consequently, the MPPT algorithm adjusts the PV array's operating voltage upward to accommodate this increase. Conversely, if solar radiation decreases, the operating voltage is reduced accordingly.

This technique relies on the slope value to sense changes in radiation levels and adapts accordingly.

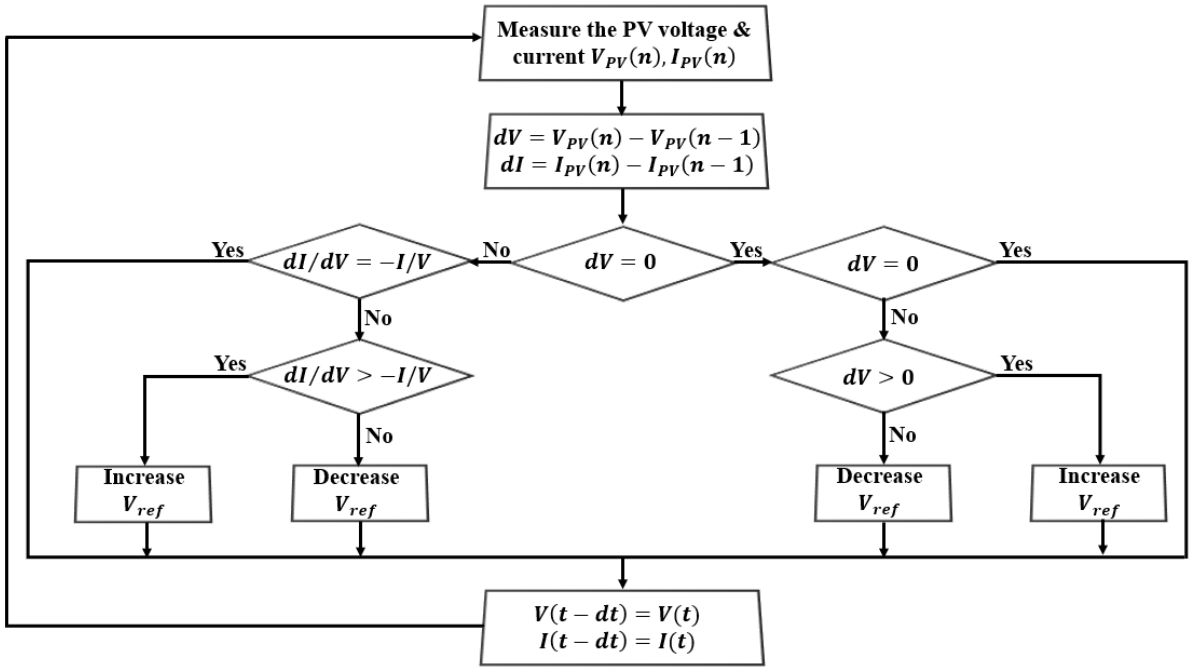

Fig. 3. 16. The Flowchart of conventional IncCon MPPT technique

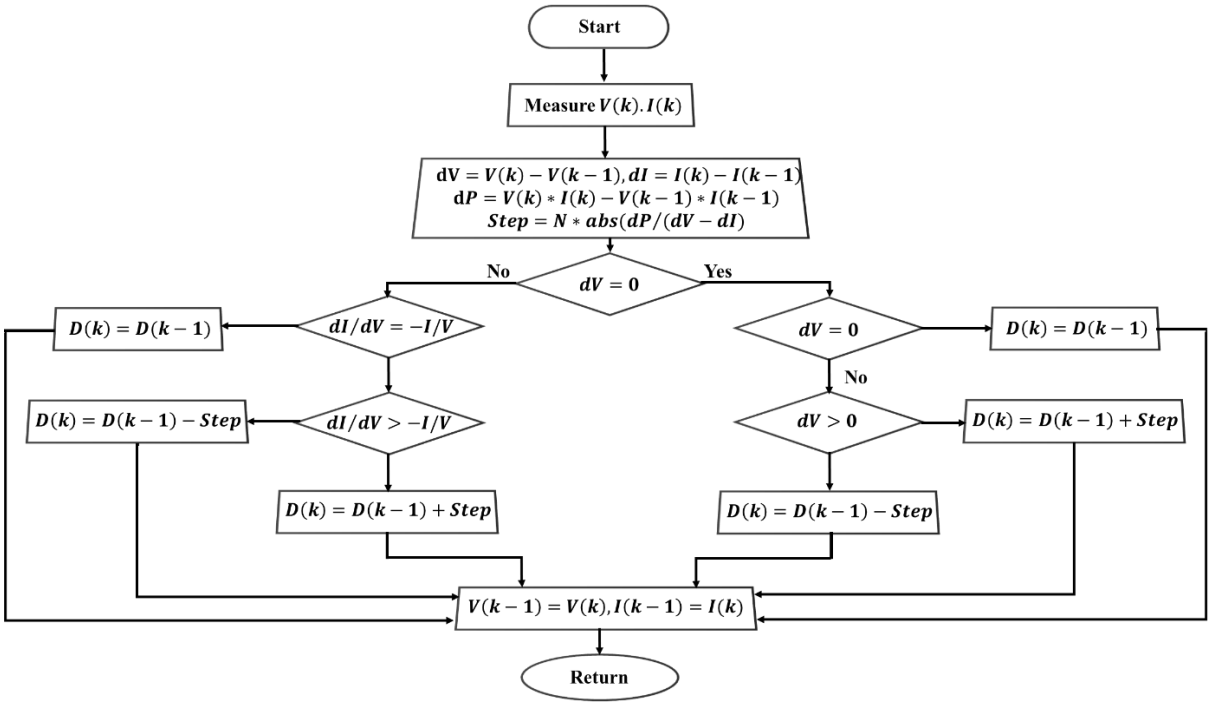

Fig. 3. 17. Variable step size IncCon MPPT technique

Additionally, the algorithm leverages past readings of the PV array generated voltage and current, denoted as dV and dI, and compares them with the current measurements to detect any changes [1]. This technique is particularly effective at detecting rapid changes, as it

continuously tracks the system's operating point, preventing any misleading tracking of the MPP of the PV array, a challenge sometimes encountered in the P&O technique. [46].

3.6.3 Fuzzy logic

The adoption of microcontrollers has propelled the popularity of fuzzy logic control techniques for MPPT tracking over the past decade. This technique offers several advantages over others: it doesn't demand precise inputs, obviates the need for an accurate mathematical model, and excels at handling nonlinearity. The process comprises three stages: fuzzification, rule-based table lookup, and defuzzification [1]. Fuzzy logic-based MPPT techniques have emerged as the most popular artificial method for MPPT, outperforming conventional techniques while offering simpler requirements. One of the standout features of this technique is its integration with existing MPPT systems, ensuring the efficient delivery of maximum power to the load [46]. The schematic diagram for Fuzzy logic MPPT technique is depicted in Figure 3.18. A membership function is used to transfer numerical input variables into linguistic variables as illustrated in the Figure 319. Where five fuzzy levels are involved in this case: NB (negative big), NS (negative small), ZE (zero), PS (positive small), and PB (positive big) [99].

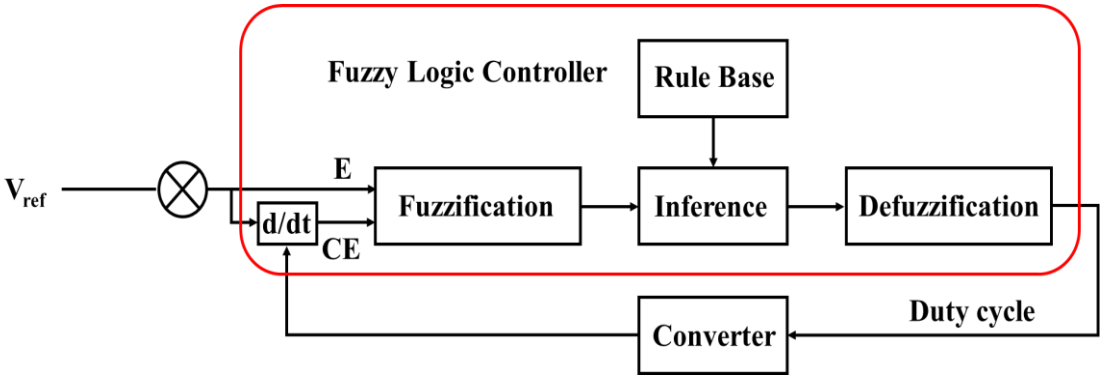

Fig. 3.18. The schematic diagram for Fuzzy logic MPPT technique [46]**.**

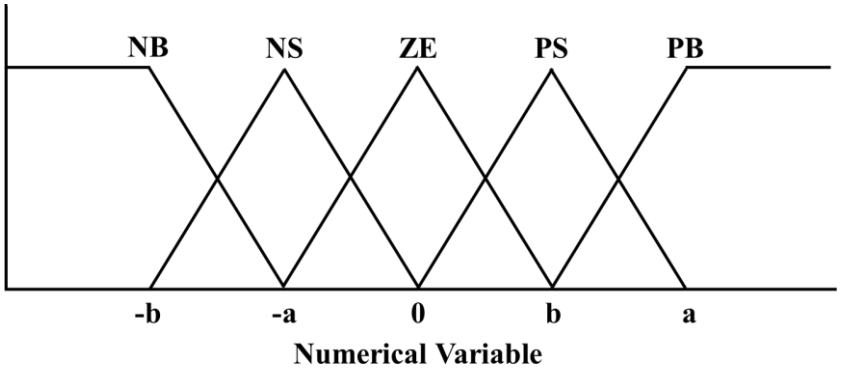

Fig. 3.19. A membership function [97].

In Figure 19, The values of "a" and "b" depend on the numerical variable's range. At times, the membership function is intentionally made asymmetric to emphasize particular fuzzy levels [97]. Figure 3.20 shows the integration of fuzzy logic controller to P&O algorithm. In this combination, the Fuzzy Logic Controller incorporates the reference input to specify the error signal, denoted as E, and the rate of change of the error, ΔE, as depicted on the left-hand side of the figure. The output signal of the fuzzy logic controller regulates the duty cycle, which in turn controls the switching period of the converter. This duty cycle is generated through a four-stage process, beginning with fuzzification, wherein numerical inputs are transformed into linguistic variables determined by the rule base and dependent on membership functions. Increasing the level of the membership functions allows for finer resolution in the calculations. Next, the input variables undergo analysis and weighting in the inference section using various methods, including Mamdani, Takagi-Sugeno, and modus ponens. Subsequently, in the last stage, which is defuzzification, the linguistic outputs of the controller are transformed back into numerical variables to find out the converter's duty cycle [46].

The user retains the ability to select how to handle the error E and its change, ΔE. where dP/dV disappears at the MPP, assumptions can be incorporated as follows [103].

$$E(n) = \frac{P(n)-P(n-1)}{V(n)-V(n-1)} \qquad (3.11)$$

$$\Delta E(n) = E(n) - E(n-1) \qquad (3.12)$$

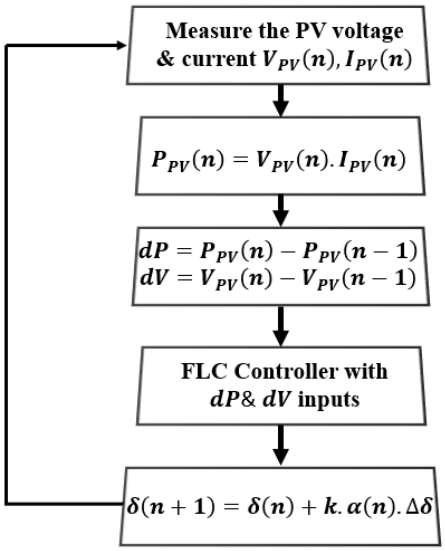

Fig. 3. 20. The integration of fuzzy logic controller to P&O algorithm.

Alternatively, the error signal can be computed as $e = I/V + dI/dV$, a widely used method. After calculating E and ΔE, and transforming them into linguistic variables, the change ratio of

the duty cycle, which serves as the output signal of the fuzzy logic controller, can be defined using a rule-based table as depicted in the Table 3.3 [98][97].

Table 3. 3. A rule-based table

	ΔE				
E	NB	NS	ZE	PS	PB
NB	ZE	ZE	NB	NB	NB
NS	ZE	ZE	NS	NS	NS
ZE	NS	ZE	ZE	ZE	PS
PS	PS	PS	PS	ZE	ZE
PB	PB	PB	PB	ZE	ZE

For instance, if the operational point lies on the far left of the MPP, indicating that the error E is PB and the change in error ΔE is ZE, a substantial increase in the duty ratio ΔD is required. This MPPT technique has been extensively studied in rapidly changing weather conditions. However, its performance is significantly reliant on the user's expertise in determining the appropriate error calculation and effectively navigating the rule-based table. [1].

3.6.4 Neural networks

The artificial neural network (ANN) draws inspiration from the functioning of the human brain, although it is not an exact replica of the biological neural network. It is a machine designed to execute tasks in a manner akin to the human brain. This technique is implemented through electronic components or software on a digital computer [1]. This technique, particularly reliant on artificial intelligence, is gaining increasing popularity day by day. Its appeal lies in its array of advantages: it doesn't necessitate extensive statistical training, it's straightforward to implement, it offers simplicity, it's adept at detecting intricate nonlinear relationships between dependent and independent variables, and it doesn't demand an accurate mathematical model. Furthermore, numerous fixed-step-based MPPT techniques have been developed and enhanced. Nevertheless, certain issues persist, such as oscillations around the MPP, sluggish convergence, precision, the inability to track the MPP swiftly in rapidly changing atmospheric conditions, and diminished accuracy, particularly pronounced in shading conditions [104]. A neural network comprises of three distinct layers: the input layer, hidden layer, and output layer, as illustrated in Figure 3.21 [105].

In the input layer, the type and number of the variables vary and depend on the user's choice. For instance, the input variables for the neural network used to track the MPP of the PV array

could include open-circuit voltage V_{OC}, short-circuit current I_{SC}, atmospheric data such as irradiation and temperature. In this scenario, the output would be the duty cycle signal, which controls the switching period of the DC converter.

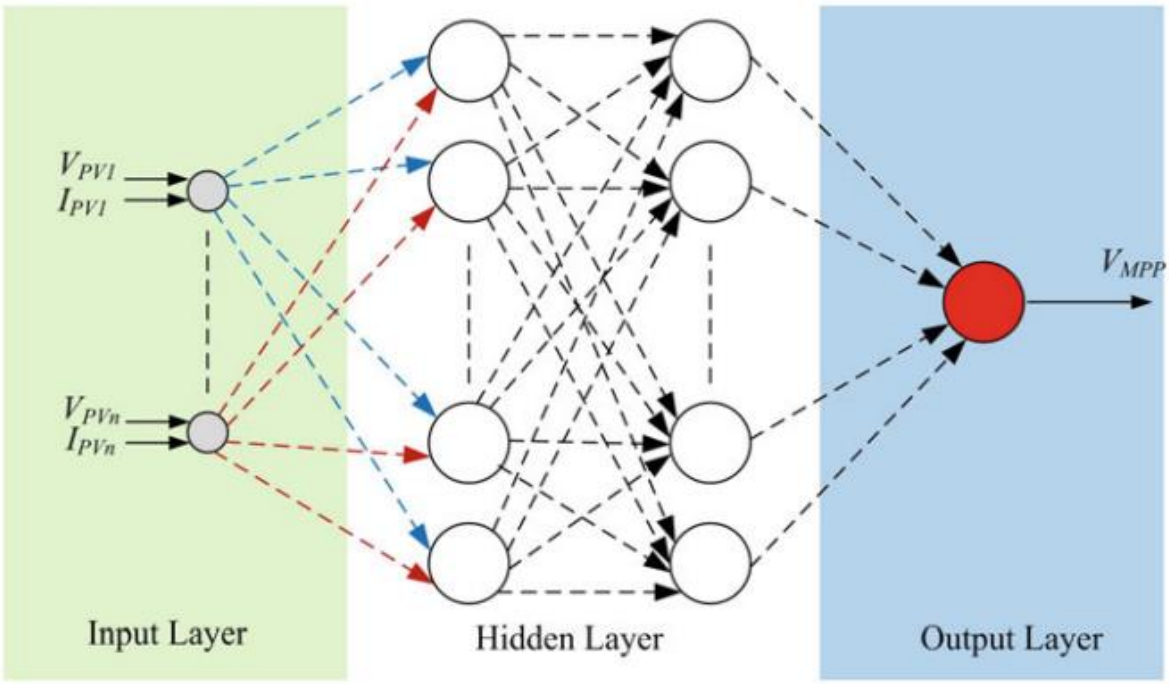

Fig. 3. 21. A neural network MPPT technique [106].

ANNs comprise a number of interconnected processors referred to as neurons, akin to cells in the human brain [1]. These neurons are linearly weighted within a function. The summation of the weighted inputs is then converted into a nonlinear function known as the activation function (AF), which is subsequently transmitted to the next layer of neurons [46]. In this technique, all neurons are integrated through a large number of weighted links. The operating point of the PV array depends on the algorithm adopted by the hidden layer and the effectiveness of training the neural network has received. The weights of these links should be appropriately adjusted to accurately extract the MPP. Usually, PV arrays are evaluated over months and years, and the relationships between the input and output variables of the neural network are established during the training process [97]. In recent studies and applications, ANN has demonstrated its ability to tackle challenging tasks related to interpretation and data processing. The process of using ANN can be broken down into four stages, beginning with training pattern generation. In this stage, offline computations are performed to cover various expected operating conditions. Next is the selection of input variables, where all parameters influencing the system's behaviour are identified and given special attention. Moving on, the stage of choosing the ANN

architecture comes into play. A multi-layered topology is the most commonly used type, consisting of an input layer, one or two hidden layers, and one output layer. Finally, there's the training and testing stage, where the training process determines the link weights that minimize errors [104].

3.7 Challenges caused by Grid-Connected PV Systems

In the majority of conventional electric power grids, power is generated by centralized generators and flows in a single direction toward the customers. However, in grid-connected solar PV systems, the generated power can flow in both directions, depending on the load demand. The challenge here is that most conventional power systems were not originally designed to handle bidirectional power flow. In remote areas, even the installation of a small number of PV systems can have an impact on grid parameters if the PV generation and the load are not well-matched [107]. With the reduction in the overall cost of installing solar systems, residential, commercial, industrial, and utility-scale entities are increasingly considering the adoption of this technology. Its appealing features, including a long lifespan (25-30 years), environmental friendliness, and minimal operational and maintenance costs, have further fuelled its popularity. However, the proliferation of grid-connected PV systems can pose certain challenges. Recent studies suggest that the hasty installation of a large number of these systems without a well-devised plan could place significant stress on the utility grid. [94]. In cases of high power production from these systems, surpassing the local power demand, the surplus power will flow through the local network, and in some instances, even though the local substations. This situation can elevate the risk of damage to the national grid and inconvenience to its customers [107]. Authors in [94] also emphasized that an increase in the installation of grid-connected photovoltaic systems (GCPVS) without simultaneous improvements in the utility grid infrastructure will result in detrimental impacts on the national network. Authors in [107] argued that the installation of large-scale solar farms necessitates substantial investments to establish the required infrastructure. This is due to the fact that large-scale PV systems are typically situated at considerable distances from consumption points, requiring extensive transmission lines. Consequently, this can lead to increased power losses in the form of heat. Authors in [108] emphasized the importance of implementing an effective control policy to manage the integration of GCPVS. Without such measures, it could pose significant challenges to the utility grid. Hossain and Ali highlighted that due to their fluctuating nature, GCPVS could potentially pose concerns for utility grids [109]. Authors in [110] stated that in the next few years, many countries will update their grid codes to

accommodate the high penetration of GCPVS and their fluctuating outputs. Additionally, new regulations will be put in place.

To address the power gap caused by the fluctuating nature of GCPVS, conventional power plants need to increase their outputs when there is insufficient power from PV systems. However, this process is technically challenging due to the time required by traditional power plants, such as steam combustion turbines and nuclear plants, to ramp up. A viable solution could involve the use of fast-ramping power plants, like gas-fired reciprocating engines and simple-cycle combustion turbines. These plants are capable of swiftly adjusting their output to alleviate stress on utility grids and can be operated as needed to bridge the energy gap. Nevertheless, this option requires years of planning, implementation, and substantial investment. Furthermore, it may not prove to be a cost-effective solution. Another critical concern is that these types of power plants operate by burning fossil fuels, which poses significant environmental challenges. To address these challenges, integrating solar systems with energy storage units has been proposed. These systems ensure a continuous power supply even after sunset. However, it's worth noting that this solution is also not cost-effective, as the cost of energy storage units remains relatively high. According to Wang and Bai, incorporating energy storage alongside solar systems could be a promising solution to enhance the reliability and stability of the system [111]. Even with these benefits, some new challenges are expected to arise since this technology is relatively new and has not been thoroughly evaluated.

3.8 Standards and requirements for safe integration of Grid- Connected PV Systems.

As the installation of distributed generator systems continues to rise, accompanied by their technical challenges, many countries have updated their grid codes and introduced new standards. These standards aim to enhance the operational process, focusing on the reliability, stability, and safe integration of grid-connected distributed generators [112]. Integrating an increasing number of PV systems into the utility grid without the introduction of proper regulations and standards may lead to significant issues regarding the integrity and stability of the grid. During the last decade, numerous industrial and academic groups have undertaken studies and evaluations of the integration of GCPVs into existing grids [94]. Their aim is to better understand the potential challenges and impacts in order to prepare effective solutions for a safe and reliable integration process. Most of these standards and guidelines related to GCPVs can be summarized as follows: [112].

- IEEE Standard 1547:

This standard, known as the Interconnecting Distributed Resources with Electric Power Systems [113], serves as a technical guideline for the integration of DG resources into national grids. It provides comprehensive information and requirements concerning the design, installation, construction, safe operation, performance, and maintenance of these systems, in alignment with local, regional, and national codes. Moreover, IEEE 1547 determines some parameters range that allow the DG to remain connected to the utility grid. These parameters encompass the power factor, voltage tolerance, frequency, anti-islanding characteristics, and fault detection. These specifications are of utmost importance to guarantee the safety of the users, other customers, and grid linemen. Within IEEE 1547, all inverters must be capable of fault detection and disconnection of the problematic part from the grid. This ensures that no power is fed into the faulty lines during maintenance, making these requirements a crucial aspect for all inverters integrated into GCPVs. Such stipulations align with those found in IEEE 929-2000 and IEC 61727 standards [114][115].

- IEEE Standard 929:

This standard applies to GCPVs and other inverter-based systems connected in parallel with the national grid, with a capacity of 10 KVA or less [116][117]. Within this standard, inverters are mandated to continuously monitor the grid to assess the behaviour of the GCPVs during irregularities. This includes monitoring synchronization loss between the grid and GCPVs, system protection, maximum trip time in cycles, and fault monitoring and isolation mechanisms [118].

- IEEE Standard 519:

This standard pertains to Recommended Practices and Requirements for Harmonic Control in Electrical Power Systems [119] [120]. It defines the acceptable range of distortion in the waveforms of current at the common coupling point (CCP) between the grid-tied system and the grid. Given the non-linear nature of voltage generated by inverters, certain harmonics are produced. These harmonic components can lead to increased heat and a greater risk of failure in the magnetic utility assets, ultimately causing power quality issues for system owners and customers. Within this standard, the acceptable limits for voltage harmonic distortion are defined as follows: 5% for normal systems, 10% for dedicated systems, and in certain exceptional circumstances, 3% at the common coupling point of the system. These limits help maintain power quality and minimize disruptions [121].

- NFPA 70:

The NFPA 70 [122], often referred to as the National Electric Code (NEC), article 690 addresses the fundamental requirements for the secure and dependable installation of PV systems. It also encompasses various crucial aspects, including ground fault protection, protection and disconnecting mechanisms for PV equipment, appropriate listing and identification of PV equipment, equipment bonding, system grounding, and wire sizing, accompanied by specific circuit protection criteria [123].

- UL standard 1741:

This standard is essential to fulfil the requirements of the IEEE 929 standard. UL standard 1741 [94] is comprehensive, addressing inverters, controllers, converters, and interconnection equipment for DG systems. It closely aligns with IEEE 1547 in three key areas: product safety, with a focus on injury prevention; coverage of various distributed generation resources, including PV systems (both grid-tied and standalone), wind, fuel cells, micro-turbines, and hydro; and regulations pertaining to the ratings, markings, and construction of these DG systems.[124].

- IEEE Standard 1547.8:

IEEE 1547.8 [125], serves as an extension of IEEE 1547, targeting larger systems ranging from 10 MVA to 20 MVA. This standard spotlights emerging technologies and industry-best practices to optimize the incorporation of DG. It hones in on specific focal points, notably the repercussions of the widespread adoption of plug-in hybrid vehicles and other energy storage systems. The standard enforces certain requirements aimed at boosting system efficiency and enhancing grid stability. One key expectation is that inverters should be capable of discerning between various fault types and general power outages. The summary of standards for grid connected DG system is shown in the Table 3.4 [94].

Table 3. 4. The summary of standards for grid connected DG system [94]

General	Safety and production	Power quality
Voltage regulation	Voltage disturbance	Harmonics mitigation
System frequency	Frequency disturbance	Direct current injection
Synchronization	Isolation device	Flicker
Monitoring provisions	Disconnect for faults	Power factor
Grounding	Reconnection	
Voltage unbalance	Anti-islanding	
Immunity	Surge capability	

3.9 Short circuit faults in grid connected PV systems.

Like most of the other renewable energy systems, in a GCPV system the PV system is integrated to the utility grid using a power electronic converter with optimised control strategy, which controls the dynamic response and stability under various conditions including normal and abnormal operation. Optimised design of the power electronic converters and associated control strategies are crucially important to maintain a reliable implementation of the system, during steady-state and transient fault conditions. With the ever-increased demand of renewable energy systems, power system authorities are more concerned about providing efficient techniques to maintain stability of the grids during abnormal operations [126]. Transient short circuit faults are one of the most common factors that make disturbance on power system and effect the power system stability. When it comes to the conventional power systems the impacts of short circuit faults are well known and well documented [127], [128]. However, in term of renewable energy resources, GCPV systems in particular, the behaviour of power system under transient short circuit scenario is still attracting more attention. Since PV systems are generally designed to deliver maximum power to the grid, they deliver the maximum power even during the fault conditions, which result in significant voltage drop at the DC busbar [129].

Due to the operating characteristics of the PV arrays and the controlled operation of the inverter, solar PV systems inject low magnitude fault currents to the grid as compared to the conventional generator [130]. For the GCPV systems, in addition to the contribution of short circuit current by the PV systems, it is crucial to analyse effects of the grid fault on the function of the PV systems. The significantly increased addition of these systems and modifications in the grid codes by regulating authorities have encouraged the researchers to evaluate the impacts of abnormal grid conditions on the various parameters of the PV systems. Moreover, key requirement for successful delivery of power from the PV systems includes various components like power electronic converters, harmonic filters, and power transformers. If the function of these components is affected due to abnormal conditions, it may cause severe disturbances in power delivery. Therefore, it is substantially important to design and evaluate a control system which can work efficiently to minimize the impacts of grid abnormalities and maintain the power system stability during and after abnormal conditions. Short circuit faults in power systems are caused by several abnormal conditions and depend on the parameters and configurations of the grid, they can inject transient fault currents of very high magnitude as compared to the rated load currents. Fault currents causes electrodynamic disruption and

significant thermal losses on power system elements, that can result sever damages [131] [132]. One approach to restrict this current is to implement suitable protective switches that can operate under short-circuit conditions, preventing damage to the power system and having the ability to isolate the faulty section of the grid. The faster these protection devices operate, the less the damage, and the greater the likelihood of maintaining system synchronization[131]. Short circuit faults are categorized to different types including symmetrical and asymmetrical short circuit faults as shown in Figure 3.22, amongst which line-to-ground (LG) faults are the most frequent, with a probability of 70 to 80 % [133]-[122].

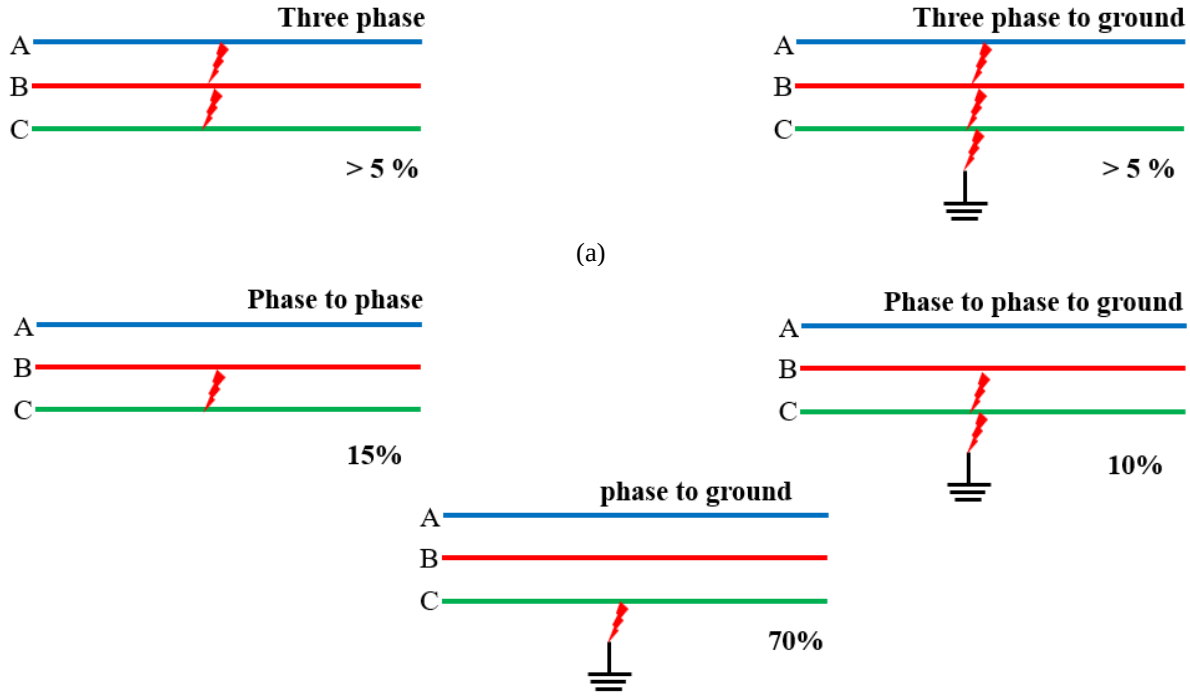

Fig. 3.22. a: Symmetrical short circuit fault; b: Asymmetrical short circuit fault.

short circuit faults in the power grid can be evaluated following different approaches as listed below [131].

1- Short-circuit currents' calculation.

2- The stability of grid connected systems and their ability to remain in synchronism up until the fault is cleared.

3- Short-circuit withstand ratings of electrical equipment such as cables, reactors, conductors, and transformers.

4- Short-circuit currents' Limitation, including the limiters of fault current as well as current-limiting fuses.

5- The impacts of short-circuit currents.

6- The switching devices' rating structure and the short-circuit currents' Interruption.

In case of a short-circuit fault, the PV system injects a certain current into the grid. The level of this current relies on the inverter's design. Whereas PV systems are configured to deliver the maximum power generated by the PV arrays into the grid, the inverter will continue injecting the same power even during a fault condition when the voltage is low. Functioning as a constant source of power, the injected current can be determined using the following equation: (3.13) [129].

$$I = (P_{PV})/V \qquad (3.13)$$

Where P_{PV} is the power generated by the PV array and V is the AC voltage. Nonetheless, the inverter restricts this current according to its predefined limits, typically set at once or twice the inverter's rated current, and it must not exceed these limits [129] [134]. In general, the short-circuit current characteristic comprises an AC component and a decaying DC component, usually diminishing in magnitude over time. Short-circuit faults can be divided into three periods: the sub-transient period, which occurs during the first few cycles after the fault started, followed by the transient period, and ultimately, the steady-state period. It's important to note that most faults are cleared before reaching the steady-state period, refer to the diagram shown in Figure 3.23 [135][136].

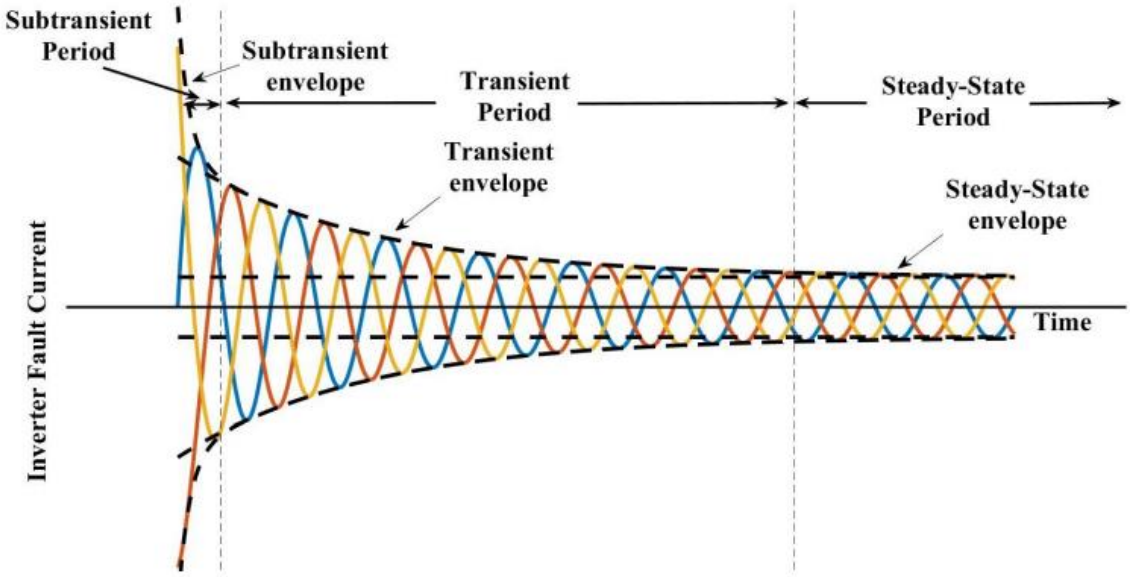

Fig. 3. 23. Transient periods of a three phase symmetric short circuit fault current [136].

GCPV systems are the most widely installed, in comparison to standalone systems [137][138]. Integrating GCPV systems with the utility grid using Voltage Source Converters (VSCs) has become a common practice [139]. These converters protect themselves against overloading by utilizing saturating current [140][141]. In the steady-state analysis of GCPV systems, it is crucial to consider the operation mode of Voltage Source Converters (VSCs), especially in terms of short-circuit analysis. It's important to note that VSCs can operate in a current-saturated state when the voltage is reduced. Therefore, various operation and control modes of VSCs, including current-saturation states, need to be taken into account when analysing short-circuit faults in GCPV systems. This consideration is vital due to the significance of the information provided by short-circuit fault analysis for the design of GCPV systems. This analysis helps to determine short-circuit equilibrium points, which serve as the foundation for the safe and reliable sizing of various system components, including cables, transformers, circuit breakers, and more. In GCPV systems, the sizing of protection components relies on the current levels that the systems may encounter at different locations when subjected to various fault scenarios [142]. The appropriate selection of short-circuit equilibrium points plays a crucial role in establishing a robust control strategy for the power converter. This strategy ensures not only high performance but also reliability, even under fault conditions. Additionally, it empowers the system with the capability for a safe and swift recovery once the fault is cleared [143]. Furthermore, short-circuit equilibrium points offer valuable insights into determining when the system should remain connected or disconnected during various fault conditions [144]. The design of the converter controller typically relies on an estimation of grid strength. Therefore, the results of short-circuit analysis facilitate an adaptive control of converters, thereby enhancing the system's dynamic performance, both during and after a fault. This is particularly crucial for applications connected to a weak grid [145]. As mentioned previously, many countries have updated their grid codes and introduced new requirements for integrating grid-tied systems into the utility grid. Among these requirements, Low Voltage Ride-Through (LVRT) is of utmost importance as it deals with the most frequent disturbance condition in the grid, which is the occurrence of grid faults and their impact on connected renewable energy systems. For this condition, LVRT regulations are devised for monitoring of system’s stability under fault conditions [146]. LVRT is a condition during which all Renewable Energy Systems (RESs) must continue operating for a specified period to guarantee that the occurred fault is transient [147]. In other word, LVRT is ability of the RESs to continue operating even during a voltage sag caused by a fault [148].

Before RES power plants can be integrated into the power grid, several tests must be conducted to evaluate their compatibility with the grid. These tests typically involve examining voltage and current fluctuations, power quality, LVRT capability, high-voltage ride through (HVRT) capability, reactive power compensation, and safety while operating in anti-islanding mode. These tests aim to assess whether the RES farms can function in compliance with the grid standards [146].

In the past LVRT requirements were mainly applied to wind turbines. This was because occurrence of three-phase fault on a transmission line could cause a complete loss of voltage at the fault point until the fault is cleared, resulting in a loss of power generation. However, with the increasing development of integrated solar power plants, there is a need to consider LVRT requirements for solar plants as well [147]-[146]. This is because when any disturbances or faults occur, complete interruption of power delivered by the solar farm can be unreliable and may lead to blackouts. Hence, it is recommended to validate LVRT capability before integrating RES with the grid. LVRT capability is generally evaluated for PV systems in the laboratory via LVRT test units [146] . In grid integrated renewable energy resources, LVRT capability is evaluated to keep converter connected with the grid during temporary fault as well as for transient stability and smooth resynchronisation when fault is cleared[149]. Figure 3.24 shows the LVRT requirements for different countries.

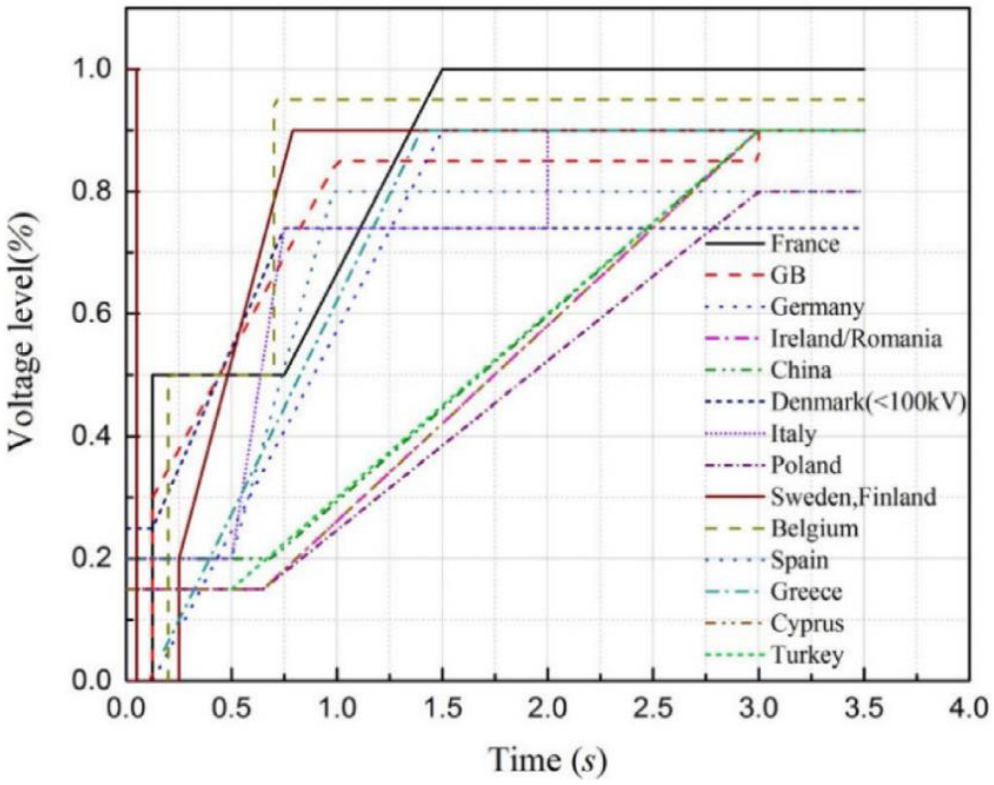

Fig. 3. 24. LVRT requirements for several countries [146].

3.10 Previous related work

Numerous studies and research related to the same field have been presented in the literature over the last two decades. For instance, the author in [150] presented a MATLAB/Simulink model for a single-phase grid-connected PV inverter, which was also experimentally tested. The study implemented the P&O MPPT technique, and the results showed that this model effectively simulates the behaviour of a single-phase grid-connected PV system. An implementation of a single-stage grid-connected PV system was proposed in [151], where all control strategies, including MPPT, harmonics reduction, and synchronization with national grid requirements, are integrated into one point. However, this approach increases the complexity of the overall control strategy. The incremental conductance technique was applied for MPPT, resulting in high efficiency and stability of the system. Reference [152], presents the design and simulation of a 100 kW hybrid grid-connected PV system. The system was designed using the MATLAB/SIMULINK environment. MPPT techniques were employed to extract maximum power available from the PV array, and a DC-DC boost converter was used to increase the level of DC voltage at the DC link busbar. The author in [153], presented a case study on designing a grid-connected PV system for the EEU building in Hawassa city. A detailed analysis of the system's power output was provided, utilizing average monthly sunshine hours to assess the effect of local solar irradiance on its performance. Moreover, various meteorological data were employed for this study. As a result, a small grid-connected PV system was installed at the EEU building. The performance of a 110 kWp grid-connected PV system installed on the rooftop of a residential hostel at MANIT, Bhopal, India, was presented in [85]. SolarGis PV planner software was used to assess the performance of different PV technologies, focusing on energy yield and performance ratio. The results show that Amorphous silicon (a-Si) and Cadmium telluride (CdTe) have performance ratios higher than 75%. The author in [154] presents a simulation study of a double-stage grid-connected PV system. The system was evaluated under two scenarios: integration to the local low-voltage grid or to the national high-voltage grid, and then compared with the existing system installed on the roof of the National Water Research Centre. The results indicate that economically, the system could save up to 235.8 thousand L.E./year when connected to the national grid, compared to 100 thousand L.E./year for the current system. A detailed modelling and control for a grid-connected PV system using MATLAB software was presented in [155] The author demonstrates a comprehensive explanation of the modelling and control of PV systems, as well as reviews different inverter topologies for such systems.

A comparison of the performance of various MPPT techniques for single-stage grid-connected PV systems was presented in [156] The results demonstrated that conventional Hill Climbing and Incremental Conductance techniques were the slowest in tracking the MPP of the system, while the modified Hill Climbing method was more accurate, with relatively small oscillations of power around the MPP. Another comparison was conducted in [97] with 19 MPPT techniques included in the study. The authors concluded that numerous MPPT techniques are available for application in PV systems. However, it is challenging to specify which one is superior. Therefore, they have identified various aspects that can aid in selecting the suitable MPPT technique for each system. These aspects include implementation, number of sensors, accuracy, performance under different weather conditions, costs, and applications. Reference [100], presents a combination of incremental conductance and integral regulator considered to extract the MP of a grid-connected PV system. The outcome of this study shows that such a combination brings high accuracy, stable operation, and mitigates the oscillations around the MPP. The author used MATLAB software to simulate the system. Author in [157] stated that while there are plenty of MPPT techniques, the Perturb and Observe (P&O) MPPT technique is considered the most common one due to its simplicity, requiring only two sensors, and its low implementation cost. On the other hand, the author in [96] presents a comparative study between two of the most common MPPT techniques, P&O and Incremental Conductance (INC), for grid-connected PV systems. The results show that the INC technique is faster in tracking the MPP and has the ability to track the MPP more accurately during rapidly changing weather conditions. The study used MATLAB software to conduct the study. Reference [142] presents a detailed analysis of short-circuit faults for grid-connected PV systems. The author stated that Thèvenin's theorem is one of the widely used methods to calculate the short-circuit current and specify the short-circuit equilibrium point. However, the short-circuit analysis can be carried out from different aspects which are mentioned in Section 3.9. A new grid support strategy for GCPV systems was presented in[143] A new grid support strategy for GCPV systems was presented in [14]. The study investigates the short-term voltage stability of the distributed generation (DG) under asymmetrical faults. The results show that the new strategy does not require accurate, fast estimation of the grid impedance at the PCC. Additionally, the new strategy demonstrated its ability to improve short-term voltage stability during voltage issues. A review study of different components of the GCPV system was presented in [91]. The study includes various topologies of grid-connected inverters. The performance of GCPV systems, including MPPT [158]-[159], harmonic emission [160], power quality aspects [161]-[162], islanding detection techniques [160], and new fault detection approach in grid connected

PV system [163] an adaptive FRT capability of virtual synchronous machine control for grid forming converter [164] , have been investigated by other researchers.

3.11 Conclusions

This chapter delves into grid-connected PV systems from various angles. It begins by exploring the primary components of the system, moves on to discuss control strategies, and delves into the challenges and issues these systems face when it comes to integration with the grid. Various standards are also covered, along with the latest requirements introduced by new grid codes. Additionally, this chapter explores the most recent research activities related to such systems. Furthermore, based on the aforementioned information, a double-stage grid-connected PV system was chosen due to its advantageous features over alternative configurations. This configuration enhances the overall controllability of the system. In contrast, in the alternative configuration, all control strategies, including MPPT, harmonics reduction, and synchronization with national grid requirements, are integrated into a single stage. This integration increases the complexity of the overall control strategy.

Moreover, the P&O MPPT technique was employed to extract the maximum power from the PV array. This selection was made for several reasons. Firstly, the P&O technique requires only two sensors, resulting in a lower implementation cost. Additionally, its simplicity makes it an attractive choice for the system design. Numerous developments have been made on this technique over the last few decades. However, the conventional approach was chosen for this study. The primary reason for this decision is to provide insights to decision-makers in Libya regarding the behaviour of such systems under their lowest expected performance conditions.

Moreover, a multistring PV inverter was selected for this study because this configuration can only be implemented with a double-stage configuration. By employing this type of inverter, the number of inverters required can be reduced, thereby lowering the overall cost of the system. Finally, a short-circuit fault analysis will be conducted to evaluate the LVRT capability of the system under this type of fault. This analysis is crucial as it is one of the most important requirements for the integration of GCPV systems.

Chapter 4:

The Principle of Dynamic Modelling for Grid-Connected PV System

4.1 Introduction

Following the literature review the key objectives of this project have been defined which include an overview of solar energy technology, as well as the current energy situation in Libya, which is the primary reason this project is being carried out. Moreover, in term of the PV system, the project has taken the essential steps towards modelling a practical grid-connected photovoltaic (GCPV) solar system; with the aid of MATLAB/SIMULINK software.

4.2 System description

In this thesis, a GCPV system is modelled and integrated with the utility grid. The system is a three-phase, two-stage GCPV system, and it was designed using the Simscape Electrical toolbox of MATLAB/SIMULINK. Figure 4.1 illustrates a schematic diagram of the simulated system. This system is composed of a PV array, a DC-DC boost converter, an MPPT control unit, an inverter with Voltage source converter VSC control, an LC filter, and a step-up power transformer.

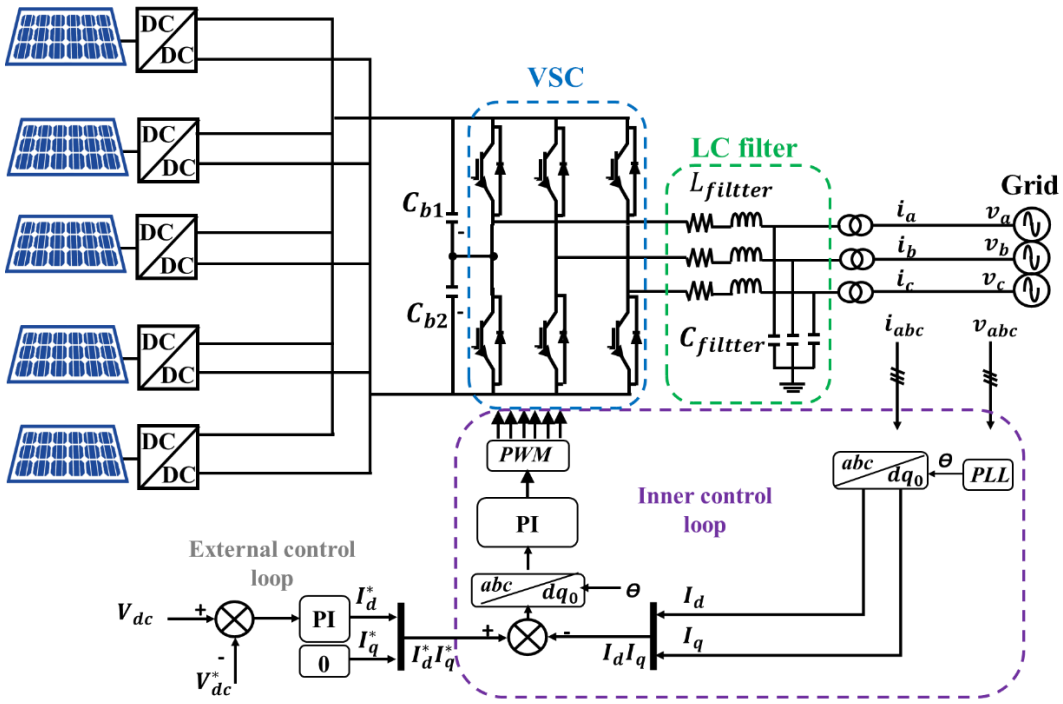

Fig. 4. 1. Schematic diagram of a GCPV system

The PV generator consists of five parallel units, each with a rated power of 400 kW, providing a total power of 2 MW. Each PV array comprises 255 shunt strings, with 5 modules connected in every string. The PV module used in the system is the SunPower SPR-315E-WHT-D, with a maximum power rating of 315 W per module. The constraints of the PV module are presented in Table 4.1.

Table 4. 1. Parameters of the PV module

SunPower SPR-315E -WHT-D		
Parameter	***Unite***	***Value***
Maximum Power ***mpp***	W	315
Cells per module	-	96
Open Circuit Voltage ***Voc***	V	65
Short circuit current ***Isc***	A	6
Voltage at maximum power point ***Vmpp***	V	55
Current at maximum power point ***Impp***	A	6
Temperature coefficient of ***Voc***	°C	-0.2727
Temperature coefficient of ***Isc***	°C	0.0617
Diode ideality factor	-	0.9507
Series Resistance ***Rs***	Ω	0.4304
Shunt Resistance ***Rsh***	Ω	430

In this system, each PV array is linked to a DC-DC boost converter and subsequently connected to the grid through a Voltage Source Converter (VSC) to convert the generated DC voltage into AC voltage. Over the past few decades, various PV system topologies have been introduced. Among them, the multi-string structure is the most commonly utilized topology for PV system installations [165] [166]. In this system each PV array is linked to its own DC-DC converter to boost the DC voltage in the DC bus. Then, all the PV arrays, along with their DC-DC converters, are connected to a centralized DC-AC inverter, which is used to connect with the utility grid. The key advantages of this topology include enhanced power source protection, safety during maintenance and installation, independent control, and cost-effectiveness. The DC-DC converter provides a pathway for implementing maximum power point tracking (MPPT) to extract the maximum power from the PV array. Various types of DC-DC converters exist, with Boost and Buck converters being the most commonly used DC/DC topologies. [1]. The multiple PV arrays are connected at a common point along with the DC link capacitors in the DC bus, and then they are linked to the DC side of the VSC. The DC link capacitors play a crucial role in regulating the DC voltage at the input terminal of the VSC. Subsequently, the output from the VSC is injected into an LC filter to get rid of high-frequency components

introduced in the generated signals. The I-V and P-V characteristics of the PV array implemented in this work for different levels of solar irradiance and temperature values are exhibited in Figure 4.2-a and 4.2-b, respectively.

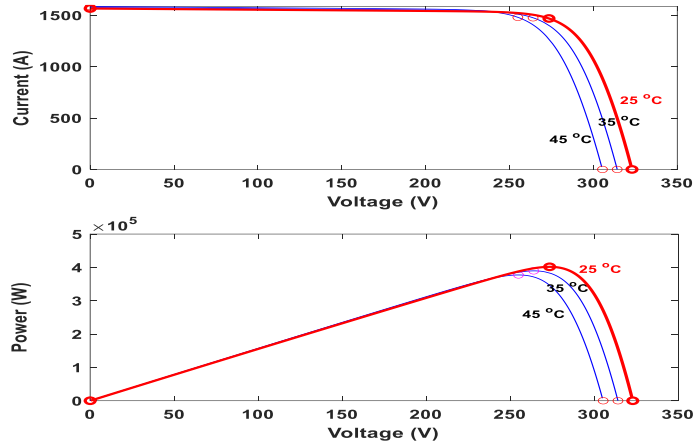

(a)

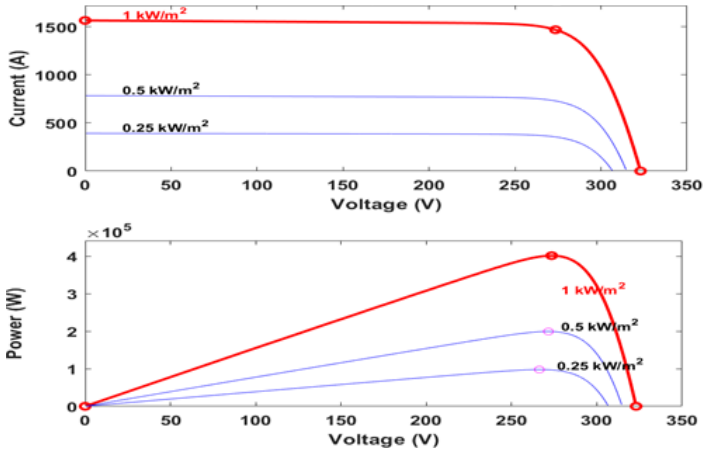

(b)

Fig. 4. 2. The I-V and P-V characteristics of the PV array (a) at varying temperature (b) at varying irradiance

4.2.1 Modelling of PV array

A solar cell is considered as the most important element in the PV solar system, where several cells are connected in series to form the PV module. Meanwhile, a combination of panels in parallel and series form a complete PV array. A basic diagram of a single diode PV cell is shown in Figure 4.3 [167]. Equation (4.1) illustrates the fundamentals of the PV cell:

$$I = I_{Ph} - I_D - I_{SH} \quad (4.1)$$

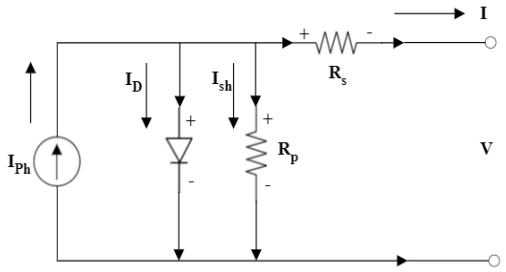

Fig. 4. 3. Single diode model of PV cell [168]**.**

where, I is the current generated by a solar cell, I_{Ph} is the photon current, I_D is the diode current and I_{SH} is the current flow through shunt resistor R_P. Whereas, the diode current can be given by using the following equation [169]:

$$I_D = I_O \left[exp\left(\frac{V + I\,R_S}{a\,V_{th}}\right) - 1 \right] \tag{4.2}$$

Additionally, the current that flows through the shunt resistance I_{SH} can be calculated using equation (4.3), as follows:

$$I_{SH} = \frac{V + I\,R_S}{R_P} \tag{4.3}$$

Therefore, equation (4.1) can be rewritten to produce a new equation, as follows:

$$I = I_{Ph} - I_O \left[exp\left(\frac{V + I\,R_S}{a\,V_{th}}\right) - 1 \right] - \frac{V + I\,R_S}{R_P} \tag{4.4}$$

where, I_O is the reverse saturation current, R_S and R_P are the series and shunt resistance of a PV cell respectively, a is diode ideality factor, V_{th} is the thermal voltage which is given by:

$$V_{th} = \frac{KT}{q} \tag{4.5}$$

where, $K = 1.38 * 10^{-23}$ J/K is Boltzmann constant, T is the cell temperature an $q = 1.6 * 10^{-19}$ C is the charge of an electron.

However, all previous equations relate to only one solar cell. Therefore, in order to calculate the energy production from the PV array, there are a number of parameters to consider. It is important to know the total number of cells connected in series N that form a solar panel/module and from the numbers of series N_s and parallel N_p connected solar panels. The current equation for a PV array is given by:

$$I = N_P I_{Ph} - N_P I_O \left[exp\left(\frac{\frac{V+I\,R_S}{N_S}}{a\,N\,V_{th}} \right) - 1 \right] - \frac{V+I\,R_S}{R_P} \qquad (4.6)$$

With the purpose of modelling a PV array, all parameters in equation (4.6) must be provided to get the energy output of the PV array. However, not all parameters are provided in the solar module datasheets. Furthermore, some parameters depend upon the materials that the solar cells are made of, so they are provided by the manufacturer. These parameters are the diode ideality factor a and Energy gap E_g values [168]. The relation between R_S and R_P can be extracted by assuming $P_{max}\ datasheet = P_{max}\ calculated$ and solving the resulting equation for R_S, as shown below [170] [168]:

$$\mathrm{P_{max\,calculated}} = \mathrm{V_{mpp}} \times \left(\mathrm{I_{pv}} - \mathrm{I_o} \left[\exp\left(\frac{\mathrm{V_{mpp}+IR_s}}{\mathrm{V_t a}} \right) - 1 \right] - \frac{\mathrm{V_{mpp}+R_s I}}{\mathrm{R_p}} \right) \qquad (4.7)$$

Rewriting equation (4.7) R_p can be realised as follow:

$$R_P = \frac{V_{mpp}\left(V_{mpp} \times I_{mpp} R_S\right)}{V_{mpp} I_{pv} - V_{mpp} I_o \left[exp\left(\frac{V_{mpp}+R_S I}{V_t a} \right) - 1 \right] + V_{mpp} I_o - P_{max}} \qquad (4.8)$$

Thus, for any value of R_s, there will be a corresponding value of R_p that causes the mathematical I–V curve to intersect with the experimental (V_{mp}, I_{mp}) point. The objective here is to determine the value of R_S (and consequently,R_P) that aligns the peak of the mathematical P–V with the experimental peak power at the (V_{mp}, I_{mp}) point. his process necessitates several iterations until $Pmax\ datasheet = Pmax\ calculated$. Each iteration updates R_S and R_P in order to reach the best model solution [1].

These values are obtained at standard conditions. Calculating R_S and R_P for the PV array at different temperature can be given by:

$$R_s = \frac{R_S\,N_s}{N_p} \qquad (4.9)$$

$$R_P = \frac{R_P\,N_s}{N_p} \qquad (4.10)$$

Temperature and the solar radiation have a direct influence on the photon current. Therefore, the photon current can be calculated by adopting the following equation [171]:

$$I_{Ph} = \left[I_{Phn} + KI\left(T - T_{ref}\right) \right] * \frac{G}{G_N} \qquad (4.11)$$

Here I_{Phn} is the photon current value at reference conditions, KI is the current temperature coefficient, $T_{ref} = 273.19\ K$ is the reference temperature, T is the cell temperature, G is the irradiance value and G_N is the irradiance value at standard temperature.

On the other hand, it is very important to calculate the reverse saturation current at any temperature in order to obtain the diode current, which is the second unknown in equation (4.1). Therefore, the reverse saturation current at standard condition must be calculated first as given by:

$$I_{on} = \frac{I_{scn}}{exp\left(\frac{V_{ocn}}{a\ N\ V_{th}}\right)-1} \tag{4.12}$$

Hence, the reverse saturation current at any temperature can be calculated by using:

$$I_o = I_{on}\ (\frac{T}{T_{ref}})^3 exp\left[q\ E_g\ \frac{\left(\frac{1}{T}-\frac{1}{T_{ref}}\right)}{Ka}\right] \tag{4.13}$$

where, I_{on} is reverse saturation current at standard temperature, E_g is energy gap value. Consequently, the current that flows through the diode in the PV array can be given by (4.14) [102]:

$$I_D = I_O\left[exp\left(\frac{\frac{V+I\ R_S}{N_S}}{a\ N\ V_{th}}\right)-1\right] \tag{4.14}$$

Therefore, a complete modelling of the PV array and the current output from the PV array can be calculated using equation (4.6).

4.2.2 DC-DC Boost Converter

Second part of the system is the DC-DC boost converter which is implemented to boost the voltage level supplied by the PV array. A DC-DC boost converter is responsible to boost the DC voltage generated by the PV array, V_{PV}, as well as to create a channel to apply the MPPT technique which improve the voltage quality and controllability of the system [7]-[92]. For the presented system, the average model of boost converter was used in which the voltage source was directly controlled by the reference voltage. An equivalent circuit of the boost converter is shown in Figure 4.10 [172].

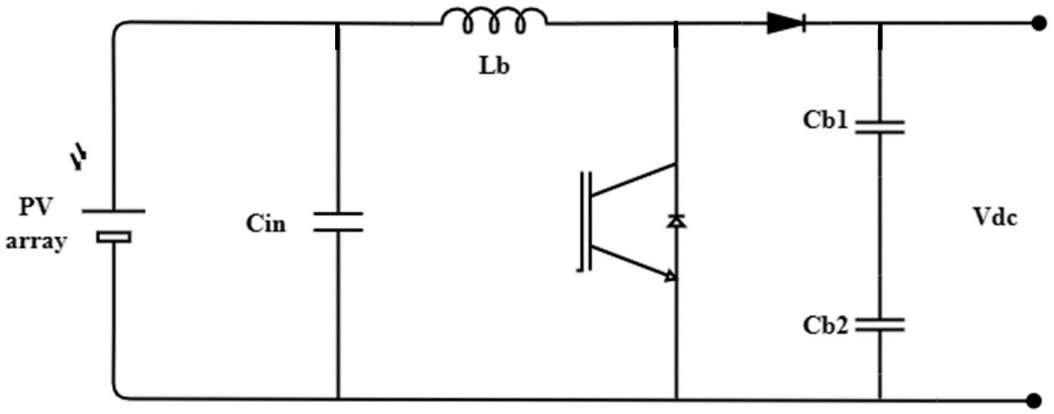

Fig. 4. 4.The average model of DC-DC boost converter [7].

The output of the boost converter is controlled by the MPPT unit which regulates the converter's duty cycle [93]. The duty cycle of the boost converter is given by:

$$D = 1 - \frac{V_{in}}{V_{out}} \tag{4.15}$$

where D is the duty cycle, $V_{in} = V_{PV}$ is the input voltage, and V_{out} is the output voltage and presents the DC link voltage V_{DC}. The values of its inductor and capacitor are given using equations (4.16) and (4.17) [1]:

$$L_b = \frac{V_{in} * D(1-D)}{\Delta I_L * f} \tag{4.16}$$

$$C_{b1} = C_{b2} = \frac{V_{in} * D(1-D)}{8 L_b \Delta V_C f^2} \tag{4.17}$$

where ΔI_L is the current ripple ΔV_C is the voltage ripple and f is the switching frequency. V_{DC} can be calculated as a function of the input voltage V_{PV} and the duty cycle of the converter. The parameters used for this boost converter are shown in Table 4.2 which are calculated based on equations (4.16) to (4.17).

Output of the DC-DC converter is then delivered to the inverter which converts the DC voltage to a Pulse Width Modulation (PWM) voltage. The output of the inverter is finally filtered using

a harmonic filter for suppression of higher frequency components and to get THD of the current and voltage below 5 % standard level as stated by the IEEE std.519 [121][173].

Table 4. 2. Parameters of the boost converter

Parameter	Symbol	Value
Input Voltage	V_{PV}	273 V
Output Voltage	V_{DC}	500 V
Inductor	L	5 mH
Input Capacitor	C_{in}	100 µF
Output Capacitor	C_b	2 F

4.2.3 LC filter

With reference to the international standards and utility grid codes it is very important to maintain the THD level of Voltage and Current for grid connected renewable energy resources below the 5% at the CCP as stated in IEEE Std. 519 and IEEE 1547-2008. [173]-[174]. Furthermore, the output voltage from the inverter contains high frequency components resulting in high level of THD which is not accepted as injecting these signals directly to the grid have destructive impacts on the grid components including accosting noise, mechanical vibration and overheating for transformer. Therefore, it is very important to filter these signals and get rid of the high frequency components and maintains the THD level at an acceptable level. In this context an LC filter was used to ensure that the output signal generated by the inverter is filtered before it injected to the transformer then the grid, as shown in Figure 4.11 highlighted in dashed green box[175]. To determine the values of the filter inductance and capacitor some other parameters are needed including current ripple, grid frequency, line to line voltage and rated power. The maximum current ripple can be calculated using (4.18) [176].

$$\Delta I_{L,max} = \frac{2V_{DC}}{3Lf_{sw}} m(m-1) \quad (4.18)$$

where f_{sw} is the inverter switching frequency m is the modulation index, so the filter inductor can be calculated using (4.19) [95].

$$L_f = \frac{V_{DC}}{6\Delta I_{L,max} f_{sw}} \quad (4.19)$$

where L_f is the filter inductor V_{DC} is the DC link voltage, usually the current ripple is counted as 5-25% of the maximum current which can be calculated by (4.20):

$$I_{L,max} = \frac{P_n\sqrt{2}}{3v_{ph}} \quad (4.20)$$

where v_{ph} indicates the RMS phase voltage, and the value of the capacitor is calculated based on the acceptable range of variation in reactive power at CCP which is considered 10% of the inverter rated power [176].

4.3 Control System Strategy

A schematic diagram of the developed control system is shown in Figure 4.11. This control system consists of two main parts: DC controller based on MPPT algorithm, and VSC control scheme for the inverter. These two parts are explained in the following subsections.

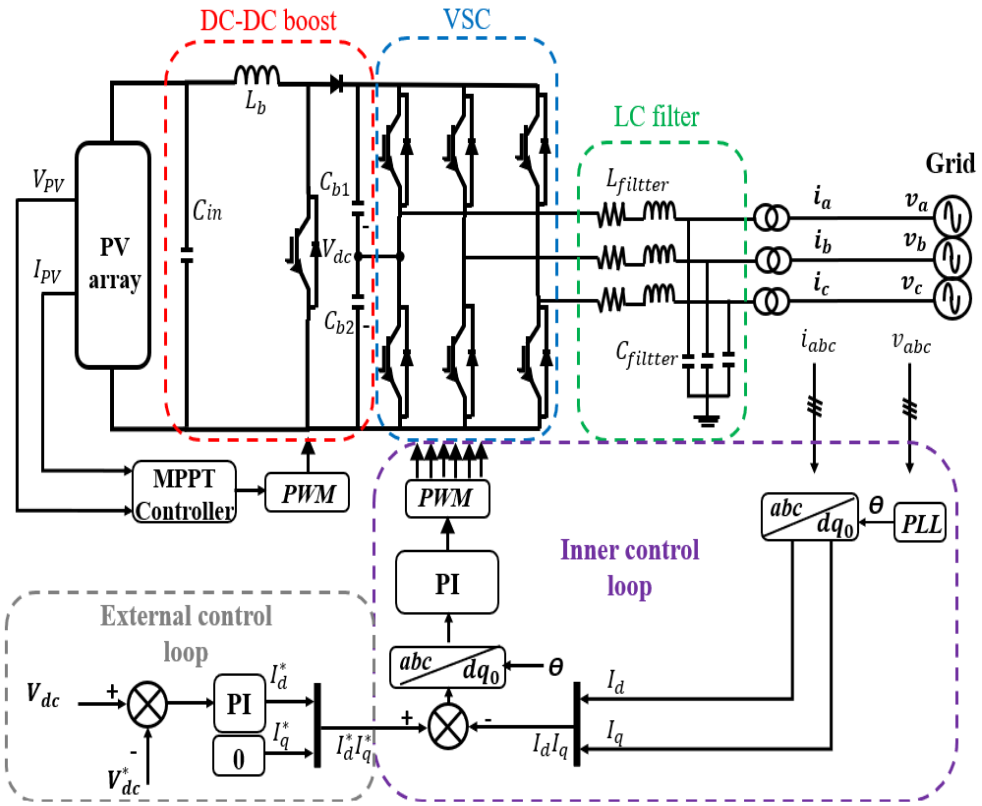

Fig. 4. 5. Block diagram of the control system of the GCPVs

4.3.1 MPPT control scheme:

The control system on the DC side is designed for maximum power extraction and to increase the voltage level of the PV array. A Perturb and Observe (P&O) algorithm based MPPT scheme was used for MPPT operation [1]. Based on the output voltage and current from the PV array, the P&O algorithm determines the duty cycle of the DC-DC converter. A flowchart of the P&O algorithm is shown in Figure 4.12.

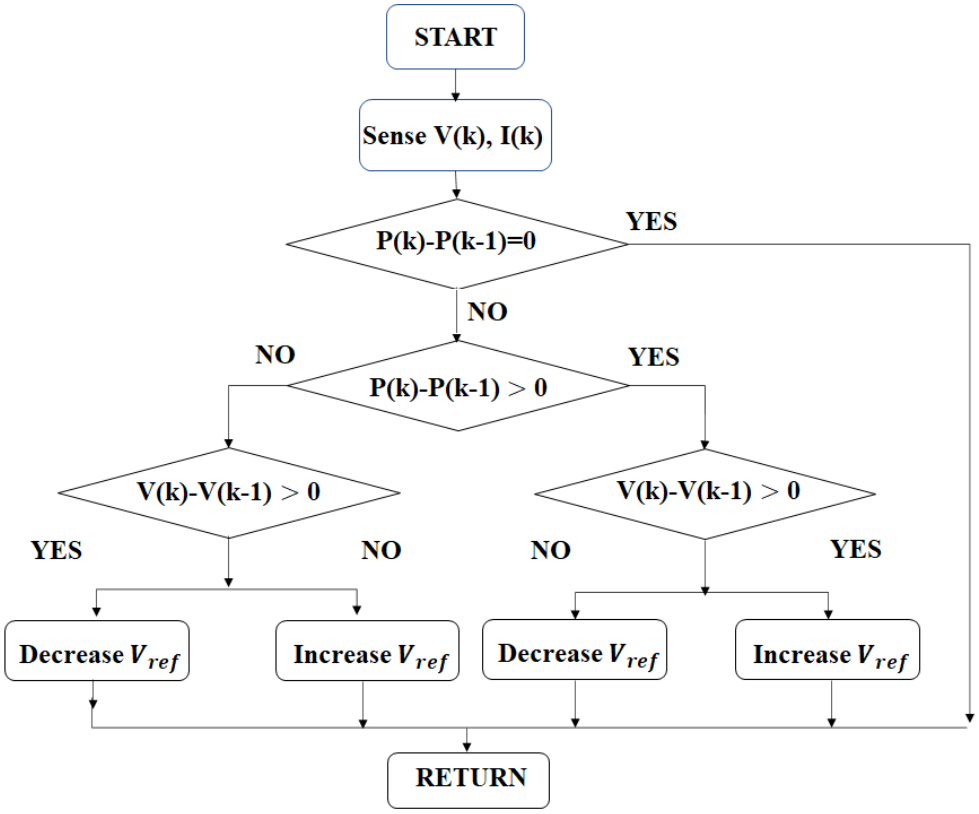

Fig. 4. 6. Flowchart for P&O MPPT technique

This algorithm determines the DC/DC converter's duty cycle based on the input parameters, i.e., voltage and current from the PV array. Output voltage of the boost converter is regulated according to the reference values. The MPPT technique and associated algorithm are implemented to obtain the maximum power from the PV array, and output power of the system according to the voltage variation [158]. In this control scheme, voltage is perturbed according to the response of the system to the previous perturb to determine the direction of the next perturbation [97]. PV characteristic curve and principle of the P&O MPPT technique are shown in Figure 4.13 and Table 4.3, respectively.

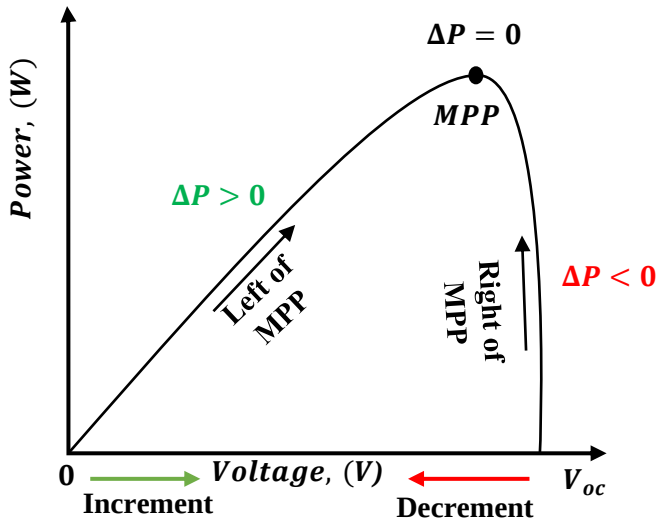

Fig. 4. 7. PV characteristics of P&O MPPT technique

It can be seen that for $\Delta P > 0$, power is increased with increasing in the voltage until MPP is achieved. After attaining MPP, where $\Delta P < 0$, any attempt to increase the voltage results in decreasing the power. Accordingly, if the power increases with the increase or decrease in the voltage, the successive perturbation remains in the same direction until MPP is achieved. On the other hand, if power decreases with the increase or decrease in voltage, the following perturbation will be reversed, as shown in Table 4.3. After reaching the MPP, the system will be continuously oscillating around this point. Level of the fluctuations across the MPP depends on the step size of the applied voltage. However, to reduce this fluctuation, smaller step-size can be used, which may slow down the MPPT process to reach the MPP [97].

Table 4. 3. Principle of the P&O algorithm

Perturbation	Change in Power	Next perturbation
Positive	Positive	Positive
Positive	Negative	Negative
Negative	Positive	Negative
Negative	Negative	Positive

4.3.2 Control strategy of the VSC:

A block diagram and the simulation model of the designed control system of the VSC is shown in Figures 4.14-a and 4.14.b, respectively. In this control system, the VSC-based control scheme is synchronized to the CCP using phase locked loop (PLL) unit which generates a reference Phase angle ω_t [177]. The error signal e_{Vdc} between the DC link voltage, generated by comparing V_{dc} and its corresponding reference value $V_{dc,ref}$, is fed to the compensator whose output u_{Vdc} is processed by a limiter to generate reference current value $I_{d,ref}$.

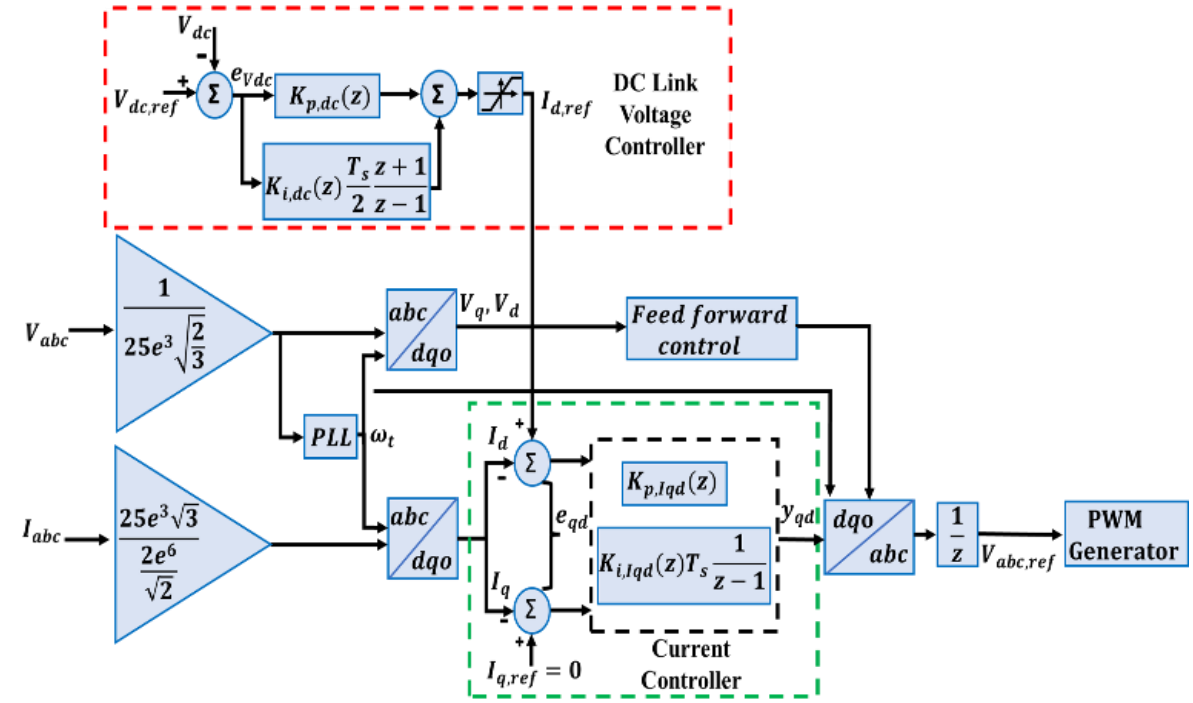

(a)

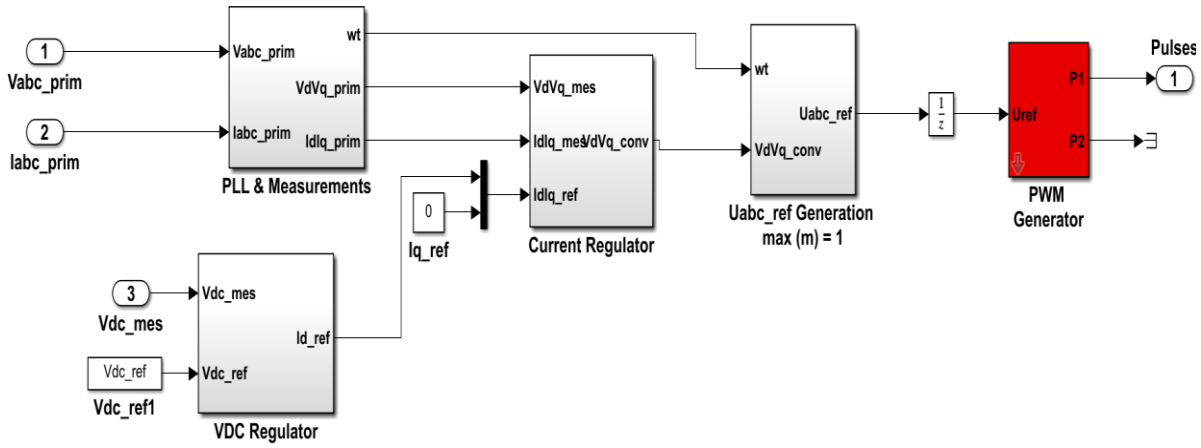

(b)

Fig. 4. 8. (a): Block diagram and (b) Simulation model of VSC control strategy.

For this system the transfer function of the control unit was determined using Z transformation, so the output U_{Vdc} can be presented mathematically as [178].

$$U_{Vdc}(z) = E_{Vdc}(z)[K_{p,dc}(z) + K_{i,dc}(z)\left(\frac{T_s}{2}\frac{z+1}{z-1}\right)] \tag{4.21}$$

where:

$$e_{Vdc} = V_{DC} - V_{DCref}\ ,\ U_{Vdc}(z) = Z(u_{Vdc}) \tag{4.22}$$

and

$$E_{Vdc}(Z) = Z(e_{Vdc}) \tag{4.23}$$

The reference signal $I_{d,ref}$ is then delivered to the current controller block. Three phase grid voltage V_{abc} and current I_{abc} are attained from the grid and converted to per unit values. After conversion, these signals are transformed to the $dq0$ reference, which is presented as ($V_d,\ V_q$) and ($I_d,\ I_q$) for the voltage and current, respectively. This transformation is given by (4.24) [179].

$$\begin{bmatrix} v_d \\ v_q \\ v_0 \end{bmatrix} = \sqrt{\frac{2}{3}} \begin{bmatrix} \cos\theta & \cos\left(\theta - \frac{2\pi}{3}\right) & \cos\left(\theta + \frac{2\pi}{3}\right) \\ -\sin\theta & -\sin\left(\theta - \frac{2\pi}{3}\right) & -\sin\left(\theta + \frac{2\pi}{3}\right) \\ \frac{1}{\sqrt{2}} & \frac{1}{\sqrt{2}} & \frac{1}{\sqrt{2}} \end{bmatrix} \begin{bmatrix} v_a \\ v_b \\ v_c \end{bmatrix} \tag{4.24}$$

Where:

$$\theta = \omega t - \frac{\pi}{2} \tag{4.25}$$

Voltage components V_d and V_q are then processed for feed forward control, which play a very important role in improving the stability of the PV system by offsetting the nonlinear characteristics of the PV arrays. The d-q components of the current, I_d and I_q, are then processed through the PI controller. For this purpose, the signals are compared with reference values, $I_{d,ref}$ and $I_{q,ref}$. These I_d and I_q components are decoupled for independent control of the active and reactive power respectively. The presented system was operated at unity power factor so $I_{q,ref}$ is set to zero [180]-[181]. Reference current $I_{d,ref}$ is obtained from the DC link voltage controller based on the values of V_{dc} and $V_{dc,ref}$ and is compared with the d-component of the grid currents, I_d. Current reference value obtained from DC control block $I_{d,ref}$ was used to

track the signal I_d and to generate error signal e_{qd}. This error signal is processed by the respective controller to provide the output y_{qd} of the current controller which can be given as: where:

$$Y_{qd}(z) = Z(y_{qd}) \text{ and } E_{qd}(z) = Z(e_{qd}) \quad (4.27)$$

The output y_{qd} represents the signal to generate reference voltage $V_{abc,ref}$ which is delivered to the PWM generator to generate pulses signals for the inverter operation. Figure 4.15 shows the simulation model for the entire system.

$$Y_{qd}(z) = E_{qd}(z)\left[K_{p,Iqd}(z) + K_{i,Iqd}(z)\left(T_s \frac{1}{z-1}\right)\right] \quad (4.26)$$

The tuning of the integral and proportional gains of the PI controller was specified using the tuning options available within the PI controller toolbox provided by MATLAB/Simulink. This tuning procedure has undergone multiple iterations to attain rapid and precise performance in tracking the MPP of the system. The values of the K_p and K_i of the V_{DC} regulator gains were 7 and 800 respectively. On the other hand, the values of the K_p and K_i of the current regulator were 0.3 and 20 respectively.

4.4 The PV system power output

The power generated by the PV system depends on two main factors: ambient temperature T_{amb} and solar irradiance. Therefore, the output power of the PV system at a selected site can be calculated as follows: [182] [183].

$$P_{PV} = N_{PV} * P_r^{PV}\left(G/G_{ref}\right)\left[1 + T_{cof}\left(T_c - T_{ref}\right)\right] \quad (4.28)$$

where N_{PV} is the number of the PV modules used in the system P_r^{PV} is the rated power of the PV panel (W), G is the incident solar irradiance (W/m^2), G_{ref} is the irradiance value at standard temperature which is constant at a value of 1000 (W/m^2) , T_{cof} is the PV module temperature coefficient, usually $-3.7 * 10^{-3}(1/℃)$ in term of poly and monocrystalline silicon PV modules [184] [185]. T_c is the cell temperature, T_{ref} is the temperature at standard test condition (STC) which equal to 25 ℃, the cell temperature T_c is effected by various factors including wind speed, ambient temperature and the solar irradiance and can be obtained using the following equation [186]:

$$T_c = T_{amb} + \left(\frac{T_{NOCT}-20}{800}\right) * G \quad (4.29)$$

where T_{NOCT} is the nominal operating cell temperature (°C) which is the cell temperature under Standard Operating Condition (SOC) according to the following parameters:

- Irradiance level of 800 (W/m^2).
- Ambient temperature of 20℃.
- Wind speed of 1 m/s.
- Power output of 0 W (no load).
- Spectral distribution of AM 1.5.

mostly T_{NOCT} values are ranging between 42℃ to 50℃ [187].

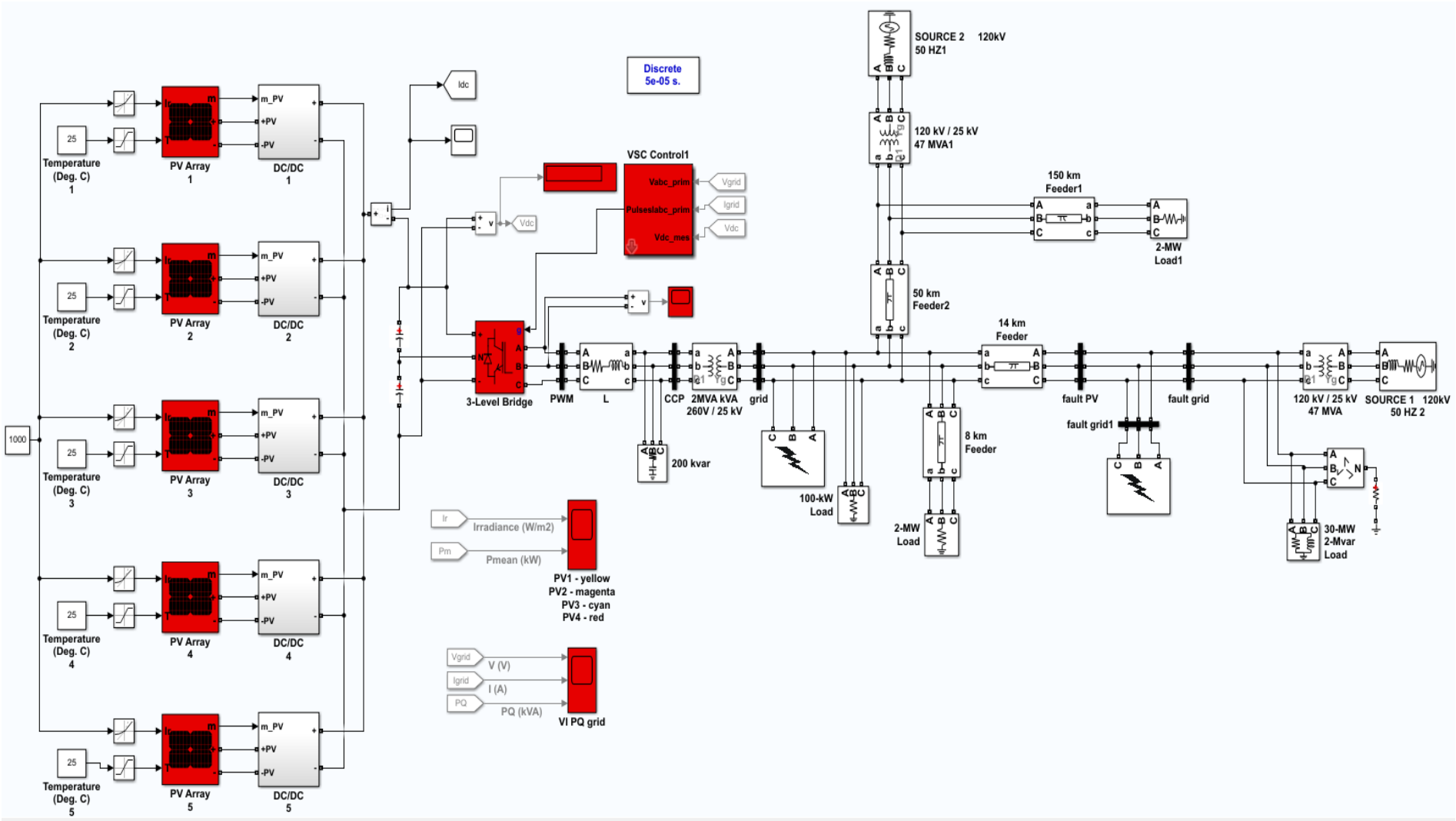

Fig. 4. 9. The simulation model for the entire system.

4.4.1 Power production under Libyan weather condition

To assess the PV system's energy production performance, MATLAB was used to apply equations (4.28) and (4.29) to calculate the hourly energy production for nine sites across Libya. The selection of these sites was based on two primary considerations: their proximity to residential areas and the aim to study as much of the Libyan landmass as possible. Two primary sources were used to obtain the hourly solar radiation and ambient temperature data for these nine sites. The first source was PVsyst software, which provided data for six out of nine of the sites used in this study. This software is considered reliable for supplying the necessary data to study the PV system's performance and has been recommended by researchers [188] [189]. PVsyst utilizes various databases to provide accurate information, including Meteonorm and NASA. Furthermore, PVsyst has been utilized in numerous research articles [190] [191]. The geographical data for the six locations illustrated in Table 4.4.

Table 4. 4. The geographical data for or the six selected locations in Libya

Location	*Latitude*	*Longitude*
Tiji	32.0°N	11.4°E
Al-Aziziyah	32.3°N	13.0°E
Sabha	27.0°N	14.3°E
Sirte	31.1°N	16.4°E
Sulug	31.68°N	20.3°E
Tawergha	32.1°N	15.0°E

The second data source was derived from actual readings recorded by the Libyan Centre for Solar Energy Research and Studies (CSESR) located in Tajoura city. The centre utilizes its own installed weather stations to measure the necessary data, encompassing solar irradiance and temperature. Each of these weather stations is equipped with the following instruments [23]:

- Kipp & Zonen “SOLYS 2” tow-axis sun tracker.
- Integrated global positioning system “GPS”.
- Kipp & Zonen pyranometers for solar radiation measurements
- Kipp & Zonen CSD 3 sunshine duration sensor.
- Anemometers to measure wind speed and direction.
- Hygrometer to measure relative humidity.
- Temperature sensors to measure ambient temperature.
- Pressure sensors to measure atmospheric pressure.

This centre provides data for the other three locations, namely Tajoura, Mslata, and Murzuq. Data was recorded at ten-minute intervals throughout the entire year. The chosen nine locations are depicted in Figure 4.16. The average solar irradiance and temperature for the first six sites that obtained by online database are shown in the Table 4.5.

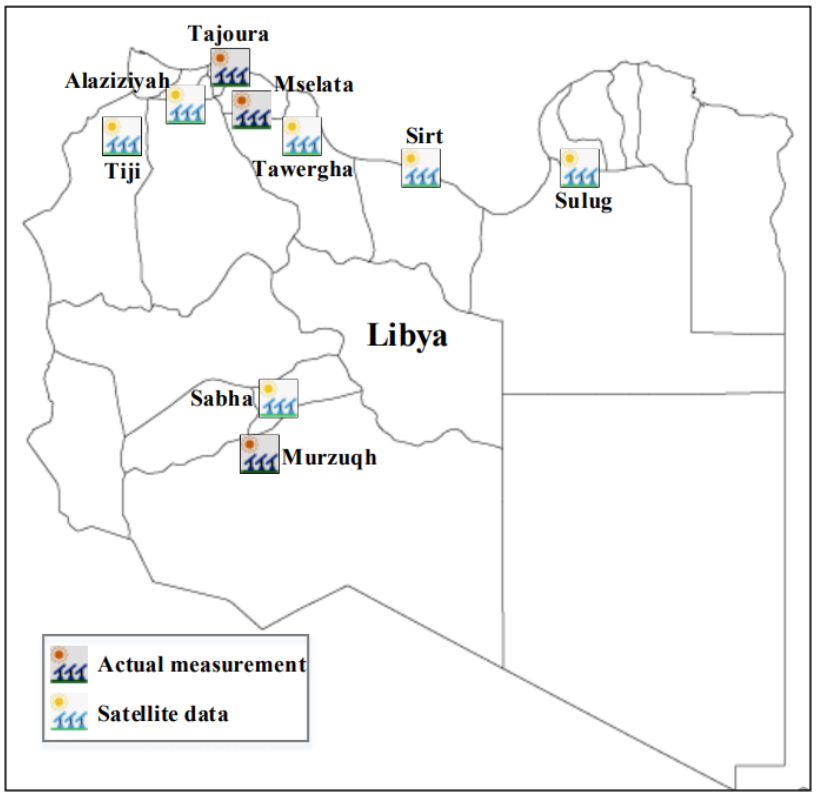

Fig. 4. 10.The potential map for installing PV system at nine locations across Libya

The table clearly illustrates that solar irradiance reaches its peak values during the summer season, while the lowest irradiance levels are recorded in the winter season. This trend is mirrored in the temperature data. From a positive perspective, this pattern of solar irradiance aligns with Libyan power consumption. where in Summer the highest power consumption is recorded as result of the increased use of air conditioners.

On the other hand, the average solar irradiance and temperature for the other three sits that obtained based on actual recorded data collected by CSESR are shown in Table 4.6. Upon closer examination of the actual measurements, it is evident that there is a close match between the data obtained from the software, provided by NASA satellites, and the actual readings collected by CSESR through its weather stations. Furthermore, it is observed that the highest solar irradiance levels were recorded during the summer season, typically around the middle of the year, while the lowest levels were observed during the winter season.

Table 4. 5. The average monthly for the six selected locations in Libya

Months	Tiji		Al-Aziziyah		Tawergha		Sirt		Sulug		Sabha	
	Irr	°C	Irr	°C	Irr	°C	Irr	°C	Irr	°C	Irr	°C
Jan	88.4	12.1	82.8	13.8	95.2	15.5	103.2	15.2	89	13.7	110.4	10.8
Feb	117.2	13.3	106.1	14.1	118.6	15.3	126.2	15.5	108.8	14.4	135.7	12.8
Mar	164.6	15.9	148.5	15.7	166.2	16.4	170.8	17.2	153.4	16.9	181.7	17.5
Apr	197.1	19.4	184.5	18.1	197.1	18.4	199.2	19.9	186.0	20.9	199.8	23.0
May	224.1	23.6	216.4	21.6	224.4	21.3	224.2	23.0	219.8	25.1	210.5	27.7
Jun	238.5	27.0	230.1	24.7	237.0	24.2	237.0	25.9	229.5	28.0	228.9	31.0
Jul	251.4	28.8	241.5	26.5	25.2	26.2	250.5	27.1	235.9	28.6	241.2	31.1
Aug	226.3	29.3	218.6	27.4	228.5	27.3	227.2	28.0	211.1	28.9	220.7	31.0
Sep	174.3	26.5	165.6	25.9	178.8	26.3	181.8	27.3	164.1	27.6	183.6	29.4
Oct	131.4	23.0	122.8	23.2	142.6	24.0	148.5	24.7	131.4	23.9	161.2	24.0
Nov	93.9	18.0	82.5	19.3	99.3	20.6	106.2	20.7	93.9	19.3	114.3	17.6
Dec	77.8	13.6	72.8	25.5	85.9	17.1	93.9	16.8	81.2	15.2	98.3	12.3

Table 4. 6. The average monthly temperature and solar irradiance recorder by CSESR

Months	**Tajoura**		**Mslata**		**Murzuq**	
	Irr	℃	Irr	℃	Irr	℃
Jan	142.87	14.20	136.68	12.72	200.51	11.7
Feb	150.95	13.73	150.40	12.26	201.40	17.03
Mar	231.37	18.99	233.48	17.45	287.29	22.19
Apr	267.54	19.89	272.20	18.48	285.59	28.44
May	299.12	22.12	291.08	21.19	292.51	32.18
Jun	312.27	25.56	301.24	24.11	309	35.29
Jul	325.30	29.04	325.45	28.47	332.46	34.40
Aug	291.60	28.39	285	26.23	299.65	35.33
Sep	241	27.65	240.73	25.80	277.68	30.15
Oct	180.47	23.29	173.60	21	205.61	27.64
Nov	135.28	18.84	135.77	17.25	195.02	19.37
Dec	119.20	13.92	113.31	12.45	184.96	12.62

4.5 Conclusions

This chapter introduces the principles of dynamic modelling for GCPV systems. It begins with the comprehensive modelling of the PV array, progressing to the DC-DC boost converter and

its control strategy, with a primary focus on the P&O MPPT technique, ensuring maximum power extraction from the PV array and elevating the voltage level for injection into the VSC. The VSC's control strategy is discussed in detail, along with the employment of an LC filter to eliminate high-frequency components from the voltage and current signals generated by the VSC, thereby guaranteeing that THD remains within the acceptable limits stipulated by grid codes, typically below 5% of the fundamental signal.

To relate this work to the Libyan context, the output power production of the simulated system was assessed for nine locations across the country. This evaluation drew upon two data sources: one based on NASA satellite data, which furnished hourly data for six sites, and the other relying on actual recorded data collected every ten minutes for three sites.

Chapter 5:

Title Impact of solar irradiance and ambient temperature on the dynamic behaviour of grid connected photovoltaic power system

5.1 Introduction

This chapter delves into the performance of a GCPV system under varying levels of solar radiation and temperature. The primary focus is on how the system responds to sudden changes in weather conditions including solar irradiance and temperature; as well as, monitoring of voltage quality at low levels of solar radiation. Additionally, Fast Fourier Transform (FFT) analysis is considered, and Total Harmonic Distortion (THD) is evaluated at different points across the system to ensure it falls within the acceptable range according to the IEEE Std 519 [173] [121]. Moreover, before proceeding further in this chapter, it is pertinent to provide a brief reminder of how the control strategy functions to synchronize the integrated system with the grid, which is summarized as follows:

The control strategy implemented on the inverter comprises two control loops: an inner control loop facilitated by a current regulator, and an external control loop managed by a DC voltage regulator. The primary objective of the VSC control strategy is to regulate the DC voltage and uphold a consistent value across the DC link. This task holds considerable importance in guaranteeing a stable DC voltage supply to the inverter. Furthermore, the control strategy regulates both the active and reactive powers delivered to the grid via the inverter.

The operation process of this control strategy begins with the inner control loop, which converts the grid voltage and current from the *abc* reference frame to the *dq0* frame. This conversion is carried out to enhance and augment the controllability of the system. The grid voltage, denoted as V_{abc}, is input into a phase-locked loop (PLL) to generate the reference phase angle. This reference angle is subsequently utilized as a reference for the inverter, ensuring that the generated signal complies with the grid requirements. In the external control loop, the actual *DC* voltage generated by the DC-DC boost converter, denoted as Vdc, is compared with a reference voltage, V_{dc}*, set at 500 V. This comparison generates an error signal, which is subsequently input into a proportional-integral (PI) controller. The output of this *DC* voltage regulator serves as the reference current, denoted as I_d*, while the reference current I_q* is set

to zero to maintain unity power factor. The current components I_d and I_q, generated by the inner control loop, are employed to regulate the injected grid current and to uphold the *DC* voltage at a constant level. Simultaneously, the reference components I_d* and I_q* generated by the *DC* regulator are compared with the actual grid current components I_d and I_q generated by the inner control loop. This comparison is facilitated by a PI controller to ensure that the steady-state error remains at zero. The output of the PI controller is then directed to a pulse-width modulation (PWM) generator to produce reference signals. These signals are integral to the control strategy of the Voltage Source Converter (VSC).

5.2 The effect of solar radiation on the PV system performance

To assess the system performance under various radiation levels, the simulated model was operated at four radiation levels: STC, 750, 500, and 250 W/m^2, with a constant temperature of 25℃. The system was run for 20 seconds, and the four scenarios were implemented. For the initial 5 seconds, solar radiation was set at 1000 W/m^2 with a temperature of 25℃. These first five seconds served as validation for the simulated system. During this stage, the system operated under Standard Test Conditions (STC) from 0 to 5 sec. The power generated by a single PV array and five PV arrays assembled in parallel for all four scenarios is depicted in Figure 5.1-a and 5.1-b, respectively.

The results indicate that the system operates at its full capacity and delivers maximum power for the first 5 sec under STC, verifying the effective functioning of the controller of the DC-DC boost converter in tracking the MPP of the PV system. When compared to the characteristic curve of the PV arrays shown in Figure 4.2, it is evident that the system generates the same amount of power as provided by the module datasheet, serving as validation for the system's operation. Moreover, it is crucial to emphasize that the P&O algorithm has been implemented for MPPT control to ensure that the system delivers maximum power by maintaining the optimized points of the PV characteristics curve of the PV arrays.

Chapter 5: ***Impact of solar irradiance and ambient temperature on the dynamic behaviour of grid connected photovoltaic power system***

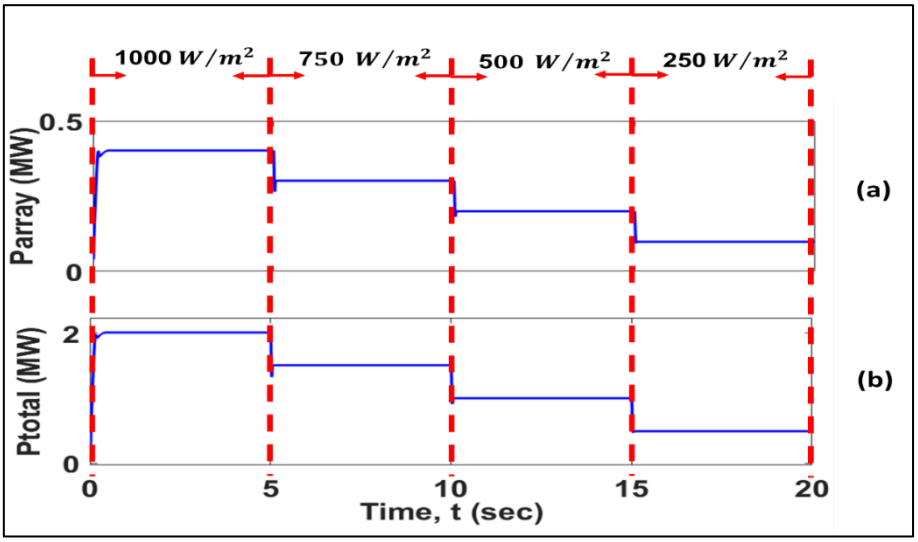

Fig. 5. 1. Output power of the PV system vs time for different irradiance level

(a) single array (b) five arrays in parallel

In the second five-second interval from 5 to 10 sec, the solar radiation was reduced to 750 W/m^2. As depicted in Figure 1, the power output is diminished, and the system exhibits a swift response to the abrupt change in irradiance levels. Nonetheless, the system remains capable of extracting the maximum available power from the PV array. The same behaviour was observed when the level of irradiance further reduced to 500 W/m^2 and 250 W/m^2. The power was reduced with a quick response from the system, yet it continued to extract the maximum available power through all four scenarios.

In the second stage of this system, the voltage at the DC busbar was monitored under the four scenarios implemented in this study. The result is presented in Figure 5.2. The DC-DC boost converter, with the designated control strategy of the MPPT algorithm, successfully boosted the DC voltage produced by the PV arrays from 273.5 V to 500 V. Figure 2 clearly shows that the voltage at the DC busbar follows the reference voltage set by the DC voltage regulator of the inverter, and the impact of irradiance variation is negligible, not disturbing the system operation. The only noticeable impact during the sudden change in irradiance level is a small, quick, and transient voltage dip of less than 4 V, as highlighted in Figure 5.2. Furthermore, the oscillation of the DC voltage around the reference value is less than ± 0.5 V. This indicates that the DC voltage supplied to the PWM inverter is effectively regulated and remains unaffected by the varying radiation. This ensures a stable AC voltage at the inverter terminal, contributing to the enhanced stability of the entire system.

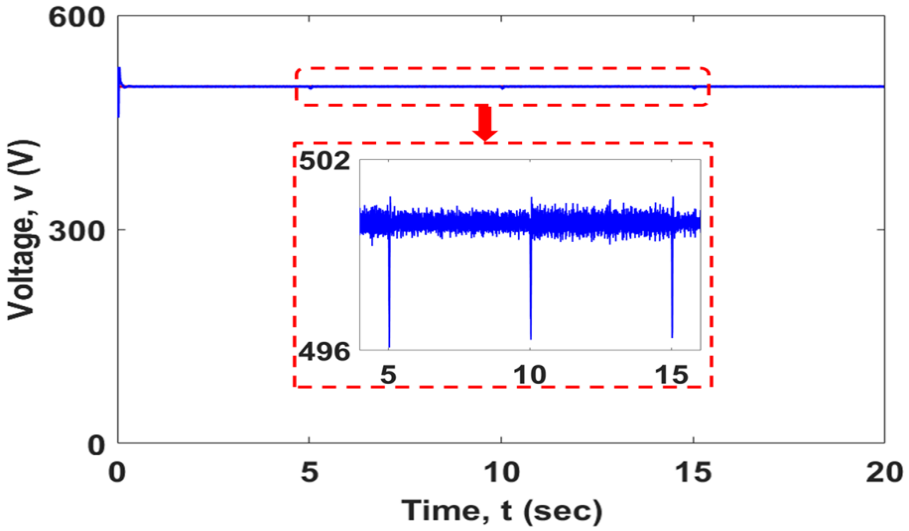

Fig. 5. 2. DC Voltage at the DC link bus bar for different irradiance level.

Moving on to the next stage, which involves the voltage and current at the terminal of the inverter. A 3-level PWM inverter with a nominal frequency of 50 Hz, synchronized with the grid power frequency, was employed. The designated control scheme monitors and controls the switching function of the inverter using the phase angle and frequency of the grid voltage as reference values. The three-phase voltages at the inverter terminal are illustrated in Figure 5.3.

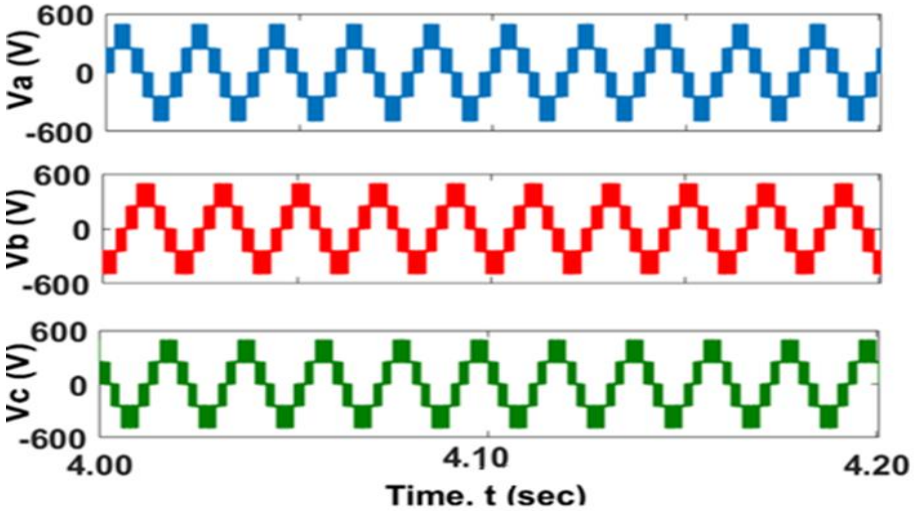

Fig. 5. 3.Phase voltage at the terminal of the PWM inverter

Since the voltage at the input side of the inverter has not been influenced by the changing irradiance, duo to the effective control strategy of the VSC and the fact that the major effects of changes in irradiance level occur on the current level, as stated by [102] [192] [193], the

output voltage at the terminal of the inverter has not been affected either, as can be seen clearly in Figure 5.3. Nevertheless, the current of the system has been affected at different points. Figure 5.4 shows the output current at the terminal of the inverter. It is evident that the current level has been significantly reduced due to the decrease in solar irradiance. The system exhibits a quick response to the change in irradiance level. However, it was capable of maintaining its balance at a low level of total harmonic distortion (THD).

In the final stage of the GCPV system, just before integration with the grid, an LC filter was implemented to eliminate the high-frequency harmonics generated by the PWM inverter. The parameters of the LC filter were carefully chosen to reduce the total harmonic distortion (THD) to well below 5%, in compliance with IEEE Std. 519.

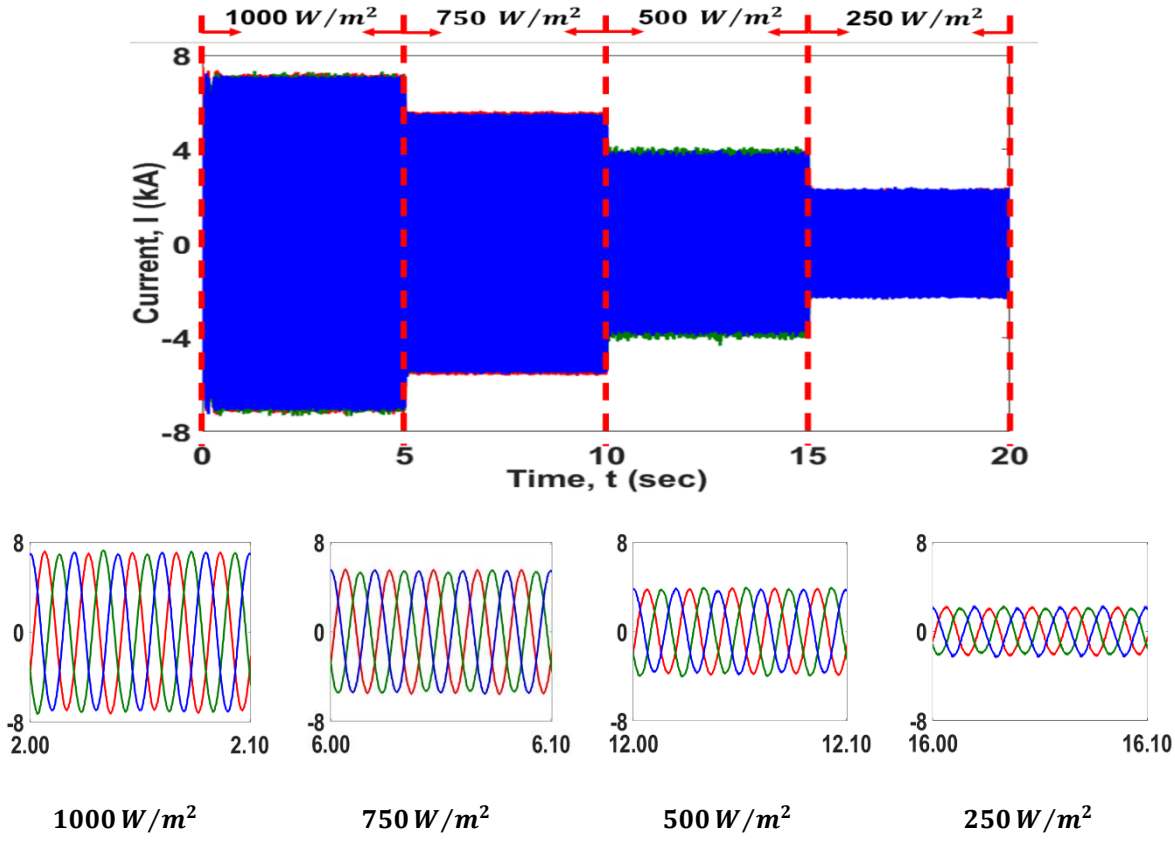

Fig. 5. 4. Current at the terminal of the inverter for different irradiance level with zoomed view for different levels of irradiance at the bottom

The same phenomenon was observed for the current at the terminal of the LC filter, where the current exhibited a rapid response to changes in solar irradiance without compromising stability. Furthermore, as the system adopts a voltage control strategy, the voltage remains

stable and constant at different points across the system. This stability is also observed at the terminal of the LC filter, which is utilized to eliminate the high-frequency components introduced by the PWM inverter. Current and voltage at the terminal of the LC filter are illustrated in Figures 5.5 and 5.6, respectively.

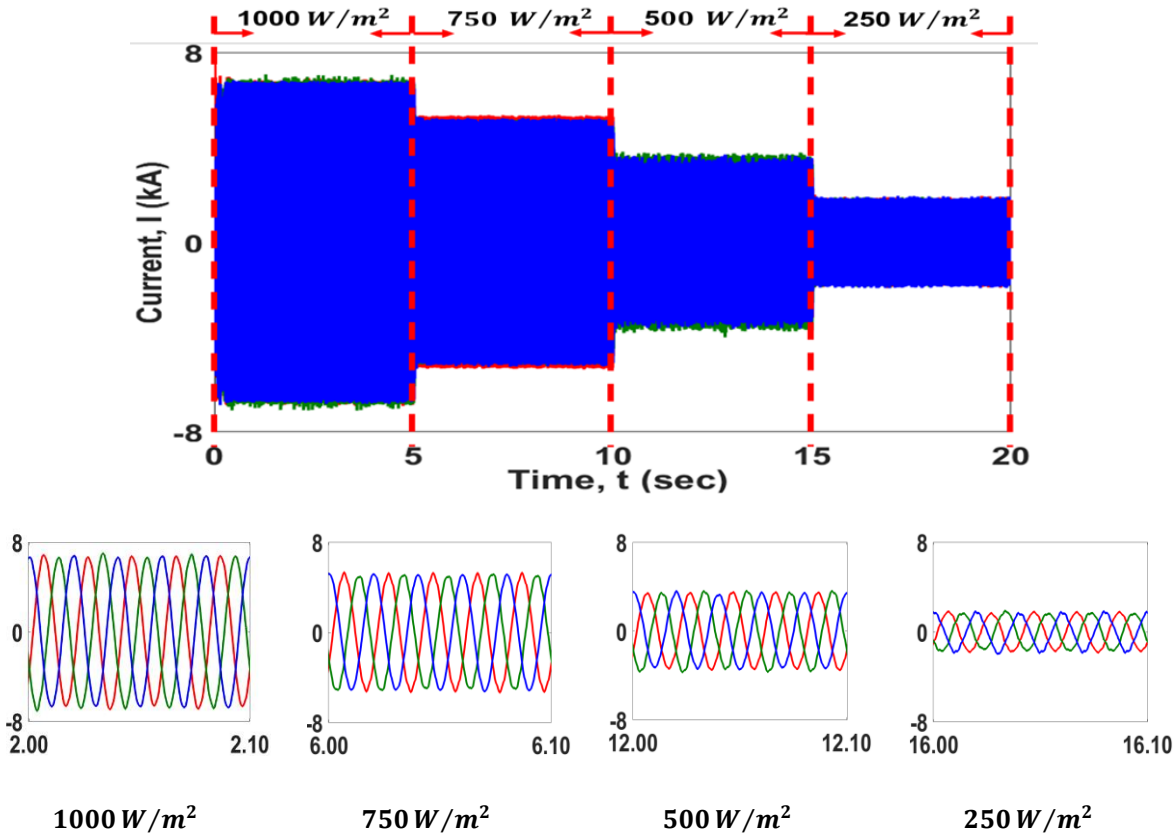

Fig. 5. 5. Current at the terminal of the LC filter for different irradiance level with zoomed view for different levels of irradiance at the bottom

5.3 The effect of Temperature on the PV system performance

To assess the influence of ambient temperature, the system was tested under four different temperature conditions: 15°C, 25°C, 35°C, and 45°C, while maintaining solar irradiance at a constant value of 1000 W/m^2. The simulation was executed for 20 seconds, with each temperature level running for 5 seconds. The findings revealed that when the system operated under the lowest ambient temperature, the produced power reached its peak, surpassing the rated power. This discrepancy can be attributed to the fact that rated power is calculated at 25°C, whereas these results were obtained under 15°C ambient temperature. Figure 5.7(a) and (b) illustrate the influence of temperature on the generated power.

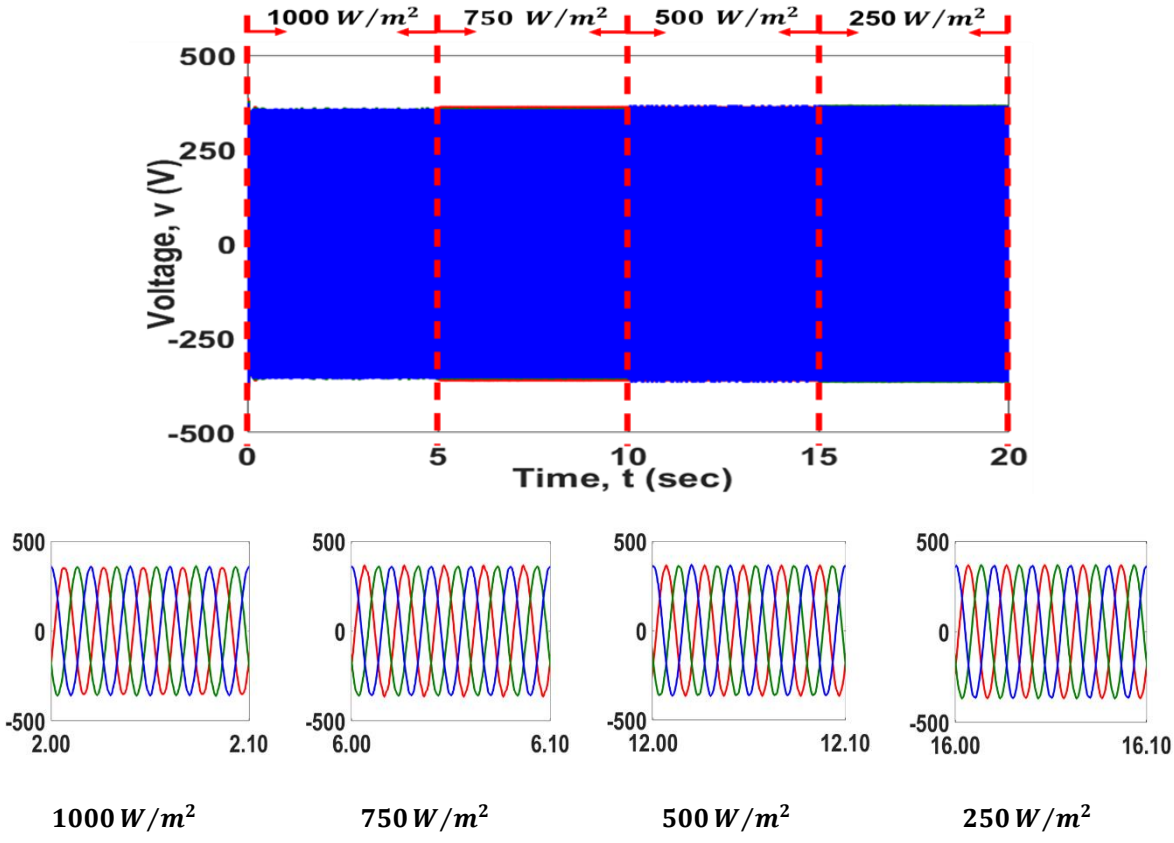

Fig. 5. 6. Voltage at the terminal of the LC filter for different irradiance level with zoomed view for different levels of irradiance at the bottom

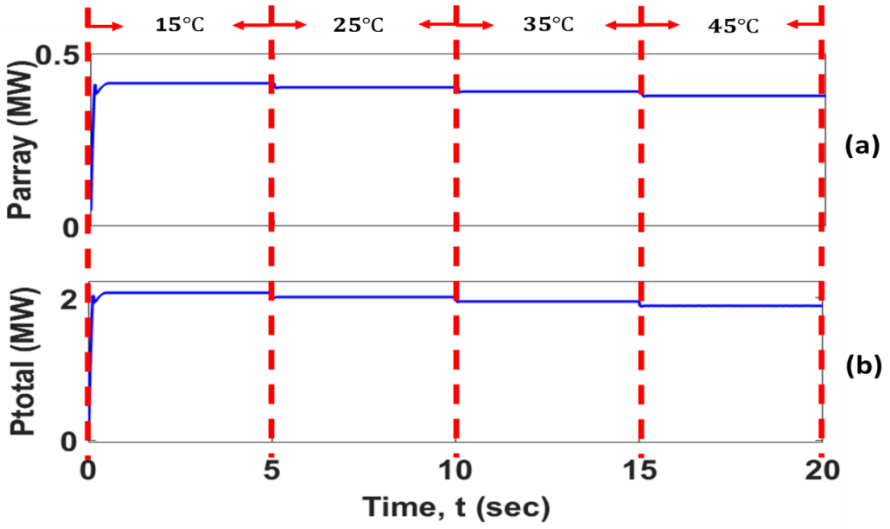

Fig. 5. 7. Output power of the PV system for different ambient temperature

(a) single array (b) five arrays in parallel

Figures 5.7(a) and (b) indicate that the influence of temperature on the generated power is less significant than the impact of solar irradiance, as depicted in Figures 5.1(a) and (b). This is due to the reduction in fallen photons carrying charges on the surface of the PV panel when solar irradiance is diminished.

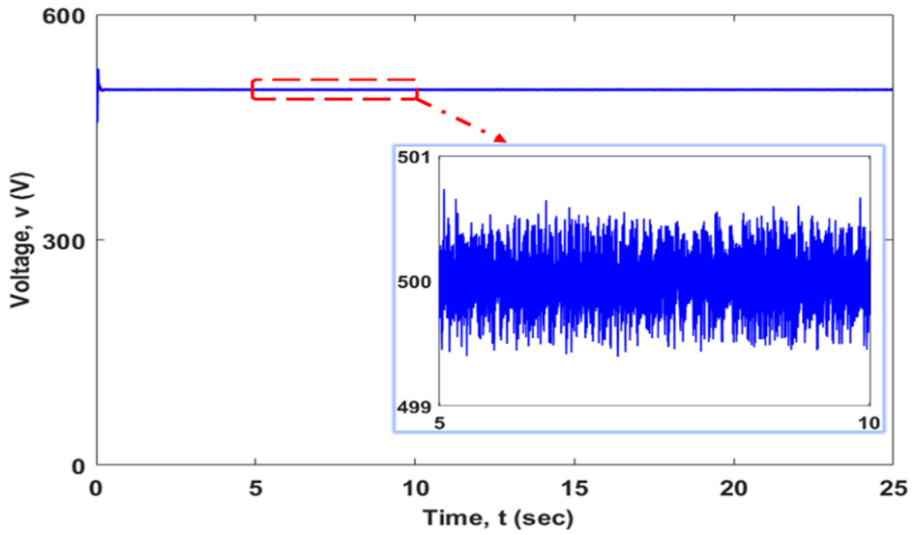

Fig. 5. 8. DC Voltage at the DC link bus bar for different ambient temperature with zoomed view.

While the voltage at the DC link busbar was not affected by the changes in ambient temperature, this is attributed to the significant role played by the system's control strategy. Additionally, the DC-DC boost converter successfully elevated the voltage level to 500V, set as the reference voltage. The implemented MPPT technique effectively extracted the maximum available power from the PV array in all four scenarios. Figure 5.8 illustrates the voltage at the DC link busbar. The generated DC voltage was subsequently fed into the PWM inverter, tasked with converting it into a PWM signal. The outcomes depicted in Figure 5.9 reveal a slight reduction in output current at higher ambient temperatures. However, this impact was not as pronounced as observed with changes in solar irradiance levels, as clearly illustrated in Figure 5.4.

The voltage remained stable under the four levels of ambient temperature, unaffected by the changing temperature. This serves as an indicator of the effective control strategy in maintaining the voltage level at the terminal of the inverter as constant as possible, regardless of any change in weather conditions. This ensures that a consistent voltage is supplied to the utility grid. Figure 5.10 illustrates a sample of the PWM voltage signal at the terminal of the inverter.

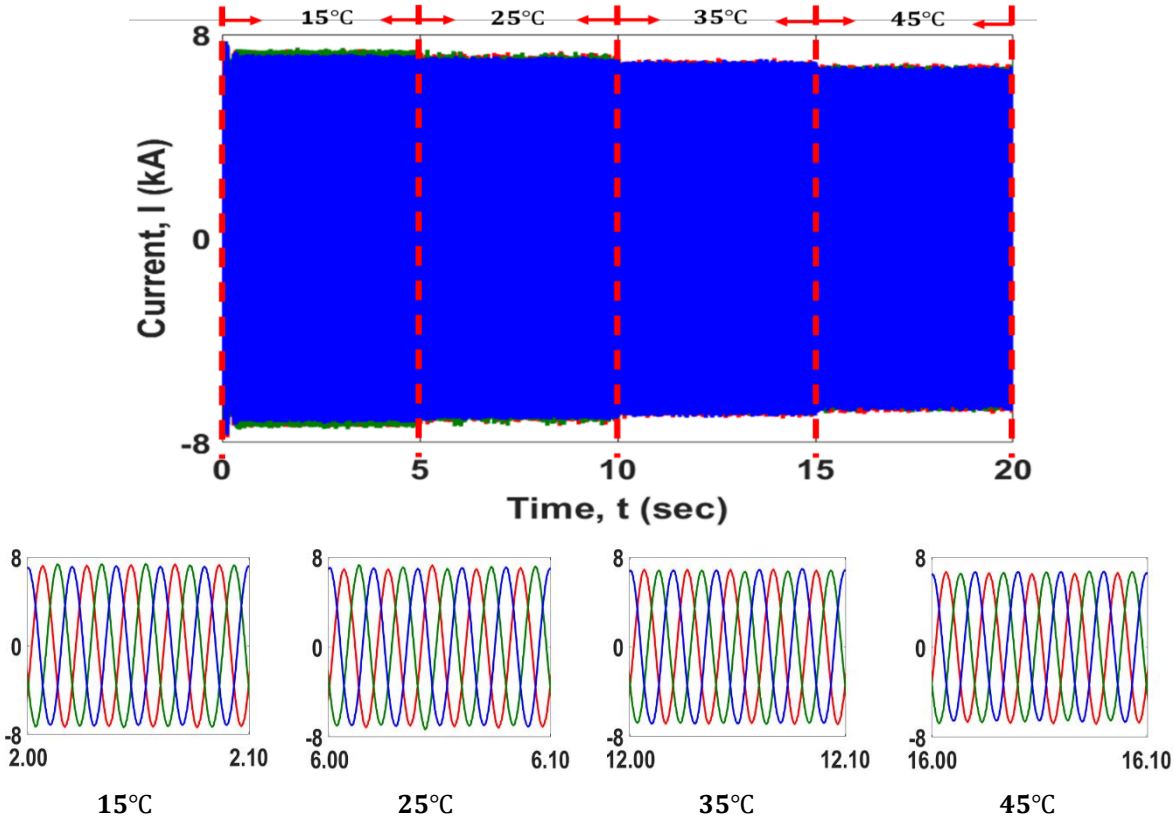

Fig. 5. 9. Current at the terminal of the inverter for different ambient temperature with zoomed view for different levels of temperature at the bottom

However, this PWM signal cannot be injected directly into the grid due to the high-frequency components introduced by the inverter. Therefore, using a filter is a compulsory requirement to eliminate the high-frequency components and ensure that the THD level is below the recommended level. Three-phase voltages and current at the LC filter terminal are illustrated in Figures 5.11 and 5.12, respectively.

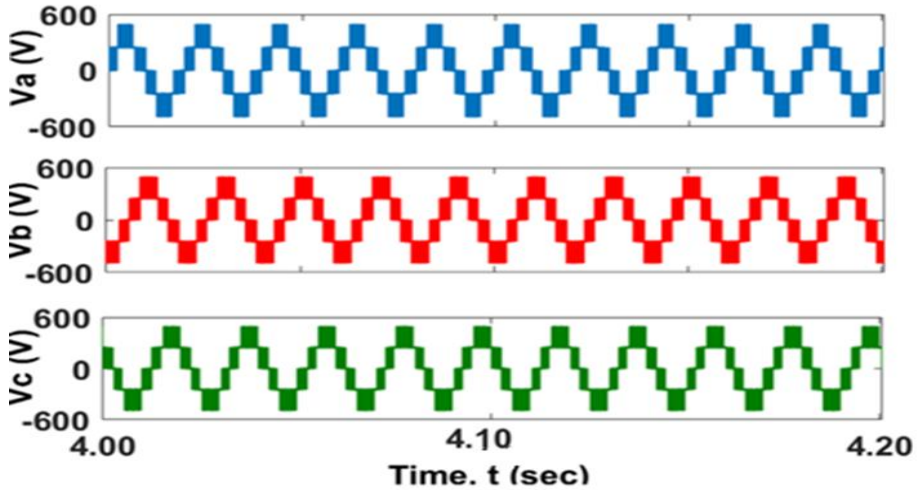

Fig. 5. 10. Phase voltage at the terminal of the PWM inverter

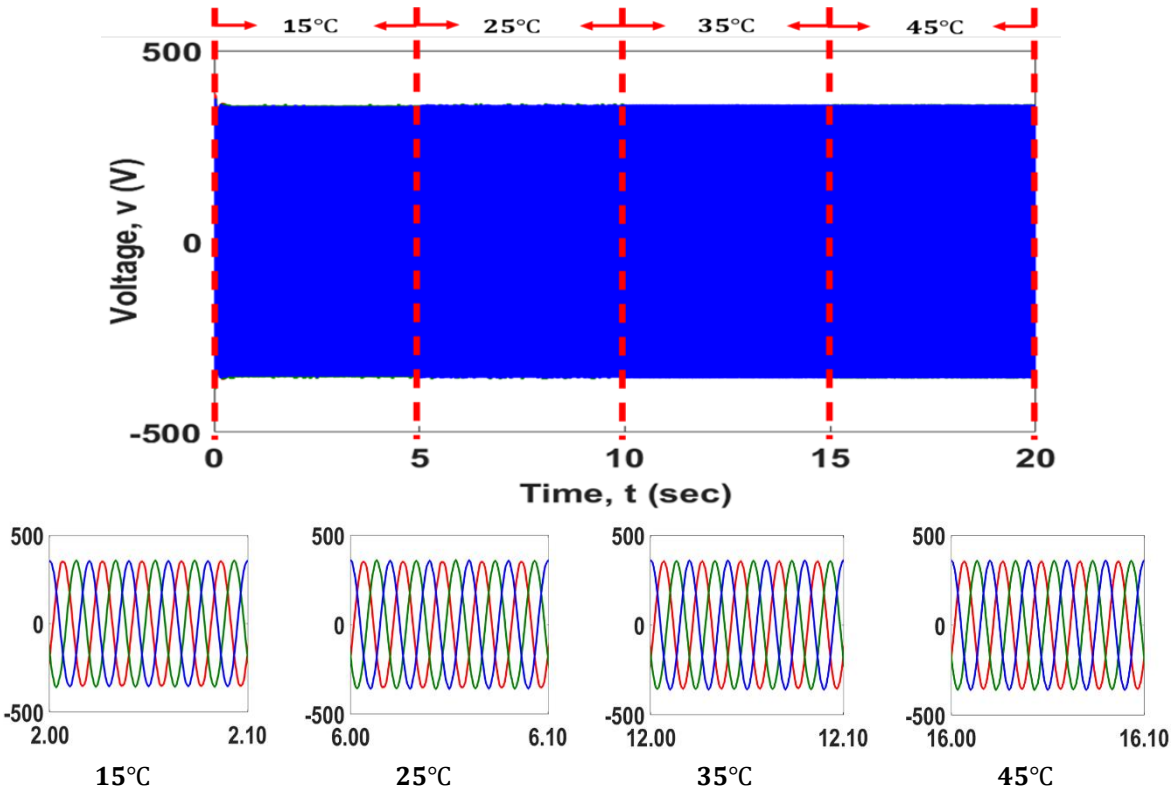

Fig. 5. 11. Voltage at the terminal of the LC filter for different ambient temperature with zoomed view for different levels of temperature at the bottom

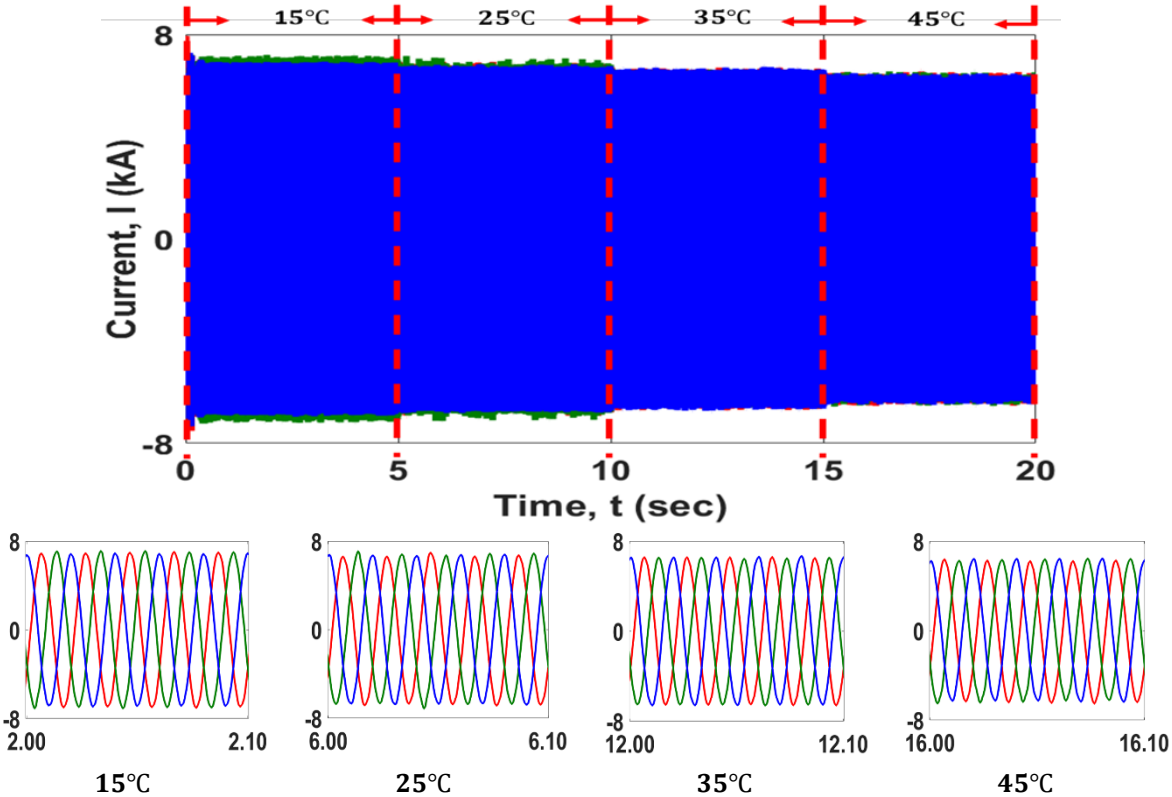

Fig. 5. 12. Current at the terminal of the LC filter for different ambient temperature with zoomed view for different levels of temperature at the bottom.

5.4 FFT analysis

A FFT analysis was conducted to examine the THD values for the voltage and current signals at three different points across the system—namely at the terminal of the inverter, at the LC filter terminal, and at the CCP. The analysis was performed under the two above-mentioned scenarios: first, under changing solar irradiance, and second, under changing ambient temperature. THD levels for the current and voltage at the inverter terminal, LC filter terminal, and CCP for both cases are presented in Figure 5.13 and 5.14, respectively.

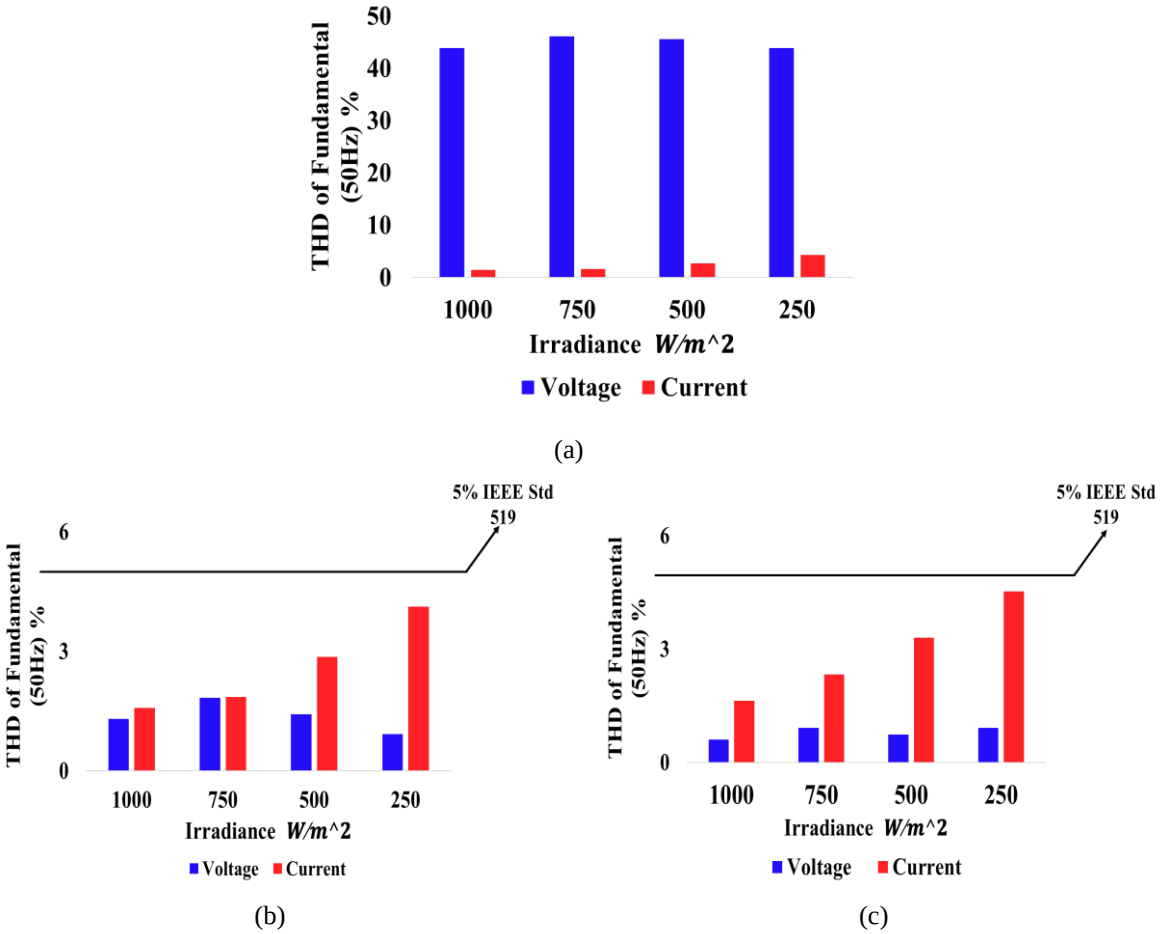

Fig. 5. 13. THD values of voltage and current under varying solar irradiance (a) at inverter terminal (b) at LC filter terminal (c) at CCP

It can be noted from Figure 13 (a) that the THD of the voltage at the inverter terminal, before the LC filter, ranges between 43% and 46% under the four levels of irradiance, which is as expected because the inverter converts the DC voltage into a PWM voltage signal. Meanwhile, the THD values of the current range between 1.48% and 4.28%. The generated signals are then fed into the LC filter, which is responsible for reducing these high-frequency components,

especially for the voltage signal. The results show that the LC filter was capable of reducing the THD level to range between 0.92% and 1.84% for the voltage under the four levels of irradiance and between 1.58% and 4.12% for the current, which is well below the acceptable level as stated in the IEEE Std. 519 [173]. Further improvement was observed at the CCP, where the transformer operates as a second filtration stage, making the filtration stage similar to an LCL filter. The results show that the THD level of voltage was further reduced to range between 0.53% and 0.92%.

Moving to the second case, the FFT analysis was conducted to evaluate the THD level under four levels of ambient temperature. Figure 5.14 illustrates the THD level for the voltage and current under the four levels of temperature at different points across the system.

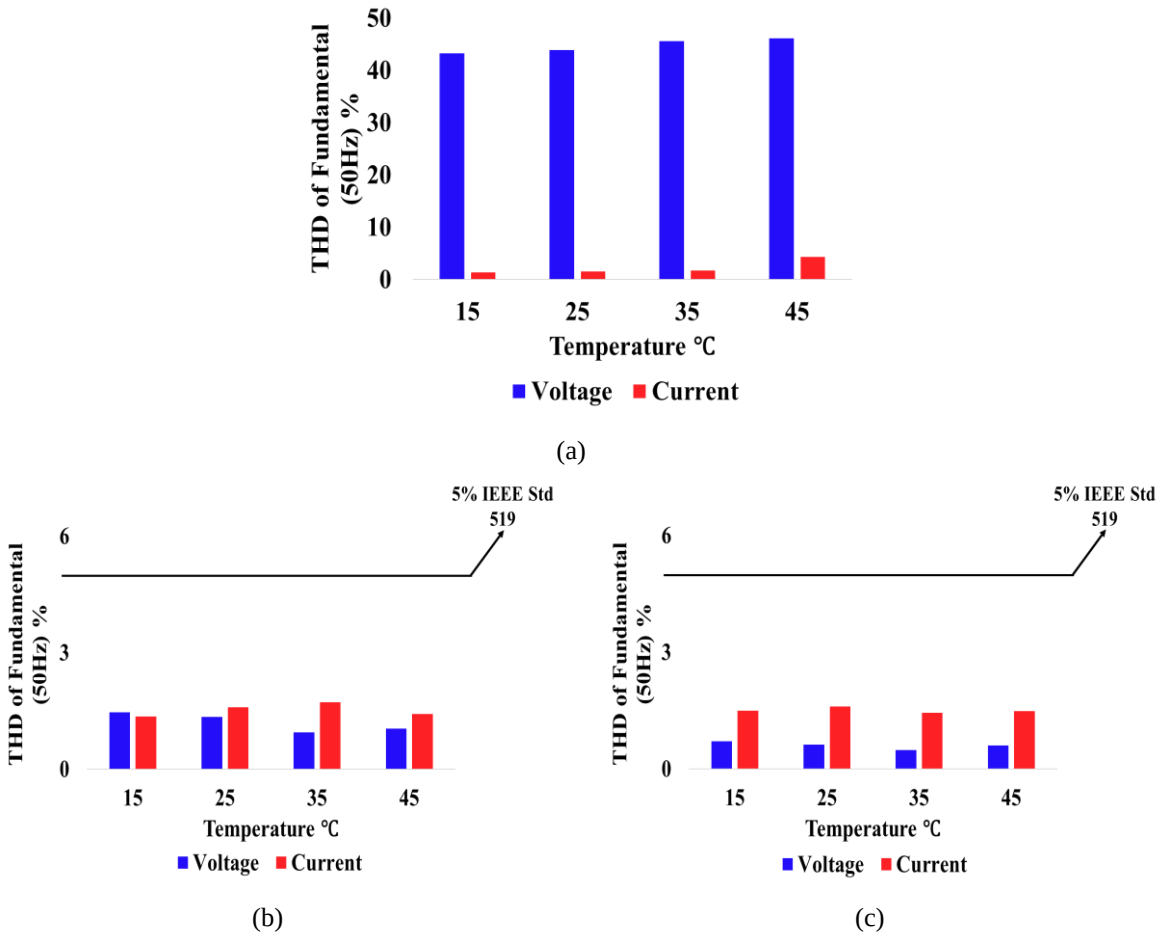

Fig. 5. 14. THD values of Voltage and current under varying ambient temperature (a) at inverter terminal (b) at LC filter terminal (c) at CCP

As can be clearly seen from Figure 5.14 (a), the THD level of voltage is quite high, ranging between 43% and 46% under the four levels of temperature. However, similar to the previous

stage, the LC filter successfully was able to get rid of these high-frequency components, ensuring that it remains well below the acceptable range. The results demonstrate that the THD level for the voltage ranged between 0.95% and 1.47%, with further improvement observed at the CCP, where the THD level ranged between 0.49% and 0.71%. On the other hand, the THD level of the current did not exceed 2% at all points and under all four levels of temperature. This highlights the effective operation of the LC filter in reducing the THD values of the voltage at the CCP. However, it is noteworthy to highlight that the THD level of the current exceeds that of the voltage. at both low levels of irradiance and high temperatures. This discrepancy may be attributed to the control strategy employed in the system, specifically a voltage-based control scheme. Additionally, the presence of inductive and capacitive components within the LC filter could contribute to this phenomenon.

5.5 Conclusions

This chapter has discussed the performance of the grid-connected PV system under various levels of solar irradiance and its response to a sudden change in weather conditions. Furthermore, the behaviour of the system under different ambient temperatures has also been covered. This chapter also evaluated the voltage and current quality in terms of THD and the ability to maintain its level below the recommended threshold. The results have shown that the system successfully extracted the maximum power under all conditions, indicating the effectiveness of the DC-DC boost converter and the designated control scheme, represented in the P&O MPPT technique. What's more, the DC-AC inverter operated efficiently in converting the DC signal into a PWM signal, and its control strategy was capable of maintaining the voltage at the DC link busbar constant at all times, unaffected by any changes in weather conditions, whether in solar irradiance or ambient temperature. Furthermore, the conducted FFT analysis demonstrated that the LC filter effectively maintained the THD well below the standard level of 5 % during all scenarios, including low levels of irradiance and high ambient temperatures. All the aforementioned results can be viewed as compelling reasons for developing countries with abundant solar irradiance to embrace these technologies. Libya, being one such country, holds the potential for solar energy to play a significant role in providing clean energy, ultimately aiding the nation in overcoming its energy crisis.

Chapter 6:

Dynamic behaviour of a grid-connected Photovoltaic power system under short circuit fault scenarios

6.1 Introduction

This chapter delves into the dynamic behaviour of grid-connected PV systems when confronted with various types of short-circuit faults on the grid side. These faults encompass both symmetrical and asymmetrical short-circuit scenarios. In power systems, short-circuit faults arise from various abnormal conditions, which depend upon the parameters and configurations of the grid. These faults have the potential to introduce transient fault currents of exceptionally high magnitude, surpassing the rated load currents. Incurring fault currents triggers electrodynamic disruptions and substantial thermal losses within power system elements, potentially leading to severe damages [131]-[132]. Short circuit faults are categorized into different types, among which line-to-ground (LG) faults are the most frequent, occurring with a probability of 70 to 80% [133]-[122]. Therefore, it is crucial to analyse the dynamic behaviour of the system when subjected to these types of faults. Moreover, power system authorities are updating the grid codes, making it compulsory to incorporate ancillary units with GCPVs for support during these abnormal conditions [178]. The emphasis on these grid codes and mandates by authorities has heightened the significance of exploring advanced control schemes, tailored to the converter types and grid codes, capable of supporting GCPVs during grid abnormalities. In the absence of a proper control scheme, it is recommended either to disconnect the PV system from the utility or to adjust the PV arrays' operating point on the characteristics curve to reduce the output power during fault conditions [194]. In this chapter two main types of faults are evaluated on the followed sections under STC with solar irradiance of 1000 W/m^2 and ambient temperature of 25℃. Before proceeding further in this chapter, it is pertinent to justify the evaluation of short circuit faults. The primary rationale for assessing the system under this scenario lies in the fact that such faults are considered among the most disruptive events encountered by power systems. Secondly, this selection is made to investigate the LVRT capability of the system, which is one of the paramount requirements in modern power systems to ensure the safe and reliable integration of solar systems.

6.2 Asymmetrical short circuit faults

6.2.1 L-G short circuit faults

In this section, the primary goal was to investigate the dynamic behaviour of the system under transient fault conditions. For this purpose, a L-G short circuit fault, representing one of the most common faults in practical power systems, was taken into account. This fault was introduced to the secondary side of the step-up transformer at t=2 sec and lasted for a duration of 1 sec at 14km from the CCP. Figure 6.1 illustrates the schematic diagram for the system highlighting the fault points. The power generated by the PV arrays during the transient fault condition was initially monitored, and the results are depicted in Figure 6.2-a and 6.2-b.

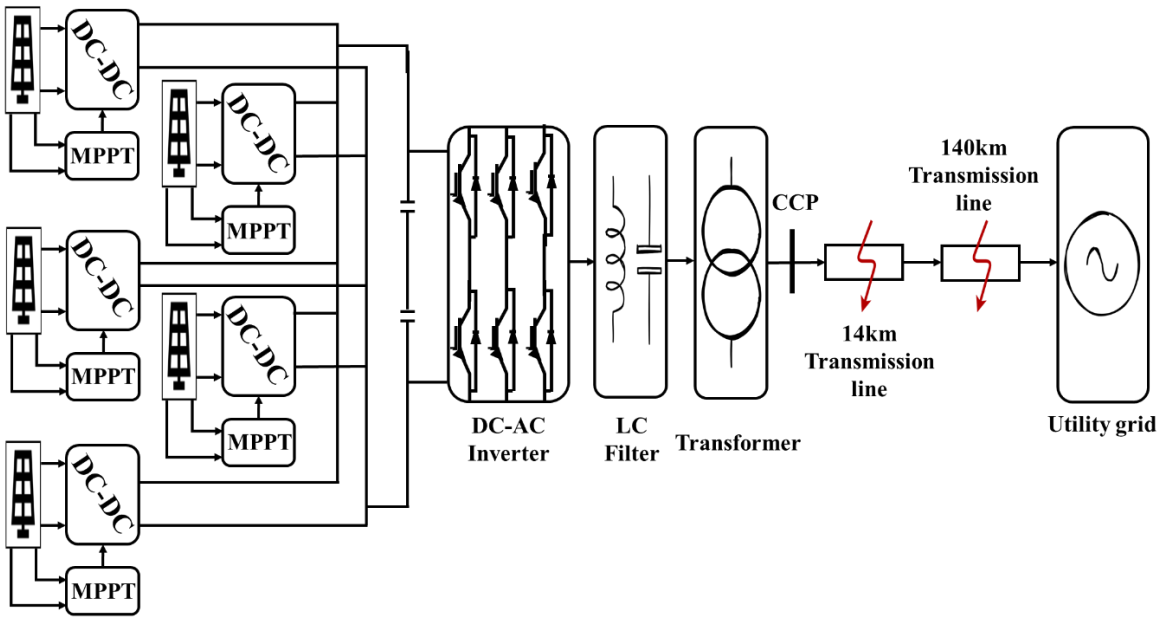

Fig. 6. 1. The schematic diagram for the GCPC with fault points

Figure 6.2 illustrates that the delivered power at the output side of the PV array remains unaffected by this short circuit fault. This explicitly confirms the effectiveness of the designed control approach in maintaining the nominal power delivered by the system at the same operating point during normal operation. This implies that, with the designated control strategy in place, this kind of fault has a negligible impact on the voltage and current output generated by the PV arrays, and therefore on the DC side of the system. This clearly demonstrates that the designated control system successfully shields the PV system from the undesirable impacts of short circuit faults. This is an essential criterion for preserving the normal function of the PV system during L-G fault conditions.

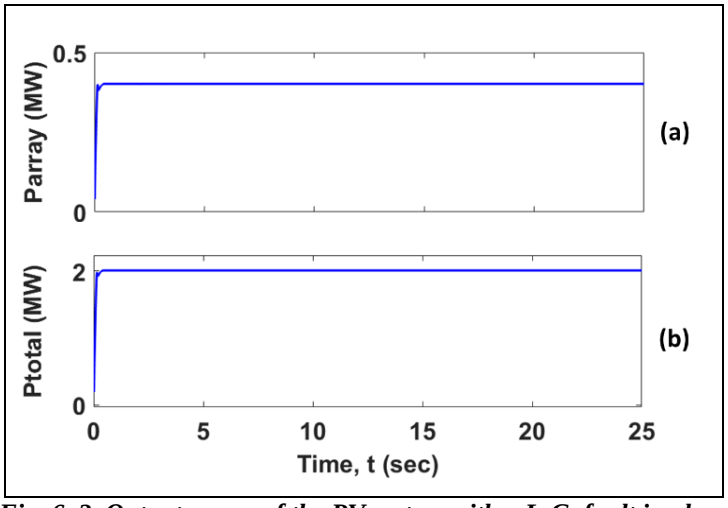

Fig. 6. 2. Output power of the PV system with a L-G fault in place

(a) single array (b) five arrays in parallel

The voltage at the DC busbar was systematically monitored, and the results are presented in Figure 6.3. It is evident that the fault originating from the grid side has a minimal impact on the DC link voltage. Subsequent to this observation, an instantaneous increase in the magnitude of oscillations occurred at t=2 sec, coinciding with the application of the fault. Notably, the overshoot of the voltage remained constrained to approximately ±5 V. Despite the transient disturbance, the system expeditiously restored its stability within a remarkably brief timeframe, achieving equilibrium within as little as 0.2 sec following the clearance of the fault. At t=3 sec, subsequent to fault clearance, the DC voltage fluctuations experienced a temporary augmentation, reverting to their standard operational state within a concise interval of 0.15 sec. This analysis emphasises the system's adeptness in promptly adapting to and recovering from transient disturbances.

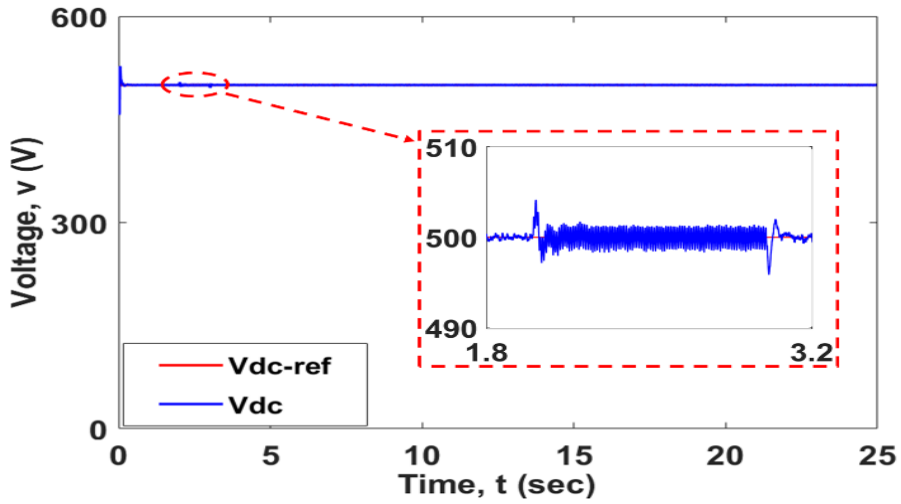

Fig. 6. 3. DC link Voltage under L-G fault with zoomed view.

These findings underscore the efficacy of the designed control system in sustaining voltage stability at the DC busbar this is mainly controlled by the external Voltage regulator which shown in Figure 6.4. Nevertheless, in the context of the AC side of the system, the impact of the L-G fault on voltage and current exceeds that observed on the DC side. The instantaneous waveforms of the three-phase voltage at the inverter terminal are illustrated in Figure 6.5.

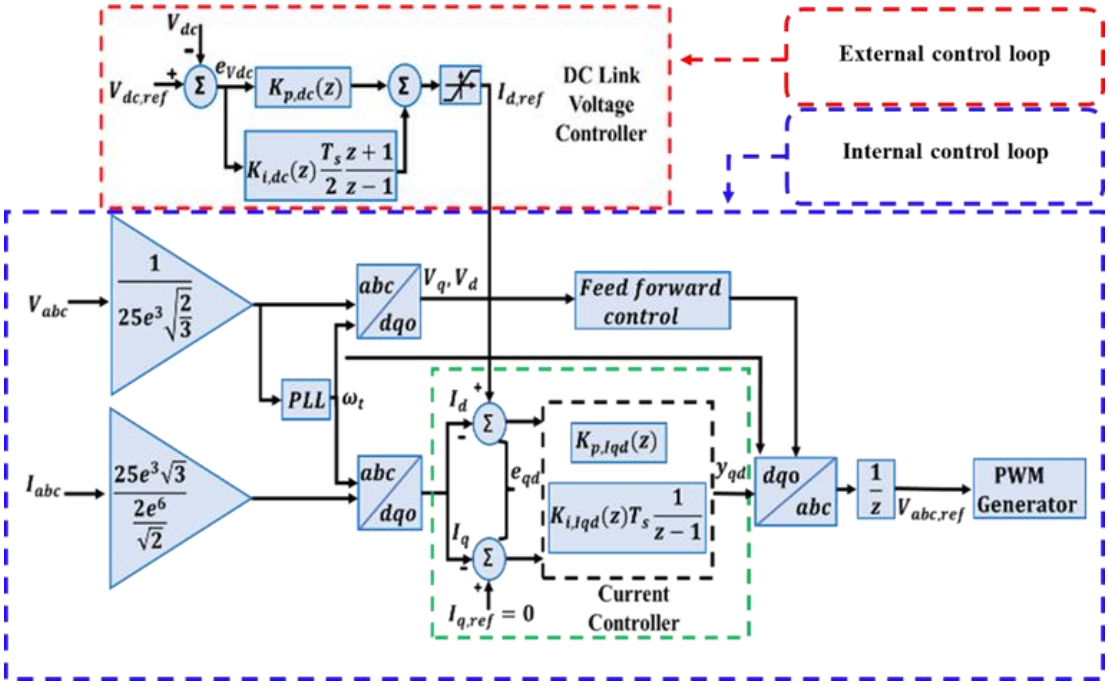

Fig. 6. 4. The GCPV system control strategy

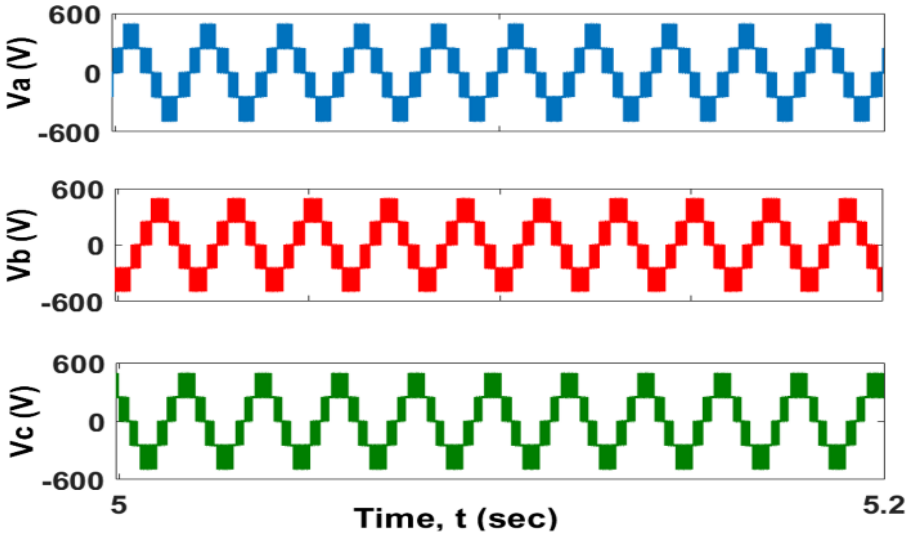

Fig. 6. 5. Three phase voltage at inverter terminal with a L-G fault in place

The impact of the aforementioned fault on the instantaneous waveforms of three-phase current and voltage signals at the CCP is depicted in Figures 6.6 and 6.7, respectively. The

results reveal that the applied fault has a more pronounced effect on voltage and current at the CCP, aligning with the principles outlined in the theory of transient fault conditions in the conventional power systems [135]. However, the implementation of the designated control system facilitated the swift restoration of currents and voltages in all three phases to their normal values, achieving this recovery within a settling time as short as 0.15 sec.

In the presented VSC-based control strategy, a control system is carefully designed in alignment with feedback obtained from grid-side parameters, as illustrated in Figure 6.4, necessitated by the imperative synchronisation between both systems. Consequently, when a fault emerges on the grid side, it promptly exerts an immediate influence on the GCPV system parameters, thereby disrupting its conventional operation. In adherence to grid code requirements, the GCPV system adheres to a specific waiting period to ascertain the clearance of a fault. If the fault is promptly cleared, the system parameters seamlessly revert to normal operation, guided by feedback signals from the grid. Conversely, if the faults persist, the system undergoes disconnection as a preventative measure against potential severe damages.

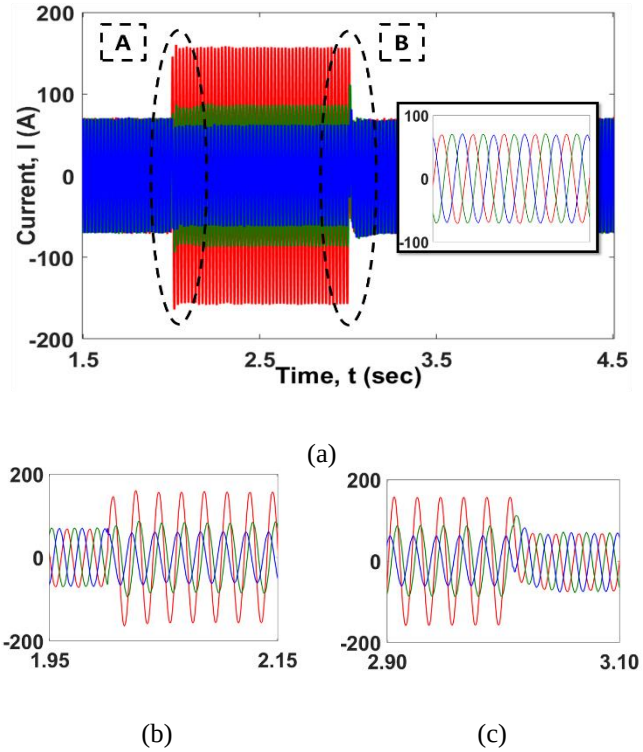

Fig. 6. 6. Instantaneous waveforms of three phase currents at CCP under L-G fault (a) complete waveforms (b) transient currents after applying the fault and (c) transient currents when the fault is cleared.

The fault can be cleared using various procedures. This includes the utilization of fuses as protective devices, which interrupt the circuit by opening it when a fault occurs in the power system. However, such devices require replacement after each fault occurrence. The second

option involves the use of circuit breakers, which are among the most prevalent protections. These devices possess the capability to isolate the faulty section of the system either manually or through remote control systems. The third procedure entails the deployment of protective relays, which function to detect faults and facilitate the operation of circuit breakers in isolating the faulty segment of the system.

The voltage and current signals at the grid side unmistakably depict that the fault condition instantaneously manifests in the parameters of the GCPV system, leading to voltage sag and an immediate increase in current coinciding with the fault occurrence. On the contrary, the minimal impact of the applied fault on the DC segment of the system can be ascribed to the fault's location and the distinct impedance levels associated with various components of the system, encompassing transmission lines, transformers, and harmonic filters. These components collectively contribute to mitigating the repercussions of the applied faults. This analysis underscores the significance of obtaining feedback from the grid side, substantiating its pivotal role in supporting the comprehensive functionality of the GCPV system. Monitoring grid conditions during the operational phase of the PV system proves crucial, exerting a significant influence on grid parameters.

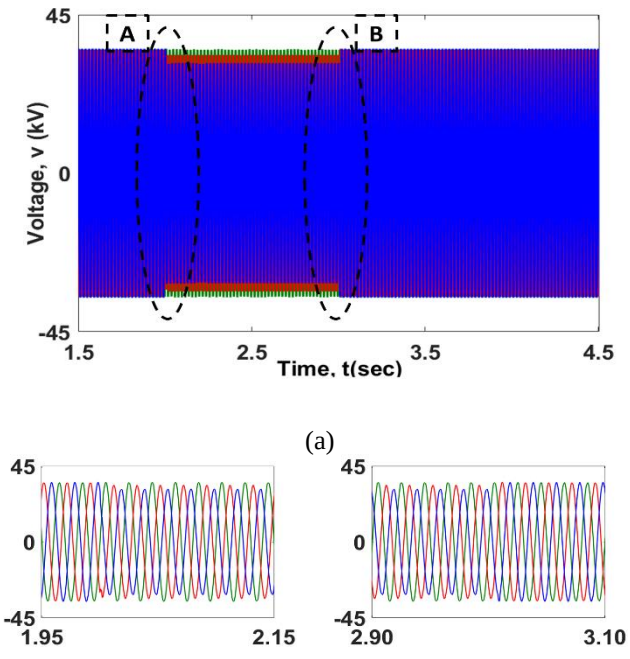

Fig. 6. 7. Instantaneous waveforms of three phase voltages at CCP under L-G fault (a) complete waveforms (b) transient voltages after applying the fault and (c) transient voltages when the fault is cleared.

6.3 Symmetrical short circuit faults

Most recent studies on the analysis of short-circuit faults in renewable energy systems predominantly focus on asymmetrical faults, such as L-G, which accounts for approximately 70% of short-circuit faults in power systems [126], as discussed in the previous section. However, it is imperative to investigate the behaviour of GCPV systems under symmetrical short-circuit faults. While such faults are infrequent in practical power systems, they are classified as the most severe faults, emphasizing the necessity for a comprehensive understanding of their impacts on modern power systems. Consequently, the primary objective of this paper is to examine the dynamic behaviour of a GCPV system under symmetrical three-line-to-ground (3L-G) short-circuit faults.

6.3.1 3L-G short circuit faults

In this study, a symmetrical 3L-G short-circuit fault was introduced at two distinct locations, positioned at distances of 14 km and 140 km from the CCP, as shown in Figure 6.1. The selection of these two distinct locations was predicated on the premise that the installation of large-scale solar farms typically occurs outside residential areas, where the power system is more susceptible to this type of fault. However, the choice of the second point was aimed at assessing the influence of power system impedance on damping the short-circuit current and its repercussions on the photovoltaic (PV) system.

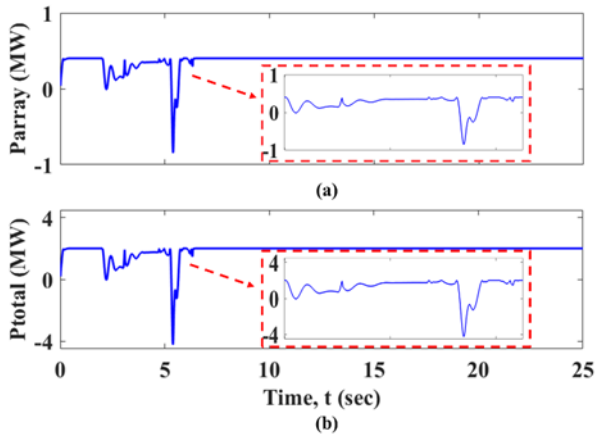

Fig. 6. 8. Power output of the PV system with 3L-G fault applied at 14km from the CCP (a) single PV array (b) total PV array

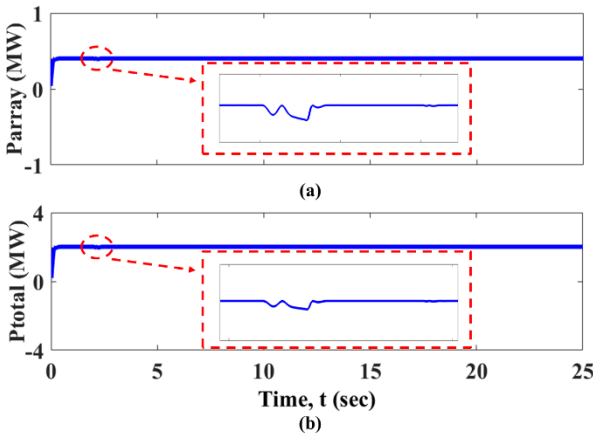

Fig. 6. 9. Power output of the PV system with 3L-G fault at 140km from the CCP (a) single PV array (b) total PV array

The dynamic behaviour, with a specific focus on the stability, of the integrated PV system was analysed during the fault occurrence and subsequent fault clearance. In the initial phase of

this investigation, the impact of this fault on the output power of the PV array and the overall power of the PV system was examined for both fault scenarios. The corresponding results are illustrated in Figures 6.8 and 6.9, respectively.

A comparison between Figures 6.8 and 6.9 clearly shows that the power system responses completely differently to these two kinds of faults. It can be seen that impacts of the short circuit faults highly depend on the physical distance between the fault point and the CCP. Figure 6.8 reveals a substantial disturbance in the output power of the PV array during the fault period. This disturbance is primarily attributed to the low inertia of the PV system, which limits its contribution to the stability of the system during the short-circuit fault. It is noteworthy that the short-circuit fault occurs at a mere 14 km distance from the CCP, exerting a significant impact on the normal operation of the PV system. However, post-fault clearance, the system promptly reverts to its normal operational condition, as explicitly illustrated in Figure 6.8. This recovery is facilitated by the designed control strategy, which relies on grid-side parameters for support which shown in Figure 6.4 highlighted under the external control loop section. Conversely, when the fault is introduced at a greater distance of 140 km from the CCP, its influence on the PV system is significantly attenuated, as depicted in Figure 6.9. This mitigation arises primarily from the higher impedance between the short-circuit point and CCP, effectively diminishing the impact of the short-circuit fault on the PV system. A comparable phenomenon was observed at the DC busbar for these two fault scenarios, as illustrated in Figures 6.10 and 6.11, respectively.

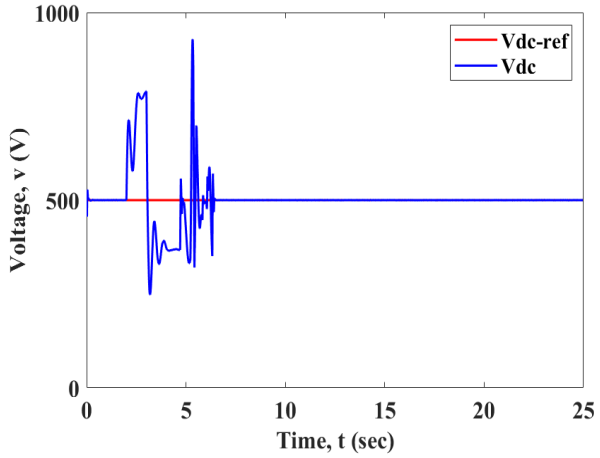

Fig. 6. 10. Voltage at the DC busbar with 3L-G fault applied at 14km from the CCP

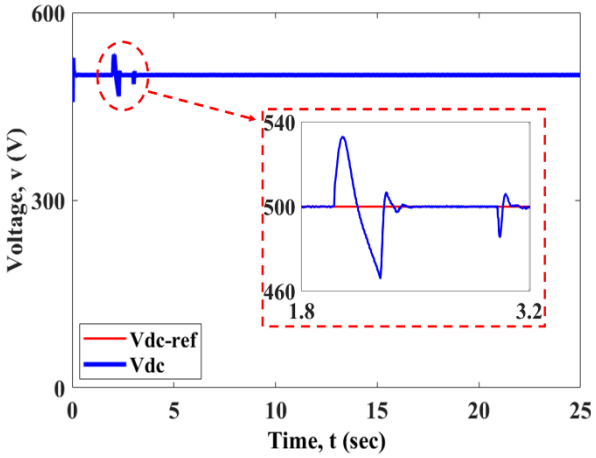

Fig. 6. 11. Voltage at the DC busbar with 3L-G fault applied at 140km from the CCP

As depicted in Figure 6.10 when the fault is introduced at the grid side, a voltage surge is evident at the DC link busbar. Upon clearance of the fault, this voltage surge diminishes. However, the impact of the fault persists, maintaining the system in a transient condition for approximately 3.5 sec. Within this transient period, another voltage surge emerges with a magnitude surpassing the preceding stage. Nevertheless, it rapidly attenuates towards the end of this transient period, initiating the restoration of the system to its normal operational condition. Following the peak surge, it takes approximately 1 sec for the DC voltage to converge to the reference value, thus re-establishing stability as defined by the control system. Nonetheless, when the fault is induced at a longer distance from the CCP, the impact of the applied fault is significantly mitigated, and the PV system sustains stability even under the same short-circuit fault condition, as illustrated in Figure 6.11. This response distinctly indicates that the primary impact of the pertinent short-circuit fault is confined to a minimal transient period, featuring an overshoot of 40V magnitude in contrast to the 450V magnitude observed in the initial fault scenario.

On the other hand, the dynamic response of voltages and currents at the inverter terminal and CCP closely aligns with that of the conventional power systems. Specifically, at the inverter terminal, the results indicate that in the first fault scenario, PWM voltage exhibits distortion, with the pulses deviating from their regular sequence and displaying an imbalance along with a slight dip in magnitude. However, in the second scenario, the system demonstrates its ability to maintain stability in terms of voltage, as transient oscillations are observed for a significantly shorter duration compared to the first scenario.

Concerning the current at the same point, in the first scenario, a surge was observed for 1 second during the fault period. Subsequent to fault clearance, the system persisted in a transient unstable condition for approximately 3.5 sec, after which it returned to normal operation. Conversely, a similar phenomenon was observed in the second scenario, albeit with a shorter transient period. Once the fault was cleared, the system swiftly restored to its normal operation, indicating the system's resilience in handling such situations. Three-phase voltage and currents at the inverter terminal are depicted in Figures 6.12 and 6.13, respectively.

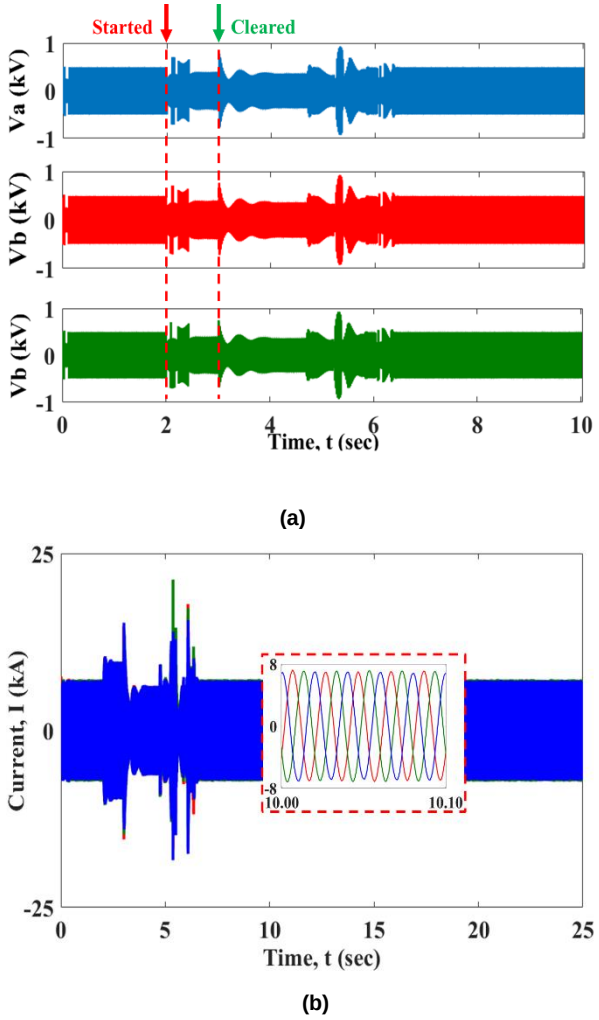

Fig. 6. 12. (a) Voltages (b) Currents at the inverter terminal with 3L-G fault applied at 14 km from the CCP

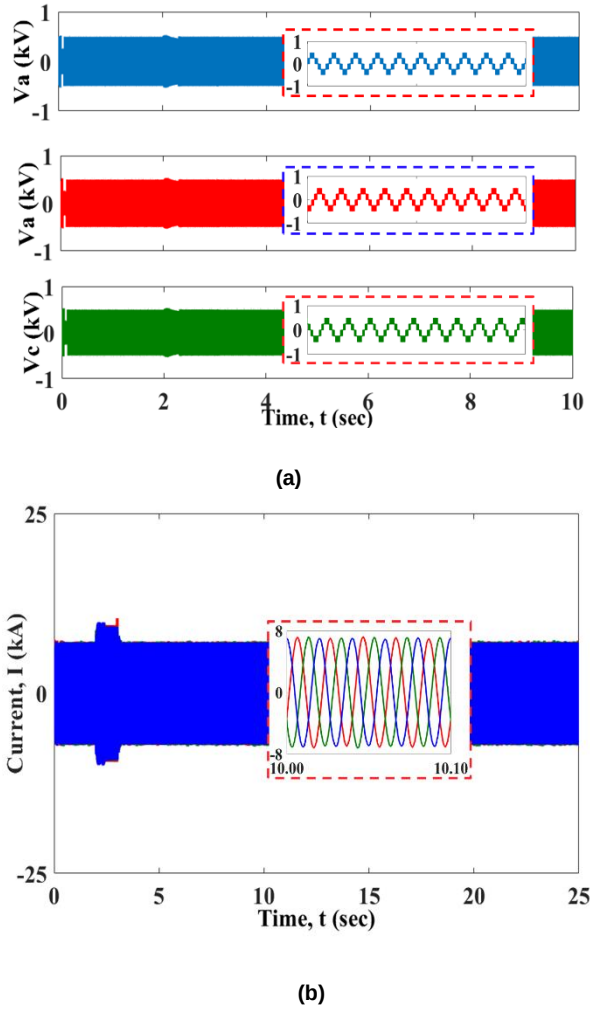

Fig. 6. 13 (a) Voltages (b) Currents at the inverter terminal with 3L-G fault applied at 140 km from the CCP

Three-phase voltages and currents at the CCP were then monitored, and the results for both short-circuit faults are presented in Figures 6.14 and 6.15, respectively. The impact of the first short-circuit fault is somewhat analogous to its effect at the inverter terminal, particularly concerning the current. A surge in the current was observed, with a transient period two to three times longer, until it returned to normal operation. However, in terms of voltage at CCP, the impact of the fault is distinctly manifested by a significant dip in the magnitude of the three phases. This can be explained by the influence of the fault on the three phases, wherein, once the fault was cleared, the voltage returned to its normal magnitude with some fluctuation during the same transient condition for about 3.5 sec.

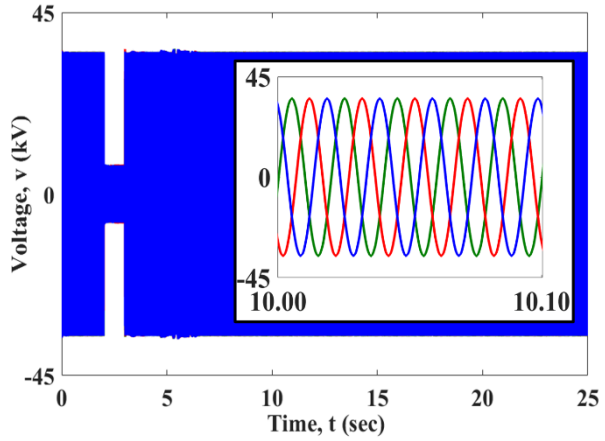

(a)

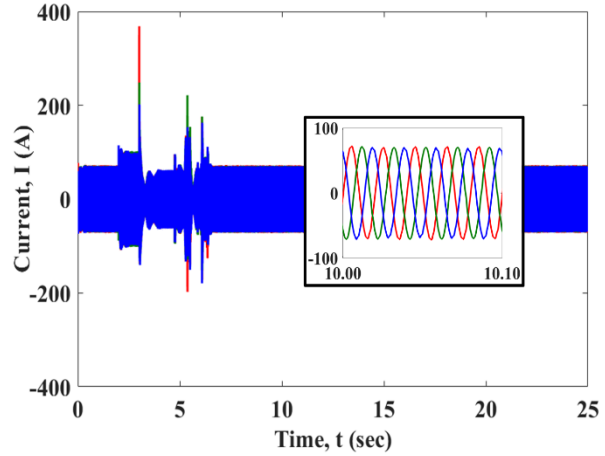

(b)

Fig. 6. 14. (a) Voltage (b) Current at the CCP with 3L-G fault applied at 14 km from the CCP

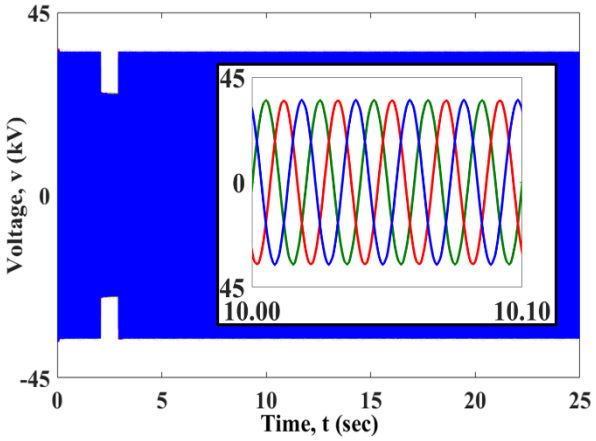

(a)

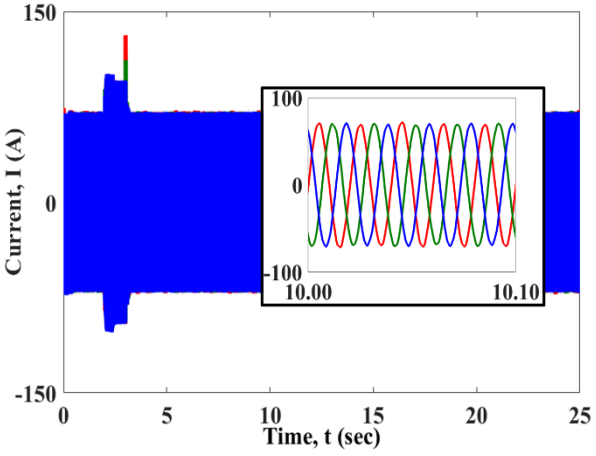

(b)

Fig. 6. 15. (a) Voltage (b) Current at the CCP with 3L-G fault applied at 140 km from the CCP

This phenomenon is primarily attributed to the presence of energy-saving components, such as inductors and capacitors, as well as the inertia of the components on the grid side. Furthermore, in the second fault scenario, a noticeable difference in terms of magnitude and time period of the oscillations was observed for both voltage and current, coupled with the system's ability to promptly restore normal operation after the fault clearance. An additional noteworthy point is the considerable reduction in the voltage dip in the second scenario, attributed to the increased distance of the fault location. This observation underscores the dependence of fault characteristics on the impedance level between the fault location and the installed PV system at the CCP. In the second case, the system maintains a higher level of impedance at the CCP, resulting in a lesser dip in the magnitude of the voltage.

6.4 LVRT Capability Analysis:

Short-circuit faults introduce voltage dips, and the grid's stipulation to remain connected during the fault period is specified through Low Voltage Ride Through (LVRT) requirements [146]. In this study, the LVRT capability of the modelled GCPV system has been analysed in accordance with the UK and Libyan grid code. Given the swift advancement of grid connected RESs, LVRT has become a mandatory requirement and has been widely incorporated into the grid codes of contemporary power systems [146] [195]. This concept is depicted graphically in Figure 6.16. In this graph, V_n indicates nominal voltage, V_F shows voltage during the period of the fault, V_{AF} represents voltage after the fault, and T_F and T_r denote the period during which voltage dipped due to the fault and the recovery time, respectively. According to the LVRT requirement, the GCPV system tolerates voltage sags to a specific ratio of the rated voltage for a certain period, as illustrated in Figure 6.16. [196].

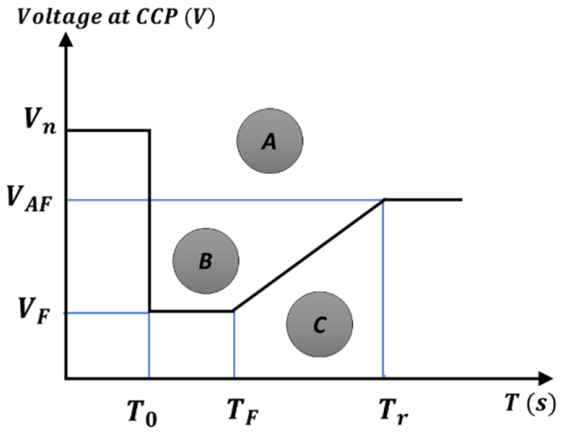

Fig. 6. 16. General curve limits of LVRT

In Figure 6.16, area Ⓐ indicates the normal operation of the GCPV system at the CCP. If the voltage magnitude at CCP falls within area Ⓑ, GCPV remains connected for a certain time (T_0 to T_F), and it should also have the ability to regain the nominal voltage magnitude at a certain rate. In area Ⓒ, the GCPV system is allowed to be disconnected. The rate of change of the voltage varies depending on the grid regulations for different countries. L-G faults, being the most prevalent type of fault in power systems, induce severe voltage sags. Therefore, it is crucial to analyse the LVRT capability of GCPV systems for the optimized setting and coordination of protection equipment.

To analyse the LVRT capability of the modelled system, a L-G fault was applied at the CCP for a duration of 140 ms, a duration recommended for this test [146]. The voltage profile was

subsequently monitored and analysed to assess the LVRT capability of the simulated system, and the results, in comparison with the UK standard, are depicted in Figure 6.17.

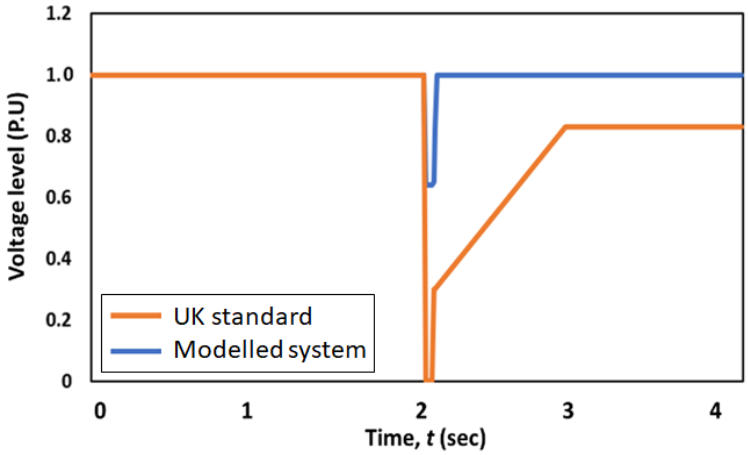

Fig. 6. 17. Comparison of LVRT of the modelled system and UK requirement

It can be clearly observed that during the time of fault, voltage at the CCP drops to 0.7 p.u. instantly and maintains the same value until fault is cleared after 140 ms. It is important to highlight that according to the UK standard [146], nominal voltage can drop to zero but for the modelled system, voltage value was maintained at a higher magnitude of 0.7 p.u.. After 140 ms of fault duration, voltage returned to its pre fault value, which is at a higher rate within 20 ms, for the modelled system, as compared to the minimum standard rate of the UK requirement.

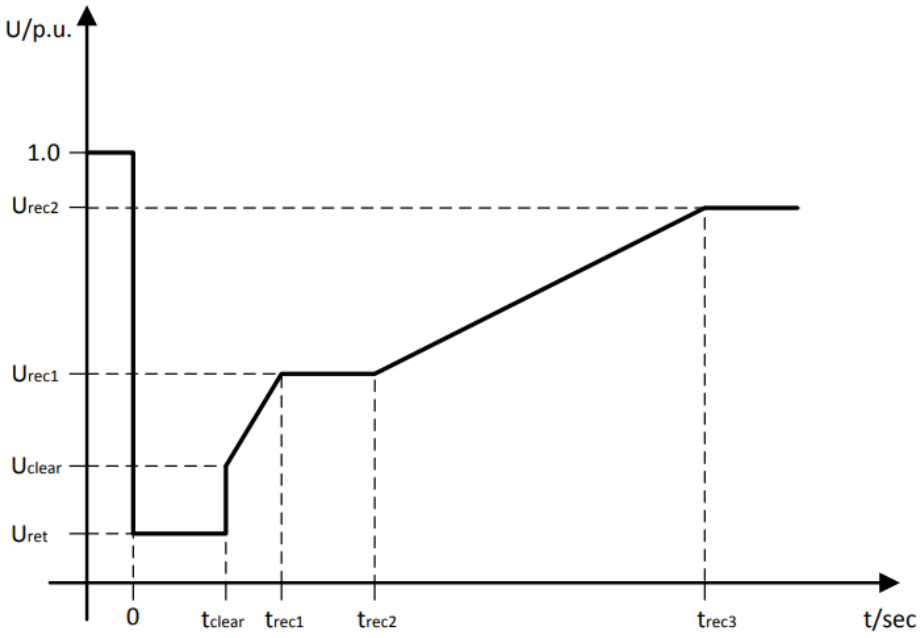

Fig. 6. 18. Low Voltage Ride Through requirement for Libyan grid codes [197]**.**

Chapter 6: ***Dynamic behaviour of a grid-connected Photovoltaic power system under short circuit fault scenarios***

According to [197], concerning the LVRT capability of a power generation system, the Libyan grid codes permit a voltage drop ranging from 5% to 15% during an asymmetrical fault at the CCP, as illustrated in Figure 6.18.

Figure 6.18 illustrates the minimum threshold for voltage at the CCP, allowing the system to remain connected to the utility grid and sustain stable operation. Here, U_{ret} represents the minimum voltage value at CCP during the fault period, t_{clear} denotes the time at which the fault is cleared, and U_{clear} signifies the lower limit of voltage after the fault clearance. Additionally, U_{rec1}, U_{rec2} denote the minimum voltage values during the recovery period at specific points in time, namely t_{rec1}, t_{rec2} and t_{rec3}. as defined by the Libyan network operator (GECOL), as indicated in Table 6.1.

Table. 6. 1. Parameters of fault-ride-through capability based on Libyan grid Codes [197]**.**

Voltage limits [p.u]		Time limits [sec]	
U_{ret}	0.5 - 0.15	t_{clear}	0.14 - 0.25
U_{clear}	$U_{ret} - 0.15$	t_{rec1}	t_{clear}
U_{rec1}	U_{clear}	t_{rec2}	t_{rec1}
U_{rec2}	0.85	t_{rec3}	1.5 – 3.0

Therefore, with an emphasis on comparing the simulation outcomes of the 2MW GCPV system under asymmetrical L-G short circuit fault presented in section 6.2.1 with the Libyan grid codes, it is evident that the system possesses the capability to ride through such faults. This is clearly demonstrated by examining the voltage level at the CCP, which only dropped to 0.7 p.u. of the rated voltage, while the Libyan grid codes permit a voltage drop of up to 0.15 p.u. Furthermore, the system swiftly restored to its pre-fault level within 0.2 sec, whereas the Libyan grid codes allow such a system 1.5 to 3.0 sec to return to 0.85 p.u. of the voltage level. The same holds true for symmetrical 3L-G short circuit faults, as evident from the results presented in section 6.3.1. The voltage dropped to 0.20 p.u. at the CCP when the fault was applied at a distance of 14km from CCP. Nonetheless, the system swiftly restored to its pre-fault level within 0.2 sec, with a sustained transient period of about 3 sec. It can be concluded that the system aligns with the requirements of the Libyan grid codes regarding LVRT capability.

6.5 Conclusions

Short-circuit faults represent the most common cause of disturbances in power systems. Therefore, it is a critical aspect that must be taken into account when modelling and integrating a PV system into the grid. Consequently, this chapter discusses and evaluates the performance of the simulated system by considering two primary short-circuit faults. Among these, L-G short-circuit faults are specifically addressed due to their frequency as the most common type of short-circuit fault occurring in power systems. The second fault is a 3L-G short-circuit fault, which is the most severe fault on the power network. By including these two types of faults, both categories of symmetrical and asymmetrical short-circuit faults were covered. The results showed that, with the designated control schemes in place, the performance of the PV side under L-G faults, including voltage at the DC busbar and MPPT, was not affected by the concerned short-circuit fault. More importantly, the system is capable of regaining its stability when the fault disappears, with a settling time of less than 0.2 seconds. On the other hand, to observe the impact of different distances of faults on the PV system, two fault scenarios with distances of 14 km and 140 km from the CCP were applied. The results show that fault characteristics and their impacts on the performance of the PV systems are highly related to the impedance level between the fault location and the CCP. The designed control system supported the system to maintain its stability, but with the increased distance of the fault, its impact was significantly reduced in terms of magnitude and period of the transient oscillation, as well as voltage sag at CCP. Moreover, it is important to highlight that with the designated control strategy in place, the system regained its stability in both fault scenarios once the fault was cleared, validating the simulation-based presented results in accordance with the definition of power system stability. The transient period after fault clearance was significantly low for the case of the second fault scenario. In terms of LVRT, the voltage at the CCP drops to 0.7 p.u. instantly and maintains the same value until the fault is cleared after 140 ms. It is important to highlight that according to the UK standard, nominal voltage can drop to zero. However, for the modelled system, the voltage value was maintained at a higher magnitude. After 140 ms of fault duration, the voltage returned to its pre-fault value, achieving this restoration at a higher rate within 20 ms for the modelled system.

Chapter 7:

Evaluation the energy production of the grid-connected Photovoltaic power system under the Libyan weather condition for different sites across Libya

7.1 Introduction

The main focus of this chapter is to assess the performance of the GCPV system in terms of energy production, with a primary emphasis on Libyan weather conditions, particularly solar irradiance and ambient temperature. The evaluation was conducted using MATLAB software across nine locations in the country, these locations are illustrated in Figure 7.1. For six of these locations, data were acquired from National Aeronautics and Space Administration (NASA) satellites through PVsyst software[198], while the remaining three locations relied on actual measurements obtained from the Libyan Centre for Solar Energy Research and Studies (CSESR). The selection of these sites was guided by two main factors: their proximity to residential areas and the goal of studying as much of the Libyan landmass as feasible.

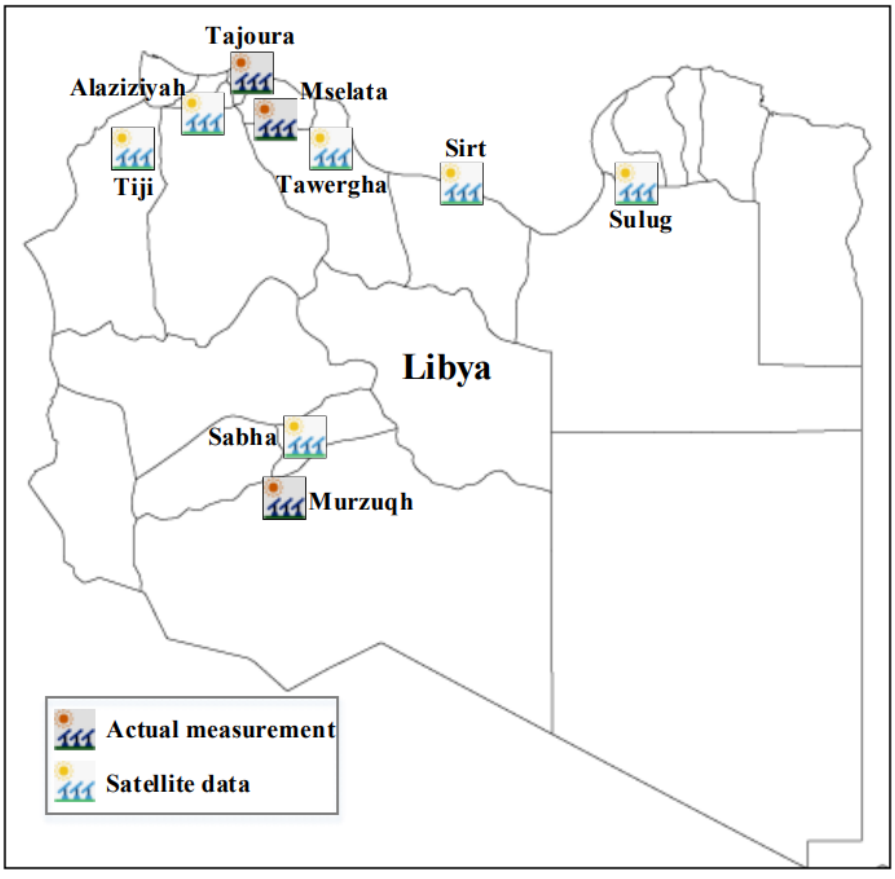

Fig. 7. 1. The potential map for installing PV system at nine locations across Libya.

The power production was evaluated using the double stage 2MW PV system developed in this work, which is consist of five PV array 400kW each, considering the equation (4.28) presented in Chapter 4, as well as the cell temperature obtained from equation (4.29). The characteristic P-V and I-V curves for single PV array are shown in Figure 7.2, (a): the PV array characteristic at different level of irradiance (b): the PV array characteristic at different temperature.

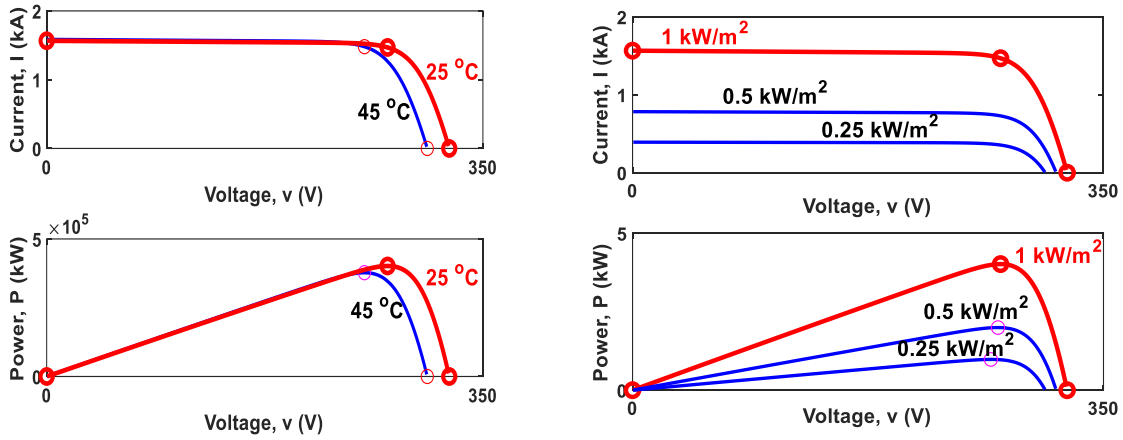

Fig. 7. 2. I-V and P-V characteristics of the PV array (a): at different temperature (b): at different radiation

7.2 The energy production based on the satellite data:

In this segment, the system's assessment was conducted for six sites using NASA's database. These sites were selected to be close to areas with the highest population density and to encompass the three main regions of the country. These cities include Tiji in the far west, AlAziziyah in the west, situated approximately 25km away from Tripoli, the capital of the country, Tawergha and Sirt in the middle of the coastal line, Sulug chosen to represent the Eastern region, and Sabha, the capital of the southern region, selected to examine the system's performance in the far south of the country. Furthermore, the number of houses that such system can be capable to provide their monthly energy demand was calculated, considering that the average Libyan household consumes approximately 20kWh per day, as indicated by [22]. This assumption was derived from the energy bills of a single Libyan household provided by General Electric Company of Libya (GECOL) over approximately 219 days throughout the year.

7.2.1 The energy production in the city of Tiji

As mentioned earlier, Tiji is situated in the far west of the country, approximately 250 km away from Tripoli, the capital. The city experiences a dry climate characterized by long hours of sunshine and relatively high ambient temperatures. The hourly solar radiation for this city is depicted in Figure 7.3.

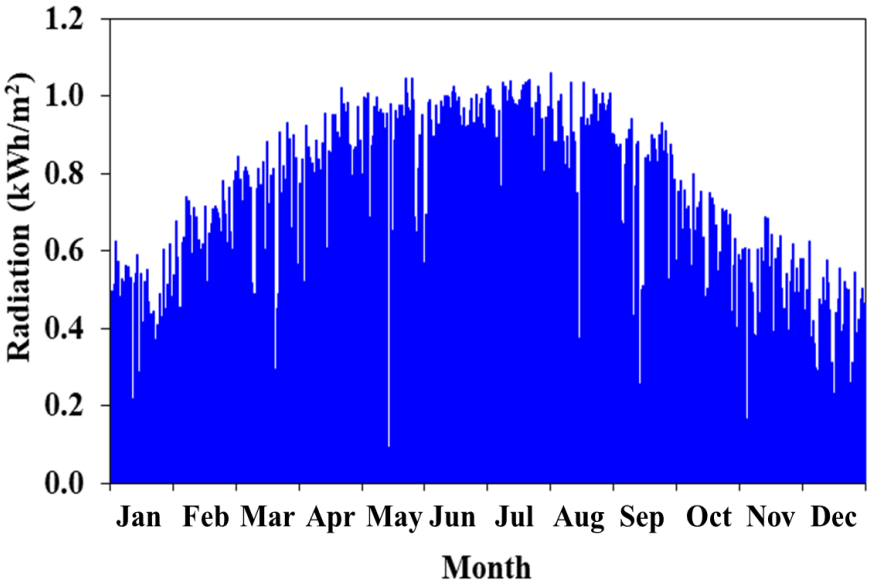

Fig. 7. 3. The hourly solar irradiance for the city of Tiji

As evident from the figure, solar irradiance reaches its peak in the middle of the year, with the highest levels recorded during the summer season, particularly in the month of July. Conversely, the lowest levels are observed at the end of the year during the winter season, specifically in December. Considering that the energy demand in Libya peaks during the summer season due to the extensive use of air conditioners, a correlation is noticeable between the pattern of solar irradiance and the energy demand, as discussed in Chapter 2. Figure 7.4 shows the hourly and monthly power and energy production for the PV system in this city. (a): The hourly PV output power (MW), (b): The average monthly energy production (MWh).

It is evident from the figure that the highest energy production was recorded in the month of July, equal to 442.44 MWh, followed by June and May with total energy production of 424.75 MWh and 403.91 MWh, respectively. Conversely, the lowest energy production was recorded in the month of December, amounting to 154.47 MWh. In terms of providing for residential energy needs, the system is capable of meeting the monthly energy demand for 714 houses in

the city during the month of July, the peak month. In the worst-case scenario, the system can still cater to the monthly energy demand for 249 houses in the month of December. The monthly energy production and the number of houses covered by this system are presented in Figure 7.5.

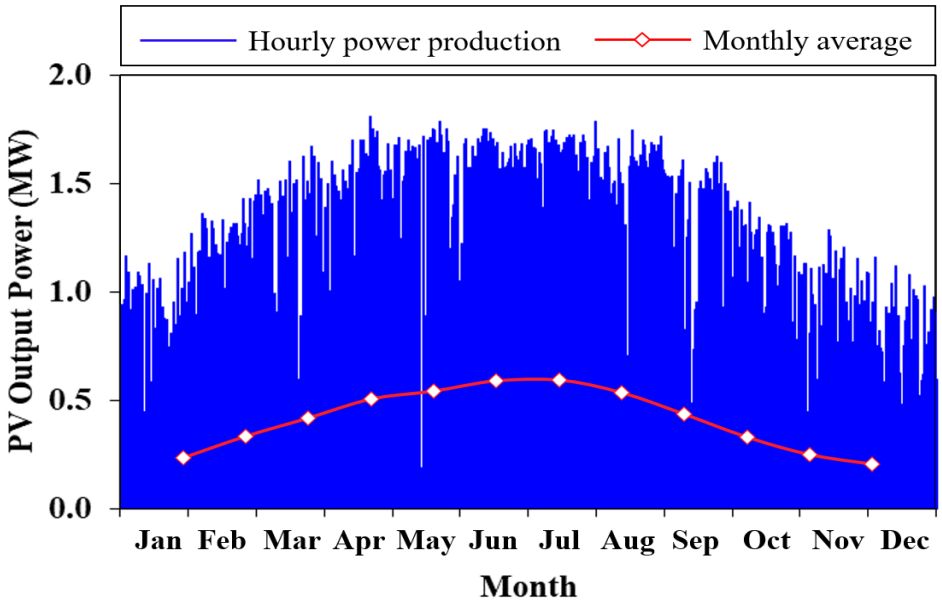

(a)

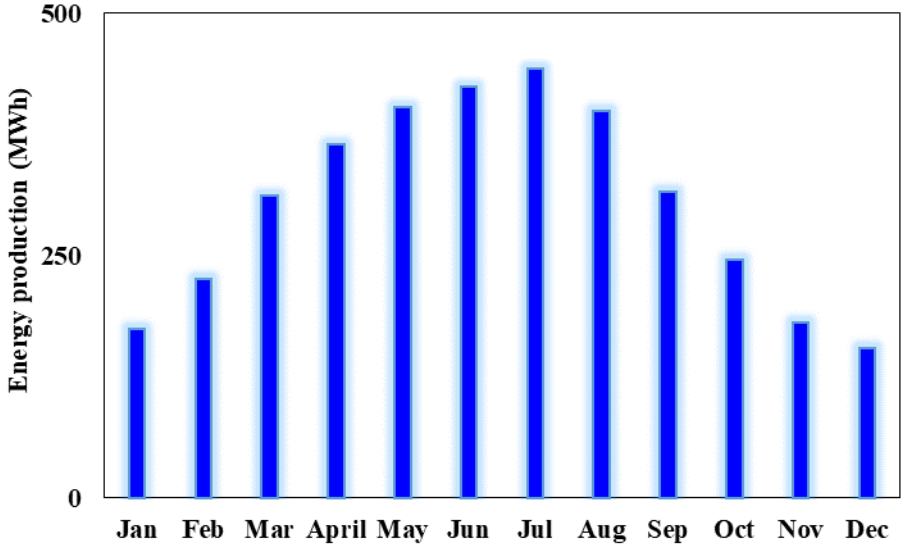

(b)

Fig. 7. 4. The hourly and monthly Power and energy production in the city of Tiji (a): Hourly Power production (b): The average monthly energy production.

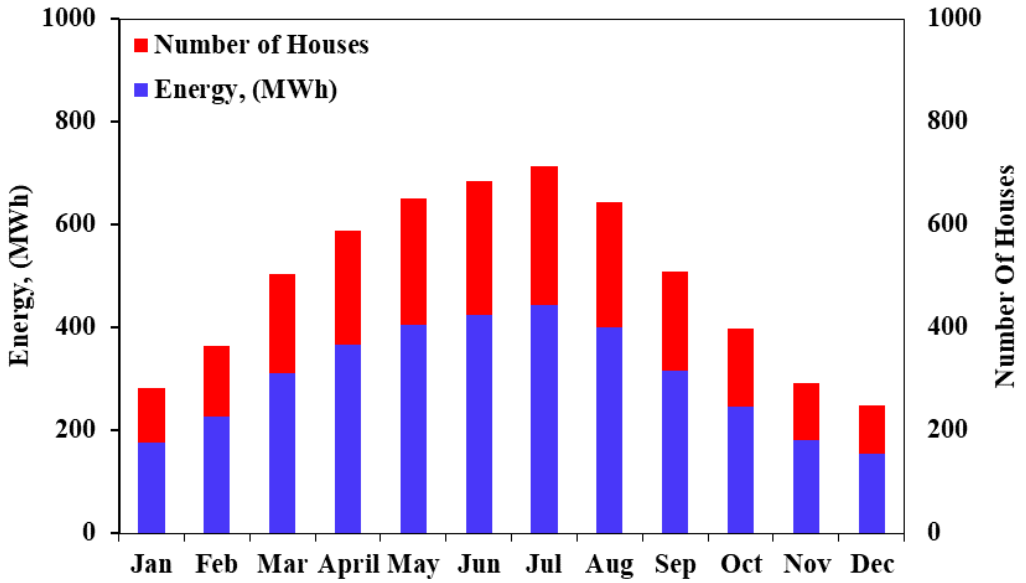

Fig. 7. 5. The monthly number of houses covered by the energy production of the system in the city of Tiji.

7.2.2 The energy production in the city of AlAziziyah

AlAziziyah city is situated in the western region of the country, a mere 25 km away from Tripoli. Renowned as one of the world's hottest places, this city has recorded some of the highest temperatures on record [199] [200]. The city experiences long hours of sunshine, with solar irradiance exceeding 1000 W/m^2 during the summer season. Figure 7.6 presents the hourly solar irradiance for a period of one year.

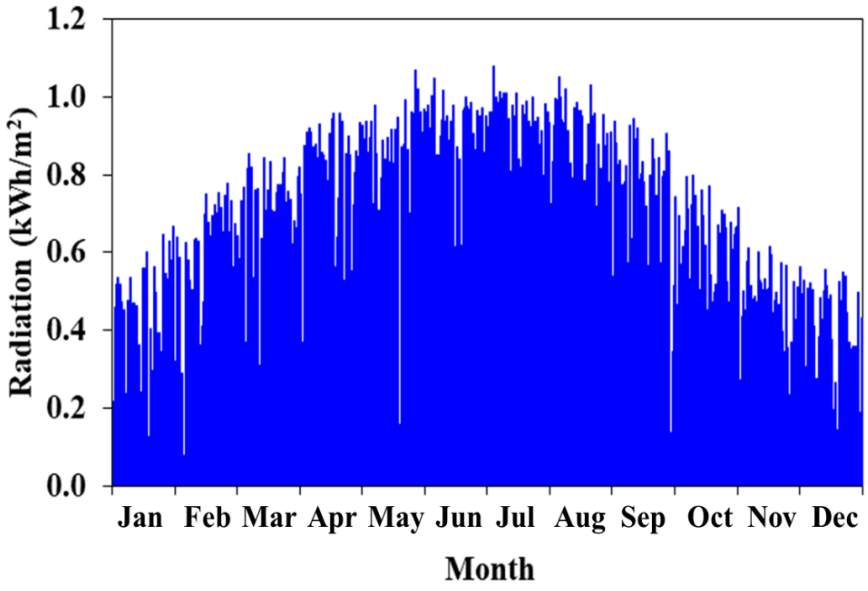

Fig. 7. 6. The hourly solar irradiance for the city of AlAziziyah.

Clearly, it can be noticed from the figure that the solar irradiance peaks in the middle of the year, specifically in the summer season, with a value of 1079 W/m^2 in the month of July. Meanwhile, the month of December shows the lowest level of solar irradiance. This is directly reflected in the monthly energy production of the system. Figure 7.7 demonstrates the hourly and monthly power and energy production for the system in this city. (a): The hourly PV output power (MW), (b): The average monthly energy production (MWh).

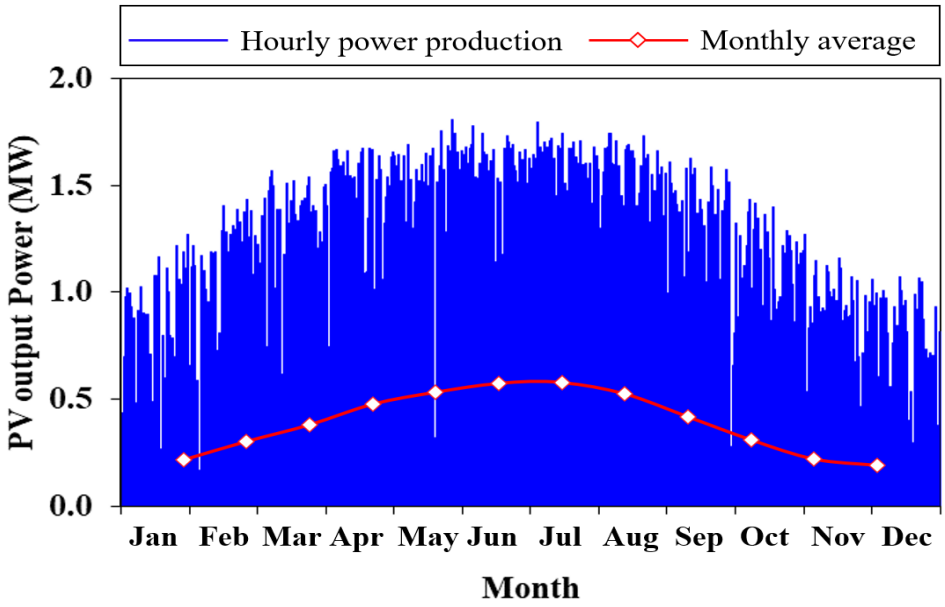

(a)

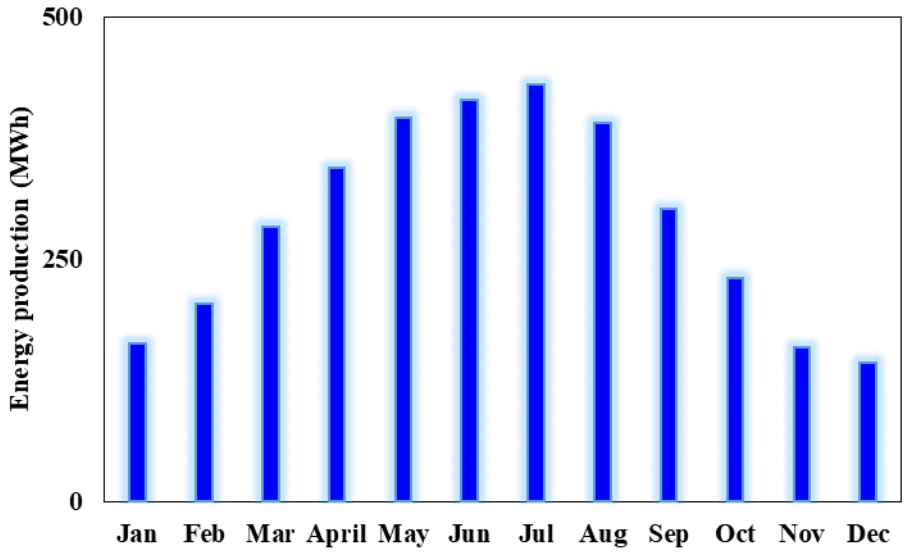

(b)

Fig. 7. 7. The hourly and monthly power and energy production in the city of AlAzizyah

(a): Hourly Power production (b): The average monthly energy production

From the figure, it can be clearly noticed that the highest energy production was recorded in the month of July, followed by June and May with values equal to 430.93, 414.64, and 396.60 MWh, respectively. The lowest energy production was recorded in the winter season, with the months of December, November, and January having energy values equal to 143.73, 159.48, and 163.22 MWh, respectively. Based on this energy production, the system will be capable of providing the energy demand for about 695 houses in the month of July during the summer season. In the winter season, when the system hits its lowest values, it will be able to provide the energy demand for about 232 houses. The monthly energy production and the number of houses covered by the system are presented in Figure 7.8 for the city of AlAziziyah.

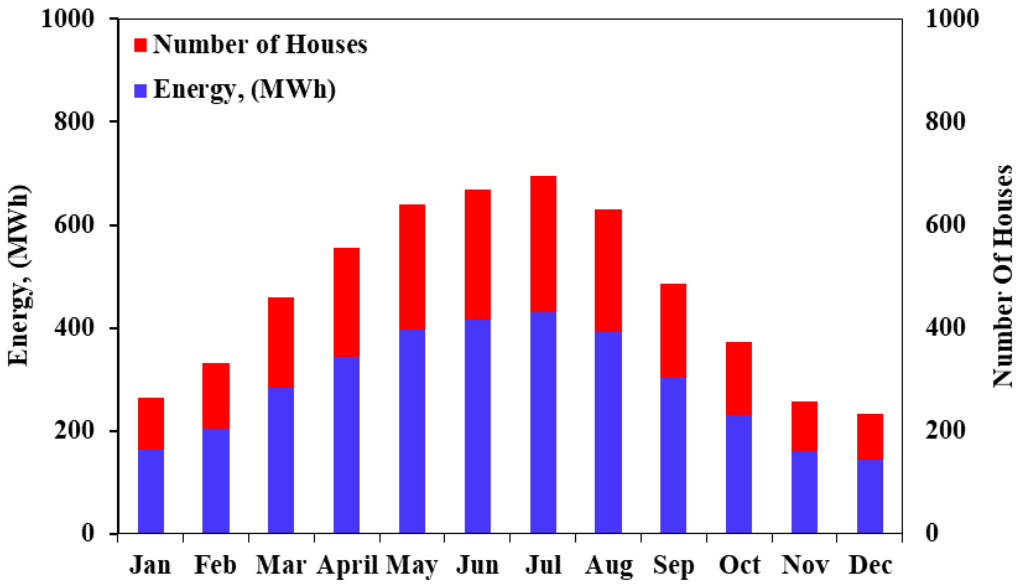

Fig. 7. 8. The monthly number of houses covered by the energy production of the system in the city of AlAziziyah

7.2.3 The energy production in the city of Tawergha

This city is located around 250 km to the east of Tripoli and is one of the coastline cities, bordered by the Mediterranean Sea to the north. Furthermore, the city experiences quite long hours of sunshine, with solar radiation reaching the level of 1000 W/m^2. Figure 7.9 shows the hourly solar irradiance for a period of one year.

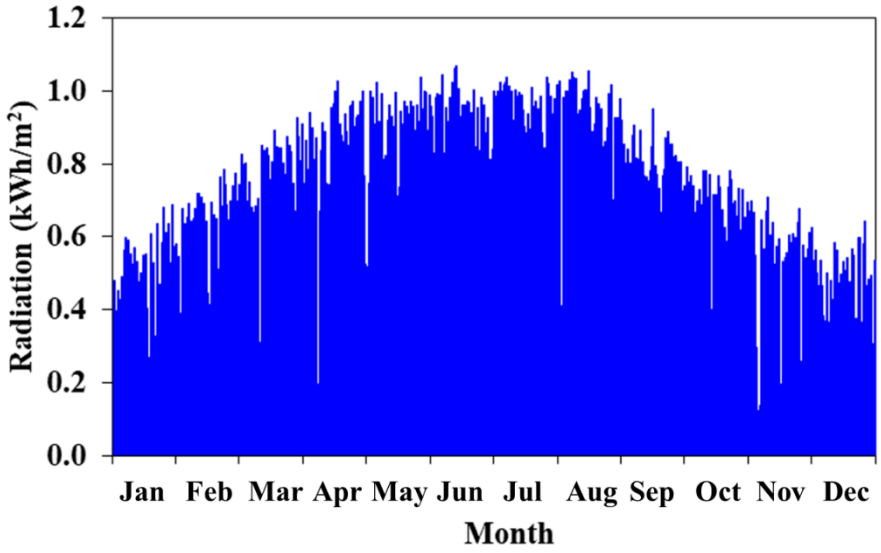

Fig. 7. 9.The hourly solar irradiance for the city of Tawergha

Similar to the previous two locations, solar irradiance reaches its highest value in the summer season. However, the highest solar irradiance point was recorded in the month of June, reaching 1069 W/m^2. Nevertheless, in terms of average monthly solar irradiance, July is the highest month, while in December, solar irradiance reaches its lowest value. The hourly and monthly power and energy production are shown in Figure 7.10. (a): The hourly PV output power (MW), (b): The average monthly energy production (MWh).

Again, it can be seen from the figure that even though temperature has a reverse impact on system performance, the highest energy production from the system was in the month of July with a total energy production of 446 MWh, followed by the months of June and May, which equal 426.73 and 410.40 MWh, respectively. While the lowest was also recorded in the month of December with a total energy of 167.35 MWh. The number of houses that the system is able to provide energy for is illustrated in Figure 7.11.

Notably, it can be seen from the figure that the energy production in the month of July could be capable of supplying the energy demands for around 719 houses, the highest during the year. Whereas in June and May, 688 and 662 houses will be covered by the energy produced by the system. While the system in its lowest performance during the month of December will be able to supply the energy demands for about 270 houses.

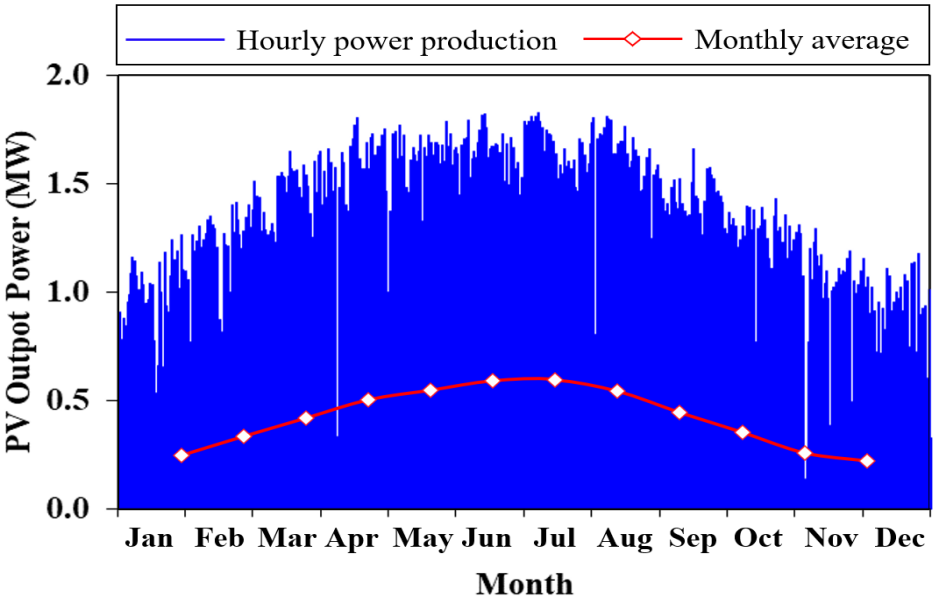

(a)

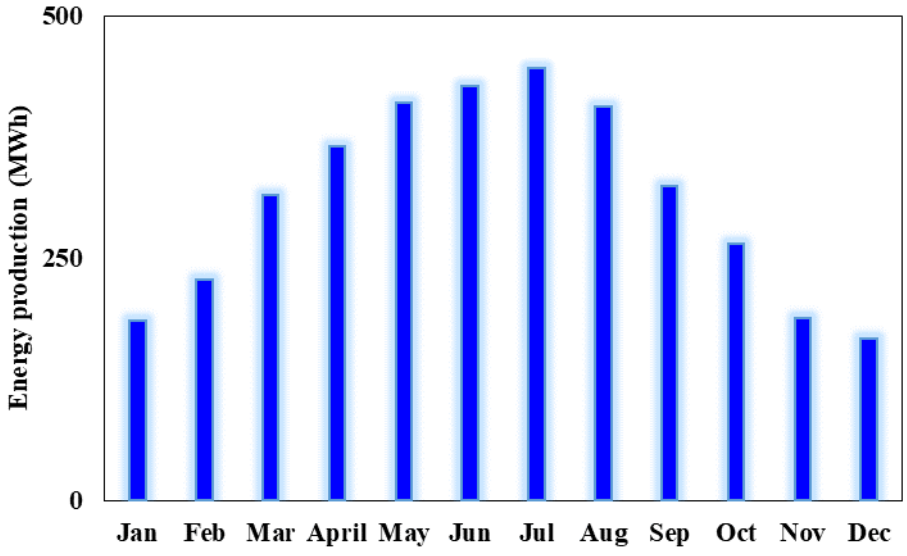

(b)

Fig. 7. 10. The hourly and monthly power and energy production in the City of Tawergha

(a): Hourly Power production (b): The average monthly energy production

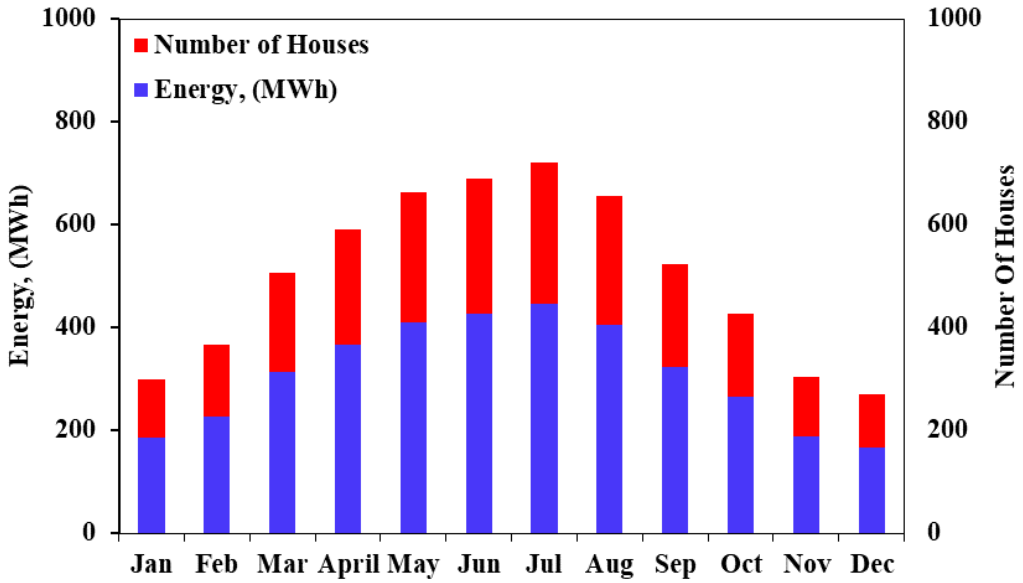

Fig. 7. 11. The monthly number of houses covered by the energy production of the system in the city of Tawergha

7.2.4 The energy production in the city of Sirt

The city of Sirt is located in the central region of the country, bordered by the Mediterranean Sea to the north and the desert to the south. It is approximately 454 km away from Tripoli and 570 km away from Benghazi, the largest city in the eastern region of the country. The city experiences moderate weather conditions with clear sky for long hours, receiving extended periods of solar irradiance as presented in Figure 7.12.

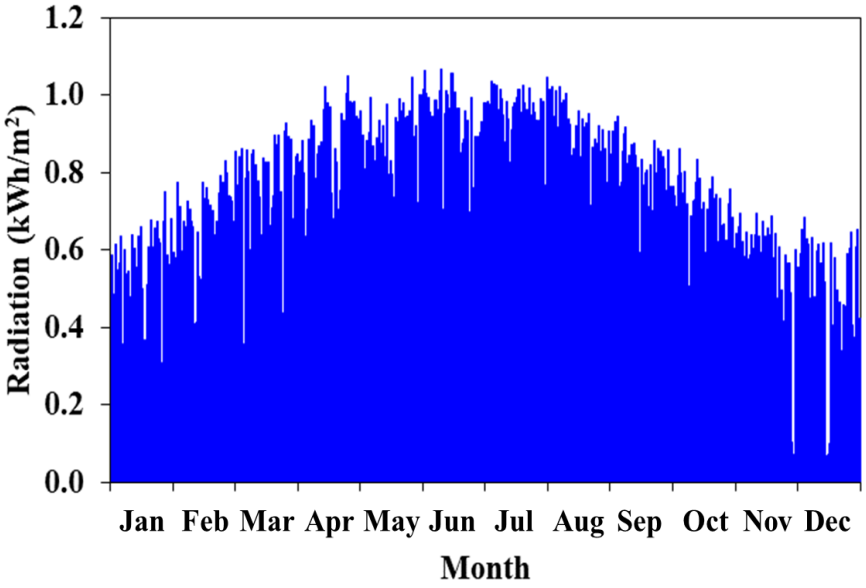

Fig. 7. 12. The hourly solar irradiance for the city of Sirt

The figure illustrates that the highest solar irradiance was recorded in the middle of the year, particularly during the months from May to August, reaching a value of 1000 W/m^2. Conversely, in the winter season, especially during the months from November to February, the surface of the earth receives the lowest level of solar irradiance. The hourly and monthly power and energy production are depicted in Figure 7.13. (a): The hourly PV output power (MW), (b): The average monthly energy production (MWh).

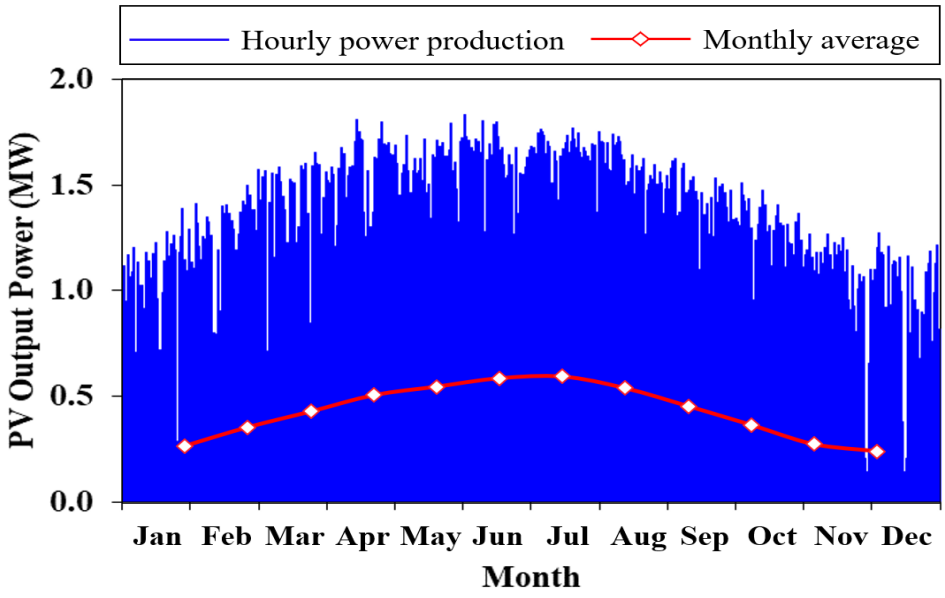

(a)

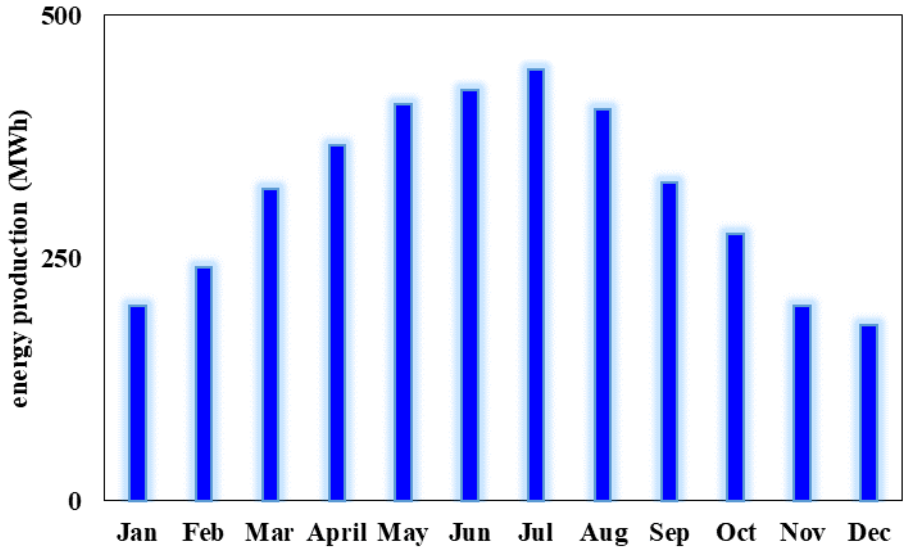

(b)

Fig. 7. 13.The hourly and monthly power and energy production in the city of Sirt

(a): Hourly Power production (b): The average monthly energy production

The same phenomenon was observed in this city, where solar irradiance reaches its peak values during the summer, thereby influencing energy production. The highest energy production was observed in the month of July, equal to 444.48 MWh, followed by June and May with total energy production of 423.79 and 408.29 MWh, respectively. Meanwhile, the lowest energy production occurred in the month of December, with amount of 181.49 MWh. The number of houses that the system is able to provide energy for is illustrated in Figure 7.14.

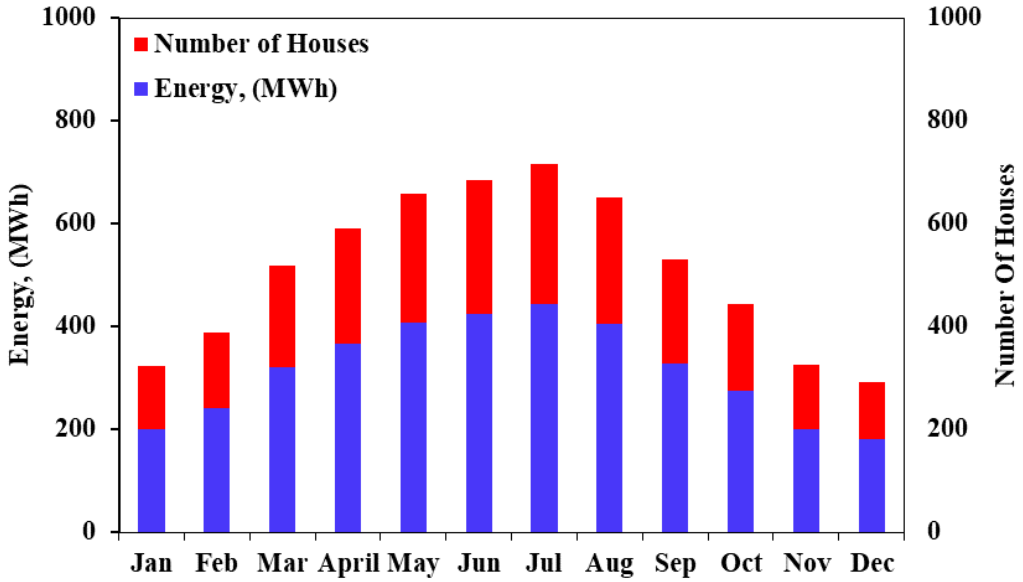

Fig. 7. 14.The monthly number of houses covered by the energy production of the system in the city of Sirt

The figure illustrates that the system is capable of producing enough energy to meet the needs of 717 houses in the month of July. In the months of June and May, the system will be able to meet the energy demand for 684 and 659 houses, respectively. Nevertheless, at its lowest performance, the system will be able to supply energy to 293 houses in the city of Sirt in the month of December.

7.2.5 The energy production in the city of Sulug

Sulug city is one of the cities located in the eastern region of the country, approximately 60 km away from Benghazi. The data provided for this city indicates that it experiences solar irradiance reaching a value of 1000 Wh/m^2, with long hours of sunshine throughout the day. Figure 7.15 displays the hourly solar irradiance for a period of one year.

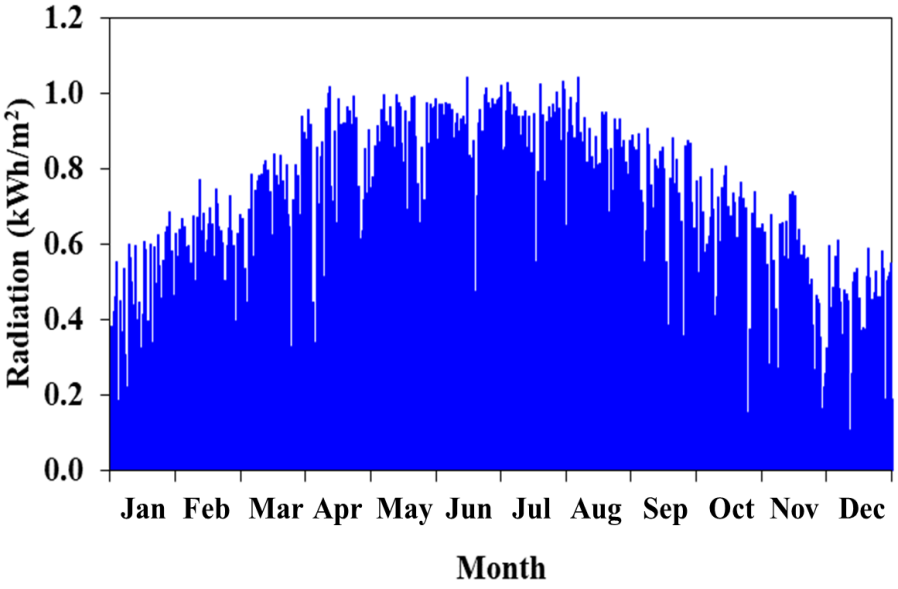

Fig. 7. 15. The hourly solar irradiance for the city of Sulug

As demonstrated by the figure, the same pattern of solar irradiance was observed here, with the highest level recorded during the summer season in the month of August, reaching a value of 1044 W/m^2. However, in terms of the average monthly level, July stood out as the highest, while the lowest average monthly level was recorded in December. The hourly and monthly Power and energy production for this city are shown in Figure 7.16. (a): The hourly PV output power (MW), (b): The average monthly energy production (MWh).

The pattern of energy production in this city matches that of the other cities mentioned above, where the highest energy production consistently occurred in the month of July, equal to 418.31 MWh. This energy output is sufficient to meet the energy needs of approximately 675 houses in July. Furthermore, the system will be capable of providing energy for 658 and 641 houses in the months of June and May, respectively. However, the lowest energy production was recorded in the month of December, which is sufficient to cover the energy needs of 257 houses. Figure 7.17 presents the monthly number of houses covered by the system in the city of Sulug.

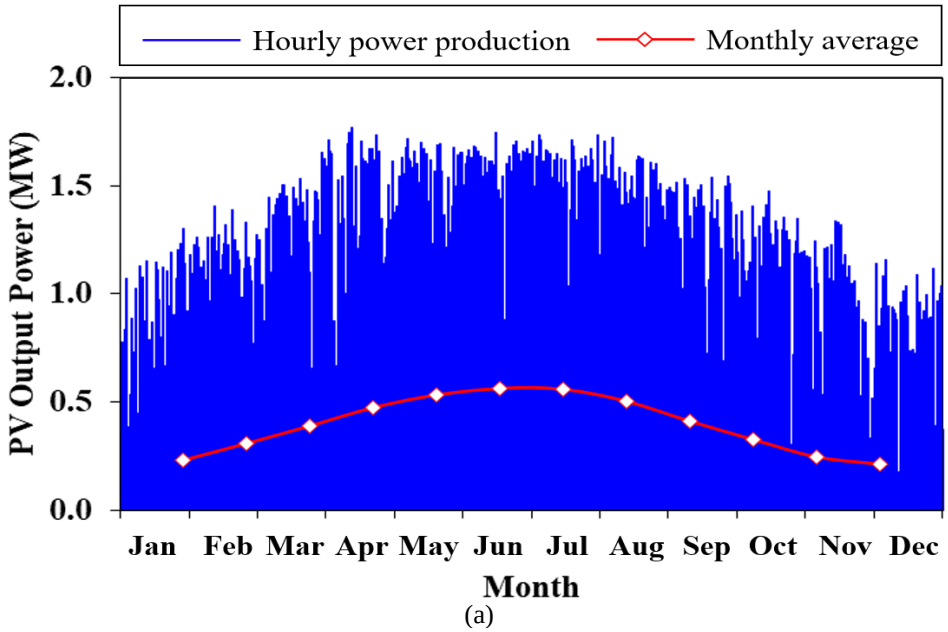

(a)

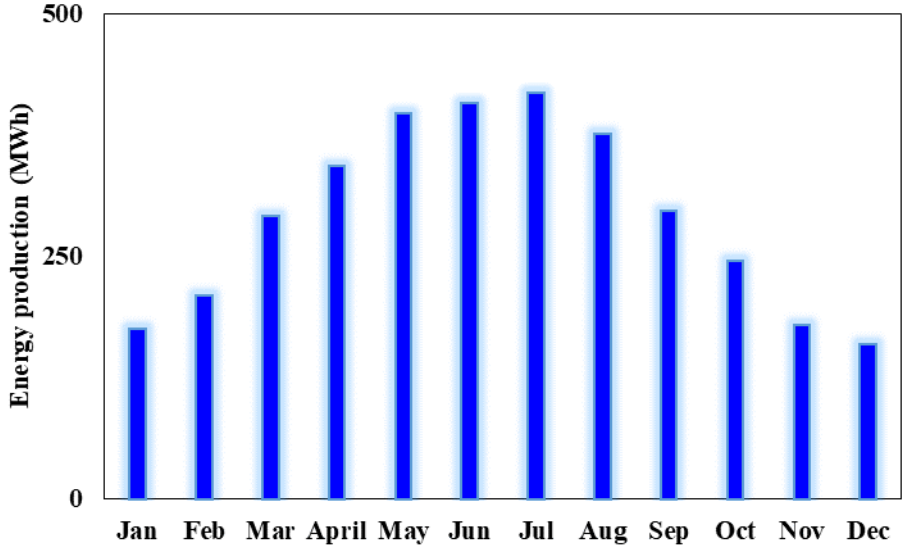

(b)

Fig. 7. 16.The hourly and monthly power and energy production in the city of Sulug

(a): Hourly Power production (b): The average monthly energy production.

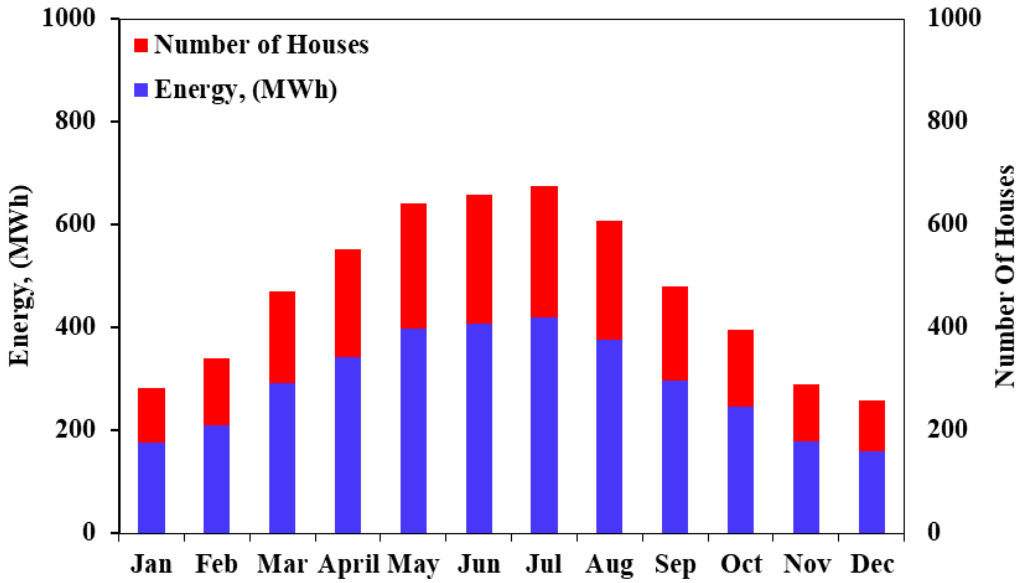

Fig. 7. 17.The monthly number of houses covered by the energy production the system in the city of Sulug.

7.2.6 The energy production in the city of Sabha

Sabha is one of the largest cities in Libya, situated in the southern region of the country and 772 km away from Tripoli. The city features a desert climate with relatively dry weather. The sun shines for extended hours, and the solar irradiance reaches 1000 W/m^2 during the summertime. Despite the fact that the southern region of Libya experiences higher levels of solar irradiance than the northern and eastern regions, as indicated by [27] [30], the high temperatures and dust have a negative impact on the system's performance in terms of energy production. Figure 7.18 illustrates the hourly solar irradiance for a period of one year.

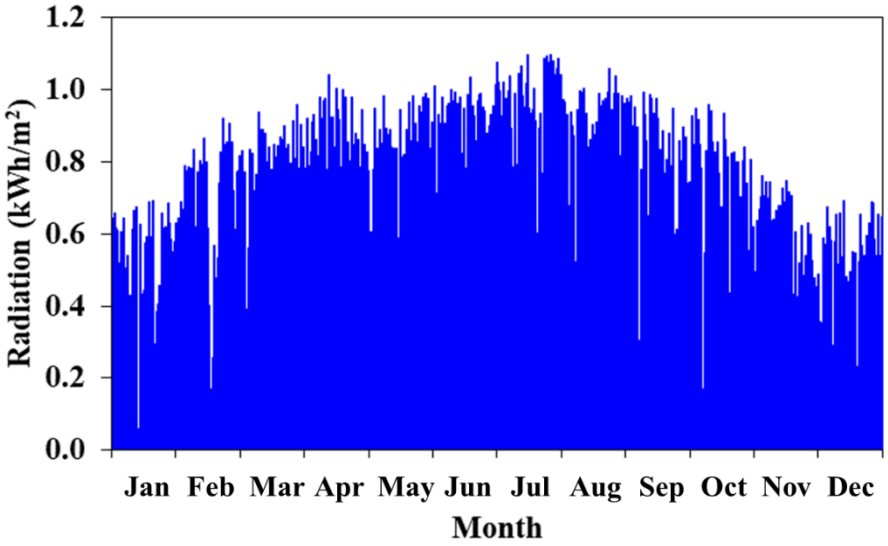

Fig. 7. 18.The hourly solar irradiance for the city of Sabha

Clearly, the figure illustrates the high levels of solar irradiance reaching the Earth's surface, peaking during the summer season from May to August. The lowest solar irradiance level occurs in the month of December. This pattern is reflected in the energy production of the system in this city. Figure 7.19 depicts the hourly and monthly power and energy production in Sabha. (a): The hourly PV output power (MW), (b): The average monthly energy production (MWh).

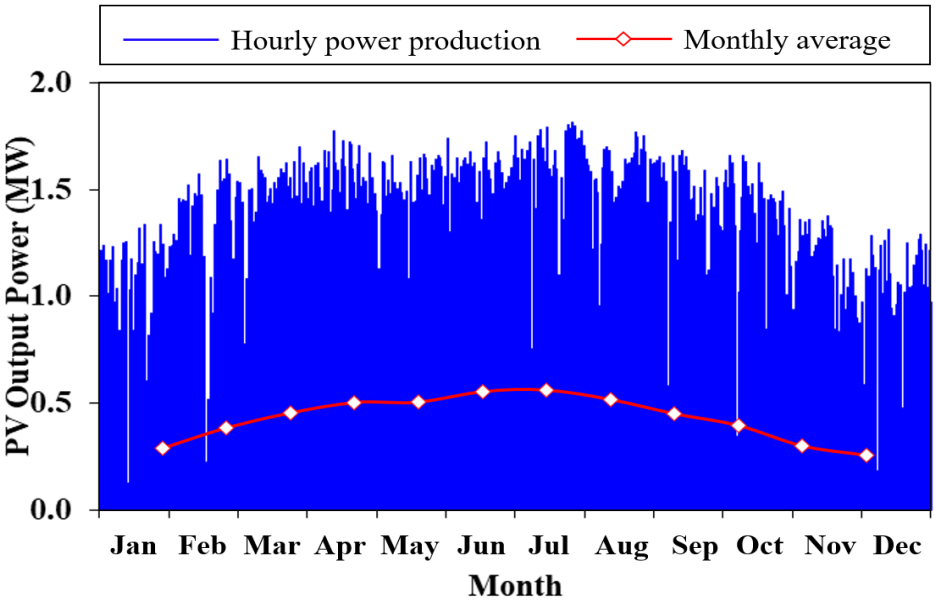

(a)

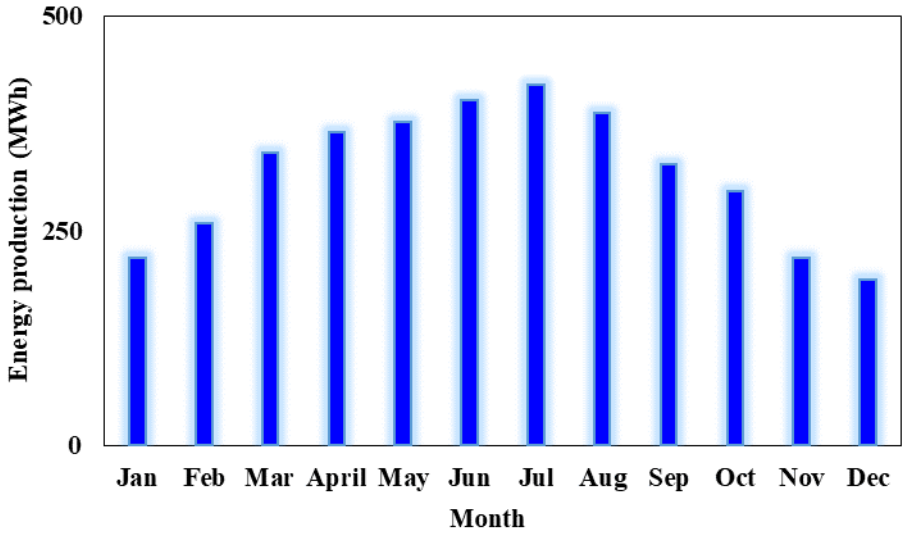

(b)

Fig. 7. 19.The hourly and monthly power energy production in the city of Sabha (a): Hourly energy production (b): The average monthly energy production

As is customary, the month of July boasts the highest energy production level, totalling 419.24 MWh, sufficient to meet the energy needs of 676 houses. Following closely, the months

of June and August contribute with total energy productions of 401.02 and 387.26 MWh, capable of supplying the energy needed for 647 and 625 houses, respectively. Conversely, the lowest energy production is recorded in the month of December, generating a total energy output of 193.08 MWh, enough to cover the energy demand for 311 houses in the city. Figure 7.20 illustrates the monthly number of houses covered by the PV system in the city of Sabha.

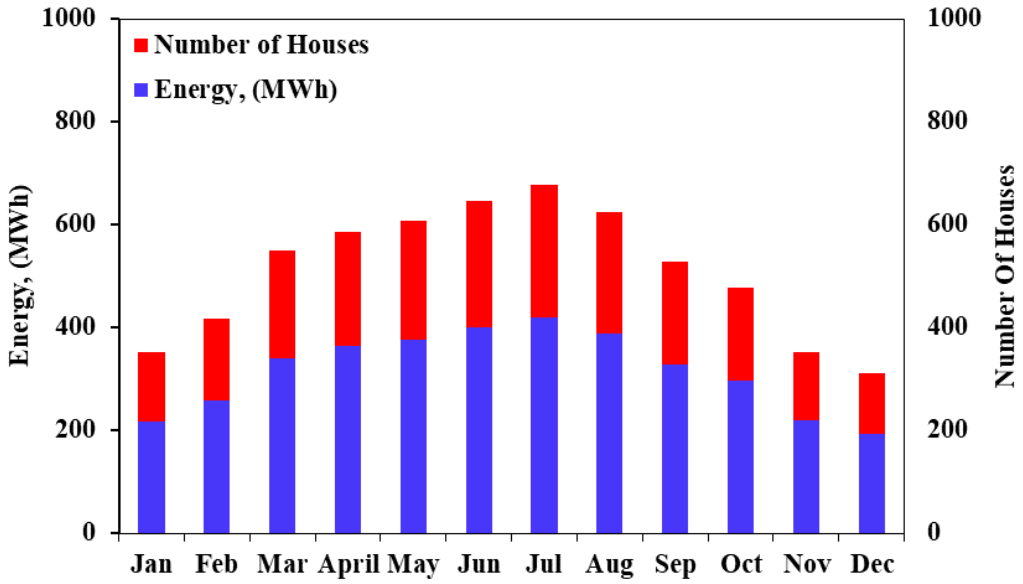

Fig. 7. 20. The monthly number of houses covered by the energy production of the system in the city of Sabha.

To conclude this section, a common thread is evident across all locations in terms of solar irradiance levels and, consequently, monthly energy production. The energy production pattern reaches its zenith during the summer season, notably in the month of July. Conversely, the lowest energy production is observed in the winter season, particularly in December. This variance can be attributed to the prevailing weather conditions, with winter bringing an increased likelihood of cloud cover, unlike the summer season characterized by predominantly clear skies. Figure 7.21 illustrates the total annual energy production alongside the total number of houses per year for these six sites, where their data was obtained based on NASA satellites using PVsyst software.

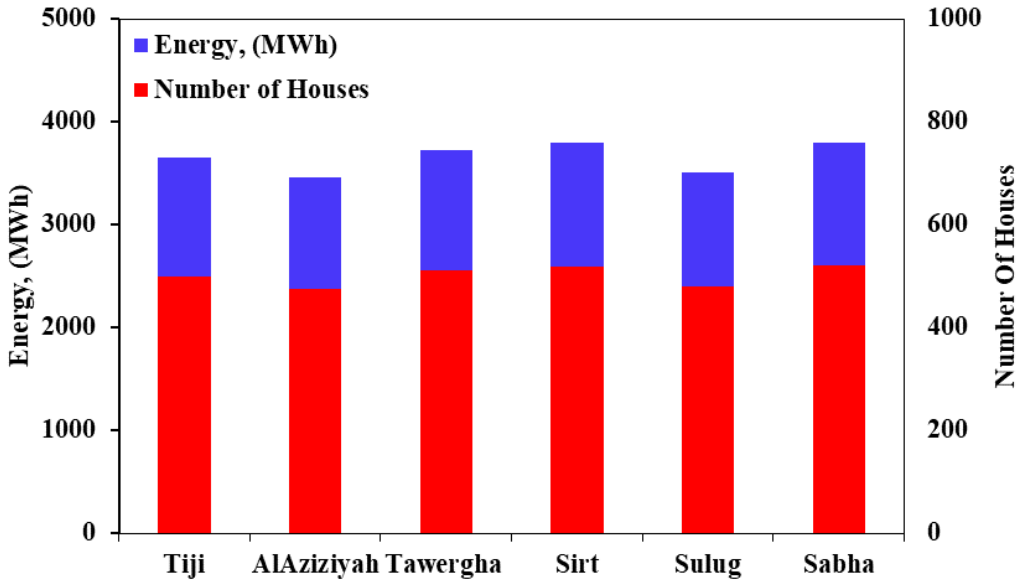

Fig. 7. 21. The annual number of houses covered by the energy production of the PV system in the six sites

It is evident that there are no significant differences in the total annual energy production among the six sites. Sabha city recorded the highest annual energy production, totalling 3798.96 MWh/year, capable of satisfying the annual energy demand for around 520 houses. Sirt follows closely with a slightly lower figure, achieving a total energy production of 3795.19 MWh/year, sufficient for the annual energy needs of 519 houses. Conversely, AlAziziyah city registered the lowest annual energy production, amounting to 3464.30 MWh/year, which is ample to meet the annual energy demand for 475 houses.

7.3 The energy production based on actual measurement:

The primary objective of this section is to assess the system's performance in terms of power production using actual readings for solar irradiance levels and ambient temperature. These authentic measurements were sourced from the CSESR and pertain to three locations in Libya: Tajoura (the centre’s location), Mselata, and Murzuqh. The data, collected every ten minutes throughout the year, was converted to an hourly basis to facilitate a comprehensive year-round analysis. The secondary goal is to compare these actual measurements with the data presented in the previous section, serving as validation, and paving the way for the study of additional locations across the country.

7.3.1 The energy production in the city of Tajoura

Tajoura, situated among Tripoli's counties and bordered by the Mediterranean Sea, hosts the CSESR. Its coastal location results in mild weather, a clear sky, and extended hours of sunshine, particularly during the summer season. Figure 7.22 illustrates the hourly solar irradiance levels for the entire year.

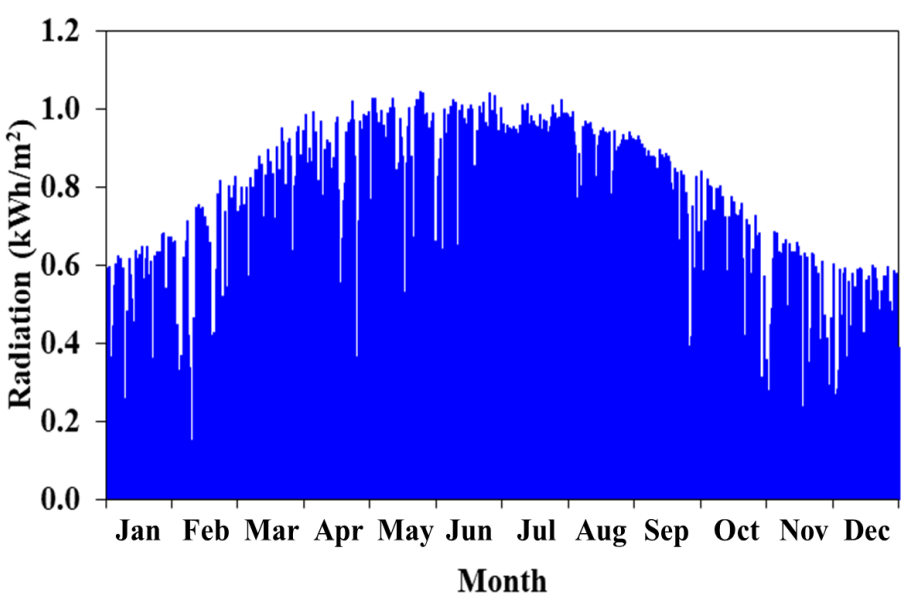

Fig. 7. 22. The hourly solar irradiance for the city of Tajoura

At first glance at the figure, it is evident that the solar irradiance pattern throughout the year aligns with that of other cities presented in the previous section. The solar irradiance peaks during the summer season, from May to August, while the lowest levels are recorded in the winter season, from November to February. This pattern directly influences the system's performance in terms of energy production. Figure 7.23 illustrates the hourly and monthly Power and energy production. (a): The hourly PV output power (MW), (b): The average monthly energy production (MWh).

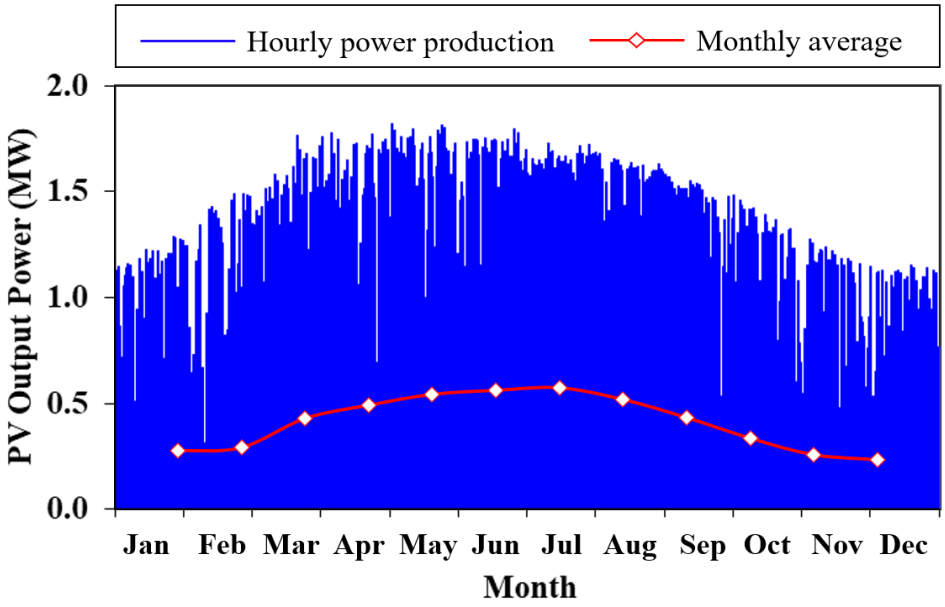

(a)

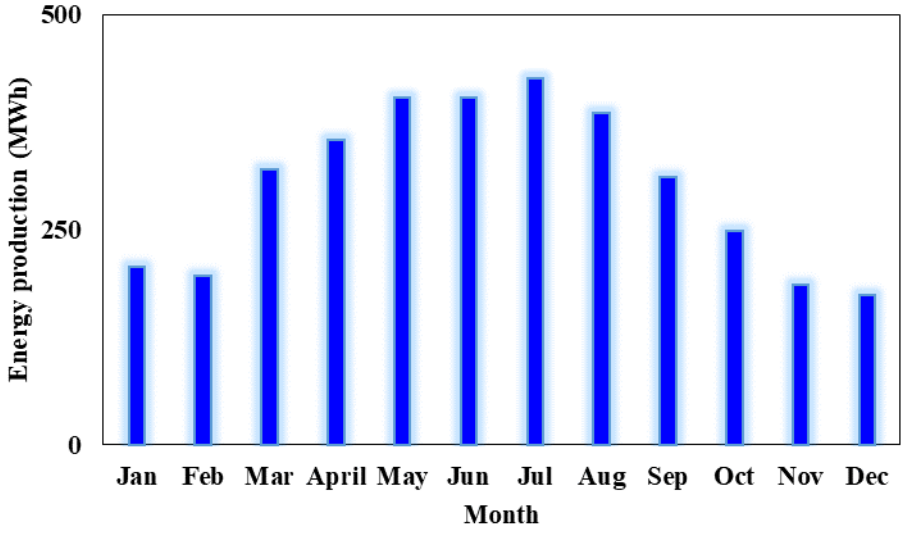

(b)

Fig. 7. 23. The hourly and monthly power and energy production in the city of Tajoura (a): Hourly Power production (b): The average monthly energy production

The figures clearly show that the month of July exhibits the highest performance in terms of energy production, reaching a value of 426.12 MWh. May and June follow closely with total production of 404.34 and 403.95 MWh, respectively. In contrast, the month of December records the lowest monthly energy production, amounting to 174.29 MWh. Furthermore, these energy production levels are sufficient to meet the energy demand for 687 houses in July, 652 houses in May and June, and 281 houses in December. Figure 7.24 illustrates the monthly number of houses covered by the system in the city of Tajoura.

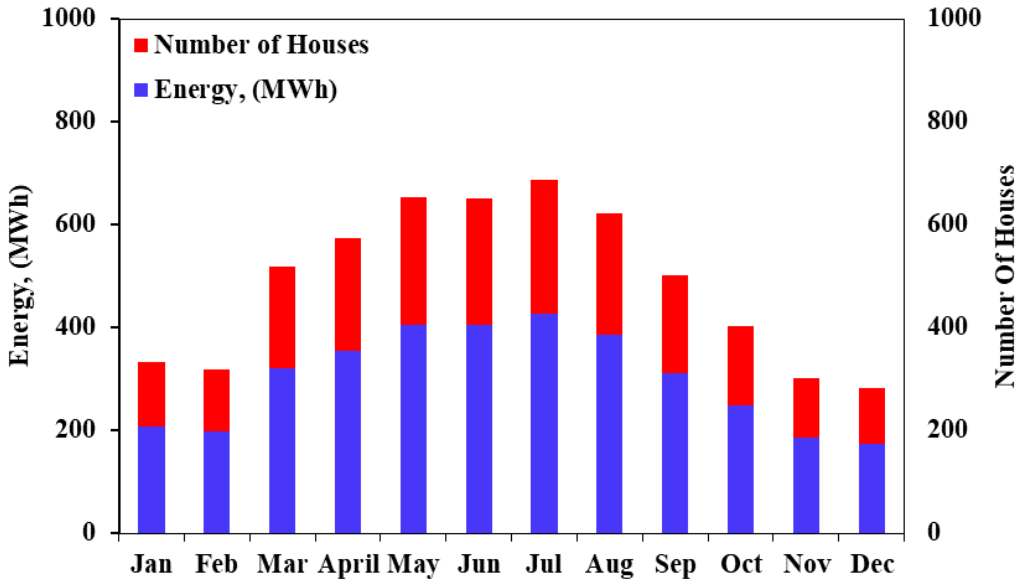

Fig. 7. 24. The monthly number of houses covered by the energy production of the system in the city of Tajoura

7.3.2 The energy production in the city of Mselata

This city, situated in the western region of the country, lies 104 km away from Tripoli. The GECOL has chosen this location for the installation of a wind farm due to its relatively high wind speed. Additionally, according to [31] [201], the city experiences relatively high solar irradiance. Proximity to the coastal line contributes to its mild weather and long hours of clear sky. The hourly solar irradiance levels for this city are depicted in Figure 7.25.

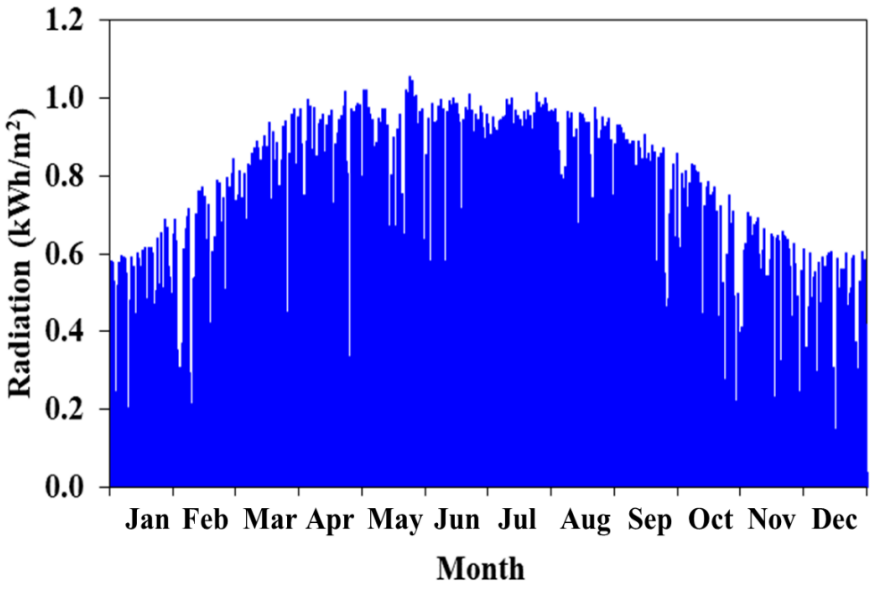

Fig. 7. 25. The hourly solar irradiance for the city of Mselata

This city exhibits a similar pattern of solar irradiance, with levels increasing from May to August during the summer season and reaching their lowest average in December. These variations directly impact the system's performance in terms of energy production. Figure 7.26 provides a visual representation of the hourly and monthly power and energy production for a 2MW system installed in this city.

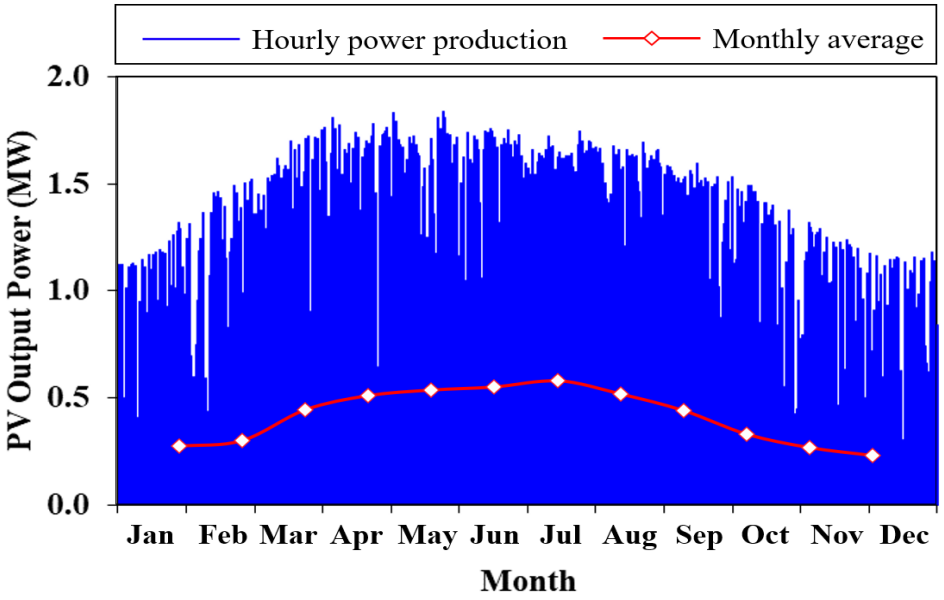

(a)

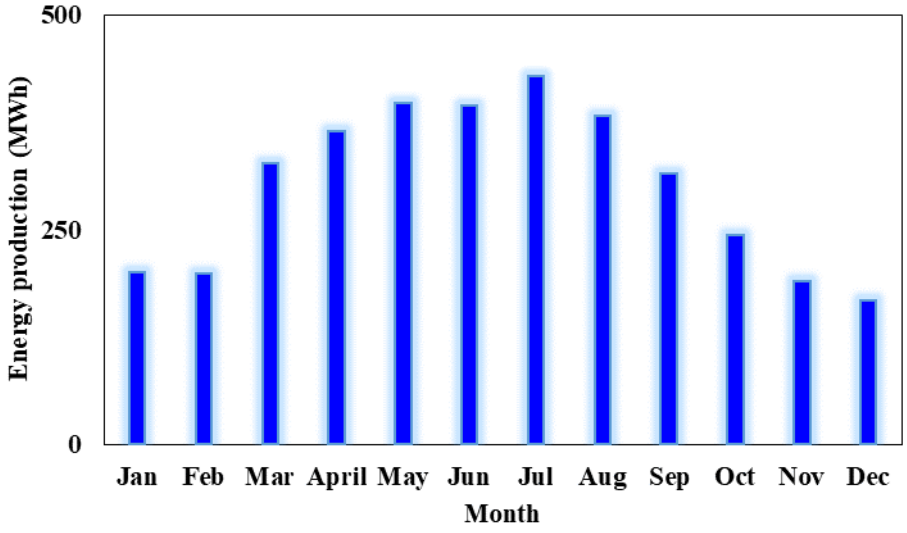

(b)

Fig. 7. 26. The hourly and monthly power energy production in the city of Mselata

(a): Hourly Power production (b): The average monthly energy production.

It's evident that the monthly energy production reaches its peak in July, totalling 428.50 MWh, and gradually decreases until it reaches its lowest average in December, with a value of 167.66 MWh. Consequently, the highest number of houses meeting their energy needs from this system was recorded in July, with a value of 691 houses. Conversely, at the lowest level, the system is capable of providing energy demand for 270 houses in the city of Mselata. Figure 7.27 visually represents the monthly number of houses covered by this system.

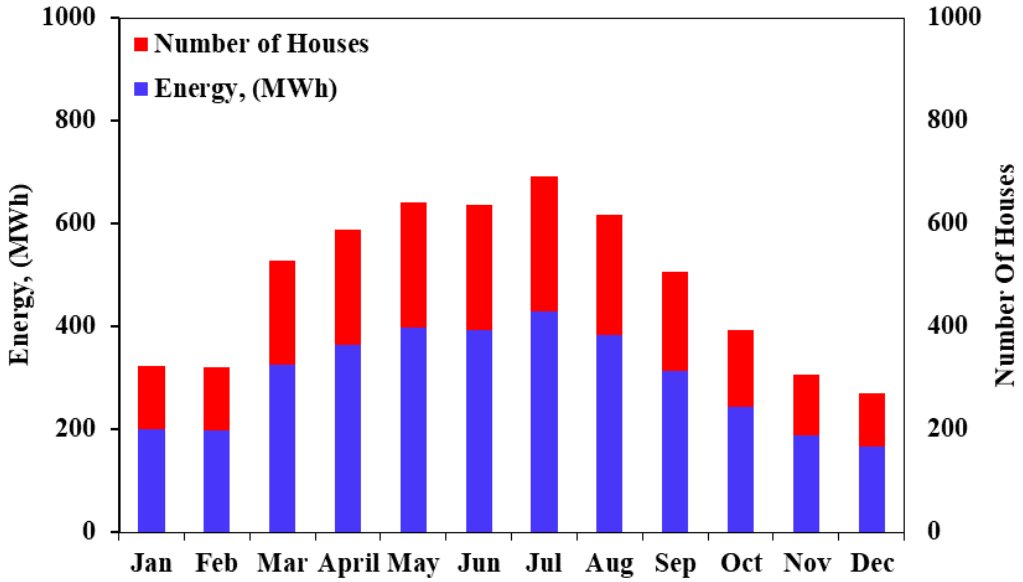

Fig. 7. 27. The monthly number of houses covered by the energy production of the system in the city of Mselata.

7.3.3 The energy production in the city of Murzuqh

The city of Murzuqh, situated in the southern region of Libya like other cities in the south, experiences a dry climate with elevated ambient temperatures. The sun shines for extended hours throughout the day, particularly in the summer season. The solar irradiance reaches the level of 1000 W/m^2 multiple times during the year, especially from the end of March to the end of August. The hourly solar irradiance levels are illustrated in Figure 7.28.

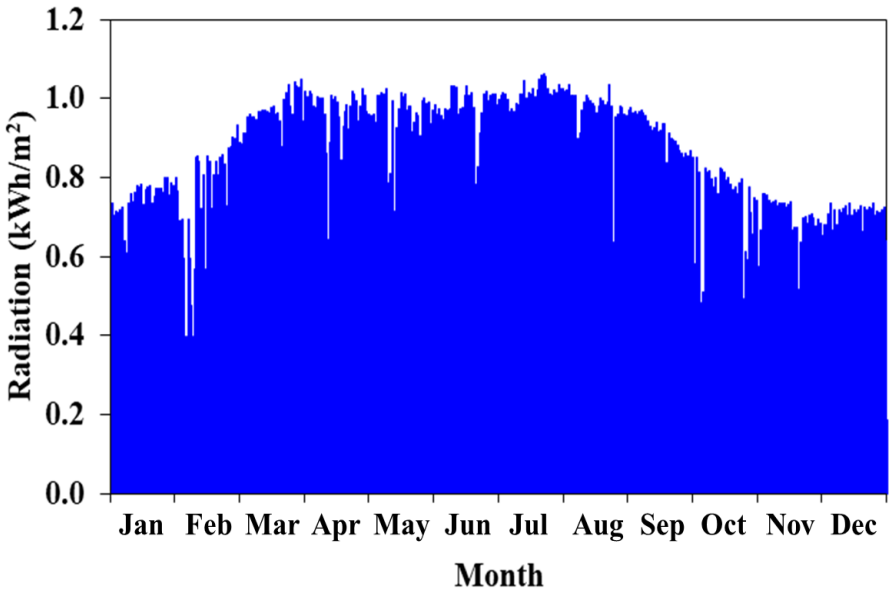

Fig. 7. 28. The hourly solar irradiance for the city of Murzuqh

It is evident that the average solar irradiance level in this city is slightly higher than in other cities, and this is reflected in the performance of the system. The hourly and monthly power and energy production is depicted in Figure 7.29. (a): The hourly PV output power (MW), (b): The average monthly energy production (MWh).

As seen from the average monthly energy production, the system's energy output surpasses the 350MWh level multiple times from March to September. The highest level was recorded in July, with a total energy production of 423.23MWh, while the lowest was in February, totalling 255.87MWh. Furthermore, the monthly number of houses covered by this system is presented in Figure 7.30. The results demonstrate that the system will be capable of providing the energy demand for 683 houses in July, and for seven months of the year, the system will supply the energy needs for more than 550 houses each month. For the remaining four months, the system will produce enough energy for over 400 houses. Thus, it can be concluded that the average annual production is higher than all previous locations.

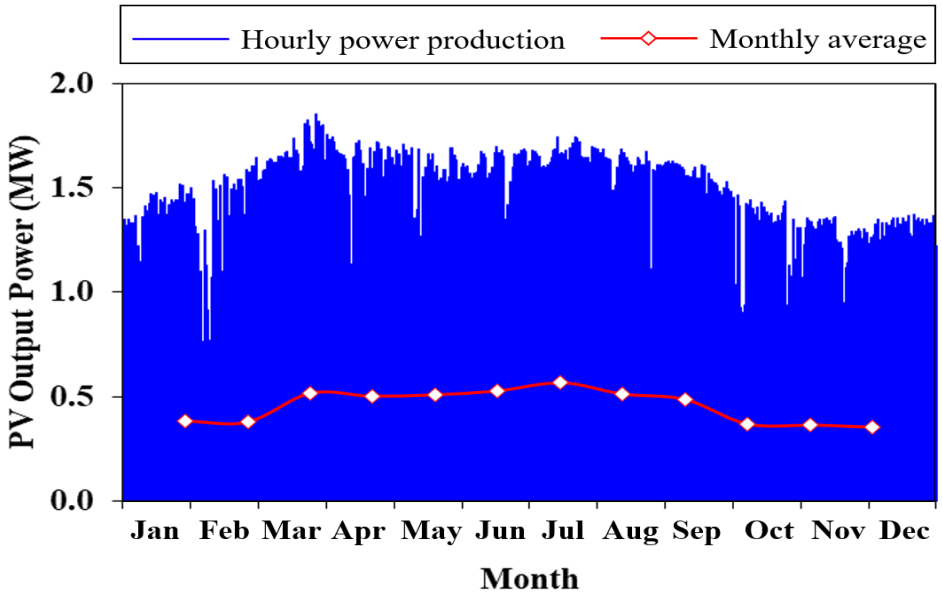

(a)

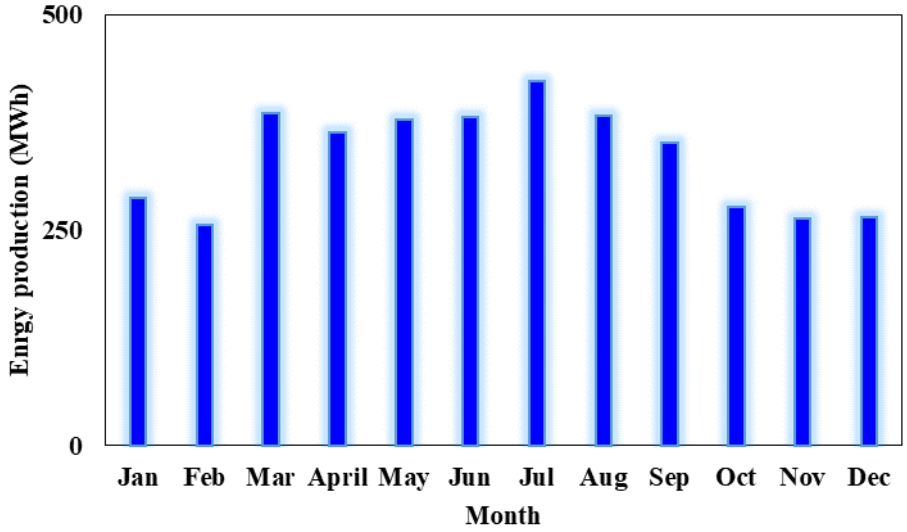

(b)

Fig. 7. 29. The hourly and monthly power and energy production in the city of Murzuqh

(a): Hourly Power production (b): The average monthly energy production

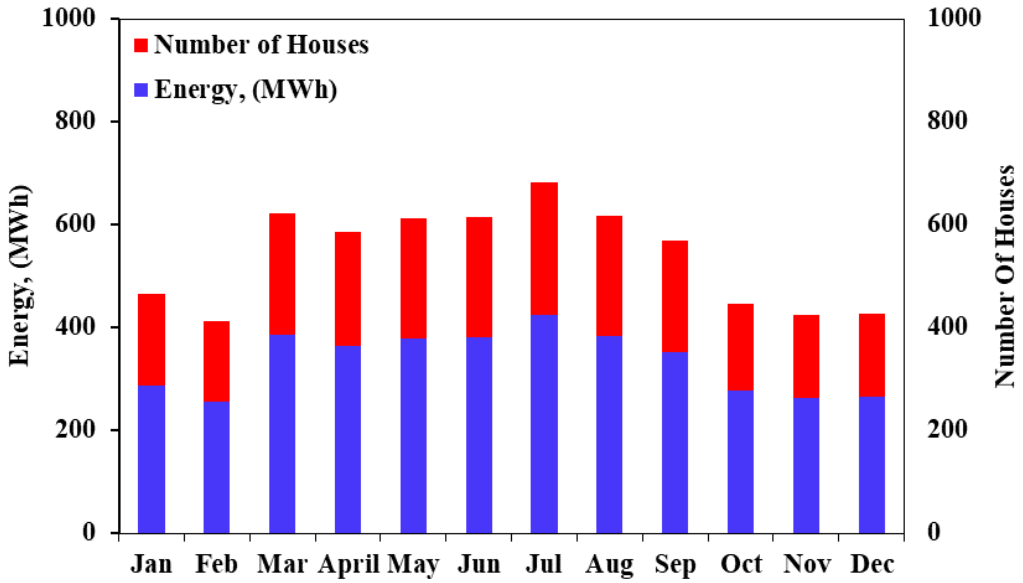

Fig. 7. 30. The monthly number of houses covered by the energy production of the system in the city of Murzuqh.

The total annual energy production and the number of houses covered by the system for the three cities presented in this section are illustrated in Figure 7.31. The results show that Murzuqh city has the highest annual energy production among all cities, with a total energy production of 4018 MWh/year. This is capable of supplying the annual energy demand for 550 houses in the city. Tajoura and Mselata follow closely, with total energy production of 3622.26 and 3607.28 MWh/year, respectively, providing annual energy for 496 and 494 houses.

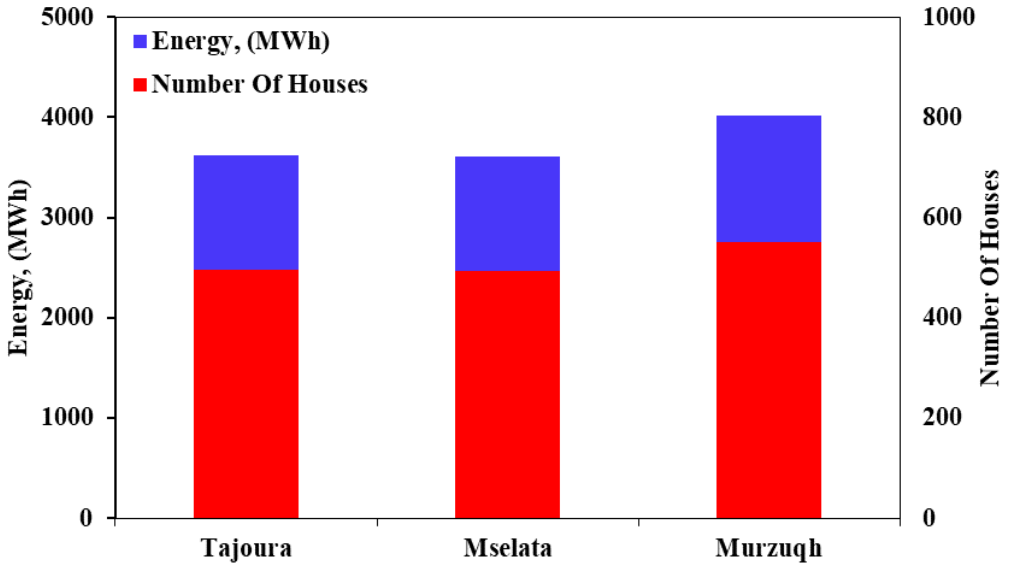

Fig. 7. 31. The annual number of houses covered by the energy production of the system in the three sites.

Considering that the data obtained from both databases exhibit relative consistency, wherein the pattern of solar irradiance demonstrates an increase during the summer season and reaches its lowest levels during the winter season, and further noting that the irradiance levels fluctuate within similar ranges across both databases, it is deemed pertinent to conduct a comparative analysis across all locations. This analysis aims to ascertain the optimal location for the installation of GCPV systems to support the grid. To this end, the performance of a 2MW grid-connected system was monitored across the four seasons. For the purpose of comparison, the system's performance during two key seasons was selected: the summer season, characterized by the system's peak performance, and the winter season, representing its lowest performance. The outcomes of this comparison are depicted in Figure 7.32 and Figure 7.33, respectively.

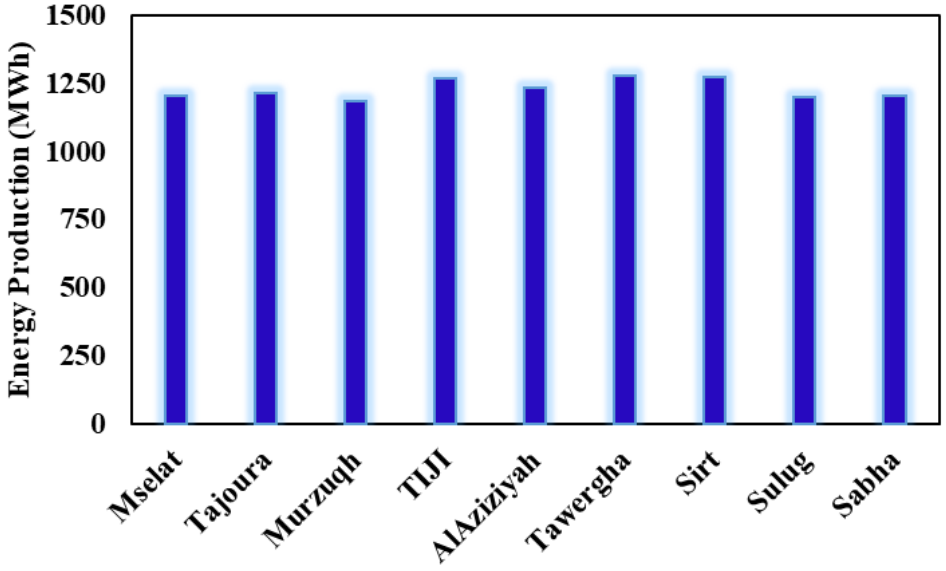

Fig. 7. 32. The performance of the system at nine locations during summer season.

The figure illustrates that the performance of the system during the summer season exhibits relatively consistent levels across the nine locations, with energy production ranging between 1180 MWh and 1280 MWh. Notably, the lowest performance was observed in Murzuqh city, likely attributable to its geographical location in the southern region of the country, characterized by desert terrain and high temperatures, as well as elevated levels of dust. Conversely, the highest performance during this season was recorded in Tawergha city, situated in the northern part of the country. This outcome may seem unexpected, however, it could be attributed to the city's proximity to the coastline, resulting in extended periods of clear skies and moderate temperature levels. Similarly, Sirt city, which shares similar weather conditions, also demonstrated comparable performance levels.

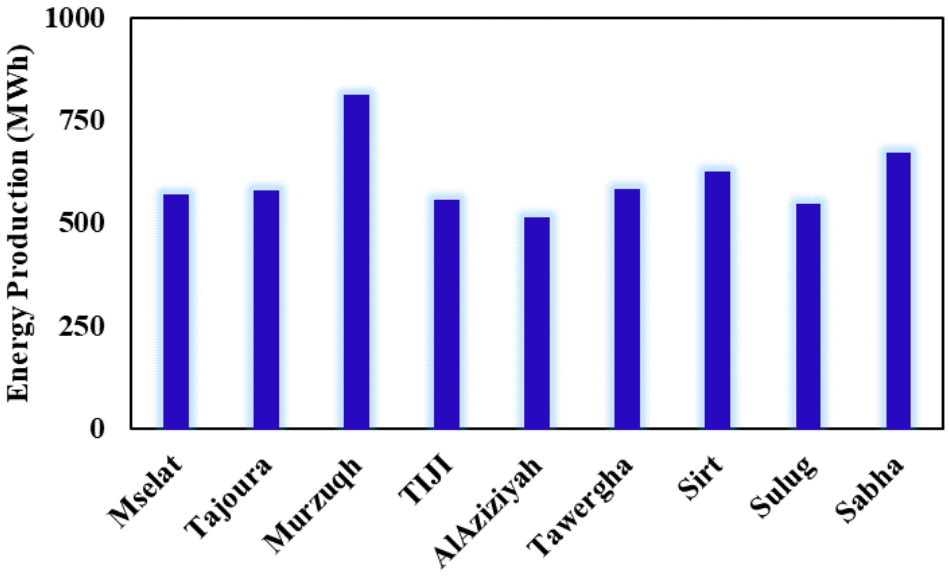

Fig. 7. 33. The performance of the system at nine locations during Winter seasons.

Conversely, during the winter seasons, the system's performance reached its lowest levels, as depicted in Figure 7.33. The figure clearly indicates that Murzuqh city exhibited the highest performance, followed by Sabha and Sirt, with energy production levels of 808 MWh, 669 MWh, and 622 MWh respectively. In contrast, AlAziziyah city recorded the lowest performance during this season, with an energy production of 511 MWh. This comparison highlights the reverse impact of temperature and dust on the system's performance. For instance, while Murzuqh and Sabha cities demonstrated lowest performance during the summer seasons, they exhibited the highest performance during the winter season. Generally, the performance of the system across all cities decreases to half or less during the winter season, except for Murzuqh city. This anomaly can be attributed to the consistent high irradiance experienced throughout the year in Murzuqh city.

7.4 Conclusions

In this chapter, the performance of the PV system in terms of energy production under Libyan weather conditions has been investigated. The analysis was based on two data resources: first, satellite data using NASA's database, and second, actual measurements obtained from the CSESR. The results reveal a consistent pattern in solar irradiance levels across all cities from both data sources. Solar irradiance peaks in the middle of the year, from May to August, reaching its zenith in July. Conversely, during the winter season, irradiance levels decrease, reaching their lowest point in December.

The findings highlight Murzuqh City as having the highest solar energy production, with a total annual output of 4018 MWh/year, sufficient to meet the annual energy needs of 550 houses in the city. Additionally, the performance of the 2MW system across all nine sites indicates a collective annual energy generation of approximately 33,180.84 MWh/year. This output is substantial, meeting the annual energy demand for 4544 houses.

Chapter 8:

8.1 Conclusion

Renewable energy resources represent one of the most promising avenues for modern energy provision, with the potential to significantly address global energy demands. Many nations have formulated strategic plans to augment the contribution of these resources within their energy sectors. Solar energy, in particular, holds a prominent position among renewable options due to its inherent characteristics. Libya is among the countries endeavouring to diversify its energy portfolio by embracing various renewable energy technologies, notably solar and wind energies. The primary objective of this thesis is to conduct an in-depth examination of the feasibility of solar energy utilization in Libya. This entails a comprehensive analysis encompassing regional climate, geographical features, and technical considerations. Additionally, the project aims to develop a prospective map delineating suitable locations for the installation of grid-connected Photovoltaic (PV) systems nationwide, thereby bolstering the national grid's capacity to mitigate energy shortages. In Chapter 2 of this thesis, an overview of the current energy situation in Libya is provided, along with a discussion of the primary factors contributing to the energy crisis that has affected the country over the past decade. Furthermore, this chapter examines the current utilization of solar energy within the country, its potential, and the prospective role this energy source could play in shaping the future of Libya's power sector. As a conclusion to this chapter, it is evident that solar energy holds significant promise and is expected to play a pivotal role in bolstering the Libyan grid to address its energy crisis. Consequently, the outcomes of this chapter align with the first part of the first objectives outlined in Chapter 1.

Furthermore, Chapter 3 of this thesis offers a comprehensive literature review that centres on recent research endeavours within the field. The chapter commences by delving into the significance of solar energy and its accessibility, followed by an elucidation of the photovoltaic phenomena and its underlying mechanisms. Moreover, various solar system configurations and the primary components of a double-stage grid-connected PV system are highlighted. Additionally, different inverter topologies and a range of MPPT techniques are discussed. Furthermore, this chapter addresses challenges stemming from grid-connected PV systems and outlines pertinent standards and requirements essential for the safe integration of such systems into the grid. Moreover, this chapter also highlights some of the most common short-circuit faults that occur in power systems, while also emphasizing the importance of LVRT capability

as a critical requirement for the integration of PV systems. The overarching aim of this chapter is to provide comprehensive knowledge about PV systems, encompassing their intricacies, challenges, and necessary conditions.

Based on the discussions and presentations in Chapter 3, a double-stage grid-connected PV system was selected for this study. Consequently, in alignment with the second objective outlined in Chapter 1, Chapter 4 presents the dynamic modelling of the grid-connected PV system. This chapter commences with a comprehensive description of the chosen system and the modelling of the PV array. Subsequently, focus shifts to the modelling of the DC-DC boost converter, which is designed to increase the DC voltage to a predetermined level, thereby facilitating the implementation of the MPPT technique. The discussion then proceeds to the modelling of the LC filter, which aims to mitigate high-frequency components introduced by the PWM inverter. This process ensures that the THD level remains within the acceptable range, aligning with the specifications outlined in the IEEE 519 standard. Furthermore, within this chapter, the control strategy of the DC-DC boost converter has been elucidated. The P&O MPPT technique has been employed to ensure the extraction of maximum power from the PV array under diverse weather conditions. Additionally, the control strategy of the DC-AC inverter has been devised to maintain the constancy of the DC voltage at the input terminal of the inverter. Simultaneously, this strategy facilitates the conversion of the DC voltage and current generated by the PV array into AC signals in accordance with grid requirements. Moreover, the primary objective of these control strategies is to restore the system to its equilibrium operational point following any encountered disturbances. Finally, this chapter provides the principle of calculating the output power of the modelled system. In this regard, this chapter clearly satisfies the second objective presented in Chapter 1.

In accordance with the presentations and models developed in Chapter 4, the system's performance was assessed in Chapter 5. This chapter evaluated the system under various levels of solar irradiance with a fixed temperature. Four irradiance levels were selected for the study: 1000, 750, 500, and 250 W/m^2, while maintaining a temperature of 25℃. Subsequently, the system was evaluated under different temperature levels while maintaining solar irradiance at a fixed level. The four temperature levels considered were 15, 25, 35 and 45℃ with an irradiance of 1000 W/m^2. This chapter also incorporates FFT analysis to ensure that the system and its components have the capability to reduce the THD to an acceptable range. The findings reveal that the system demonstrated rapid responsiveness to environmental fluctuations, with solar irradiance exerting a more significant influence than temperature. Particularly noteworthy is

the substantial impact of variations in solar irradiance on the system's power output, while maintaining a constant DC voltage. The most notable changes were observed in the system's current.

FFT analysis reveals that the THD remained within the limits specified by the IEEE 519 standard under both irradiance and temperature scenarios. Specifically, the results demonstrate that the designated LC filter effectively reduced THD levels to a range between 0.92% and 1.84% for voltage across the four irradiance levels, and between 1.58% and 4.12% for current. Meanwhile, under varying temperature conditions, THD levels for voltage ranged from 0.95% to 1.47%, with further improvement observed at the CCP, where THD ranged between 0.49% and 0.71%. Conversely, the THD level for current did not exceed 2% at any of the specified points. It is noteworthy that the current exhibited a higher THD level than voltage, possibly due to the voltage-based control strategy employed and the selection of system parameters at STC, while the evaluation was conducted at relatively low levels of irradiance and high temperatures. In conclusion, this chapter satisfies a part of the main aim of this thesis by studying the system under various technical considerations.

Further technical considerations are presented in Chapter 6. Short circuit fault analysis was conducted in this chapter to evaluate the behaviour of the system under short circuit fault scenarios and to investigate its LVRT capability. The first scenario considers L-G short circuit faults, recognized as the most frequent fault in power systems. The second scenario examines 3L-G short circuit faults, acknowledged as the most severe fault in power systems. The results reveal that the GCPV system demonstrated greater equilibrium and quicker restoration to its operational point when subjected to L-G short circuit faults. Notably, the power output remained unaffected by this fault, and the DC-DC boost converter, particularly employing the P&O MPPT strategy, efficiently extracted maximum power despite the applied fault. Furthermore, the control strategy implemented in the DC-AC inverter successfully maintained the DC voltage at the busbar consistently, even during the fault occurrence. On the AC side of the system, the impact of this fault was more pronounced, resulting in voltage sag and current surge at the inverter and CCP terminals. However, the system exhibited the capability to swiftly restore its equilibrium operational point, accomplishing this within a very short timeframe, specifically less than 0.2 ms.

On the contrary, the dynamic behaviour of the PV system under 3L-G faults was relatively more adverse. These faults were introduced at two distinct points: the first at a distance of 14

km from the CCP, and the second at a distance of 140 km from the CCP. The results demonstrated that the power system responded differently to these two kinds of faults. It can be observed that the impacts of the short circuit faults highly depend on the physical distance between the fault point and the CCP. The power output of the system experienced severe repercussions when the fault occurred at a distance of 14 km from the CCP, displaying substantial fluctuations. Similar observations were noted for the voltage and current at various points in the system. Upon fault clearance, the system remained in a transient state for approximately 3.5 seconds before regaining its equilibrium point. Nevertheless, when the fault occurred at a greater distance, the dynamic behaviour of the system exhibited greater balance, and the impact of the fault on power output became negligible. Similarly, the DC voltage at the busbar demonstrated minimal transient fluctuations, underscoring the effectiveness of the control strategy implemented in the DC-AC inverter to maintain constant DC voltage during the fault. Additionally, the voltage sag experienced a reduction when the fault was applied at a longer distance. This observation highlights the dependence of fault characteristics on the impedance level between the fault location and the installed PV system at the CCP. In the second scenario, the system maintained a higher level of impedance at the CCP, resulting in a less pronounced dip in the voltage magnitude. Furthermore, the system swiftly returned to its normal operating point once the fault was cleared, achieving a very brief settling time of less than 0.2 ms. The outcome of this chapter supports and satisfy the main aim of this thesis as well as the third objective.

Transitioning to Chapter 7, the evaluation of the system's performance in terms of energy production across various locations in Libya, the study encompassed nine locations spanning the country's three primary regions. The principal objective of this chapter is to assess the energy production of the 2MW system and conduct a comparative analysis between online data obtained from NASA satellites using PVsyst software and actual measurements collected by the CSESR. Additionally, to create a potential map for the installation of GCPV systems to support the grid in facing its energy crisis, the main aim of this chapter is to fulfil the primary objective of the thesis and identify a realistic horizon for solar energy technology in Libya.

The findings indicate a consistent pattern of solar irradiance across all nine locations, reaching its peak during the summer season and registering the lowest levels in winter. A parallel pattern is observed in the energy production of the system. This variability can be attributed to prevailing weather conditions, with winter introducing an increased likelihood of cloud cover in contrast to the predominantly clear skies during the summer season.

For locations relying on satellite-derived data, there are no significant differences in the total annual energy production among the six sites. Sabha city recorded the highest annual energy production, totalling 3798.96 MWh/year, capable of satisfying the annual energy demand for approximately 520 houses. Sirt closely follows with a slightly lower figure, achieving a total energy production of 3795.19 MWh/year, sufficient for the annual energy needs of 519 houses. Conversely, AlAziziyah city registered the lowest annual energy production at 3464.30 MWh/year, ample to meet the annual energy demand for 475 houses.

For locations relying on actual measurements, the results underscore Murzuqh City as exhibiting the highest solar energy production, boasting a total annual output of 4018 MWh/year. This capacity is adequate to fulfil the annual energy needs of 550 houses in the city. Furthermore, the overall performance of the 2MW system across all nine sites indicates a cumulative annual energy generation of approximately 33,180.84 MWh/year. This substantial output can cater to the annual energy demand of 4544 houses.

To this end, it can be noted that the main aim and objectives of this thesis were met. As a general conclusion, it is worth mentioning that the potential of solar energy exists, and the performance of the system at all locations was satisfactory. Therefore, it is expected that this energy source can and will play a significant role in supporting the Libyan grid, enabling it to address its energy crisis. It is also anticipated that this research and its associated achievements will be implemented by the General Electricity Company of Libya (GECOL) and other Libyan authorities in future energy plans to tackle the current energy crisis in the country. Finally, the main research contributions and future work are summarized in the next two sections.

8.2 Contribution of the research

1- This thesis includes the creation of a potential map for installing a centralized solar system. The system is evaluated at nine different locations across Libya, spanning the country's three main regions. Consideration is given to the proximity of these locations to residential areas, aiming to minimize the distance between generating points and consuming points to mitigate power losses during the transmission stage.

2- This thesis provides an evaluation of a 2 MW grid-connected PV system in terms of power production at nine locations across the country and calculates the number of houses that can benefit from this power production, considering the energy consumption for a typical Libyan house. Electricity bills obtained from the General Electricity Company of Libya (GECOL) were used for this calculation.

3- The thesis also presents a comparison between two weather data resources, including online data obtained from the NASA database and actual data measurements obtained from the Libyan Centre for Solar Energy Research and Studies (CSESR).

8.3 Recommendation and future work

Although significant work has been undertaken in this thesis concerning the current energy situation and the potential of solar energy in Libya, as well as the modeling of grid-connected Photovoltaic (PV) systems, including different components of the system, further investigation in certain areas is recommended.

1- In this work, the performance of the GCPV system under short-circuit faults was studied from the perspective of transient stability in interconnected systems, aiming to ensure the system remains in synchronism until the faulty section of the power system is isolated. Therefore, it is recommended that further analysis on short-circuit faults, such as the calculation of short-circuit current, could be a fruitful area of research.
2- In this thesis, two main short-circuit faults on the grid side have been studied. However, it is highly recommended to investigate the performance of the GCPV system under additional short-circuit fault scenarios, including L-L, 2L-G, and 3L together short-circuit faults. Additionally, studying the system's performance under short-circuit faults at the DC side, such as short-circuit faults at the DC-DC boost converter and short-circuit faults at the PV array, would be beneficial.
3- The performance of the system at different locations in Libya was investigated. However, it is highly recommended to extend the study to encompass more locations throughout the country.
4- Although the LC filter has successfully maintained the THD at the CCP within the acceptable level recommended by the IEEE 519 standard, the use of LCL filter configuration is worthy of further study.
5- The focus of this work was on grid-connected Photovoltaic (PV) system technology. However, exploring more solar energy technologies could be a fruitful area of research, such as concentrated solar power (CSP).
6- Studying the performance of other renewable energy technologies in Libya is highly recommended to assess their capability in helping the country overcome its energy crisis.

References

[1] S. Sumathi, L. Ashok Kumar, and P. Surekha, *Solar PV and Wind Energy Conversion Systems*. 2015.

[2] S. Mekhilef, R. Saidur, and A. Safari, "A review on solar energy use in industries," *Renew. Sustain. Energy Rev.*, vol. 15, no. 4, pp. 1777–1790, 2011, doi: 10.1016/j.rser.2010.12.018.

[3] A. Kumar, O. Prakash, and A. Dube, "A review on progress of concentrated solar power in India," *Renew. Sustain. Energy Rev.*, vol. 79, no. February 2016, pp. 304–307, 2017, doi: 10.1016/j.rser.2017.05.086.

[4] K. Kaygusuz, "Renewable energy: Power for a sustainable future," *Energy Explor. Exploit.*, vol. 19, no. 6, pp. 603–626, 2001, doi: 10.1260/0144598011492723.

[5] J. Everett, Robert; Boyle, Godfrey; Peake, Stephen and Ramage, *Renewable Energy: Power for a Sustainable Future*, 3rd ed. Oxford Univerity Press, 2012.

[6] M. Z. Jacobson and M. A. Delucchi, "Providing all global energy with wind, water, and solar power, Part I: Technologies, energy resources, quantities and areas of infrastructure, and materials," *Energy Policy*, vol. 39, no. 3, pp. 1154–1169, 2011, doi: 10.1016/j.enpol.2010.11.040.

[7] T. Suntio and T. Messo, "Power electronics in renewable energy systems," *Energies*, vol. 12, no. 10, 2019, doi: 10.3390/en12101852.

[8] M. A. Eltawil and Z. Zhao, "Grid-connected photovoltaic power systems: Technical and potential problems-A review," *Renew. Sustain. Energy Rev.*, vol. 14, no. 1, pp. 112–129, 2010, doi: 10.1016/j.rser.2009.07.015.

[9] L. A *et al.*, "Smart energy monitoring and power quality performance based evaluation of 100-kW grid tied PV system," *Heliyon*, vol. 9, no. 6, p. e17274, 2023, doi: 10.1016/j.heliyon.2023.e17274.

[10] Y. Chen *et al.*, "From laboratory to production: Learning models of efficiency and manufacturing cost of industrial crystalline silicon and thin-film photovoltaic technologies," *IEEE J. Photovoltaics*, vol. 8, no. 6, pp. 1531–1538, 2018, doi: 10.1109/JPHOTOV.2018.2871858.

References

[11] G. Najafi, B. Ghobadian, R. Mamat, T. Yusaf, and W. H. Azmi, "Solar energy in Iran: Current state and outlook," *Renew. Sustain. Energy Rev.*, vol. 49, pp. 931–942, 2015, doi: 10.1016/j.rser.2015.04.056.

[12] C. Phil, *Solar energy perspectives*, vol. 1. 2011.

[13] N. L. Panwar, S. C. Kaushik, and S. Kothari, "Role of renewable energy sources in environmental protection: A review," *Renew. Sustain. Energy Rev.*, vol. 15, no. 3, pp. 1513–1524, 2011, doi: 10.1016/j.rser.2010.11.037.

[14] N. Kannan and D. Vakeesan, "Solar energy for future world: - A review," *Renew. Sustain. Energy Rev.*, vol. 62, pp. 1092–1105, 2016, doi: 10.1016/j.rser.2016.05.022.

[15] S. Sharma, K. K. Jain, and A. Sharma, "Solar Cells: In Research and Applications—A Review," *Mater. Sci. Appl.*, vol. 06, no. 12, pp. 1145–1155, 2015, doi: 10.4236/msa.2015.612113.

[16] Y. Chu, "Review and Comparison of Different Solar Energy Technologies August 2011 Table of Contents," 2011.

[17] V. G. Gude, N. Nirmalakhandan, and S. Deng, "Desalination using solar energy: Towards sustainability," *Energy*, vol. 36, no. 1, pp. 78–85, 2011, doi: 10.1016/j.energy.2010.11.008.

[18] V. Nian, "Impacts of changing design considerations on the life cycle carbon emissions of solar photovoltaic systems," *Appl. Energy*, vol. 183, pp. 1471–1487, 2016, doi: 10.1016/j.apenergy.2016.08.176.

[19] P. G. V. Sampaio and M. O. A. González, "Photovoltaic solar energy: Conceptual framework," *Renew. Sustain. Energy Rev.*, vol. 74, no. February, pp. 590–601, 2017, doi: 10.1016/j.rser.2017.02.081.

[20] RCREEE, "RCREEE Country Profile Renewable Energy in Libya," 2019. [Online]. Available: https://www.rcreee.org/content/Libya. [Accessed: 15-Oct-2019].

[21] A. Ehtiwesh, C. Kutlu, Y. Su, and S. Riffat, "Modelling and performance evaluation of a direct steam generation solar power system coupled with steam accumulator to meet electricity demands for a hospital under typical climate conditions in Libya," *Renew. Energy*, vol. 206, no. November 2022, pp. 795–807, 2023, doi: 10.1016/j.renene.2023.02.075.

References

[22] M. Almaktar, A. M. Elbreki, and M. Shaaban, “Revitalizing operational reliability of the electrical energy system in Libya: Feasibility analysis of solar generation in local communities,” *J. Clean. Prod.*, vol. 279, p. 123647, 2021, doi: 10.1016/j.jclepro.2020.123647.

[23] B. Belgasim, Y. Aldali, M. J. R. Abdunnabi, G. Hashem, and K. Hossin, “The potential of concentrating solar power (CSP) for electricity generation in Libya,” *Renew. Sustain. Energy Rev.*, vol. 90, no. March, pp. 1–15, 2018, doi: 10.1016/j.rser.2018.03.045.

[24] M. A. Al-refai, “Optimal Design and Simulation of a Grid-Connected Photovoltaic (PV) Power System for an Electrical Department in University of Tripoli-Libya,” *Int. J. Electr. Comput. Eng.*, vol. 8, no. 6, pp. 855–859, 2014, doi: 10.5281/zenodo.2825884.

[25] A. M. A. Mohamed, A. Al-Habaibeh, H. Abdo, and S. Elabar, “Towards exporting renewable energy from MENA region to Europe: An investigation into domestic energy use and householders’ energy behaviour in Libya,” *Appl. Energy*, vol. 146, pp. 247–262, 2015, doi: 10.1016/j.apenergy.2015.02.008.

[26] A. M. A. Mohamed, A. Al-Habaibeh, and H. Abdo, “An investigation into the current utilisation and prospective of renewable energy resources and technologies in Libya,” *Renew. Energy*, vol. 50, pp. 732–740, 2013, doi: 10.1016/j.renene.2012.07.038.

[27] M. Almaktar and M. Shaaban, “Prospects of renewable energy as a non-rivalry energy alternative in Libya,” *Renew. Sustain. Energy Rev.*, vol. 143, no. March, p. 110852, 2021, doi: 10.1016/j.rser.2021.110852.

[28] D. Pamučar, I. Badi, K. Sanja, and R. Obradović, “A novel approach for the selection of power-generation technology using a linguistic neutrosophic CODAS method: A case study in Libya,” *Energies*, vol. 11, no. 9, pp. 1–25, 2018, doi: 10.3390/en11092489.

[29] A. O. M. Maka, S. Salem, and M. Mehmood, “Solar photovoltaic (PV) applications in Libya: Challenges, potential, opportunities and future perspectives,” *Clean. Eng. Technol.*, vol. 5, p. 100267, 2021, doi: 10.1016/j.clet.2021.100267.

[30] M. A. Almaktar, “Towards an extensive exploitation of solar PV technology in Libya :

References

Legislative , economic and environmental considerations," vol. 2, no. August, 2018.

[31] Y. F. Nassar, H. J. El-khozondar, G. Ghaboun, M. Khaleel, Z. Yusupov, and Abdussalam Ahmed; Abdulgader Alsharif, "Solar and Wind Atlas for Libya," *Int. J. Electr. Eng. Sustain.*, vol. 1, no. 3, pp. 27–43, 2023.

[32] T. A. Hamad, A. A. Agll, Y. M. Hamad, and J. W. Sheffield, "Solid waste as renewable source of energy: Current and future possibility in Libya," *Case Stud. Therm. Eng.*, vol. 4, pp. 144–152, 2014, doi: 10.1016/j.csite.2014.09.004.

[33] F. Amara, J. Darkwa, J. Calautit, and I. Sharfeddin, "The Potential and analysis of Grid-connected Photovoltaic System in residential houses in Libya : Near-term solution of electricity shortage: A case study in Tripoli," *2019 IEEE 2nd Int. Conf. Renew. Energy Power Eng.*, pp. 125–129, 2020, doi: 10.1109/repe48501.2019.9025125.

[34] Y. Kassem, H. Camur, and O. A. M. Abughinda, "Solar Energy Potential and Feasibility Study of a 10MW Grid-connected Solar Plant in Libya," *Eng. Technol. Appl. Sci. Res.*, vol. 10, no. 4, pp. 5358–5366, 2020, doi: 10.48084/etasr.3607.

[35] PWC, "Task A : Sector performance and structural sector reform," *Pricewaterhouse Coopers*, no. September, 2017.

[36] A. Kadem, Z. Rajab, A. Khalil, A. Tahir, A. Alfergani, and F. A. Mohamed, "Economic feasibility, design, and simulation of centralized PV power plant," *2018 9th Int. Renew. Energy Congr. IREC 2018*, no. March, pp. 1–6, 2018, doi: 10.1109/IREC.2018.8362448.

[37] F. Mosbah and T. Iqbal, "Sizing of A Large Isolated Solar Energy System for Bani Walid, Libya," *J. Clean Energy Technol.*, vol. 6, no. 6, pp. 385–393, 2018, doi: 10.18178/jocet.2018.6.6.495.

[38] Y. Kassem, H. Çamur, and R. A. F. Aateg, "Exploring solar and wind energy as a power generation source for solving the electricity crisis in Libya," *Energies*, vol. 13, no. 14, 2020, doi: 10.3390/en13143708.

[39] S. Alweheshi, A. Abdelali, Z. Rajab, A. Khalil, and F. Mohamed, "Photovoltaic Solar Energy Applications in Libya: A Survey," *2019 10th Int. Renew. Energy Congr. IREC 2019*, no. April, 2019, doi: 10.1109/IREC.2019.8754527.

References

[40] A. Khalil, Z. Rajab, M. Amhammed, and A. Asheibi, “The benefits of the transition from fossil fuel to solar energy in Libya: A street lighting system case study,” *Appl. Sol. Energy (English Transl. Geliotekhnika)*, vol. 53, no. 2, pp. 138–151, 2017, doi: 10.3103/S0003701X17020086.

[41] I. Conference, H. Tatras, and S. Republic, “POWER FLOW MODELLING IN ELECTRIC NETWORKS WITH RENEWABLE ENERGY SOURCES IN LARGE AREAS,” 2012.

[42] O. A. Mohamed and S. H. Masood, “A brief overview of solar and wind energy in Libya: Current trends and the future development,” *IOP Conf. Ser. Mater. Sci. Eng.*, vol. 377, no. 1, 2018, doi: 10.1088/1757-899X/377/1/012136.

[43] A. Khalil, Z. Al Faituri, and A. Asheibi, “The Economic Feasibility of Photovoltaic Systems for Electricity Production in Libya,” *7th Int. Renew. Energy Congr. IREC’2016*, 2016.

[44] K. A. Glaisa, M. E. Elayeb, and M. A. Shetwan, “Potential of hybrid system powering school in Libya,” *Energy Procedia*, vol. 57, pp. 1411–1420, 2014, doi: 10.1016/j.egypro.2014.10.132.

[45] I. Dincer, C. O. Colpan, O. Kizilkan, and M. A. Ezan, *Progress in clean energy*, vol. 1. 2015.

[46] N. Bizon, N. M. Tabatabaei, F. Blaabjerg, and E. Kurt, *Energy Harvesting and Energy Efficiency: Technology, Methods, and Applications*. 2017.

[47] Z. Rajab, A. Khalil, M. Amhamed, and A. Asheibi, “Economic feasibility of solar powered street lighting system in Libya,” *2017 8th Int. Renew. Energy Congr. IREC 2017*, no. March, 2017, doi: 10.1109/IREC.2017.7926027.

[48] A. Khalil, A. Khalil, and A. Asheibi, “The Chances and Challenges for Renewable Energy in Libya The Chances and Challenges for Renewable Energy in Libya,” no. February, pp. 22–25, 2016.

[49] SolarGIS, “olar resource maps and GIS data for 180+ countries,” *solargis.com*, 2019. [Online]. Available: https://solargis.com/maps-and-gis-data/download/libya. [Accessed: 10-Dec-2019].

[50] M. Almaktar, A. M. Elbreki, and M. Shaaban, “Revitalizing operational reliability of

the electrical energy system in Libya: Feasibility analysis of solar generation in local communities," *J. Clean. Prod.*, vol. 279, no. January, 2021, doi: 10.1016/j.jclepro.2020.123647.

[51] S. Alweheshi, A. Abdelali, Z. Rajab, A. Khalil, and F. Mohamed, "Photovoltaic Solar Energy Applications in Libya: A Survey," *2019 10th Int. Renew. Energy Congr. IREC 2019*, no. Irec, pp. 1–6, 2019, doi: 10.1109/IREC.2019.8754527.

[52] A. M. A. Mohamed, A. Al-habaibeh, and H. Abdo, "Future Prospects of the Renewable Energy sector in Libya," *SBE16 Dubai*, no. 17-19 January, p. 8, 2016.

[53] I. M. Saleh, H. M. Abufares, and H. M. Snousi, "Three-Year Performance Evaluation of Single Junction Amorphous Solar Cells Grid-Connected Power Station in Libya," *Conf. Pap. Eng.*, vol. 2013, no. September 2012, pp. 1–5, 2013, doi: 10.1155/2013/950195.

[54] M. Elmnifi and H. Moria, "Feasibility Study into Possibility Potentials and Challenges of Renewable Energy in Libya," *Artic. Int. J. Adv. Sci. Technol.*, vol. 29, no. 03, pp. 12546–12560, 2020.

[55] M. Zuheir *et al.*, "A comparison between solar thermal and photovoltaic/thermal (PV/T) systems for typical household in Libya," *4th IEEE Int. Conf. Eng. Technol. Appl. Sci. ICETAS 2017*, vol. 2018-Janua, pp. 1–6, 2018, doi: 10.1109/ICETAS.2017.8277877.

[56] Y. Aldali, D. Henderson, and T. Muneer, "A 50 MW very large-scale photovoltaic power plant for Al-Kufra, Libya: Energetic, economic and environmental impact analysis," *Int. J. Low-Carbon Technol.*, vol. 6, no. 4, pp. 277–293, 2011, doi: 10.1093/ijlct/ctr015.

[57] S. S. M Sbeta, "on field performance of PV water pumping system in Libya.," *Cent. Sol. Energy Res. Stud. Tripoli*, pp. 1–7, 2012.

[58] A. S. A. M. T. Kagilik, "Performance analysis of a grid-connected photovoltaic system," *Sol. Energy Sustain. Dev.*, vol. 4, no. 2, pp. 93–102, 2015, doi: 10.1016/S0360-5442(98)00084-X.

[59] A. Kadem, Z. Rajab, A. Khalil, A. Tahir, A. Alfergani, and F. A. Mohamed, "Economic feasibility, design, and simulation of centralized PV power plant," *2018*

9th Int. Renew. Energy Congr. IREC 2018, pp. 1–6, 2018, doi: 10.1109/IREC.2018.8362448.

[60] F. Abusief, R. Caldon, and R. Turri, "Implementation of distributed generation (DG) using solar energy resource to improve power system security in southern area in Libya," *Proc. Univ. Power Eng. Conf.*, pp. 1–6, 2014, doi: 10.1109/UPEC.2014.6934755.

[61] E. Kabir, P. Kumar, S. Kumar, A. A. Adelodun, and K. H. Kim, "Solar energy: Potential and future prospects," *Renew. Sustain. Energy Rev.*, vol. 82, no. August 2017, pp. 894–900, 2018, doi: 10.1016/j.rser.2017.09.094.

[62] S. Gorjian, B. N. Zadeh, L. Eltrop, R. R. Shamshiri, and Y. Amanlou, "Solar photovoltaic power generation in Iran: Development, policies, and barriers," *Renew. Sustain. Energy Rev.*, vol. 106, no. October 2018, pp. 110–123, 2019, doi: 10.1016/j.rser.2019.02.025.

[63] B. Aboagye, S. Gyamfi, E. A. Ofosu, and S. Djordjevic, "Degradation analysis of installed solar photovoltaic (PV) modules under outdoor conditions in Ghana," *Energy Reports*, vol. 7, pp. 6921–6931, 2021, doi: 10.1016/j.egyr.2021.10.046.

[64] P. Gevorkian, *Solar Power Generation Problems, Solutions, and Monitoring*. Cambridge University Press, 2016.

[65] H. Machrafi, *Green Energy and Technology*. 2012.

[66] M. C. Argyrou, P. Christodoulides, C. C. Marouchos, and S. A. Kalogirou, "A grid-connected photovoltaic system: Mathematical modeling using MATLAB/Simulink," *2017 52nd Int. Univ. Power Eng. Conf. UPEC 2017*, vol. 2017-Janua, pp. 1–6, 2017, doi: 10.1109/UPEC.2017.8232009.

[67] P. Hersch and K. Zweibel, "Basic photovoltaic principles and methods," *Antimicrob. Agents Chemother.*, vol. 58, no. 12, pp. 7250–7, 1982, doi: 10.2172/5191389.

[68] T. Markvart, "Light harvesting for quantum solar energy conversion," *Prog. Quantum Electron.*, vol. 24, no. 3, pp. 107–186, 2000, doi: 10.1016/S0079-6727(00)00003-3.

[69] N. A. Mehedi Fahad, Mohammed Ali, Nahar Islam, "A New Approach to Design of an optimized Grid Tied Smart Solar," vol. 1, pp. 3–7, 2012.

References

[70] A. M. Humada, M. Hojabri, S. Mekhilef, and H. M. Hamada, “Solar cell parameters extraction based on single and double-diode models: A review,” *Renew. Sustain. Energy Rev.*, vol. 56, pp. 494–509, 2016, doi: 10.1016/j.rser.2015.11.051.

[71] A. Younis, A. Bakhit, M. Onsa, and M. Hashim, “A comprehensive and critical review of bio-inspired metaheuristic frameworks for extracting parameters of solar cell single and double diode models,” *Energy Reports*, vol. 8, pp. 7085–7106, 2022, doi: 10.1016/j.egyr.2022.05.160.

[72] N. M. A. Alrahim Shannan, N. Z. Yahaya, and B. Singh, “Single-diode model and two-diode model of PV modules: A comparison,” *Proc. - 2013 IEEE Int. Conf. Control Syst. Comput. Eng. ICCSCE 2013*, pp. 210–214, 2013, doi: 10.1109/ICCSCE.2013.6719960.

[73] A. Kassis and M. Saad, “Analysis of multi-crystalline silicon solar cells at low illumination levels using a modified two-diode model,” *Sol. Energy Mater. Sol. Cells*, vol. 94, no. 12, pp. 2108–2112, 2010, doi: 10.1016/j.solmat.2010.06.036.

[74] R. Chenni, M. Makhlouf, T. Kerbache, and A. Bouzid, “A detailed modeling method for photovoltaic cells,” *Energy*, vol. 32, no. 9, pp. 1724–1730, 2007, doi: 10.1016/j.energy.2006.12.006.

[75] F. E. Ndi, S. N. Perabi, S. E. Ndjakomo, G. Ondoua Abessolo, and G. Mengounou Mengata, “Estimation of single-diode and two diode solar cell parameters by equilibrium optimizer method,” *Energy Reports*, vol. 7, pp. 4761–4768, 2021, doi: 10.1016/j.egyr.2021.07.025.

[76] A. M. Humada, A. M. Aaref, H. M. Hamada, M. H. Sulaiman, N. Amin, and S. Mekhilef, “Modeling and characterization of a grid-connected photovoltaic system under tropical climate conditions,” *Renew. Sustain. Energy Rev.*, vol. 82, no. July 2015, pp. 2094–2105, 2018, doi: 10.1016/j.rser.2017.08.053.

[77] N. Barth, R. Jovanovic, S. Ahzi, and M. A. Khaleel, “PV panel single and double diode models: Optimization of the parameters and temperature dependence,” *Sol. Energy Mater. Sol. Cells*, vol. 148, pp. 87–98, 2016, doi: 10.1016/j.solmat.2015.09.003.

[78] P. R. Rivera, “Grid-connected photovoltaic systems based on nonlinear control,”

University of Louisville, 2018.

[79] E. Romero-Cadaval, G. Spagnuolo, L. G. Franquelo, C. A. Ramos-Paja, T. Suntio, and W. M. Xiao, "Grid-connected photovoltaic generation plants: Components and operation," *IEEE Ind. Electron. Mag.*, vol. 7, no. 3, pp. 6–20, 2013, doi: 10.1109/MIE.2013.2264540.

[80] R. G. Vieira, F. M. U. de Araújo, M. Dhimish, and M. I. S. Guerra, "A comprehensive review on bypass diode application on photovoltaic modules," *Energies*, vol. 13, no. 10, pp. 1–21, 2020, doi: 10.3390/en13102472.

[81] R. Ramaprabha and B. L. Mathur, "A comprehensive review and analysis of solar photovoltaic array configurations under partial shaded conditions," *Int. J. Photoenergy*, vol. 2012, 2012, doi: 10.1155/2012/120214.

[82] P. Bauwens and J. Doutreloigne, "Reducing partial shading power loss with an integrated Smart Bypass," *Sol. Energy*, vol. 103, pp. 134–142, 2014, doi: 10.1016/j.solener.2014.01.040.

[83] A. C. de W. and W. G. J. H. M. van S. Boudewijn B. Pannebakker, "Photovoltaics in the shade: one bypass diode per solar cell revisited," *Prog. Photovoltaics Res. Appl.*, vol. 25, no. 1, pp. 836–849, 2017, doi: 10.1002/pip.

[84] H. Shamatah, S. Azouz, A. Khalil, and Z. Rajab, "The potential of the rooftop grid-connected PV systems in Benghazi," *2017 IEEE Jordan Conf. Appl. Electr. Eng. Comput. Technol. AEECT 2017*, vol. 2018-Janua, pp. 1–6, 2017, doi: 10.1109/AEECT.2017.8257778.

[85] A. K. Shukla, K. Sudhakar, and P. Baredar, "Simulation and performance analysis of 110 kWp grid-connected photovoltaic system for residential building in India: A comparative analysis of various PV technology," *Energy Reports*, vol. 2, pp. 82–88, 2016, doi: 10.1016/j.egyr.2016.04.001.

[86] T. Khatib, A. Mohamed, and K. Sopian, "A review of photovoltaic systems size optimization techniques," *Renew. Sustain. Energy Rev.*, vol. 22, pp. 454–465, 2013, doi: 10.1016/j.rser.2013.02.023.

[87] A. Loukriz, M. Haddadi, and S. Messalti, "Simulation and experimental design of a new advanced variable step size Incremental Conductance MPPT algorithm for PV

systems," *ISA Trans.*, vol. 62, pp. 30–38, 2016, doi: 10.1016/j.isatra.2015.08.006.

[88] C. Lupangu and R. C. Bansal, "A review of technical issues on the development of solar photovoltaic systems," *Renew. Sustain. Energy Rev.*, vol. 73, no. February, pp. 950–965, 2017, doi: 10.1016/j.rser.2017.02.003.

[89] K. Zeb *et al.*, "A comprehensive review on inverter topologies and control strategies for grid connected photovoltaic system," *Renew. Sustain. Energy Rev.*, vol. 94, no. July, pp. 1120–1141, 2018, doi: 10.1016/j.rser.2018.06.053.

[90] B. G. Sujatha and G. S. Anitha, "Enhancement of PQ in grid connected PV system using hybrid technique," *Ain Shams Eng. J.*, vol. 9, no. 4, pp. 869–881, 2018, doi: 10.1016/j.asej.2016.04.007.

[91] A. Cabrera-Tobar, E. Bullich-Massagué, M. Aragüés-Peñalba, and O. Gomis-Bellmunt, "Topologies for large scale photovoltaic power plants," *Renew. Sustain. Energy Rev.*, vol. 59, pp. 309–319, 2016, doi: 10.1016/j.rser.2015.12.362.

[92] M. H. De Freitas Takami, S. A. Oliveira Da Silva, and L. P. Sampaio, "Dynamic performance comparison involving grid-connected PV systems operating with active power-line conditioning and subjected to sudden solar irradiation changes," *IET Renew. Power Gener.*, vol. 13, no. 4, pp. 587–597, 2019, doi: 10.1049/iet-rpg.2018.5810.

[93] A. Costa De Souza, F. Cardoso Melo, T. Lima Oliveira, and C. Eduardo Tavares, "Performance Analysis of the Computational Implementation of a Simplified PV Model and MPPT Algorithm," *IEEE Lat. Am. Trans.*, vol. 14, no. 2, pp. 792–798, 2016, doi: 10.1109/TLA.2016.7437224.

[94] M. Obi and R. Bass, "Trends and challenges of grid-connected photovoltaic systems - A review," *Renew. Sustain. Energy Rev.*, vol. 58, pp. 1082–1094, 2016, doi: 10.1016/j.rser.2015.12.289.

[95] Ö. Çelik and A. Teke, "A Hybrid MPPT method for grid connected photovoltaic systems under rapidly changing atmospheric conditions," *Electr. Power Syst. Res.*, vol. 152, pp. 194–210, 2017, doi: 10.1016/j.epsr.2017.07.011.

[96] S. A. Mohamed and M. Abd El Sattar, "A comparative study of P&O and INC maximum power point tracking techniques for grid-connected PV systems," *SN Appl.*

Sci., vol. 1, no. 2, pp. 1–13, 2019, doi: 10.1007/s42452-018-0134-4.

[97] T. Esram and P. L. Chapman, "Comparison of photovoltaic array maximum power point tracking techniques," *IEEE Trans. Energy Convers.*, vol. 22, no. 2, pp. 439–449, 2007, doi: 10.1109/TEC.2006.874230.

[98] T. Thumma and S. R. Sheri, "Comparison of Photovoltaic Array Maximum Power Point Tracking Techniques," *Int. Adv. Res. J. Sci. Eng. Technol.*, vol. 2, no. 2, pp. 197–205, 2015, doi: 10.17148/IARJSET.

[99] M. Dehghani, M. Taghipour, G. B. Gharehpetian, and M. Abedi, "Optimized Fuzzy Controller for MPPT of Grid-connected PV Systems in Rapidly," pp. 1–8, 2019, doi: 10.35833/MPCE.2019.000086.

[100] P. K. Mishra and P. Tiwari, "Incremental conductance MPPT in grid connected PV system," *Int. J. Eng. Sci. Technol.*, vol. 13, no. 1, pp. 138–145, 2021, doi: 10.4314/ijest.v13i1.21s.

[101] M. H. Ibrahim, S. P. Ang, M. N. Dani, M. I. Rahman, R. Petra, and S. M. Sulthan, "Optimizing Step-Size of Perturb & Observe and Incremental Conductance MPPT Techniques Using PSO for Grid-Tied PV System," *IEEE Access*, vol. 11, no. February, pp. 13079–13090, 2023, doi: 10.1109/ACCESS.2023.3242979.

[102] R. Chedid, R. Tajeddine, F. Chaaban, and R. Ghajar, "Modeling and simulation of PV arrays under varying conditions," *Proc. Mediterr. Electrotech. Conf. - MELECON*, no. April 2014, pp. 536–542, 2014, doi: 10.1109/MELCON.2014.6820592.

[103] N. Khaehintung, K. Pramotung, and P. Sirisuk, "RISC microcontroller built-in fuzzy logic controller for maximum power point tracking in solar-powered for battery charger," *IEEE Reg. 10 Annu. Int. Conf. Proceedings/TENCON*, vol. D, no. 1, pp. 637-640 Vol. 4, 2004, doi: 10.1109/tencon.2004.1415013.

[104] S. Messalti, A. Harrag, and A. Loukriz, "A new variable step size neural networks MPPT controller: Review, simulation and hardware implementation," *Renew. Sustain. Energy Rev.*, vol. 68, no. September 2016, pp. 221–233, 2017, doi: 10.1016/j.rser.2016.09.131.

[105] H. Boumaaraf, A. Talha, and O. Bouhali, "A three-phase NPC grid-connected inverter for photovoltaic applications using neural network MPPT," *Renew. Sustain. Energy*

Rev., vol. 49, pp. 1171–1179, 2015, doi: 10.1016/j.rser.2015.04.066.

[106] S. A. Rizzo and G. Scelba, "ANN based MPPT method for rapidly variable shading conditions," *Appl. Energy*, vol. 145, pp. 124–132, 2015, doi: 10.1016/j.apenergy.2015.01.077.

[107] K. N. Nwaigwe, P. Mutabilwa, and E. Dintwa, "An overview of solar power (PV systems) integration into electricity grids," *Mater. Sci. Energy Technol.*, vol. 2, no. 3, pp. 629–633, 2019, doi: 10.1016/j.mset.2019.07.002.

[108] P. P. Zarina, S. Mishra, and P. C. Sekhar, "Deriving inertial response from a non-inertial PV system for frequency regulation," *PEDES 2012 - IEEE Int. Conf. Power Electron. Drives Energy Syst.*, pp. 1–5, 2012, doi: 10.1109/PEDES.2012.6484409.

[109] M. K. Hossain and M. H. Ali, "Small scale energy storage for power fluctuation minimization with spatially diverged PV plants," *Conf. Proc. - IEEE SOUTHEASTCON*, pp. 1–6, 2013, doi: 10.1109/SECON.2013.6567358.

[110] W. A. Omran, M. Kazerani, and M. M. A. Salama, "Investigation of methods for reduction of power fluctuations generated from large grid-connected photovoltaic systems," *IEEE Trans. Energy Convers.*, vol. 26, no. 1, pp. 318–327, 2011, doi: 10.1109/TEC.2010.2062515.

[111] H. Wang and X. Bai, "Adequacy assessment of generating systems incorporating wind, PV and energy storage," *2012 IEEE Innov. Smart Grid Technol. - Asia, ISGT Asia 2012*, pp. 1–6, 2012, doi: 10.1109/ISGT-Asia.2012.6303229.

[112] A. Anzalchi and A. Sarwat, "Overview of technical specifications for grid-connected photovoltaic systems," *Energy Convers. Manag.*, vol. 152, no. September, pp. 312–327, 2017, doi: 10.1016/j.enconman.2017.09.049.

[113] J. C. Boemer, M. Huque, B. Seal, T. Key, D. Brooks, and C. Vartanian, "Status of revision of IEEE Std 1547 and 1547.1," *IEEE Power Energy Soc. Gen. Meet.*, vol. 2018-Janua, pp. 1–5, 2018, doi: 10.1109/PESGM.2017.8274554.

[114] W. Group, *IEEE Application Guide for IEEE Std 1547, IEEE Standard for Interconnecting Distributed Resources with Electric Power Systems*, no. April. 2008.

[115] S. Chatterjee, P. Kumar, and S. Chatterjee, "A techno-commercial review on grid connected photovoltaic system," *Renew. Sustain. Energy Rev.*, vol. 81, no. March

2017, pp. 2371–2397, 2018, doi: 10.1016/j.rser.2017.06.045.

[116] B. Kroposki and R. DeBlasio, “Technologies for the new millennium: Photovoltaics as a distributed resource,” *Proc. IEEE Power Eng. Soc. Transm. Distrib. Conf.*, vol. 3, no. c, pp. 1798–1801, 2000, doi: 10.1109/pess.2000.868807.

[117] Y. K. Wu, J. H. Lin, and H. J. Lin, “Standards and Guidelines for Grid-Connected Photovoltaic Generation Systems: A Review and Comparison,” *IEEE Trans. Ind. Appl.*, vol. 53, no. 4, pp. 3205–3216, 2017, doi: 10.1109/TIA.2017.2680409.

[118] A. American and N. Standard, “An American National Standard IEEE Recommended Practice for Utility Interface of Residential and Intermediate Photovoltaic (PV) Systems,” 1991.

[119] M. J. R. Arseneau, G. T. Heydt, Kempker, “Application of IEEE Standard 519-1992 Harmonic Limits for Revenue Billing Meters,” *IEEE Trans. Power Deliv.*, vol. 12, no. 1, pp. 346–353, 1997.

[120] T. M. Blooming and D. J. Carnovale, “Application of IEEE STD 519-1992 harmonic limits,” *IEEE Conf. Rec. Annu. Pulp Pap. Ind. Tech. Conf.*, pp. 1–9, 2006, doi: 10.1109/papcon.2006.1673767.

[121] IEEE Std 519, “IEEE Recommended Practice and Requirements for Harmonic Control in Electric Power Systems Sponsored by the Transmission and Distribution Committee IEEE Power and Energy Society,” *IEEE Stand.*, vol. 2014, pp. 1–29, 2014.

[122] D. S. Pillai, J. P. Ram, N. Rajasekar, A. Mahmud, Y. Yang, and F. Blaabjerg, “Extended analysis on Line-Line and Line-Ground faults in PV arrays and a compatibility study on latest NEC protection standards,” *Energy Convers. Manag.*, vol. 196, no. April, pp. 988–1001, 2019, doi: 10.1016/j.enconman.2019.06.042.

[123] M. W. Earley, J. S. Sargent, J. V Sheehan, and E. W. Buss, *National electrical code*, vol. 44, no. 11. 2013.

[124] D. S. Pillai and R. Natarajan, “A Compatibility Analysis on NEC, IEC, and UL Standards for Protection Against Line-Line and Line-Ground Faults in PV Arrays,” *IEEE J. Photovoltaics*, vol. 9, no. 3, pp. 864–871, 2019, doi: 10.1109/JPHOTOV.2019.2900706.

[125] D. L. Bassett, “Update of the status of IEEE 1547.8, expanding on IEEE Standard

1547," *Proc. IEEE Power Eng. Soc. Transm. Distrib. Conf.*, pp. 1–3, 2012, doi: 10.1109/TDC.2012.6281453.

[126] O. Goksu, R. Teodorescu, B. Bak-Jensen, F. Iov, and P. C. Kjar, "An iterative approach for symmetrical and asymmetrical Short-circuit calculations with converter-based connected renewable energy sources. Application to wind power," *IEEE Power Energy Soc. Gen. Meet.*, pp. 1–8, 2012, doi: 10.1109/PESGM.2012.6344906.

[127] N. Zhou, J. Wu, and Q. Wang, "Three-phase short-circuit current calculation of power systems with high penetration of VSC-based renewable energy," *Energies*, vol. 11, no. 2, 2018, doi: 10.3390/en11030537.

[128] V. N. Kumar, N. B. Pea, R. Kiranmayi, P. Siano, and G. Panda, "Improved Power Quality in a Solar PV Plant Integrated Utility Grid by Employing a Novel Adaptive Current Regulator," *IEEE Syst. J.*, vol. 14, no. 3, pp. 4308–4319, 2020, doi: 10.1109/JSYST.2019.2958819.

[129] H. Hooshyar and M. E. Baran, "Fault analysis on distribution feeders with high penetration of PV systems," *IEEE Trans. Power Syst.*, vol. 28, no. 3, pp. 2890–2896, 2013, doi: 10.1109/TPWRS.2012.2227842.

[130] R. K. Varma, S. A. Rahman, V. Atodaria, S. Mohan, and T. Vanderheide, "Technique for Fast Detection of Short Circuit Current in PV Distributed Generator," *IEEE Power Energy Technol. Syst. J.*, vol. 3, no. 4, pp. 155–165, 2016, doi: 10.1109/jpets.2016.2592465.

[131] J. C. Das, *Power system*. New York: Marcel Dekker, Inc., 2002.

[132] B. Vahidi, S. A. Agheli, and S. Jazebi, "Teaching short-circuit withstand test on power transformers to M.Sc. students and junior engineers using MATLAB-SIMULINK," *Comput. Appl. Eng. Educ.*, vol. 20, no. 3, pp. 484–492, 2012, doi: 10.1002/cae.20416.

[133] H. Zahloul, H. Hamzehbahmani, A. Khaliq, and S. Veremieiev, "An Approach to Dynamic Behaviour of a Grid Connected PV System during Symmetrical Short Circuit Fault," *2022 13th Int. Renew. Energy Congr. IREC 2022*, no. Irec, 2022, doi: 10.1109/IREC56325.2022.10002093.

[134] I. Standards, C. Committee, D. Generation, and E. Storage, *IEEE Guide for Conducting Distribution Impact Studies for Distributed Resource Interconnection*.

2014.

[135] K. Prabha, “Power System Stability and Control.” p. 1176, 1994.

[136] R. Mahmud, D. Narang, and A. Hoke, “Reduced-Order Parameterized Short-Circuit Current Model of Inverter-Interfaced Distributed Generators,” *IEEE Trans. Power Deliv.*, vol. 36, no. 6, pp. 3671–3680, 2021, doi: 10.1109/TPWRD.2020.3046966.

[137] S. Kouro, J. I. Leon, D. Vinnikov, and L. G. Franquelo, “Grid-connected photovoltaic systems: An overview of recent research and emerging PV converter technology,” *IEEE Ind. Electron. Mag.*, vol. 9, no. 1, pp. 47–61, 2015, doi: 10.1109/MIE.2014.2376976.

[138] K. Shivam, J. C. Tzou, and S. C. Wu, “A multi-objective predictive energy management strategy for residential grid-connected PV-battery hybrid systems based on machine learning technique,” *Energy Convers. Manag.*, vol. 237, no. 195, p. 114103, 2021, doi: 10.1016/j.enconman.2021.114103.

[139] A. Yazdani *et al.*, “Modeling guidelines and a benchmark for power system simulation studies of three-phase single-stage photovoltaic systems,” *IEEE Trans. Power Deliv.*, vol. 26, no. 2, pp. 1247–1264, 2011, doi: 10.1109/TPWRD.2010.2084599.

[140] G. P. Adam, K. H. Ahmed, S. J. Finney, and B. W. Williams, “AC fault ride-through capability of a VSC-HVDC transmission systems,” *2010 IEEE Energy Convers. Congr. Expo. ECCE 2010 - Proc.*, pp. 3739–3745, 2010, doi: 10.1109/ECCE.2010.5617786.

[141] S. F. Zarei, H. Mokhtari, M. A. Ghasemi, and F. Blaabjerg, “Reinforcing Fault Ride through Capability of Grid Forming Voltage Source Converters Using an Enhanced Voltage Control Scheme,” *IEEE Trans. Power Deliv.*, vol. 34, no. 5, pp. 1827–1842, 2019, doi: 10.1109/TPWRD.2018.2844082.

[142] J. Song, M. Cheah-Mane, E. Prieto-Araujo, and O. Gomis-Bellmunt, “Short-circuit analysis of grid-connected PV power plants considering inverter limits,” *Int. J. Electr. Power Energy Syst.*, vol. 149, no. July 2022, p. 109045, 2023, doi: 10.1016/j.ijepes.2023.109045.

[143] M. Islam, M. Nadarajah, and M. J. Hossain, “A Grid-Support Strategy with PV Units to Boost Short-Term Voltage Stability under Asymmetrical Faults,” *IEEE Trans.*

Power Syst., vol. 35, no. 2, pp. 1120–1131, 2020, doi: 10.1109/TPWRS.2019.2942094.

[144] I. S. Association, *IEEE Std. 1547-2018. Standard for Interconnection and Interoperability of Distributed Energy Resources with Associated Electric Power Systems Interfaces*, no. February. 2018.

[145] K. Givaki, D. Chen, and L. Xu, "Current Error Based Compensations for VSC Current Control in Weak Grids for Wind Farm Applications," *IEEE Trans. Sustain. Energy*, vol. 10, no. 1, pp. 26–35, 2019, doi: 10.1109/TSTE.2018.2820386.

[146] M. Yadav, N. Pal, and D. K. Saini, "Low voltage ride through capability for resilient electrical distribution system integrated with renewable energy resources," *Energy Reports*, vol. 9, pp. 833–858, 2023, doi: 10.1016/j.egyr.2022.12.023.

[147] I. Yahyaoui, *Advances in renewable energies and power technologies: solar and wind energies*. Elsevier, 2018.

[148] J. Mohammadi, S. Afsharnia, and S. Vaez-Zadeh, "Efficient fault-ride-through control strategy of DFIG-based wind turbines during the grid faults," *Energy Convers. Manag.*, vol. 78, pp. 88–95, 2014, doi: 10.1016/j.enconman.2013.10.029.

[149] T. Qoria, X. Wang, and R. Kadri, "Grid-forming control VSC-based including current limitation and re-synchronization functions to deal with symmetrical and asymmetrical faults," *Electr. Power Syst. Res.*, vol. 223, no. December 2022, p. 109647, 2023, doi: 10.1016/j.epsr.2023.109647.

[150] S. G. P. System, M. E. Ropp, and S. Gonzalez, "Development of a MATLAB / Simulink Model of a," pp. 1–8, 2009.

[151] W. Libo, Z. Zhengming, S. Member, and L. Jianzheng, "A Single-Stage Three-Phase Grid-Connected Photovoltaic System With Modified MPPT Method and Reactive Power Compensation," vol. 22, no. 4, pp. 881–886, 2007.

[152] P. R. Kumar *et al.*, "DESIGN AND SIMULATION OF 100KW HYBRID GRID CONNECTED SOLAR PV SYSTEM BY USING MATLAB / SIMULINK," vol. 6, no. 1, pp. 136–142, 2019.

[153] Y. K. Baseem Khan, "Designing and modelling of grid connected photovoltaic system (case study : EEU Building at Hawassa City) Yishak Kifle and Baseem Khan * Jitendra Singh," vol. 3, no. 1, pp. 20–34, 2018.

References

[154] R. Abdelhady and R. Abdelhady, “Modeling and simulation of a micro grid- connected solar PV system Modeling and simulation of a micro grid-connected solar PV system,” *TITLE=Water Sci.*, vol. 31, no. 1, pp. 1–10, 2017, doi: 10.1016/j.wsj.2017.04.001.

[155] M. G. Molina, *Modelling and Control of Grid-connected Solar Photovoltaic Systems*. 2016.

[156] S. Jain and V. Agarwal, “Comparison of the performance of maximum power point tracking schemes applied to single-stage grid-connected photovoltaic systems,” no. Ccm, pp. 753–762, doi: 10.1049/iet-epa.

[157] P. System, “A Review on Perturb and Observe Maximum Power Point Tracking in A Review on Perturb and Observe Maximum Power Point Tracking in Photovoltaic System,” no. February 2016, 2015, doi: 10.12928/telkomnika.v13i3.1439.

[158] A. I. M. Ali, M. A. Sayed, and E. E. M. Mohamed, “Modified efficient perturb and observe maximum power point tracking technique for grid-tied PV system,” *Int. J. Electr. Power Energy Syst.*, vol. 99, no. February, pp. 192–202, 2018, doi: 10.1016/j.ijepes.2017.12.029.

[159] L. P. Sampaio, M. V. Da Rocha, S. A. O. Da Silva, and M. H. T. De Freitas, “Comparative analysis of MPPT algorithms bio-inspired by grey wolves employing a feedforward control loop in a three-phase gridconnected photovoltaic system,” *IET Renew. Power Gener.*, vol. 13, no. 8, pp. 1379–1390, 2019, doi: 10.1049/iet-rpg.2018.5941.

[160] A. K. Verma and B. Singh, “Harmonics and Reactive Current Detection of a Grid-Interfaced PV Generation in a Distribution System,” *IEEE Trans. Ind. Appl.*, vol. 54, no. 5, pp. 4786–4794, 2018, doi: 10.1109/TIA.2018.2830752.

[161] L. B. G. Campanhol, S. A. O. Da Silva, A. A. De Oliveira, and V. D. Bacon, “Power flow and stability analyses of a multifunctional distributed generation system integrating a photovoltaic system with unified power quality conditioner,” *IEEE Trans. Power Electron.*, vol. 34, no. 7, pp. 6241–6256, 2019, doi: 10.1109/TPEL.2018.2873503.

[162] A. Khaliq, H. Zahloul, and H. Hamzehbahmani, “A control approach for power quality improvement of a large-scale grid connected PV system at standard test conditions,”

vol. 1, pp. 241–245, 2022, doi: 10.1049/icp.2022.1836.

[163] S. Silvestre, M. A. Da Silva, A. Chouder, D. Guasch, and E. Karatepe, “New procedure for fault detection in grid connected PV systems based on the evaluation of current and voltage indicators,” *Energy Convers. Manag.*, vol. 86, pp. 241–249, 2014, doi: 10.1016/j.enconman.2014.05.008.

[164] T. Lin, M. Das, A. Gole, and A. Isaacs, “Adaptive fault ride through control of VSM Grid-forming converters ☆,” *Electr. Power Syst. Res.*, vol. 223, no. December 2022, p. 109606, 2023, doi: 10.1016/j.epsr.2023.109606.

[165] M. Calais, J. Myrzik, T. Spoone, and V. G. Agelidis, “Inverters for Single-phase Grid Connected Photovoltaic Systems - An Overview,” vol. 2, pp. 1995–2000, 2002.

[166] G. R. Walker and P. C. Sernia, “Cascaded DC – DC Converter Connection of Photovoltaic Modules,” vol. 19, no. 4, pp. 1130–1139, 2004.

[167] R. Kadri, J. Gaubert, and G. Champenois, “An Improved Maximum Power Point Tracking for Photovoltaic Grid-Connected Inverter Based on Voltage-Oriented Control,” *IEEE Trans. Ind. Electron.*, vol. 58, no. 1, pp. 66–75, 2011, doi: 10.1109/TIE.2010.2044733.

[168] J. Atiq and P. K. Soori, “Modelling of a grid connected solar PV system using MATLAB/simulink,” *Int. J. Simul. Syst. Sci. Technol.*, vol. 17, no. 41, pp. 45.1-45.7, 2017, doi: 10.5013/IJSSST.a.17.41.45.

[169] A. M. Humada, A. M. Aaref, H. M. Hamada, and M. Herwan, “Modeling and characterization of a grid-connected photovoltaic system under tropical climate conditions,” *Renew. Sustain. Energy Rev.*, vol. 82, no. July 2015, pp. 2094–2105, 2018, doi: 10.1016/j.rser.2017.08.053.

[170] M. G. Villalva, J. R. Gazoli, and E. R. Filho, “Comprehensive approach to modeling and simulation of photovoltaic arrays,” *IEEE Trans. Power Electron.*, vol. 24, no. 5, pp. 1198–1208, 2009, doi: 10.1109/TPEL.2009.2013862.

[171] H. Bellia, R. Youcef, and M. Fatima, “A detailed modeling of photovoltaic module using MATLAB,” *NRIAG J. Astron. Geophys.*, vol. 3, no. 1, pp. 53–61, 2014, doi: 10.1016/j.nrjag.2014.04.001.

[172] R. Errouissi, A. Al-Durra, and S. M. Muyeen, “A Robust Continuous-Time MPC of a

DC-DC Boost Converter Interfaced with a Grid-Connected Photovoltaic System," *IEEE J. Photovoltaics*, vol. 6, no. 6, pp. 1619–1629, 2016, doi: 10.1109/JPHOTOV.2016.2598271.

[173] M. Bajaj and A. K. Singh, "Grid integrated renewable DG systems: A review of power quality challenges and state-of-the-art mitigation techniques," *Int. J. Energy Res.*, vol. 44, no. 1, pp. 26–69, 2020, doi: 10.1002/er.4847.

[174] F. Li, X. Zhang, H. Zhu, H. Li, and C. Yu, "An LCL - LC Filter for Grid-Connected Converter :," vol. 30, no. 9, pp. 5067–5077, 2015.

[175] P. Cortés, G. Ortiz, J. I. Yuz, J. Rodríguez, S. Vazquez, and L. G. Franquelo, "Model predictive control of an inverter with output LC filter for UPS applications," *IEEE Trans. Ind. Electron.*, vol. 56, no. 6, pp. 1875–1883, 2009, doi: 10.1109/TIE.2009.2015750.

[176] M. H. Mahlooji, H. R. Mohammadi, and M. Rahimi, "A review on modeling and control of grid-connected photovoltaic inverters with LCL filter," *Renew. Sustain. Energy Rev.*, vol. 81, no. November 2016, pp. 563–578, 2018, doi: 10.1016/j.rser.2017.08.002.

[177] R. N. Kalaam, S. M. Muyeen, A. Al-Durra, H. M. Hasanien, and K. Al-Wahedi, "Optimisation of controller parameters for grid-tied photovoltaic system at faulty network using artificial neural network-based cuckoo search algorithm," *Front. Cell Dev. Biol.*, vol. 9, pp. 1517–1526, 2017, doi: 10.1049/iet-rpg.2017.0040.

[178] M. Graungaard Taul, X. Wang, P. Davari, and F. Blaabjerg, "Current Reference Generation Based on Next-Generation Grid Code Requirements of Grid-Tied Converters during Asymmetrical Faults," *IEEE J. Emerg. Sel. Top. Power Electron.*, vol. 8, no. 4, pp. 3784–3797, 2020, doi: 10.1109/JESTPE.2019.2931726.

[179] R. Madnani and M. K. Mishra, "A visual understanding of electrical transformations and generalized abc to αβ0 and dq0 transformation," *Int. J. Circuit Theory Appl.*, no. April 2022, pp. 963–978, 2022, doi: 10.1002/cta.3439.

[180] N. Cao and J. Liu, "An improved maximum power point tracking for photovoltaic grid-connected inverter," *2013 IEEE Int. Conf. Mechatronics Autom. IEEE ICMA 2013*, vol. 58, no. 1, pp. 616–621, 2013, doi: 10.1109/ICMA.2013.6617987.

References

[181] S. Prakash and S. Mishra, "VSC Control of Grid Connected PV for Maintaining Power Supply during Open-Phase Condition in Distribution Network," *IEEE Trans. Ind. Appl.*, vol. 55, no. 6, pp. 6211–6222, 2019, doi: 10.1109/TIA.2019.2932697.

[182] A. L. Bukar, C. W. Tan, L. K. Yiew, R. Ayop, and W. S. Tan, "A rule-based energy management scheme for long-term optimal capacity planning of grid-independent microgrid optimized by multi-objective grasshopper optimization algorithm," *Energy Convers. Manag.*, vol. 221, no. June, p. 113161, 2020, doi: 10.1016/j.enconman.2020.113161.

[183] A. Seifi, M. H. Moradi, M. Abedini, and A. Jahangiri, "An optimal programming among renewable energy resources and storage devices for responsive load integration in residential applications using hybrid of grey wolf and shark smell algorithms," *J. Energy Storage*, vol. 27, no. December 2019, 2020, doi: 10.1016/j.est.2019.101126.

[184] A. Alsharif *et al.*, "Impact of Electric Vehicle on Residential Power Distribution Considering Energy Management Strategy and Stochastic Monte Carlo Algorithm," *Energies*, vol. 16, no. 3, pp. 1–22, 2023, doi: 10.3390/en16031358.

[185] A. Maleki and F. Pourfayaz, "Optimal sizing of autonomous hybrid photovoltaic/wind/battery power system with LPSP technology by using evolutionary algorithms," *Sol. Energy*, vol. 115, pp. 471–483, 2015, doi: 10.1016/j.solener.2015.03.004.

[186] A. Alsharif, C. W. Tan, R. Ayop, K. Y. Lau, and A. M. d. Dobi, "A rule-based power management strategy for Vehicle-to-Grid system using antlion sizing optimization," *J. Energy Storage*, vol. 41, no. April, p. 102913, 2021, doi: 10.1016/j.est.2021.102913.

[187] H. Louie, *Off-Grid Electrical Systems in Developing Countries*. Cham: Springer, 2018.

[188] M. Baqir and H. K. Channi, "Analysis and design of solar PV system using Pvsyst software," *Mater. Today Proc.*, vol. 48, pp. 1332–1338, 2021, doi: 10.1016/j.matpr.2021.09.029.

[189] N. H. Umar, B. Bora, C. Banerjee, N. Umar, and B. S. Panwar, "Comparison of different PV power simulation softwares: case study on performance analysis of 1 MW grid-connected PV solar power plant," *Int. J. Eng. Sci. Invent.*, vol. 7, no. 7, pp. 11–24, 2018.

References

[190] B. Wittmer, A. Mermoud, and T. Schott, “Analysis of Pv Grid Installations Performance, Comparing Measured Data To Simulation Results To Identify Problems in Operation and Monitoring,” *Eur. Photovolt. Sol. Energy Conf.*, no. September, pp. 14–18, 2015.

[191] A. Villoz, B. Wittmer, A. Mermoud, M. Oliosi, and A. Bridel-Bertomeu, “a Model Correcting the Effect of Sub-Hourly Irradiance Fluctuations on Overload Clipping Losses in Hourly Simulations,” no. September, pp. 26–30, 2022.

[192] C. G. Popovici, S. V. Hudişteanu, T. D. Mateescu, and N. C. Cherecheş, “Efficiency Improvement of Photovoltaic Panels by Using Air Cooled Heat Sinks,” *Energy Procedia*, vol. 85, no. November 2015, pp. 425–432, 2016, doi: 10.1016/j.egypro.2015.12.223.

[193] Q. M. Aish, “Temperature Effect on Photovoltaic Modules Power Drop,” *J. Al-Khwarizmi Eng. J.*, vol. 11, no. 2, pp. 62–73, 2015.

[194] M. Mirhosseini, J. Pou, and V. G. Agelidis, “Single- and Two-Stage Inverter-Based Grid-Connected Photovoltaic Power Plants With Ride-Through Capability Under Grid Faults,” *IEEE Trans. Sustain. Energy*, vol. 6, no. 3, pp. 1150–1159, 2015, doi: 10.1109/TSTE.2014.2347044.

[195] Y. L. Hu, Y. K. Wu, C. K. Chen, C. H. Wang, W. T. Chen, and L. Il Cho, “A Review of the Low-Voltage Ride-Through Capability of Wind Power Generators,” *Energy Procedia*, vol. 141, pp. 378–382, 2017, doi: 10.1016/j.egypro.2017.11.046.

[196] R. Ntare, N. H. Abbasy, and K. H. M. Youssef, “Low Voltage Ride through Control Capability of a Large Grid Connected PV System Combining DC Chopper and Current Limiting Techniques,” *J. Power Energy Eng.*, vol. 07, no. 01, pp. 62–79, 2019, doi: 10.4236/jpee.2019.71004.

[197] T. W. Bank *et al.*, “Libya - Supporting Electricity Sector Reform Contract No . 7181909 - Task D : Strategic Plan for Renewable Energy Development Least Cost Expansion Plan Report Technology Review,” 2017.

[198] “PVsyst software.” Geneve, 2011.

[199] D. J. Mildrexler, M. Zhao, and S. W. Running, “Where are the hottest spots on Earth?,” *Eos (Washington. DC).*, vol. 87, no. 43, 2006, doi: 10.1029/2006EO430002.

References

[200] C. C. Burt, “The World’s Hottest Recorded Air Temperatures,” *Weatherwise*, vol. 64, no. 2, pp. 26–33, 2011, doi: 10.1080/00431672.2011.551594.

[201] G. Ali, H. N. Musbah, H. H. Aly, and T. Little, “Hybrid Renewable Energy Resources Selection Based on Multi Criteria Decision Methods for Optimal Performance,” *IEEE Access*, vol. 11, no. February, pp. 26773–26784, 2023, doi: 10.1109/ACCESS.2023.3254532.

Appendix

Appendix A

List of publications:

Refereed conference papers:

1. **Hussin Zahloul**, Arjmand Khaliq, Hamed Hamzehbahmani, and Sergii Veremieiev, "*An Approach to Dynamic Behaviour of a Grid Connected PV System During Symmetrical Short Circuit Fault"*, IEEE 13th International Renewable Energy Congress (IREC), Hammamet, Tunisia, Dec 2022

2. Arjmand Khaliq, **Hussin Zahloul** and Hamed Hamzehbahmani, "*A Control Approach for Power Quality Improvement of a Large-Scale Grid Connected PV System at Standard Test Conditions*", The 11th IET International Conference on Renewable Power Generation, London, UK, Sep 2022

3. Arjmand Khaliq, **Hussin Zahloul** and Hamed Hamzehbahmani, "*Performance evaluation of VSC based control strategy for a large-scale grid connected PV system and harmonics analysis under sudden changes in weather conditions*" IET Renewable Power Generation and Future Power Systems Conference, 15 - 16 November 2023, Glasgow UK

Submitted journal papers:

1. **Hussin Zahloul**, Arjmand Khaliq, Hamed Hamzehbahmani, Sergii Veremieiev and Sana Salous "*Evaluation of LVRT Capability and Stability Analysis of VSC based Advanced Control Strategy for Grid Connected PV System under Grid Fault Conditions*", Heliyon, Oct 2023
2. Arjmand Khaliq, **Hussin Zahloul,** Hamed Hamzehbahmani, and Sana Salous "Harmonics analysis and attenuation using optimised LCL filter for grid tied inverters with deployment of large-scale grid connected PV system under sudden changes in weather conditions".

Appendix B

➢ MATLAB CODE FOR P&O MPPT

```
function D  = PandO(Param, Enabled, V, I)


% MPPT controller based on the Perturb & Observe algorithm.


% D output = Duty cycle of the boost converter (value between 0 and 1)
%
% Enabled input = 1 to enable the MPPT controller
% V input = PV array terminal voltage (V)
% I input = PV array current (A)
%
% Param input:
Dinit = Param(1);  %Initial value for D output
Dmax = Param(2);   %Maximum value for D
Dmin = Param(3);   %Minimum value for D
deltaD = Param(4); %Increment value used to increase/decrease the duty cycle D
% ( increasing D = decreasing Vref )
%


persistent Vold Pold Dold;


dataType = 'double';


if isempty(Vold)
    Vold=0;
    Pold=0;
    Dold=Dinit;
end
P= V*I;
dV= V - Vold;
dP= P - Pold;

if dP ~= 0 & Enabled ~=0
    if dP < 0
        if dV < 0
            D = Dold - deltaD;
        else
            D = Dold + deltaD;
        end
    else
        if dV < 0
            D = Dold + deltaD;
        else
            D = Dold - deltaD;
        end
    end
else D=Dold;
end
```

Appendix

```
if D >= Dmax | D<= Dmin
    D=Dold;
end

Dold=D;
Vold=V;
Pold=P;
```

➢ MATLAB CODE FRO POWER OUTPUT OF PV SYSTEM

```
solar=xlsread('Tiji_1.xlsx',1,'B14:B8773')';         %% solar irradiance data
W/m^2
Temp=xlsread('Tiji_1.xlsx',1,'C14:C8773')';           %% temperature data 0C
T_amb=Temp;                                          %% ambient temperature 0C


Gref=1000;                %% reference solar radiation (W/m^2)
NOCT=47;                  %% Nominal  operating cell temperature
TC=-3.7e-3;               %% Temperature coeeficient
T_ref=25;                  %% Temperature at reference condition
Tc=T_amb+((NOCT-20)/800).*solar;  % cell temperature
P_max=0.315;                %%  Rated power under reference condition (kwh)
G=solar;
PV_out=6375*(P_max.*(G/Gref)).*(1+TC.*(Tc-T_ref));         %PV output power
(kW)
pp=PV_out;

figure ;plot(pp);axis tight;box  on;xlabel('Time (hours)');ylabel('PV output
power (kW)');title(' Output power generated from PV','Fontsize',15)

%%%%%% solar radiation%%%%%%%___
figure ;plot(G);axis tight;box  on;xlabel('Time (hours)');ylabel('radiation
(W/m^2) (kW)');title(' Solar Radiation','Fontsize',15)
```

Appendix

Appendix C

- **The submitted journal article.**

Evaluation of LVRT Capability and Stability Analysis of VSC based Advanced Control Approach for Grid Connected PV System under Grid Fault Conditions

Hussin Zahloul[1,2]*, Arjmand Khaliq[1,3], Hamed Hamzehbahmani[1], *Senior Member IEEE*, Sergii Veremieiev[1] and Sana Salous[1]
[1]Department of engineering, Durham University, DH1 3LE, Durham, United Kingdom
[2]Electrical engineering department, High Institute of Science and Technology, Tiji, Libya
[3]Architectural engineering and design department, University of Engineering and Technology Lahore, Lahore, Pakistan
*hussin.a.zahloul@durham.ac.uk

***Abstract*— Short circuit faults are a prevalent issue in power systems, causing disruptions to the grid's normal operation. Dynamic behaviours of the conventional power systems during short circuit faults have been extensively studied and understood. The bulk of ongoing research and development are focusing on the dynamic performance of grid-connected renewable energy systems under these fault conditions, due to changes in the grid code and a decrease in system inertia. The development of effective control strategies to enhance the system's reliability during fault conditions is of paramount importance. In this paper, a two-stages grid-connected photovoltaic system (GCPV) having a rated power of 2 MW was created in the MATLAB/Simulink environment. The dynamic behaviour of the presented system was evaluated in two scenarios: steady state conditions and short circuit faults. A line-to-ground short circuit fault was created at the grid side, and its effect on the PV system's operation was observed. An advanced control system was designed to maintain stability during fault conditions. The results demonstrated the efficiency of the designated control system in minimizing the effects of short circuit faults on the GCPV system's function, and restoring the system promptly after the fault was cleared. Furthermore, considering modifications in grid regulations, the low voltage ride through (LVRT) capability of the designed system was analysed and validated according to the UK standards. The Total Harmonic Distortion (THD) level at the common coupling point was also analysed for voltage and current, remaining below the acceptable level of 5% as specified in the IEEE Std. 519.**

***keywords*— Grid connected PV system, short circuit faults, VSC control, voltage stability, Low Voltage Ride Through (LVRT).**

1. INTRODUCTION

RENEWABLE energy resources have drawn great attention around the world due to the increased energy demand and concerns about climate change and global warming. As a result, a rapid increase in energy generation from renewable energy resources have been observed in the past few decades. Among all renewable resources, photovoltaic (PV) systems dominated other resources due to its advantages of easy installation, simple operation, and low maintenance cost [1][2]. Consistent with the International Renewable Energy Agency (IREA) it is expected that by 2050, 15 % of the whole renewable energy of the world would be from solar PV systems [3][4].

Solar Power generators are mainly characterised based on operation into two categories: grid connected, and standalone systems [5]. Grid Connected Photovoltaic Systems (GCPV) are more common because of their advantages over the standalone systems. With the GCPV, energy is delivered to the grid according to the load demand. Furthermore, in GCPV systems there is no need for energy storage or back up system, which reduce the overall cost. It also increases the system's total efficiency by reducing the power losses caused by the energy storage units [6]. Due to the numerous features of the PV systems, it is expected that they will play a key role in Net-Zero economy[7]. However, to guarantee a stability and reliability as well as secure operation of the system an in-depth analysis on the integration criteria to the utility grid is required [8]-[9]. This is a one of the fundamental factors in the improved design and successful control of GCPV systems to prevent unfavourable consequences including voltage fluctuations, harmonics emission at the Common Coupling Point (CCP) and instability to the grid [10].

Connecting the renewable energy resources with power grid supports the operation of grid in meeting the growing energy demand though the increased ratio of these resources arises the concerns about its stable operation. With the changing scenarios by the addition of these renewable energy resources, power grid operators are continuously focusing and revising the grid codes and standards which can support the system according to new requirements. One of the most frequent conditions in such system is occurrence of grid faults and its impact on connected RE systems. For this condition, Low Voltage Ride Through (LVRT) regulations are devised for monitoring of system's stability under fault conditions [11]. LVRT is a condition during which all Renewable Energy Systems (RESs) must continue operating for a specified period to guarantee that the occurred fault is transient [12]. In other word, LVRT is ability of the RESs to remain in service during a voltage dip caused by a fault [13].

Before RES power plants can be integrated into the power grid, several tests must be conducted to evaluate their compatibility with the grid. These tests typically involve examining voltage and current fluctuations, power quality, LVRT capability, high-voltage ride through (HVRT) capability, reactive power compensation, and safety while operating in anti-islanding mode. These tests aim to assess whether the RES farms can function in compliance with the grid standards [11].

In the past LVRT requirements were mainly applied to wind turbines. This was because occurrence of three-phase fault on a

transmission line could cause a complete loss of voltage at the fault point until the fault is cleared, resulting in a loss of power generation. However, with the increasing development of integrated solar power plants, there is a need to consider LVRT requirements for solar plants as well [12]-[11]. This is because when any disturbances or faults occur, complete interruption of power delivered by the solar farm can be unreliable and may lead to blackouts. Hence, it is recommended to validate LVRT capability before integrating RES with the grid. LVRT capability is generally evaluated for PV systems in the laboratory via LVRT test units [11] . In grid integrated renewable energy resources, LVRT capability is evaluated to keep converter connected with the grid during temporary fault as well as for transient stability and smooth resynchronisation when fault is cleared[14].

Performance of the GCPV systems including Maximum Power-Point Tracking (MPPT) [15]-[16], harmonic emission [17], power quality aspects [18]-[19], islanding detection techniques [17], and new fault detection approach in grid connected PV system [20] an adaptive FRT capability of virtual synchronous machine control for grid forming converter [21] , have been investigated by other researchers. Like most of the other renewable energy systems, in a GCPV system the PV system is integrated to the utility grid using a power electronic converter with optimised control strategy, which controls the dynamic response and stability under various conditions including normal and abnormal operation. Optimised design of the power electronic converters and associated control strategies are crucially important to maintain a reliable implementation of the system, during steady-state and transient fault conditions. With the ever-increased demand of renewable energy systems, power system authorities are more concerned about providing efficient techniques to maintain stability of the grids during abnormal operations [22]. This requires improved control approaches for the power electronic converters.

Due to the operating characteristics of the PV arrays and the controlled operation of the inverter, solar PV systems inject low magnitude fault currents to the grid as compared to the conventional generator [23]. For the GCPV systems, in addition to the contribution of short circuit current by the PV systems, it is crucial to analyse effects of the grid fault on the function of the PV systems. The significantly increased addition of these systems and modifications in the grid codes by regulating authorities have encouraged the researchers to evaluate the impacts of abnormal grid conditions on the various parameters of the PV systems. Moreover, key requirement for successful delivery of power from the PV systems includes various components like power electronic converters, harmonic filters, and power transformers. If the function of these components is affected due to abnormal conditions, it may cause severe disturbances in power delivery. Therefore, it is substantially important to design and evaluate a control system which can work efficiently to minimize the impacts of grid abnormalities and maintain the power system stability during and after abnormal conditions.

Short circuit faults in power systems are caused by several abnormal conditions and depend on the parameters and configurations of the grid, they can inject transient fault currents of very high magnitude as compared to the rated load currents. Fault currents causes electrodynamic disruption and significant thermal losses on power system elements, that can result sever damages [24]-[25]. Short circuit faults are categorized to different types, amongst which line-to-ground (LG) faults are the most frequent, with a probability of 70 to 80 % [26]-[27]. Therefore, it is vital to analyse dynamic behaviour of the system while subjected to these types of faults. Moreover, power system authorities are updating the grid codes and making it compulsory to incorporate ancillary units with GCPVs for their support during these abnormal conditions [28]. The focus on these grid codes and compulsions by authorities have increased the importance of exploring advanced control schemes, depending upon the converter types and grid codes, which can support GCPVs during grid abnormalities. In absence of a proper control scheme, it is recommended to either disconnect the PV system from the utility, or to change the PV arrays operating point on the characteristics curve to reduce the output power during fault conditions [29].

The key objective of this paper is to propose an advanced control system to enhance stability of GCPV systems under normal and abnormal conditions. The proposed scheme was validated on a large-scale GCPV system having installed capacity of 2 MW. Initial parameters were calculated based on the equations and were tuned to meet the generation capacity of the large scale of proposed system. Furthermore, the findings proved that the developed control system is successfully maintained the stability of the system during short circuit fault conditions. This is significant for renewable energy systems and more broadly for modern power systems. An in-depth FFT analysis was initially performed to monitor voltage quality at the CCP under normal operation. The results showed that, with the developed control system, Total Harmonic Distortion (THD) at the CCP is well below the standard level defined in the IEEE Std. 519 [30]. The main contributions of the work are summarized as:

- A Voltage Source Converter (VSC) control system is modified and validated for a large-scale PV system during steady state conditions.
- Ability and performance of the designated control system is validated during short circuit fault. To this end, a L-G fault condition was applied at the grid side and an in-depth analysis was carried out to evaluate the control scheme.
- A comprehensive analysis of the LVRT was undertaken to prove the capability of the modified VSC control strategy for voltage stability of the same system during fault conditions.

In this study and associated analysis, L-G fault is considered predominantly in line with the UK regulations and LVRT grid code.

2. SYSTEM DESCRIPTION

A three phase two stages GCPV system was designed using the Simscape Electrical toolbox of MATLAB/SIMULINK;

Appendix

Fig 1 exhibits a schematic diagram of the simulated system. This system composes of a PV array, DC-DC boost converter, control part for MPPT, inverter with VSC control, LC filter and step-up power transformer.

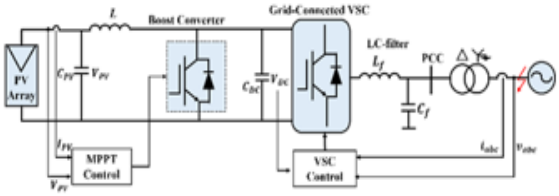

Fig. 1. Schematic of a GCPV system

The PV generator consists of five parallel units, with rated power of 400 kW each and 2 MW in total. Each PV array comprises of 255 shunt strings and 5 modules coupled in every string. The PV module employed in the presented system is SunPower SPR-315E-WHT-D including a highest power rating of 315 W per module. Applied constraints of the PV module are displayed in Table I.

Table I Parameters of the PV module

SunPower SPR-315E -WHT-D		
Parameter	**Value**	**Unite**
Maximum Power	315	W
Cells per module	96	-
Open Circuit Voltage	65	V
Short circuit current	6	A
Voltage at maximum power point	55	V
Current at maximum power point	6	A
Temperature coefficient of V_{oc}	-0.2727	°C
Temperature coefficient of I_{sc}	0.0617	°C
Diode ideality factor	0.9507	-
Series Resistance	0.4304	Ω
Shunt Resistance	430	Ω

A single solar cell is the fundamental element for solar PV generator scheme. An assembly of PV cells mounted on a framework forms a solar panel, also known as PV module. A combination of the PV modules connected in series and shunt arrangement constructs a complete PV array. Fig 2 shows a basic circuit diagram of a solar cell circuit [17].

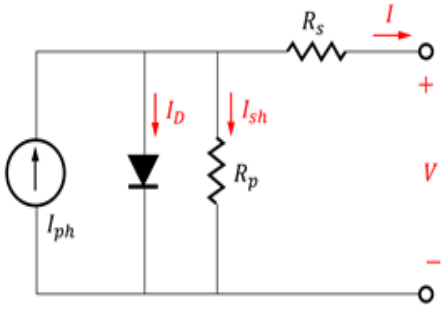

Fig. 2. Single diode structure of the PV cell

From the circuit diagram of Fig 2, current supplied by each PV cell is given as:

$$I = I_{ph} - I_D - I_{sh} \quad (1)$$

where, I gives the current produced using a solar cell, I_{ph} gives the photon current, I_D indicates the value of diode current and I_{SH} represents current magnitude passing in the parallel resistor R_P, while R_S is the series resistance of a PV cell [31]. Total current supplied by a PV array is defined by [32]-[33]:

$$I = N_P I_{ph} - N_P I_O \left[exp\left(\frac{\frac{V+I R_S}{N_S}}{a N V_{th}} \right) - 1 \right] - \left(\frac{V+I R_S}{R_P} \right) \quad (2)$$

where N_S and N_P are number of solar cells arranged in series and parallel configuration in each PV array, I_O gives the value of reverse saturation current, a indicates the diode ideality factor while V_{th} represents the thermal voltage. These constraints are controlled by the solar irradiance value, cell temperature, and reference values. The reference values for PV modules are usually given by the manufacturers at a standard test condition having irradiance level of 1000 W/m^2 and temperature value of 25 °C [34]. The I-V and P-V characteristics of the PV array implemented in this work for different levels of solar irradiance and temperature values are exhibited in Figs 3-a and 3-b, respectively.

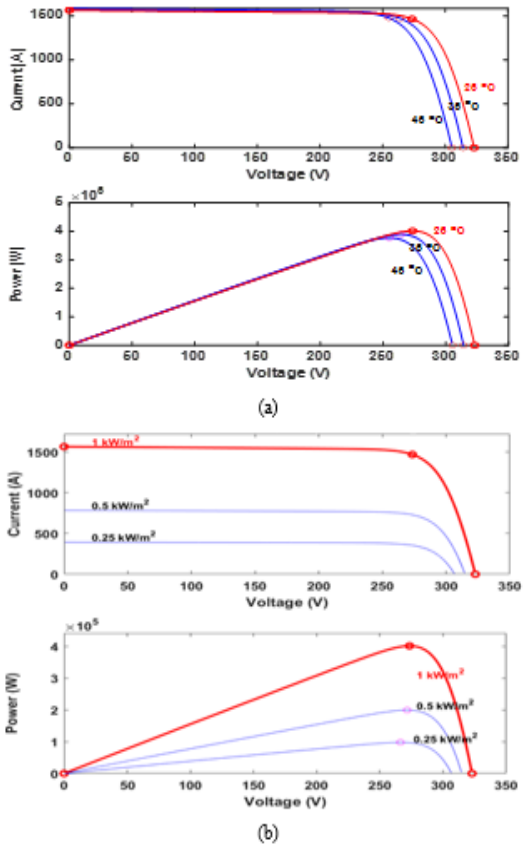

Fig. 3. The I-V and P-V characteristic of the PV array (a) at varying temperature (b) at varying irradiance

Second part of the system is the DC-DC boost converter which is implemented to boost the voltage magnitude supplied by the PV array. A DC-DC boost converter is responsible to

boost the DC voltage level produced by the PV array, V_{PV}, as well as to create a channel to apply the MPPT technique which improve the voltage quality and controllability of the system [35]-[36]. For the presented system, the average model of boost converter was used in which supply voltage was precisely controlled according to the reference voltage for developing the function of the converter. An equivalent circuit of the boost converter is illustrated in Fig 4 [37].

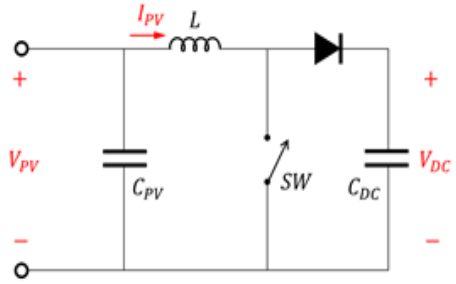

Fig. 4. The average model of boost converter

The generated signal of the boost converter is controlled by the MPPT unit which regulates the duty cycle for the converter [38]. The following equation is applied to obtain the duty cycle for boost converter:

$$D = 1 - \frac{V_{PV}}{V_{DC}} \tag{3}$$

Inductance and capacitance for the boost converter design are specified as [5]:

$$L = \frac{V_{DC} \times D(1-D)}{\Delta I_{DC} \times f} \tag{4}$$

$$C_{DC} = \frac{V_{PV} \times D(1-D)}{8Lf^2 \Delta V_c} \tag{5}$$

where V_{DC} is voltage at the terminal of the DC-DC boost converter and I_{DC} indicates the value of the current supplied to the inverter. V_{DC} is determined with reference to the input voltage V_{PV} and the duty cycle of the converter. The parameters used for this boost converter are demonstrated in table II which are calculated applying equations (4) to (5).

Table II Parameters of the boost converter

Parameter	Symbol	Value
Input Voltage	V_{PV}	273 V
Output Voltage	V_{DC}	500 V
Inductor	L	5 mH
Input Capacitor	C_{PV}	100 µF
Output Capacitor	C_{DC}	2 F

Output of the DC-DC converter is delivered to the inverter which transforms the DC voltage to a Pulse Width Modulation (PWM) voltage signal. The obtained signal at the output of the inverter is then filtered via harmonic filter for suppression of higher frequency components and to get THD of the current and voltage below 5 % standard level as stated by the IEEE std.519 [30]-[39].

3. CONTROL SYSTEM STRATEGY

A schematic diagram of the established control scheme is explained in Fig 5. This control unite comprises of two main parts: DC controller based on MPPT algorithm, and VSC control scheme for the inverter. These two parts are described in the succeeding subsections.

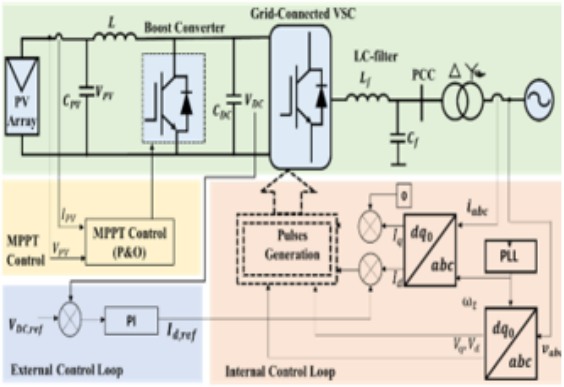

Fig. 5. Block diagram of the control system of the GCPVS

3.1 MPPT control scheme:

The control system on the DC side is designed for maximum power extraction and to increase the voltage level of the PV array. A Perturb and Observe (P&O) algorithm based MPPT scheme was used for MPPT operation. Considering the output voltage and current signals of the PV array, the P&O algorithm determines the duty cycle of the DC-DC converter. A flowchart of the P&O algorithm is shown in Fig. 6.

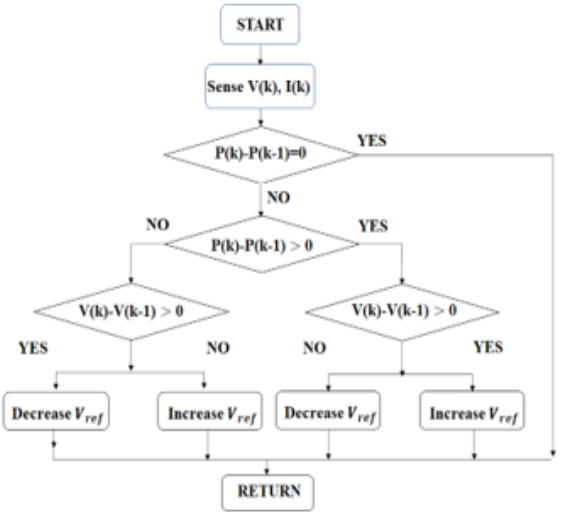

Fig. 6. Flowchart for P&O MPPT technique

This algorithm determines the duty cycle of the DC-DC boost converter based on the input parameters, i.e., voltage and current from the PV array. Output voltage of the boost converter is regulated according to the reference values. The MPPT technique and associated algorithm are implemented to get the maximum power delivered by the PV array and output power of the system is maintained with reference to the voltage

variation [15]. In this control scheme, voltage is perturbed according to the response of the system to the previous perturb to decide the direction of the following perturbation [40]. PV characteristic curve and principle of the P&O based MPPT technique are demonstrated in Fig 7 and Table III, respectively.

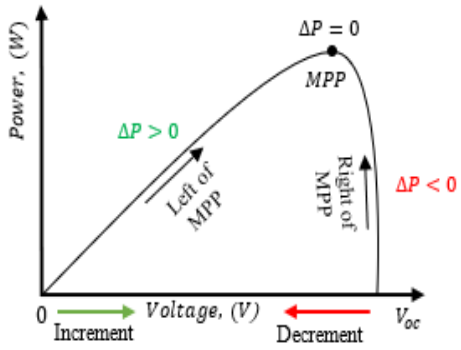

Fig. 7. PV characteristics of P&O MPPT technique

For $\Delta P > 0$, power is increased with increasing the voltage until MPP is achieved. After attaining MPP, where $\Delta P < 0$, any attempt to increase the voltage results in decreasing the power. Accordingly, if increasing or decreasing the voltage led to an increase in the power output, the successive perturbation continues the same direction until MPP is achieved. On the other hand, if power decreases with the increase or decrease in voltage, the following perturbation will be reversed, as shown in Table III. After reaching the MPP, the system will be continuously oscillating around this point. Level of the fluctuations across the MPP alters with reference to the step size of the supplied voltage. However, to decrease these fluctuations, reduced step-size can be applied, which may slow down the MPPT process to reach the MPP [40].

Table III Principle of the P&O algorithm

Perturbation	Change in Power	Next perturbation
Positive	Positive	Positive
Positive	Negative	Negative
Negative	Positive	Negative
Negative	Negative	Positive

3.2 Control scheme of the Voltage Source Converter:

A block diagram of the designed control system of the VSC is presented in Fig 8. In this control system, the VSC-based control scheme is synchronized to the CCP using phase locked loop (PLL) unit which generate a reference angle ω_t [41]. The error signal e_{Vdc} between the DC link voltage, generated by comparing V_{dc} and its corresponding reference value $V_{dc,ref}$, is fed to the compensator whose output u_{Vdc} is processed by a limiter to generate reference current value $I_{d,ref}$.

For this system the transfer function of the control unit was determined using Z transformation, so the output U_{Vdc} can be presented mathematically as [28]:

$$U_{Vdc}(z) = E_{Vdc}(z)[K_{p,dc}(z) + K_{i,dc}(z)\left(\frac{T_s}{2}\frac{z+1}{z-1}\right)] \quad (6)$$

where:

$$e_{Vdc} = V_{DC} - V_{DCref}\ ,\ U_{Vdc}(z) = Z(u_{Vdc}) \quad (7)$$

and

$$E_{Vdc}(Z) = Z(e_{Vdc}) \quad (8)$$

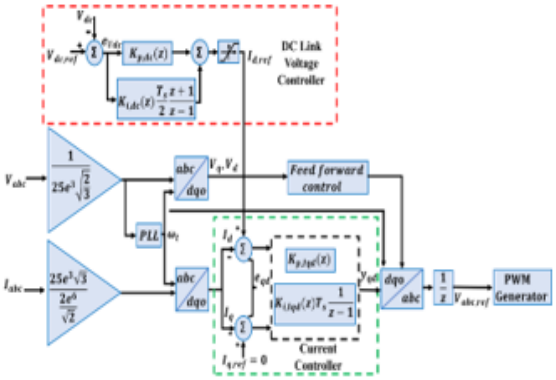

Fig. 8. Block diagram of VSC control strategy.

The reference signal $I_{d,ref}$ is then delivered to the current controller block. Three phase grid voltage V_{abc} and current I_{abc} are attained from the grid and converted to per unit values. After conversion, these signals are converted to $dq0$ reference, which is presented as (V_d, V_q) and (I_d, I_q) for the voltage and current, respectively. Voltage components V_d and V_q are then processed for feed forward control, which play a crucial function in improving the stability of the PV system by offsetting the nonlinear characteristics of the PV arrays. The d-q parts of the current, I_d and I_q, are then processed through the PI controller. For this purpose, the signals are compared with reference values, $I_{d,ref}$ and $I_{q,ref}$. These I_d and I_q components are decoupled for decoupled control of the active and reactive power respectively. The presented system was operated at unity power factor, so $I_{q,ref}$ is set to zero [42]-[43]. Reference current $I_{d,ref}$ is gained from the external control loop based on the values of V_{dc} and $V_{dc,ref}$ and is compared with the d-component of the grid currents, I_d. Current reference value obtained from DC control block $I_{d,ref}$ was used to track the signal I_d and to produce error signal e_{qd}. The gained error signal is processed by the respective controller to provide the output signal y_{qd} of the current controller which can be given as:

$$Y_{qd}(z) = E_{qd}(z)[K_{p,Iqd}(z) + K_{i,Iqd}(z)\left(T_s\frac{1}{z-1}\right)] \quad (9)$$

where:

$$Y_{qd}(z) = Z(y_{qd}) \text{ and } E_{qd}(z) = Z(e_{qd}) \quad (10)$$

The output y_{qd} represents the signal to generate reference voltage $V_{abc,ref}$ which is delivered to the PWM generator to generate pulses signals for the inverter operation.

4. RESULTS AND DISCUSSION

Dynamic performance of the GCPV solar system was

evaluated under two different conditions: steady state operation, and L-G short circuit fault condition. Results of each study is presented and discussed in the following subsections.

4.1 Steady state operation

In this stage the system was operated at Standard Test Conditions (STC) with solar irradiance level of 1000 W/m^2 and ambient temperature value of 25°C. The power generated by a single PV array and five PV arrays assembled in parallel, are shown in Figs 9-a and 9-b, respectively. The results show that the system operates at its full capacity and delivers maximum power, which verify that the controller of the DC-DC boost converter works effectively to track the MPP of the PV system. It is important to highlight that the P&O algorithm has been implemented for MPPT control to confirm that maximum power is delivered from the system by maintaining the optimized points of the PV characteristics curve of the PV arrays.

In the second stage of this study, voltage at the DC busbar was monitored, the result is presented in Fig 10. The DC-DC boost converter with the designated control strategy of the MPPT algorithm, successfully boost the DC voltage produced by the PV arrays from 273.5 V to 500 V. Fig 10 clearly shows that voltage at the DC busbar follows the reference voltage that has been set by the DC voltage regulator of the inverter. Furthermore, the oscillation of the DC voltage across the reference value is less than $\pm$ 0.5 V, this means the DC voltage supplied to the PWM inverter is effectively regulated. This will ensure a stable AC voltage at the inverter terminal as well as the enhanced stability of the whole system.

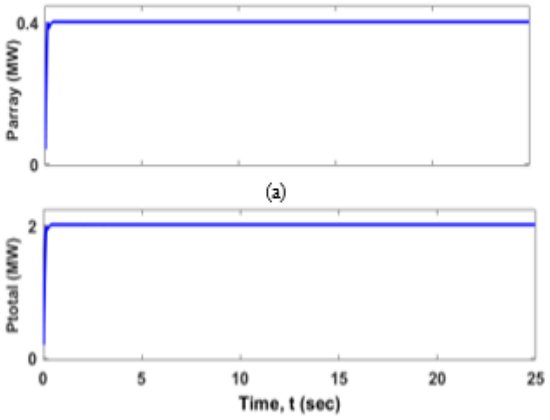

Fig. 9. Output power of the PV system
(a) single array (b) five arrays in parallel

A 3-level PWM inverter with a nominal frequency of 50 Hz, synchronized with the grid power frequency was employed. The designated control scheme monitors and controls the switching function of the inverter using phase angle and frequency of the grid voltage as reference values. Three phase voltages at the inverter terminal are illustrated in Fig. 11.

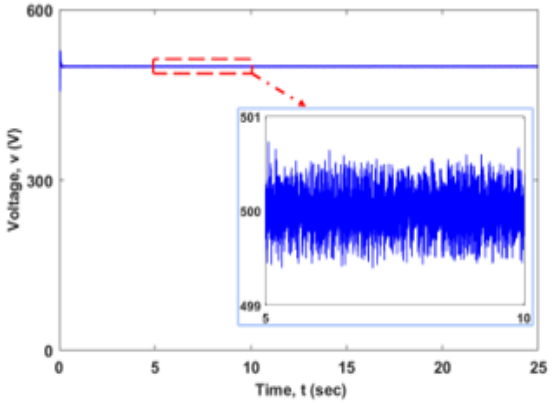

Fig. 10. DC Voltage at the DC link bus bar.

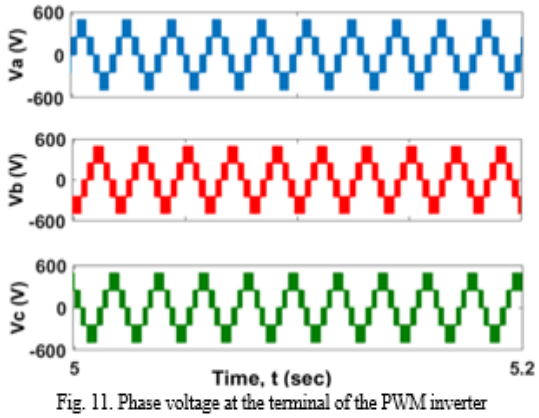

Fig. 11. Phase voltage at the terminal of the PWM inverter

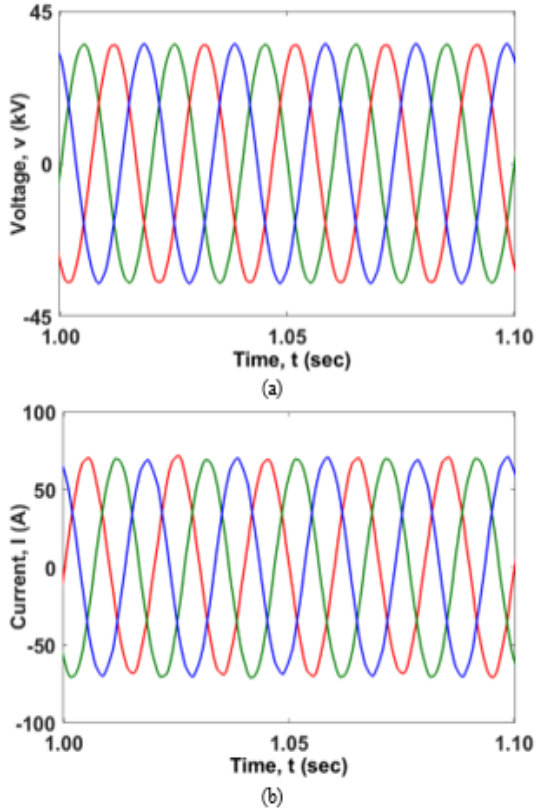

Fig. 12 Instantaneous wave shapes of three phase
(a) voltages and (b) currents at CCP

Appendix

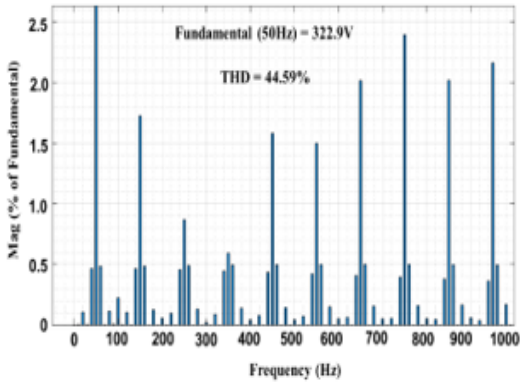

(a)

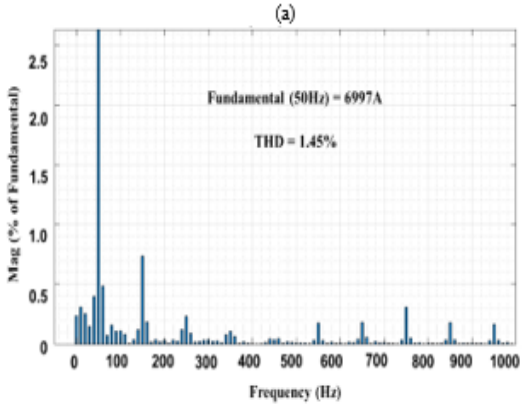

(b)

Fig. 13 Frequency spectrum and THD level of
(a) voltage and (b) current at the inverter terminal

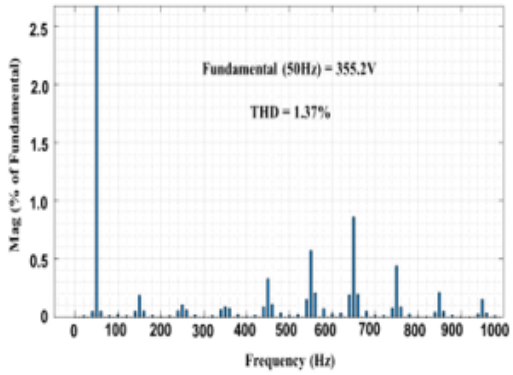

(a)

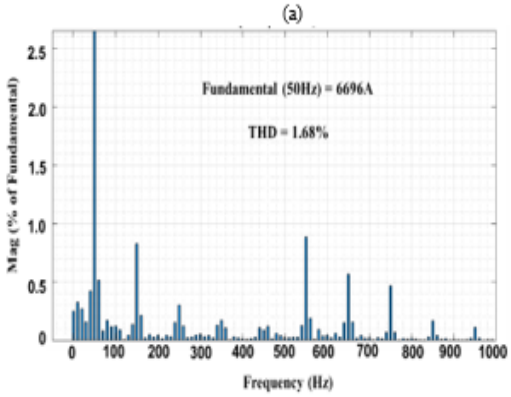

(b)

Fig. 14 Frequency spectrum and THD values of
(a) voltage and (b) current at CCP

In the last stage of the GCPV system and before integrating at the grid side, a LC filter was implemented to filter the high- frequency harmonics generated by the PWM inverter. To this end, parameters of the LC filter were determined to bring the THD level well below 5 %, which comply with the IEEE Std. 519 [39]. Three phase voltage and current signals at the CCP are represented in Fig 12-a and 12-b, respectively. A FFT analysis was performed to examine the THD values for the voltage and the current signals at different points across the system.

Frequency spectrum and THD level for the current and voltage at the inverter terminal and CCP are presented in Figs 13 and 14, respectively. It can be noted from Fig 13 THD of the voltage at the inverter terminal, before the LC filter, is 44.59 %. THD values of the current and voltage signals at the CCP were recorded1.68 % and 1.37 %, respectively; which is well below the acceptable level as stated in the IEEE Std. 519 [39].

This explicitly highlights the effective operation of the LC filter to reduce the THD values of the voltage at the CCP. Finally, the PV system was integrated with the gride using a step-up power transformer.

4.2 Short circuit faults analysis:

As the key objective of this work, dynamic behaviour of the system under transient fault condition was studied. For this purpose, a L-G short circuit fault, as the most frequent fault in practical power systems, was considered. This fault was introduced to the secondary side of the step-up transformer at $t = 2\ sec$ for a duration of $1\ sec$. The produced power by the PV arrays during the transient fault condition was initially monitored, the results are shown in Fig 15.

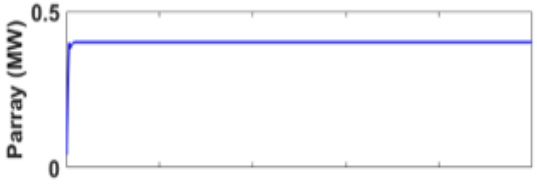

(a)

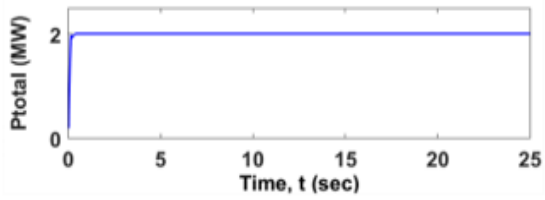

(b)

Fig. 15 Output power of the PV system with a L-G fault in place
(a) single array (b) five arrays in parallel

Fig 15 exhibits that the delivered power at the output side of the PV array is not affected by this short circuit fault. This

explicitly verifies the efficiency of the designed control approach to maintain the nominal power delivered by the system as the same operating point during normal operation. This implies that, with the designated control strategy in place, this kind of fault has negligible impact on the voltage and current output generated by the PV arrays, and therefore on the DC side of the system. This evidently shows that the designated control system successfully protects the PV system from the undesirable impacts of short circuit faults. This is an essential criterion for maintaining the normal function of the PV system during L-G fault conditions.

Voltage at the DC busbar was then monitored, the result is exhibited in Fig 16. As can be seen the concerned fault at the grid side makes a minor impact on the DC link voltage. From this outcome, the magnitude of the oscillations increased instantly at $t = 2\ sec$, when the fault is applied, but overshoot of the voltage is limited to about $\pm 5\ V$. However, the system regained its stability within a very short time of as low as $0.2\ sec$, after the fault is cleared. At $t = 3\ sec$, when the fault is cleared, the DC voltage fluctuations increased for a short period, and restored to its normal operation within $0.15\ sec$.

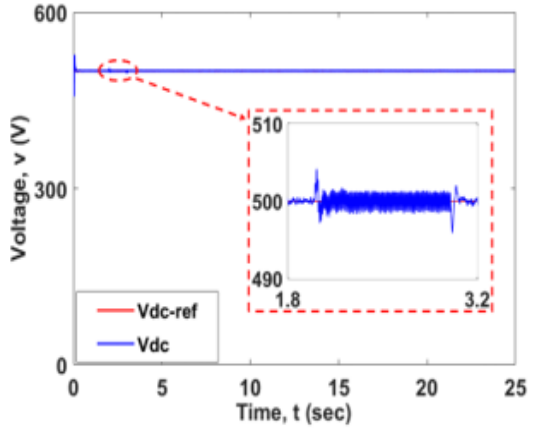

Fig. 16. DC link Voltage under L-G fault.

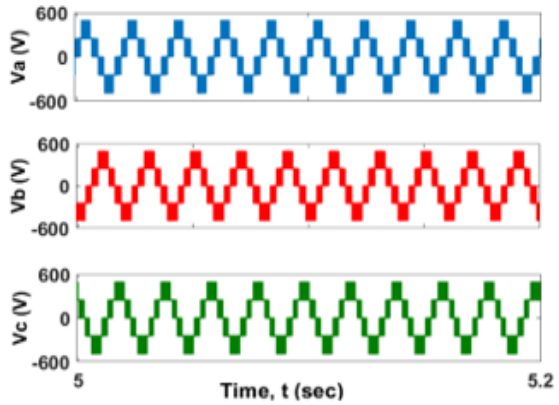

Fig. 17. Three phase voltage at inverter terminal with a L-G fault in place

These findings show the capability of the designed control system for maintaining the voltage stability at the DC busbar. However, when it comes to the AC side of the system, the L-G fault impacts on the voltage and current are higher than that on the DC side. The instantaneous waveforms of the three-phase voltage at the inverter terminal are shown in Figs 17.

Impact of the concerned fault on the instantaneous waveforms and rms ratings of three-phase current and voltage signals at the CCP are illustrated in Figs 18 to 21, respectively. The results show that, impact of the applied fault on voltage and current at the CCP is more severe, which comply with the theory of transient fault conditions in the conventional power systems [44]. However, with the designated control system in place, currents and voltage in all three phases returned to the normal value in a settling time of as low as $0.15\ sec$.

In the presented VSC based control strategy, a control system is designed in accordance with the feedback from the grid side parameters as shown in Fig 8, due to the required synchronization of both systems. So, as a fault arises at the grid side, it has immediate impact on the GCPV system parameters and disrupts its normal operation.

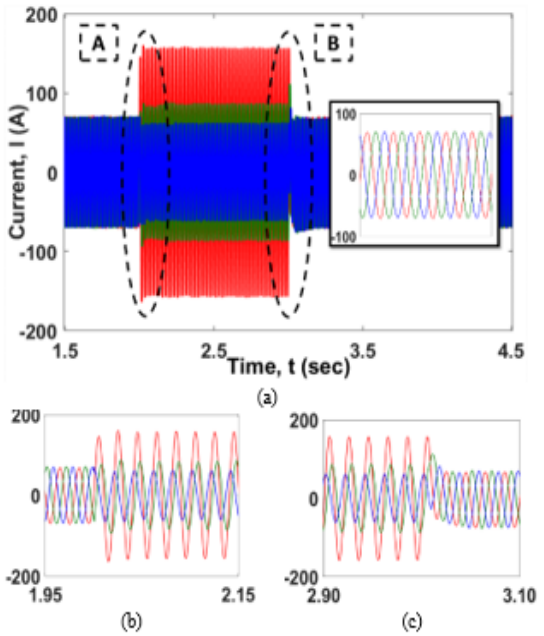

Fig. 18. Instantaneous waveforms of three phase currents at CCP under L-G fault (a) complete waveforms (b) transient currents after applying the fault and (b) transient currents when the fault is cleared

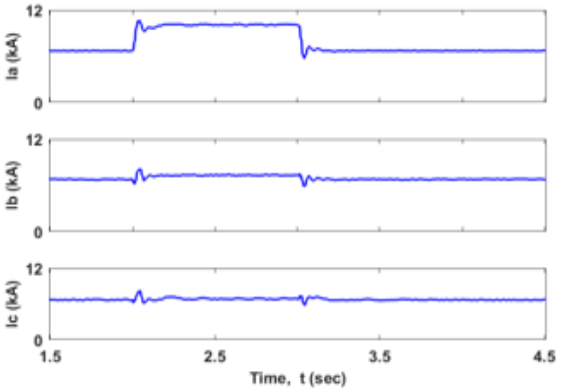

Fig. 19 Three phase rms currents at CCP under L-G fault

Based on the grid codes requirements, the GCPV system waits for a particular period whether fault to be cleared; if so, system parameters regain the normal operation based on the feedback signals from the gird. In contrast, if the faults are prolonged,

system is disconnected to prevent severe damages. The voltage and current signals at the grid side clearly show that the fault condition is immediately reflected in the parameters of the GCPV system and caused the voltage sag and increased current at the same instant when the fault occurred. On the other hand, the negligible impact of the applied fault on the DC part of the system can be attributed to the position of the fault and the role played by different impedance levels for various components of the system, including transmission lines, transformers, and harmonic filters. These components help in mitigating the impacts of the applied faults. From this analysis it is evident that getting feedback from the grid side supports the overall function of the GCPV system as it is important to monitor the grid conditions while the PV system is in operation and has great impact on the grid parameters

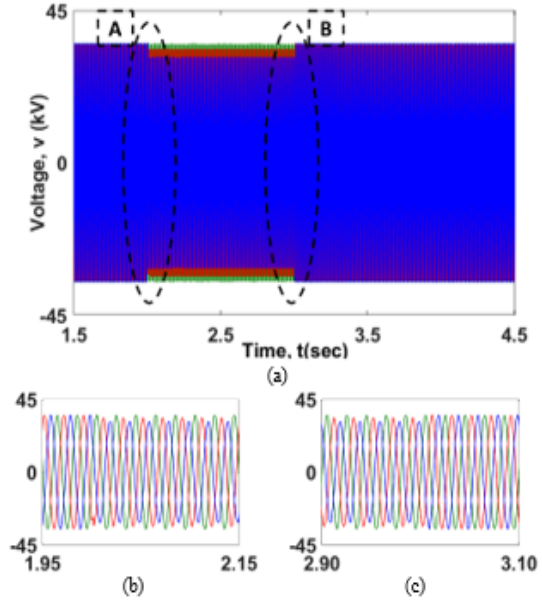

Fig. 20 Instantaneous waveforms of three phase voltages at CCP under L-G fault (a) complete waveforms (b) transient voltages after applying the fault and (b) transient voltages when the fault is cleared

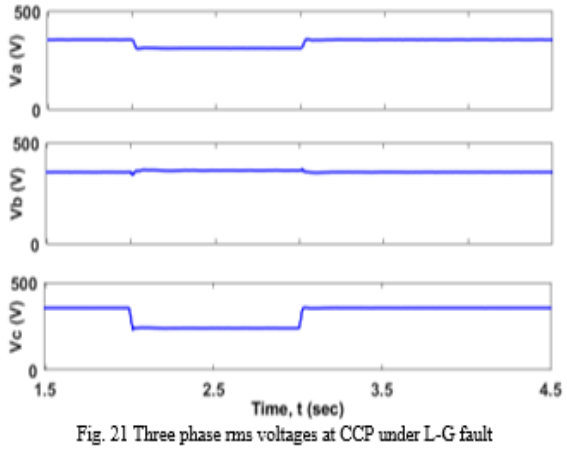

Fig. 21 Three phase rms voltages at CCP under L-G fault

4.3 LVRT Capability Analysis:

Short circuit faults impose voltage dip, and the grid requirements to maintain connected during the fault period is defined by means of LVRT [9]-[10]. In this work, the LVRT capability of the modelled GCPV system has been analysed in line with the UK grid code. Considering the rapid development of grid connected RESs, LVRT becomes a mandatory requirement and have been broadly adopted in the grid codes of modern power systems. This concept is shown graphically in Fig 22. In this graph, V_n indicates nominal voltage, V_F shows voltage during the period of fault, V_{AF} represents voltage after fault, and T_F and T_r denote the period at which voltage dipped because of fault and recovery time, respectively. According to the LVRT requirement, the GCPV system tolerates voltage sags to a specific ratio of the rated voltage for a certain period, as shown in Fig 22 [45].

In Fig 22, area Ⓐ indicates the normal operation of the GCPV system at the CCP. If the voltage magnitude at CCP falls in area Ⓑ, GCPV remains connected for a certain time (T_0 to T_F), and it should also have ability to regain nominal voltage magnitude at a certain rate. In area Ⓒ, GCPV system is allowed to be disconnected. Rate of change of the voltage varies depending upon the grid regulations for different countries. L-G faults, as the most frequent type of fault in the power system, cause severe voltage sags. Therefore, it is crucial to analyse the LVRT capability of GCPV systems for the optimized setting and coordination of protection equipment.

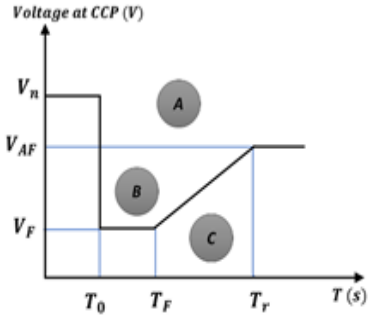

Fig. 22 General curve limits of LVRT

To analyse the LVRT capability of the modelled system, a L-G fault was applied at the CCP for a duration of 140 ms, which is recommended duration for this test [11]. Voltage profile was then monitored and analysed to assess the LVRT capability of the simulated system, the results in comparison with the UK standard is shown in Fig 23.

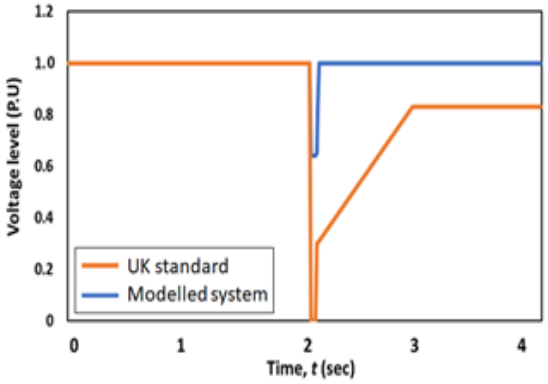

Fig. 23 Comparison of LVRT of the modelled system and UK requirement

Appendix

It can be observed that during the time of fault, voltage at the CCP drops to 0.7 p.u. instantly and maintains the same value until fault is cleared after 140 ms. It is important to highlight that according to the UK standard [11], nominal voltage can drop to zero but for the modelled system, voltage value was maintained at a higher magnitude. After 140 ms of fault duration, voltage returned to its pre fault value, which is at a higher rate within 20 ms, for the modelled system, as compared to the minimum standard rate of the UK requirement.

5. CONCLUSIONS

In this paper a dynamic model was developed for a grid connected solar PV system having power production capacity of 2 MW. Dynamic function of the designed system was studied under steady state and transient fault conditions. Two control systems, one for controlling the function of DC-DC boost converter, and the other one to control the VSC were designed and implemented. The key function of the DC-DC controller is to achieve MPP, while the VSC controller is to maintain voltage quality at the CCP, and stability of the system during short circuit faults. The results showed that, the designated control systems can effectively provide clean voltage at the CCP with a THD of 1.39 %, which is well below the threshold level of the IEEE Std. 519.

As a key objective of this work, dynamic performance of the system subjected to a L-G fault at the CCP was evaluated, as well as LVRT analysis was also considered. The results showed that, with the designated control schemes in place, performance of the PV side including voltage at the DC busbar and MPPT were not affected by the concerned short circuit fault. More importantly, the system is capable to regains its stability when the fault is disappeared having a settling time of less than 0.2 sec.

ACKNOWLEDGMENTS

This paper is based on PhD research projects which are funded by Libyan government for author[1] and by Commonwealth Scholarship commission and the foreign, Commonwealth and development office in the UK for author[2]. We are grateful for their support. All views here are those of the authors[1,2]not the funding bodies.

CONFLICT OF INTEREST STATEMENT

The authors declare no conflict of interest.

DATA AVAILABILITY STATEMENT

The data that support the findings of this study are available from the corresponding author upon reasonable request.

REFERENCES

[1] M. A. Eltawil and Z. Zhao, "Grid-connected photovoltaic power systems: Technical and potential problems-A review," *Renew. Sustain. Energy Rev.*, vol. 14, no. 1, pp. 112–129, 2010, doi: 10.1016/j.rser.2009.07.015.

[2] L. A *et al.*, "Smart energy monitoring and power quality performance based evaluation of 100-kW grid tied PV system," *Heliyon*, vol. 9, no. 6, p. e17274, 2023, doi: 10.1016/j.heliyon.2023.e17274.

[3] G. Rajgor, "Greater acceleration of renewables required to meet COP21 goal," *Renew. Energy Focus*, vol. 17, no. 5, pp. 175–177, 2016, doi: 10.1016/j.ref.2016.08.007.

[4] T. Ruan, M. Topel, W. Wang, and B. Laumert, "Potential of grid-connected decentralized rooftop PV systems in Sweden," *Heliyon*, vol. 9, no. 6, p. e16871, 2023, doi: 10.1016/j.heliyon.2023.e16871.

[5] S. Sumathi, L. Ashok Kumar, and P. Surekha, *Solar PV and Wind Energy Conversion Systems*. 2015.

[6] N. A. Mehedi Fahad, Mohammed Ali, Nahar Islam, "A New Approach to Design of an optimized Grid Tied Smart Solar," vol. 1, pp. 3–7, 2012.

[7] D. B. Aeggegn, T. F. Agajie, Y. G. Workie, B. Khan, and A. Fopah-Lele, "Feasibility and techno-economic analysis of PV-battery priority grid tie system with diesel resilience: A case study," *Heliyon*, vol. 9, no. 9, p. e19387, 2023, doi: 10.1016/j.heliyon.2023.e19387.

[8] A. K. Shukla, K. Sudhakar, and P. Baredar, "Simulation and performance analysis of 110 kWp grid-connected photovoltaic system for residential building in India: A comparative analysis of various PV technology," *Energy Reports*, vol. 2, pp. 82–88, 2016, doi: 10.1016/j.egyr.2016.04.001.

[9] R. T. Juarez, C. R. Fuerte-Esquivel, E. Espinosa-Juarez, and U. Sandoval, "Steady-State Model of Grid-Connected Photovoltaic Generation for Power Flow Analysis," *IEEE Trans. Power Syst.*, vol. 33, no. 5, pp. 5727–5737, 2018, doi: 10.1109/TPWRS.2018.2817585.

[10] A. Chidurala, T. K. Saha, and N. Mithulananthan, "Harmonic impact of high penetration photovoltaic system on unbalanced distribution networks - Learning from an urban photovoltaic network," *IET Renew. Power Gener.*, vol. 10, no. 4, pp. 485–494, 2016, doi: 10.1049/iet-rpg.2015.0188.

[11] M. Yadav, N. Pal, and D. K. Saini, "Low voltage ride through capability for resilient electrical distribution system integrated with renewable energy resources," *Energy Reports*, vol. 9, pp. 833–858, 2023, doi: 10.1016/j.egyr.2022.12.023.

[12] I. Yahyaoui, *Advances in renewable energies and power technologies: solar and wind energies*. Elsevier, 2018.

[13] J. Mohammadi, S. Afsharnia, and S. Vaez-Zadeh, "Efficient fault-ride-through control strategy of DFIG-based wind turbines during the grid faults," *Energy Convers. Manag.*, vol. 78, pp. 88–95, 2014, doi: 10.1016/j.enconman.2013.10.029.

[14] T. Qoria, X. Wang, and R. Kadri, "Grid-forming control VSC-based including current limitation and re-synchronization functions to deal with symmetrical and asymmetrical faults," *Electr. Power Syst. Res.*, vol. 223, no. December 2022, p. 109647, 2023, doi: 10.1016/j.epsr.2023.109647.

[15] A. I. M. Ali, M. A. Sayed, and E. E. M. Mohamed, "Modified efficient perturb and observe maximum power point tracking technique for grid-tied PV system," *Int. J. Electr. Power Energy Syst.*, vol. 99, no. February, pp. 192–202, 2018, doi: 10.1016/j.ijepes.2017.12.029.

[16] L. P. Sampaio, M. V. Da Rocha, S. A. O. Da Silva, and M. H. T. De Freitas, "Comparative analysis of MPPT algorithms bio-inspired by grey wolves employing a feedforward control loop in a three-phase gridconnected photovoltaic system," *IET Renew. Power Gener.*, vol. 13, no. 8, pp. 1379–1390, 2019, doi: 10.1049/iet-rpg.2018.5941.

[17] A. K. Verma and B. Singh, "Harmonics and Reactive Current Detection of a Grid-Interfaced PV Generation in a Distribution System," *IEEE Trans. Ind. Appl.*, vol. 54, no. 5, pp. 4786–4794, 2018, doi: 10.1109/TIA.2018.2830752.

[18] L. B. G. Campanhol, S. A. O. Da Silva, A. A. De Oliveira, and V. D. Bacon, "Power flow and stability analyses of a multifunctional distributed generation system integrating a photovoltaic system with unified power quality conditioner," *IEEE Trans. Power Electron.*, vol. 34, no. 7, pp. 6241–6256, 2019, doi: 10.1109/TPEL.2018.2873503.

[19] A. Khaliq, H. Zahloul, and H. Hamzehbahmani, "A control approach for power quality improvement of a large-scale grid connected PV system at standard test conditions," vol. 1, pp. 241–245, 2022, doi: 10.1049/icp.2022.1836.

[20] S. Silvestre, M. A. Da Silva, A. Chouder, D. Guasch, and E. Karatepe, "New procedure for fault detection in grid connected PV systems based on the evaluation of current and voltage indicators," *Energy Convers. Manag.*, vol. 86, pp. 241–249, 2014, doi: 10.1016/j.enconman.2014.05.008.

[21] T. Lin, M. Das, A. Gole, and A. Isaacs, "Adaptive fault ride through control of VSM Grid-forming converters ☆," *Electr. Power Syst.*

Appendix

Res., vol. 223, no. December 2022, p. 109606, 2023, doi: 10.1016/j.epsr.2023.109606.

[22] O. Goksu, R. Teodorescu, B. Bak-Jensen, F. Iov, and P. C. Kjar, "An iterative approach for symmetrical and asymmetrical Short-circuit calculations with converter-based connected renewable energy sources. Application to wind power," *IEEE Power Energy Soc. Gen. Meet.*, pp. 1–8, 2012, doi: 10.1109/PESGM.2012.6344906.

[23] R. K. Varma, S. A. Rahman, V. Atodaria, S. Mohan, and T. Vanderheide, "Technique for Fast Detection of Short Circuit Current in PV Distributed Generator," *IEEE Power Energy Technol. Syst. J.*, vol. 3, no. 4, pp. 155–165, 2016, doi: 10.1109/jpets.2016.2592465.

[24] J. C. Das, *Power system*. 2002.

[25] B. Vahidi, S. A. Agheli, and S. Jazebi, "Teaching short-circuit withstand test on power transformers to M.Sc. students and junior engineers using MATLAB-SIMULINK," *Comput. Appl. Eng. Educ.*, vol. 20, no. 3, pp. 484–492, 2012, doi: 10.1002/cae.20416.

[26] H. Zahloul, H. Hamzehbahmani, A. Khaliq, and S. Veremieiev, "An Approach to Dynamic Behaviour of a Grid Connected PV System during Symmetrical Short Circuit Fault," *2022 13th Int. Renew. Energy Congr. IREC 2022*, no. Irec, 2022, doi: 10.1109/IREC56325.2022.10002093.

[27] D. S. Pillai, J. P. Ram, N. Rajasekar, A. Mahmud, Y. Yang, and F. Blaabjerg, "Extended analysis on Line-Line and Line-Ground faults in PV arrays and a compatibility study on latest NEC protection standards," *Energy Convers. Manag.*, vol. 196, no. April, pp. 988–1001, 2019, doi: 10.1016/j.enconman.2019.06.042.

[28] M. Graungaard Taul, X. Wang, P. Davari, and F. Blaabjerg, "Current Reference Generation Based on Next-Generation Grid Code Requirements of Grid-Tied Converters during Asymmetrical Faults," *IEEE J. Emerg. Sel. Top. Power Electron.*, vol. 8, no. 4, pp. 3784–3797, 2020, doi: 10.1109/JESTPE.2019.2931726.

[29] M. Mirhosseini, J. Pou, and V. G. Agelidis, "Single- and Two-Stage Inverter-Based Grid-Connected Photovoltaic Power Plants With Ride-Through Capability Under Grid Faults," *IEEE Trans. Sustain. Energy*, vol. 6, no. 3, pp. 1150–1159, 2015, doi: 10.1109/TSTE.2014.2347044.

[30] IEEE Std 519, "IEEE Recommended Practice and Requirements for Harmonic Control in Electric Power Systems Sponsored by the Transmission and Distribution Committee IEEE Power and Energy Society," *IEEE Stand.*, vol. 2014, pp. 1–29, 2014.

[31] A. M. Humada, A. M. Aaref, H. M. Hamada, and M. Herwan, "Modeling and characterization of a grid-connected photovoltaic system under tropical climate conditions," *Renew. Sustain. Energy Rev.*, vol. 82, no. July 2015, pp. 2094–2105, 2018, doi: 10.1016/j.rser.2017.08.053.

[32] A. M. Humada, A. M. Aaref, H. M. Hamada, M. H. Sulaiman, N. Amin, and S. Mekhilef, "Modeling and characterization of a grid-connected photovoltaic system under tropical climate conditions," *Renew. Sustain. Energy Rev.*, vol. 82, no. July 2015, pp. 2094–2105, 2018, doi: 10.1016/j.rser.2017.08.053.

[33] H. A. Kazem, M. T. Chaichan, A. H. A. Al-Waeli, and K. Sopian, "A novel model and experimental validation of dust impact on grid-connected photovoltaic system performance in Northern Oman," *Sol. Energy*, vol. 206, no. May, pp. 564–578, 2020, doi: 10.1016/j.solener.2020.06.043.

[34] J. Atiq and P. K. Soori, "Modelling of a grid connected solar PV system using MATLAB/simulink," *Int. J. Simul. Syst. Sci. Technol.*, vol. 17, no. 41, pp. 45.1-45.7, 2017, doi: 10.5013/IJSSST.a.17.41.45.

[35] T. Suntio and T. Messo, "Power electronics in renewable energy systems," *Energies*, vol. 12, no. 10, 2019, doi: 10.3390/en12101852.

[36] M. H. De Freitas Takami, S. A. Oliveira Da Silva, and L. P. Sampaio, "Dynamic performance comparison involving grid-connected PV systems operating with active power-line conditioning and subjected to sudden solar irradiation changes," *IET Renew. Power Gener.*, vol. 13, no. 4, pp. 587–597, 2019, doi: 10.1049/iet-rpg.2018.5810.

[37] R. Errouissi, A. Al-Durra, and S. M. Muyeen, "A Robust Continuous-Time MPC of a DC-DC Boost Converter Interfaced with a Grid-Connected Photovoltaic System," *IEEE J. Photovoltaics*, vol. 6, no. 6, pp. 1619–1629, 2016, doi: 10.1109/JPHOTOV.2016.2598271.

[38] A. Costa De Souza, F. Cardoso Melo, T. Lima Oliveira, and C. Eduardo Tavares, "Performance Analysis of the Computational Implementation of a Simplified PV Model and MPPT Algorithm," *IEEE Lat. Am. Trans.*, vol. 14, no. 2, pp. 792–798, 2016, doi: 10.1109/TLA.2016.7437224.

[39] M. Bajaj and A. K. Singh, "Grid integrated renewable DG systems: A review of power quality challenges and state-of-the-art mitigation techniques," *Int. J. Energy Res.*, vol. 44, no. 1, pp. 26–69, 2020, doi: 10.1002/er.4847.

[40] T. Esram and P. L. Chapman, "Comparison of photovoltaic array maximum power point tracking techniques," *IEEE Trans. Energy Convers.*, vol. 22, no. 2, pp. 439–449, 2007, doi: 10.1109/TEC.2006.874230.

[41] R. N. Kalaam, S. M. Muyeen, A. Al-Durra, H. M. Hasanien, and K. Al-Wahedi, "Optimisation of controller parameters for grid-tied photovoltaic system at faulty network using artificial neural network-based cuckoo search algorithm," *Front. Cell Dev. Biol.*, vol. 9, pp. 1517–1526, 2017, doi: 10.1049/iet-rpg.2017.0040.

[42] N. Cao and J. Liu, "An improved maximum power point tracking for photovoltaic grid-connected inverter," *2013 IEEE Int. Conf. Mechatronics Autom. IEEE ICMA 2013*, vol. 58, no. 1, pp. 616–621, 2013, doi: 10.1109/ICMA.2013.6617987.

[43] S. Prakash and S. Mishra, "VSC Control of Grid Connected PV for Maintaining Power Supply during Open-Phase Condition in Distribution Network," *IEEE Trans. Ind. Appl.*, vol. 55, no. 6, pp. 6211–6222, 2019, doi: 10.1109/TIA.2019.2932697.

[44] K. Prabha, "Power System Stability and Control." p. 1176, 1994.

[45] R. Ntare, N. H. Abbasy, and K. H. M. Youssef, "Low Voltage Ride through Control Capability of a Large Grid Connected PV System Combining DC Chopper and Current Limiting Techniques," *J. Power Energy Eng.*, vol. 07, no. 01, pp. 62–79, 2019, doi: 10.4236/jpee.2019.71004.